

Universität
Rostock



Traditio et Innovatio



Influence of the Ligand Structure on the Hydroformylation of Olefins

Dissertation

zur

Erlangung des akademischen Grades
doctor rerum naturalium (Dr. rer. nat.)

der Mathematisch-
Naturwissenschaftlichen Fakultät
der Universität Rostock

vorgelegt von

Svenja Kloß, geb. am 18. Februar 1992 in Wolfsburg
aus Rostock

Rostock, 20. April 2020

https://doi.org/10.18453/rosdok_id00002870

Gutachter:

Prof. Dr. Armin Börner, Leibniz-Institut für Katalyse, Universität Rostock

Prof. Dr. Mark Gandelman, Schulich Faculty of Chemistry, Technion - Israel Institute of Technology

Jahr der Einreichung: 2020

Jahr der Verteidigung: 2020

Danksagung

An dieser Stelle möchte ich mich herzlich bei allen bedanken, ohne die die Fertigstellung dieser Arbeit nicht möglich gewesen wäre.

Mein besonderer Dank gilt Prof. Dr. Armin Börner, der mich nicht nur herzlich in seinem Arbeitskreis aufgenommen, sondern mir außerdem die Möglichkeit gegeben hat dieses spannende Themengebiet im Rahmen meiner Promotionsarbeit zu bearbeiten. Außerdem möchte ich mich besonders für die Unterstützung, das in mich gesetzte Vertrauen und die zahlreichen motivierenden Worte bedanken.

Many thanks to Prof. Dr. Mark Gandelman for giving me the opportunity to work in his research group at the Technion in Haifa for three months. It was a pleasure to be part of your cordial group and the time in Israel really was an unforgettable experience for me.

Außerdem möchte ich mich herzlich bei allen meinen Kollegen der Arbeitsgruppe Börner für die Unterstützung und die angenehme Arbeitsatmosphäre bedanken. Mein besonderer Dank gilt hierbei Dr. Baoxin Zhang und Maria Lange, die mir immer mit Rat und Tat zur Seite standen. Es war mir wirklich eine Freude mit euch zu arbeiten. Des Weiteren gilt mein Dank Dr. Detlef Selent und Kerstin Romeike für die Bereitstellung von Druckversuchen und die Unterstützung in fachlichen Fragen.

Gleichfalls gebührt mein Dank den technischen Mitarbeitern des Instituts für Chemie und des Leibniz-Instituts für Katalyse für die analytischen Messungen. Besonders bedanken möchte ich mich für die Unterstützung von Dr. Dirk Michalik und Dr. Anke Spannenberg für Hilfestellungen bei der Problemlösung hinsichtlich NMR-Spektroskopie und Röntgenstrukturanalyse. Meinen ausdrücklichen Dank möchte ich auch an Heike Borgwald für die Durchführung von unzähligen NMR-Messungen sowie Susann Buchholz, Susanne Schareina und Astrid Lehmann aussprechen, die immer auch kurzfristige Messungen möglich machten.

Außerdem möchte ich mich bei meiner Mittagsrunde und meinen Freunden für die vielen mal mehr, mal weniger fachlichen Gespräche verdanken. Bei euch konnte ich immer runterkommen und neue Energie für den Arbeitstag sammeln. Ich werde immer gerne an die Zeit mit euch zurückdenken.

Von ganzem Herzen danke ich meiner ganzen Familie, vor allem aber meinen Eltern und meiner Schwester, für die stetige, bedingungslose und auch finanzielle Unterstützung in allen Lebenslagen. Ihr habt mich aufgebaut und mich immer und immer wieder ermutigt weiterzumachen, wenn mich mal der Mut verließ.

Abschließend möchte ich noch Sebastian Boldt danken, ohne den ich die Promotion wohl nicht durchgezogen hätte. Du hast mich immer wieder motiviert, mich nach Rückschlägen aufgeheitert und Erfolge mit mir gefeiert. Ich bin übergücklich und dankbar, dass ich dich an meiner Seite habe. Ich freue mich auf alles was kommt!

Contents

| | | |
|-------------|--|------------|
| I. | List of figures | I |
| II. | List of schemes | III |
| III. | List of tables | IV |
| IV. | List of abbreviations..... | V |
| 1 | Introduction | 1 |
| 1.1 | Hydroformylation..... | 1 |
| 1.1.1 | Introduction to hydroformylation | 1 |
| 1.1.2 | Ligands for hydroformylation..... | 6 |
| 1.1.3 | Phosphites as ligands for hydroformylation | 7 |
| 1.1.4 | Potentially polydentate coordinating ligands in hydroformylation | 10 |
| 1.1.4.1 | PNP-ligands in hydroformylation..... | 11 |
| 1.1.4.2 | Triphosphorus ligands in hydroformylation | 14 |
| 1.2 | Hydrolysis of phosphites | 16 |
| 2 | Aim of investigations | 22 |
| 3 | Results and discussion | 24 |
| 3.1 | Investigations of substituent effects of mono- and bidentate phosphites on hydroformylation performance and hydrolysis stability | 24 |
| 3.1.1 | Biphenolphosphites | 24 |
| 3.1.1.1 | Synthesis | 24 |
| 3.1.1.2 | Hydroformylation experiments | 28 |
| 3.1.1.3 | Hydrolysis experiments..... | 31 |
| 3.1.1.4 | Conclusion..... | 35 |
| 3.1.2 | Benzopinacolphosphites..... | 37 |
| 3.1.2.1 | Synthesis | 37 |
| 3.1.2.2 | Hydroformylation experiments | 40 |
| 3.1.2.3 | Hydrolysis experiments..... | 42 |
| 3.1.2.4 | Conclusion..... | 46 |
| 3.2 | Investigations of hemilabile potentially tridentate coordinating PNP-ligands | 48 |
| 3.2.1 | Synthesis of PNP-ligands | 48 |
| 3.2.2 | Synthesis of cationic and neutral rhodium complexes..... | 49 |
| 3.2.3 | Hydroformylation experiments with PNP-complexes..... | 54 |
| 3.2.4 | Conclusion..... | 59 |
| 3.3 | Investigation of a potentially tridentate coordinating ferrocenyl ligand..... | 60 |
| 3.3.1 | Investigation of the complexation behavior of HiersoPHOS-2 to rhodium | 61 |

| | | |
|----------|--|-----------|
| 3.3.2 | Application of HiersoPhos-2 in hydroformylation..... | 66 |
| 3.3.3 | Factorial Design..... | 71 |
| 3.3.3.1 | Determination of the yield of the reaction..... | 72 |
| 3.3.3.2 | Determination of the regioselectivity of the reaction..... | 78 |
| 3.3.4 | Conclusion..... | 84 |
| 4 | Concluding remarks..... | 86 |
| 5 | Appendix..... | i |
| 5.1 | Experimental section..... | i |
| 5.1.1 | Synthesis procedures of phosphites with biphenol structure..... | ii |
| 5.1.2 | Hydroformylation with phosphites with biphenol structure..... | xii |
| 5.1.3 | Synthesis of phosphites with benzopinacol structure..... | xiii |
| 5.1.4 | Hydroformylation with phosphites with benzopinacol structure..... | xxviii |
| 5.1.5 | Hydrolysis of phosphites with biphenol and benzopinacol structure..... | xxix |
| 5.1.5.1 | Hydrolysis diagrams of biphenolphosphites..... | xxix |
| 5.1.5.2 | NMR spectra of hydrolysis reactions of biphenolphosphites..... | xxxii |
| 5.1.5.3 | Hydrolysis diagrams of benzopinacolphosphites..... | xxxvii |
| 5.1.5.4 | NMR spectra of hydrolysis reactions of benzopinacolphosphites..... | xl |
| 5.1.6 | Synthesis of PNP-ligands and -complexes..... | lii |
| 5.1.7 | Hydroformylation experiments with PNP-complexes..... | lvii |
| 5.1.8 | Synthesis of HiersoPHOS-2 complexes..... | lviii |
| 5.1.9 | Hydroformylation with HiersoPHOS-2..... | lix |
| 6 | References..... | lx |

I. List of figures

| | |
|--|----|
| Figure 1: Hedione®..... | 4 |
| Figure 2: Structure of Alkanox® 240 and BIPHEPHOS..... | 7 |
| Figure 3: Structures of a tridentate phosphite by Börner and a tetradentate phosphine by Zhang. | 11 |
| Figure 4: Systematic structure of PNP-ligands..... | 11 |
| Figure 5: PNP-pincer ligands used for hydroformylation by Chen..... | 13 |
| Figure 6: PNP-pincer ligands used for hydroformylation by Keglevich..... | 13 |
| Figure 7: Investigated bi- and triphosphine ligands..... | 15 |
| Figure 8: Structures of Bisbi, Tribi and selected phosphoramidites..... | 16 |
| Figure 9: Structure of the investigated nonsymmetric bisphosphite..... | 20 |
| Figure 10: Effect of substituents on the hydrolysis stability of an acylphosphite..... | 21 |
| Figure 11: Investigated structures..... | 23 |
| Figure 12: Structures of the bidentate phosphites 3a and 3b..... | 28 |
| Figure 13: The 16 ml autoclave manufactured by HEL Group..... | 29 |
| Figure 14: Direct and logarithmized plots of the concentration profile of 3a during hydrolysis. Conditions: [L] = 0.049 mol·L ⁻¹ ; H ₂ O/L = 100; T = 90 °C; solvent: 1,4-dioxane..... | 32 |
| Figure 15: Hydrolysis of 2a and 2e at 90 °C..... | 35 |
| Figure 16: Half-life times of biphenolphosphites at room temperature..... | 36 |
| Figure 17: Molecular structure of 8a in the solid state. Displacement ellipsoids correspond to 30 % probability. Hydrogen atoms are omitted for clarity. Selected bond lengths [Å] and angles [°]: P1–O1 1.6275(9), P1–O2 1.6223(9), P1–O3 1.6403(9); O2–P1–O1 94.20(4), O2– P1–O3 106.71(5), O1–P1–O3 94.53(5)..... | 40 |
| Figure 18: Molecular structure of 8c in the solid state. Displacement ellipsoids correspond to 30 % probability. Hydrogen atoms are omitted for clarity. Selected bond lengths [Å] and angles [°]: P1–O1 1.6292(9), P1–O2 1.6189(9), P1–O3 1.6397(9); O2–P1–O1 94.10(4), O2– P1–O3 105.61(5), O1–P1–O3 95.53(5)..... | 40 |
| Figure 19: Direct and logarithmized plots of the concentration profile of 8a during hydrolysis. Conditions: [L] = 0.049 mol·L ⁻¹ ; H ₂ O/L = 100; T = room temperature; solvent: 1,4-dioxane. | 43 |
| Figure 20: Hydrolysis of 8f, 8g and 8h at 90 °C..... | 45 |
| Figure 21: Complete decomposition times of biphenolphosphites at room temperature..... | 46 |
| Figure 22: 3D-plot of aldehyde yield and <i>n</i> -selectivity under optimized reaction conditions and the complete decomposition at room temperature..... | 47 |
| Figure 23: ³¹ P NMR spectra of the reaction mixture (a), the purified desired complex (b) and the dimer side-product (c)..... | 50 |
| Figure 24: Molecular structure of Rh(PNP ^{<i>i</i>Pr})Cl-complex (15b) in the solid state from two different angles. Displacement ellipsoids correspond to 30 % probability. Selected interatomic distances [Å]: P1–Rh1, 2.2389(4); Cl1–Rh1, 2.3481(5); N1–Rh1, 2.0212(18). Selected angles [°]: P1–Rh–Cl1, 95.428(10); Cl1–Rh1–N1, 180.000; P1–Rh1–P1, 169.14(2); N1–Rh1–P1, 84.572(10). Selected torsion angles [°]: P1–Rh1–N1–C3, -11.63(11)..... | 53 |
| Figure 25: Yields of aldehydes obtained with complexes 15a and 15b at different reaction conditions..... | 55 |
| Figure 26: Volumetric uptake of syngas during the hydroformylation with 15a at 20 bar..... | 56 |
| Figure 27: Volumetric uptake of syngas during the hydroformylation with 15a at 50 bar..... | 56 |
| Figure 28: GC spectrum of the hydroformylation reaction with 15a at 20 bar and 100 °C..... | 56 |

| | |
|---|----|
| Figure 29: <i>n</i> -Selectivities of the hydroformylation of 1-octene with 15a and 15b at different reaction conditions..... | 57 |
| Figure 30: GC spectrum for the hydroformylation reaction with 15a at 50 bar and 100 °C..... | 58 |
| Figure 31: GC spectrum of the hydroformylation reaction with 15b at 50 bar and 120 °C..... | 58 |
| Figure 32: ³¹ P NMR spectra of HiersoPHOS-2 (a) and of the rhodium acetylacetonato complex (b)..... | 63 |
| Figure 33: ³¹ P NMR spectra of the rhodium HiersoPHOS-2 complex at elevated temperatures.. | 64 |
| Figure 34: ³¹ P NMR spectra of HiersoPHOS-2 (a) and the corresponding rhodium complex with alternative rhodium precursor (b)..... | 65 |
| Figure 35: 150 ml autoclave by Premex Solutions GmbH..... | 66 |
| Figure 36: Gas consumption of the reaction with a P/Rh ratio of 2/1 at 120 °C and 20 bar (Table 11, entry 1)..... | 68 |
| Figure 37: GC spectrum of the hydroformylation reaction at a phosphorus to rhodium ratio of 2/1, at 120 °C and 20 bar (Table 11, entry 1)..... | 68 |
| Figure 38: Yield of aldehydes, hydrogenation product and the <i>n</i> -selectivity at different ratios of P/Rh and a temperature of 120 °C and syngas pressure of 20 bar..... | 69 |
| Figure 39: Yield of aldehydes and <i>n</i> -selectivity at varying reaction temperatures, P/Rh ratio of 3/1 and a syngas pressure of 20 bar..... | 70 |
| Figure 40: Yield of aldehydes and <i>n</i> -selectivity at varying syngas pressure, P/Rh ratio of 3/1 and at temperatures of 80 °C and 120 °C..... | 71 |
| Figure 41: Three-dimensional representation of the response surface of yield derived from equation (9)..... | 77 |
| Figure 42: Projection of the yield of aldehyde = 0 % line onto the pressure/temperature plane. | 78 |
| Figure 43: Projection of the yield of aldehyde = 100 % line onto the pressure/temperature plane..... | 78 |
| Figure 44: Three-dimensional representation of the response surface of regioselectivity derived from equation (12)..... | 83 |
| Figure 45: Projection of the <i>n</i> -selectivity = 0 % line onto the pressure/temperature plane..... | 83 |
| Figure 46: Projection of the <i>n</i> -selectivity = 100 % line onto the pressure/temperature plane..... | 83 |

II. List of schemes

| | |
|---|----|
| Scheme 1: Principle of hydroformylation..... | 1 |
| Scheme 2: Simplified reaction mechanism of the hydroformylation..... | 2 |
| Scheme 3: Products and reactions based on aldehydes..... | 3 |
| Scheme 4: Application of hydroformylation in the total synthesis of Vitamin A acetate by BASF. . | 3 |
| Scheme 5: Synthesis of α -hexyl cinnamaldehyde by different hydroformylation procedures. | 4 |
| Scheme 6: Phosphorus compounds commonly used as ligands. | 6 |
| Scheme 7: Equilibria between different Rh-complexes leading to different rhodium catalysts. | 7 |
| Scheme 8: General routes for the synthesis of phosphites..... | 8 |
| Scheme 9: Synthesis of nonsymmetrically substituted phosphites..... | 9 |
| Scheme 10: Synthesis of symmetric and nonsymmetric potentially bidentate phosphites. | 9 |
| Scheme 11: Enhanced chelating ability of a tetraphosphine ligand through multiple chelating modes and increased local phosphorus concentration at the metal center. | 10 |
| Scheme 12: Synthesis routes for PNP-phosphine ligands. | 12 |
| Scheme 13: PNP-pincer ligand by Mathey and application thereof in the hydroformylation of α -pinene. | 14 |
| Scheme 14: Degradation of phosphites by (autocatalytic) hydrolysis. | 17 |
| Scheme 15: Mechanism of the hydrolysis of phosphites..... | 17 |
| Scheme 16: Degradation of <i>O,O'</i> -3,3'-di- <i>tert</i> -butyl-5,5'-dimethoxy-1,1'-biphenyl-2,2'-diylphosphonate and its tautomeric equilibrium between pentavalent and trivalent structure. | 18 |
| Scheme 17: Hydrolysis stability of bulky phosphites..... | 19 |
| Scheme 18: Proposed catalytic cycle for the phosphite hydrolysis reaction in the coordination sphere of platinum(II)..... | 20 |
| Scheme 19: Synthesis of a biphenolphosphorochloridite. | 24 |
| Scheme 20: General synthesis of biphenolphosphites..... | 25 |
| Scheme 21: Synthesis of 2c in the presence of triethylamine. | 26 |
| Scheme 22: Reaction scheme for the synthesis of the hydroxyl protected phosphites 2d and 2e. | 26 |
| Scheme 23: Hydrolysis conditions for biphenolphosphites..... | 31 |
| Scheme 24: Synthesis of phosphorochloridite 7 with benzopinacol moiety..... | 37 |
| Scheme 25: Synthesis of benzopinacolphosphites 8a-l..... | 38 |
| Scheme 26: The order of activity in hydroformylation in dependence on position and nature of substituents..... | 42 |
| Scheme 27: Synthesis of PNP ^{Ph} (9a)..... | 48 |
| Scheme 28: Synthesis of PNP ^{iPr} (9b)..... | 48 |
| Scheme 29: Routes for the synthesis of cationic rhodium complexes..... | 49 |
| Scheme 30: Synthesis of [Rh(PNP ^{Ph})(COE)]X..... | 50 |
| Scheme 31: Synthesis of [Rh(PNP ^{Ph})(C ₂ H ₄)]BF ₄ (13). | 51 |
| Scheme 32: Synthesis of [Rh(PNP ^{iPr})(COE)]BF ₄ (14)..... | 52 |
| Scheme 33: Synthesis of Rh(PNP)Cl (15)..... | 52 |
| Scheme 34: Synthesis procedure of HiersoPHOS-2..... | 60 |
| Scheme 35: Coordination mode of HiersoPHOS-2 to copper iodide..... | 60 |
| Scheme 36: Coordination mode of HiersoPHOS-2 to palladium..... | 61 |
| Scheme 37: Synthesis of the rhodium complex 16 with HiersoPHOS-2..... | 62 |

III. List of tables

| | |
|--|-------|
| Table 1: Reaction conditions and yields of monophosphites synthesized..... | 25 |
| Table 2: Optimization of Suzuki–Miyaura coupling reactions for the synthesis of the protected biphenols 6a and 6b..... | 27 |
| Table 3: Hydroformylation ^a of <i>n</i> -octenes ^b with biphenolphosphites..... | 30 |
| Table 4: Hydrolysis ^a of biphenolphosphites at room temperature..... | 33 |
| Table 5: Hydrolysis ^a of biphenolphosphites at 90 °C..... | 34 |
| Table 6: Reaction conditions and yields of the benzopinacolphosphites..... | 38 |
| Table 7: Hydroformylation ^a of <i>n</i> -octenes ^b with benzopinacolphosphites..... | 41 |
| Table 8: Hydrolysis ^a of benzopinacolphosphites at room temperature..... | 43 |
| Table 9: Hydrolysis ^a of benzopinacolphosphites at 90 °C..... | 44 |
| Table 10: Hydroformylation ^a of 1-octene with PNP-complexes..... | 54 |
| Table 11: Hydroformylation ^a of 1-octene with HiersoPHOS-2..... | 67 |
| Table 12: Selected results for the hydroformylation ^a of 1-octene with obtained yield of aldehyde and coding according to Factorial Design..... | 73 |
| Table 13: Design matrix <i>D</i> for the investigation concerning the yield of aldehyde..... | 73 |
| Table 14: Values for <i>a</i> , experimental (<i>y</i>) and estimated (<i>y</i> [̂]) results for the yield of aldehyde..... | 74 |
| Table 15: Coded design matrix <i>D</i> _C for the yield of aldehyde..... | 74 |
| Table 16: Matrix (<i>D</i> _C '· <i>D</i> _C) ⁻¹ | 75 |
| Table 17: Values of <i>t</i> and significance..... | 76 |
| Table 18: Selected results for the hydroformylation ^a of 1-octene with obtained <i>n</i> -selectivity and coding according to Factorial Design..... | 79 |
| Table 19: Design matrix <i>D</i> for the investigation concerning the <i>n</i> -selectivity of the reaction..... | 79 |
| Table 20: Values for <i>a</i> , experimental (<i>y</i>) and estimated (<i>y</i> [̂]) results for the <i>n</i> -selectivity..... | 80 |
| Table 21: Coded design matrix <i>D</i> _C for the <i>n</i> -selectivity..... | 80 |
| Table 22: Matrix (<i>D</i> _C '· <i>D</i> _C) ⁻¹ | 80 |
| Table 23: Values of <i>t</i> and significance..... | 81 |
| Table 24: Crystallographic details of 8a..... | xv |
| Table 25: Crystallographic details of 8c..... | xviii |
| Table 26: Crystallographic details of 15b..... | lvi |

IV. List of abbreviations

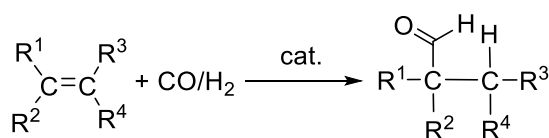
| | |
|-------------|--|
| Ac | acetyl |
| acac | acetylacetonate |
| Alk | alkyl substituent |
| Bn | benzyl |
| BuLi | butyllithium |
| COE | cyclooctene |
| cp | cyclopentadienyl |
| d | doublet |
| DCPD | dicyclopentadiene |
| dppe | 1,2-bis(diphenylphosphino)ethane |
| EI | electron ionization |
| ESI | electrospray ionization |
| Et | ethyl |
| GC | gas chromatography |
| h | hours |
| HASPO | heteroatom-substituted phosphine oxide |
| <i>i</i> Pr | <i>iso</i> -propyl |
| <i>m</i> - | <i>meta</i> - |
| m | multiplet |
| Me | methyl |
| min | minutes |
| MS | mass spectroscopy |
| NBD | 2,5-norbornadiene |
| <i>n</i> Bu | <i>n</i> -butyl |
| NMP | <i>N</i> -methyl-2-pyrrolidone |
| NMR | nuclear magnetic resonance |
| <i>o</i> - | <i>ortho</i> - |
| OTf | trifluoromethanesulfonate |
| <i>p</i> | pressure |
| <i>p</i> - | <i>para</i> - |
| Ph | phenyl |
| q | quartet |
| r.t. | room temperature |
| s | singlet |
| <i>T</i> | temperature |
| t | triplet |
| TIPS | triisopropylsilyl |
| TBS | <i>tert</i> -butyldimethylsilyl |
| <i>t</i> Bu | <i>tert</i> -butyl |
| THF | tetrahydrofuran |
| TMEDA | tetramethylethylenediamine |
| TOF | time of flight |
| v | virtual |

1 Introduction

1.1 Hydroformylation

1.1.1 Introduction to hydroformylation

The hydroformylation of olefins is one of the most relevant industrially applied chemical reactions worldwide in homogeneous catalysis.¹⁻⁶ The annual production of over 10 million tons of aldehydes reflects its importance.² Principally, homogeneously catalyzed hydroformylation describes the reaction of synthesis gas (“syngas”) — a mixture of hydrogen and carbon monoxide — with alkenes under the formation of aldehydes (Scheme 1). Formally, this reaction can be described as the addition of hydrogen (“hydro”) and a formyl group to the double bond of the alkene in an atom-economical manner.²

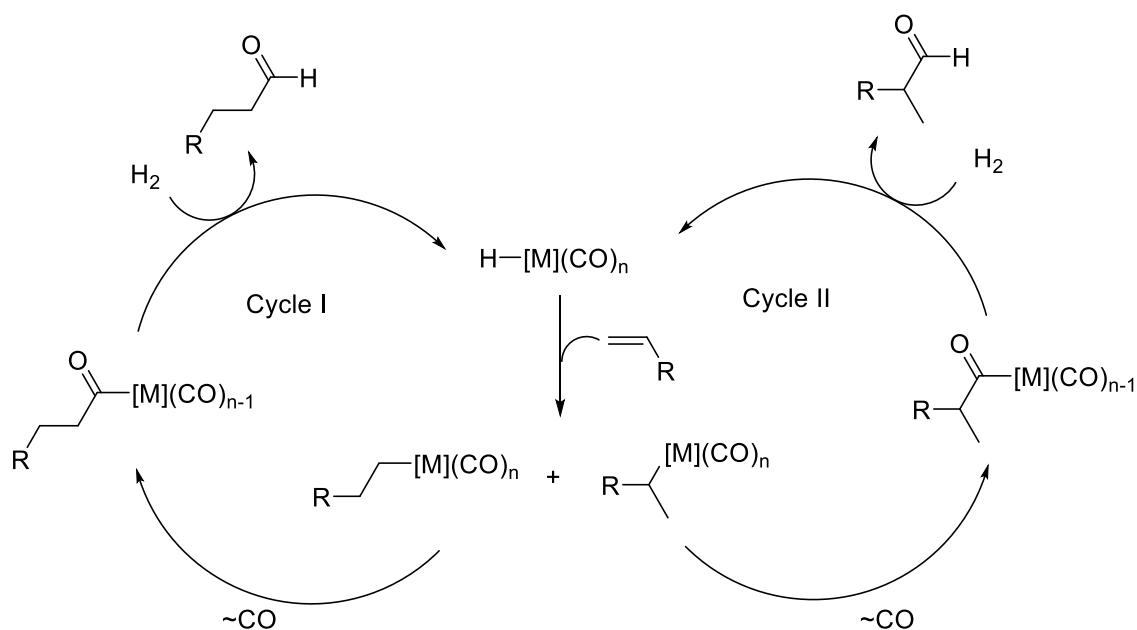


Scheme 1: Principle of hydroformylation.

With the exception of ethylene as substrate, this reaction leads to a mixture of isomeric aldehydes. In the case of terminal alkenes (R^1 and $\text{R}^2 = \text{H}$) the formation of the *n*-aldehyde and *iso*-aldehyde is possible, as well as several other branched aldehydes, when double bond isomerization takes place. In this case the description as linear (*l*) and branched (*b*) aldehydes is more precise. The same applies when functionalized substrates are used. The two simplified reaction mechanisms for the formation of *n*-aldehyde (Cycle I) and *iso*-aldehyde (Cycle II) are shown in Scheme 2.⁷ Additionally, if a prochiral substrate is used, the newly formed branched aldehydes are chiral, which increases the possibilities of stereoselective conversions even further. The regioselectivity of the reaction, meaning the ratio of isomers formed, are a decisive factor of every hydroformylation reaction. It can be influenced by several reaction parameters: for example, the applied catalyst system (metal and ligand) and reaction conditions such as temperature, pressure and syngas composition. The developments of the past decades show that the rhodium based catalysts in hydroformylation can offer excellent regioselectivities, chemoselectivities and functional group tolerance at relatively low temperature and pressure.⁸⁻¹⁰

1 Introduction

1.1 Hydroformylation

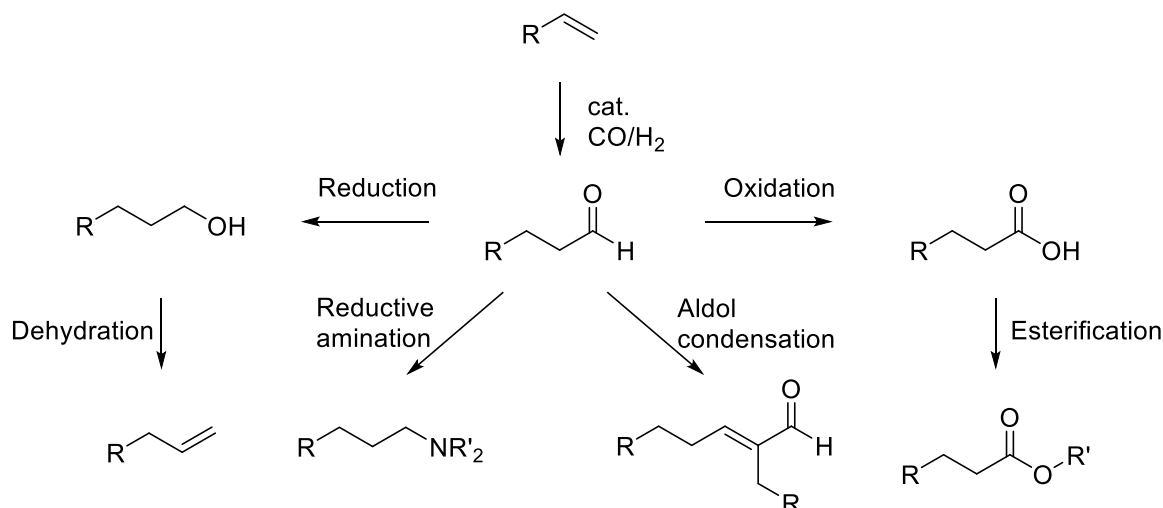


Scheme 2: Simplified reaction mechanism of the hydroformylation.

Although aldehydes themselves are less commercially interesting (with the exception of perfume ingredients, see Scheme 5), they are important intermediates for further reactions. They can be transformed into alcohols by reduction, to carboxylic acids by oxidation, or to amines by reductive amination. These in turn represent important starting materials for further conversions. Alcohols can be dehydrated to alkenes which inherit one more carbon atom than the original alkene (olefin homologization). Carboxylic acids can be converted into the corresponding esters. An overview about important reactions and subsequent transformations is shown in Scheme 3. Some of these final products are also synthesized in one-pot and tandem reactions in which the aldehydes as intermediates are not isolated. Such subsequent reactions are e.g. hydrogenations, acetalizations or C-C-coupling reactions.¹¹⁻¹³ These industrially applied transformation further emphasize the importance of a high stability paired with high stereoselectivity of the applied catalyst under quite different and sometimes very severe reaction conditions. Sometimes the assistance of the hydroformylation catalyst in the following reaction step is necessary.

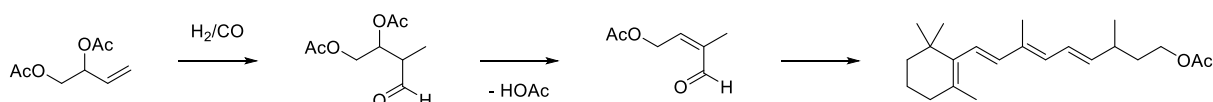
1 Introduction

1.1 Hydroformylation



Scheme 3: Products and reactions based on aldehydes.

Even though the reaction can also be used to synthesize fine-chemicals like pharmaceuticals, scents and flavors, the field of hydroformylation is mainly dominated by bulk processes with respect to the production scale.¹⁴⁻¹⁹ One example for the application of hydroformylation in a commercially used synthesis route in the field of fine-chemicals is the synthesis of vitamin A acetate by BASF (Scheme 4). The first step of this approach is the rhodium-catalyzed hydroformylation of 1,2-diacetoxy-3-butene to the corresponding branched aldehyde. Final elimination of acetic acid leads to the α,β -unsaturated aldehyde which gives vitamin A acetate by a Wittig reaction.¹⁴



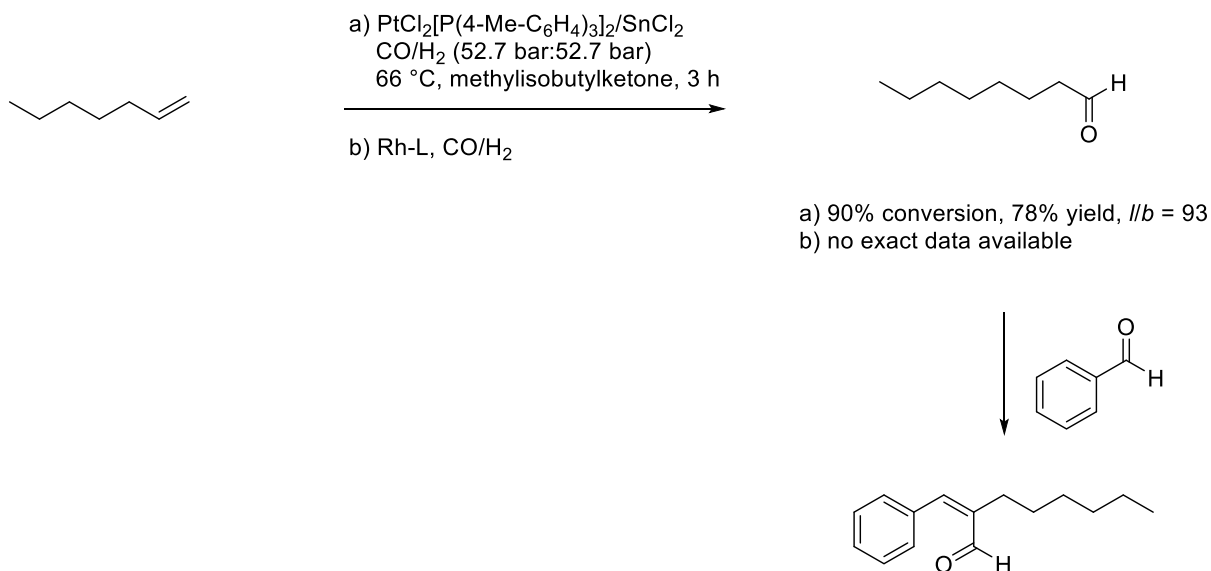
Scheme 4: Application of hydroformylation in the total synthesis of Vitamin A acetate by BASF.

Another field that is highly dependent on the production of aldehydes by hydroformylation is the field of scents. An example is the synthesis of *n*-octanal (caprylaldehyde) shown in Scheme 5. This compound can be synthesized by Pt/Sn-catalyzed hydroformylation of *n*-heptene^{20,21} or by a rhodium-catalyzed route developed by Sasol. This second variant gives probably 85 % yield of the linear aldehyde when PPh_3 is used as a ligand.²² Naturally caprylaldehyde is part of several citrus oils and has a pungent odor in high concentrations. On the other hand, it has a typical citrus scent in low concentrations, and therefore it is used sparingly in fragrances. A final aldol condensation of octanal with benzaldehyde gives α -hexyl cinnamaldehyde, which has an elegant, transparent floral, jasmine note with a fresh citrus scent. This odor is very similar to the popular methyl

1 Introduction

1.1 Hydroformylation

dihydrojasmonate (also known as Hedione®), which is added to almost every fine fragrance. Therefore α -hexyl cinnamaldehyde is used as an inexpensive alternative.²³



Scheme 5: Synthesis of α -hexyl cinnamaldehyde by different hydroformylation procedures.

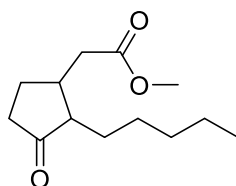


Figure 1: Hedione®.

Hydroformylation was discovered accidentally in 1938 by Otto Roelen (Ruhchemie AG), who called it the “oxo process”.^{24,25} The process is also referred to as “oxonation”. Roelen discovered the formation of small amounts of propanal and diethylketone as he was introducing ethylene and synthesis gas to a heterogeneous catalyst while he was studying the Fischer–Tropsch reaction.²⁶ Only four years later the first plant started to operate. Following Roelen’s original procedure, the first generation of hydroformylation processes applied cobalt catalysts and rather gentle reaction conditions.⁵

Similar to the first generation, the second generation of processes employed unmodified Co-catalysts but under more severe reaction conditions. Furthermore, the methods of recovering the catalyst from the product changed. Either redox processes or transformation of the precatalyst $[\text{HCo}(\text{CO})_4]$ into water-soluble salts were applied. Moreover, instead of alkenes with longer carbon chain mainly propylene was used as a substrate. Already in this generation outlets of up to 300 kt per year were achieved. Major drawbacks of unmodified Co-catalysts are the rather low I/b -ratios,

1 Introduction

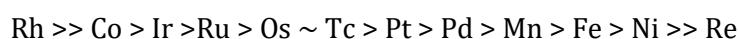
1.1 Hydroformylation

which can be improved by monodentate organic phosphine ligands. However, this leads to a lower activity and the undesired formation of alcohols and alkanes.^{27,28} This improved process can be performed under lower synthesis gas pressure (120–190 °C, CO/H₂ pressure 4–30 MPa) and is still used today mainly in the synthesis of aldehydes or alcohols from long-chain or branched alkenes.

The third generation of hydroformylation processes was developed in the late 1970s and operates with rhodium catalysts that are modified by organic, mainly phosphorus containing, ligands. Similar to the processes of the second generation rather low syngas pressures (1.8–6.0 MPa) and temperatures (85–130 °C) are applied. These are also the conditions predominantly used until now. About 70 % of the processes today are based on rhodium catalysts. In addition, nowadays short-chain alkenes like ethylene, propylene and isomeric butenes represent the majority of the substrates. One main difference between the second and third generation concerns the way of catalyst recycling. Due to its high price compared to cobalt the recovery of rhodium has a significant impact on the whole economic efficiency of a process. The estimated annual financial loss can reach up to several million euros in a 400 kt/a plant, when only 1 ppm Rh/kg product is lost.⁶ There are mainly two different methods used in industry for recovering the catalyst. The first is the so called “gas recycle” whereby the resulting product is separated from the catalyst solution with the support of a syngas stream. In the second method, the newly formed aldehyde is separated by distillation.

The fourth generation employs another very efficient method for separating catalyst and product: It is based on liquid-liquid biphasic processes in which an aqueous phase is used to immobilize the rhodium complex which is water-soluble due to sulfonated phosphine ligands (TPPTS). The formed aldehyde is mainly dissolved in the organic phase and can be separated from there.²⁹

As already mentioned in the previous paragraphs, the metals typically used in hydroformylation are rhodium and cobalt. Due to the high price of rhodium, alternative metals gained importance as well, but up to now they only play a role in academic research due to their relatively low reactivity.³⁰ A generally accepted row of the activity of the non-modified metals can be described as below.³¹



As a catalyst usually a homogeneous hydrido complex of the type $[\text{HM}(\text{CO})_x\text{L}_y]$, with M representing the metal and L representing carbon monoxide or an organic ligand, is submitted to

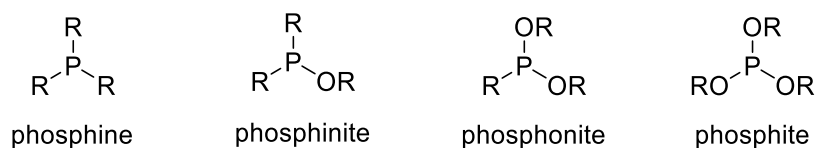
1 Introduction

1.1 Hydroformylation

the reaction. A hydrido complex with exclusively CO-ligands is called unmodified or “naked” catalyst, while a catalyst with CO and additional organic ligands is called “modified” catalyst.

1.1.2 Ligands for hydroformylation

Ligands in modern hydroformylation processes fulfil several crucial tasks. They improve the general catalysis properties, such as activity, regio- and chemoselectivity. Moreover, they can significantly contribute to the stability of the organometallic complex towards other components like water, aldehydes or acids during the hydroformylation process. Besides the alteration of the catalytic properties, other incentives for the development of new ligands may be the circumvention of existing patents or a better separability of the catalyst from the product. For several decades, mainly trivalent phosphorus containing organic compounds — like phosphines, phosphinites, phosphonites and phosphites — have been used (Scheme 6). A perusal of the patent literature indicates that phosphites are the most common.



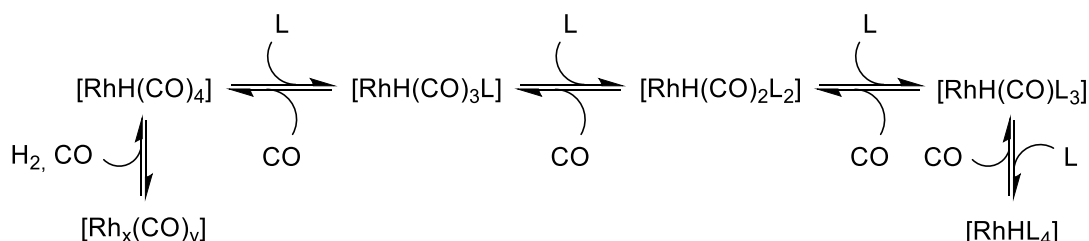
Scheme 6: Phosphorus compounds commonly used as ligands.

In general, every organic ligand has to compete with CO for the free coordination sites of the metal center. This results in an equilibrium of several complexes of the type $[\text{HM}(\text{CO})_x\text{L}_y]$, which differ in the number of CO and organic ligand coordinated to the metal, as shown in Scheme 7 using rhodium as an example. It is important to note that only the complexes $[\text{RhH}(\text{CO})_3\text{L}]$ and $[\text{RhH}(\text{CO})_2\text{L}_2]$ are the desired catalytically active complexes. A higher coordination number of carbon monoxide leads to the unmodified catalyst, which is usually less active and has a lower regioselectivity. Eventually, even higher coordination of CO to the metal can lead to the formation of rhodium clusters and the precipitation of these from the reaction solution. On the other hand, a high number of coordinated organic ligands can inhibit the coordination of CO, which leads in consequence to hydrogenation or no activity at all. The shift of equilibria depends on the CO-pressure as well as on the ratio of rhodium to phosphorus ligand. The coordination properties of a ligand are determined by electronic and steric properties.^{32,33} In comparison to phosphines phosphites are better π -acceptors, and therefore they accelerate the CO dissociation from the metal which is a precondition for the generation of the catalyst from the relevant precatalyst as well as for the insertion in the rhodium-alkyl bond during the reaction.³⁴ To generate the desired

1 Introduction

1.1 Hydroformylation

catalyst complexes usually a large excess of ligand is needed, which has to compete with CO for free coordination sites on the metal. Dependent on the efforts for the ligand synthesis, this may inherit a significant economic factor. Strategies in this matter will be further addressed in chapter 1.1.4.



Scheme 7: Equilibria between different Rh-complexes leading to different rhodium catalysts.

1.1.3 Phosphites as ligands for hydroformylation

Phosphites are triesters of phosphorous acid. Compared to phosphines they are characterized by three aryloxy and alkoxy groups, respectively. They play a crucial role as mono-, bi- or polydentate ligands in rhodium-catalyzed hydroformylation and many other catalytic applications.³⁵ Over the years, a comprehensive library of numerous ligands following this basic motive were synthesized, incorporating varying steric, electronic or even chiral moieties.^{36,37} Two of the most prominent examples of this group of ligands are tris[2,4-di-*tert*-butylphenyl]phosphite (also known as Alkanox[®] 240)³⁸⁻⁴² and 6,6'-[(3,3'-di-*tert*-butyl-5,5'-dimethoxy-1,1'-biphenyl-2,2'-diyl)bis(oxy)]bis(dibenzo[*d,f*][1,3,2]) which is also known by the name BIPHEPHOS claimed by Union Carbide Corporation (now Dow Chemical).⁴³⁻⁴⁵

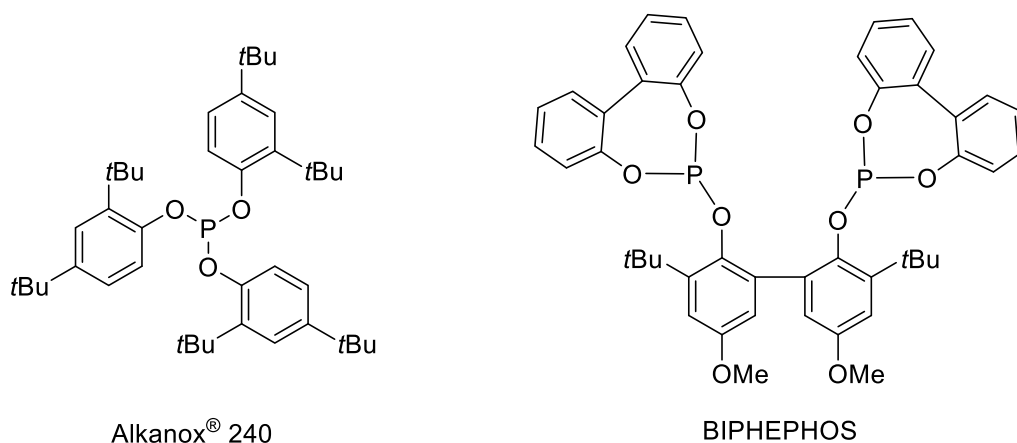
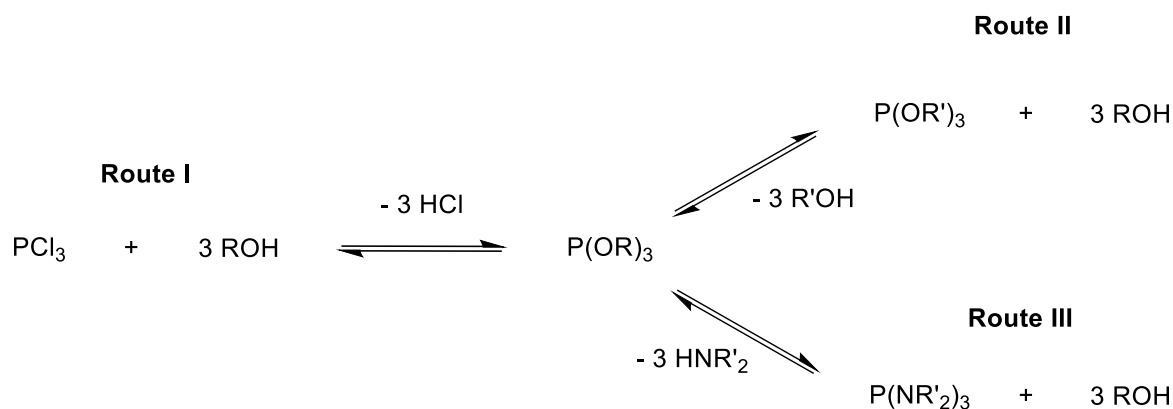


Figure 2: Structure of Alkanox[®] 240 and BIPHEPHOS.

1 Introduction

1.1 Hydroformylation

Phosphites are synthesized by substitution reactions of various trivalent phosphorus compounds with alcohols. The most common method is the reaction of phosphorus trichloride with substituted phenols or alkanols (Scheme 8, Route I). It is also possible to carry out transesterifications of phosphites (Route II)^{46,47} or the substitution reaction of phosphorous triamides with alcohols (Route III).⁴⁸ The latter are less frequently applied.



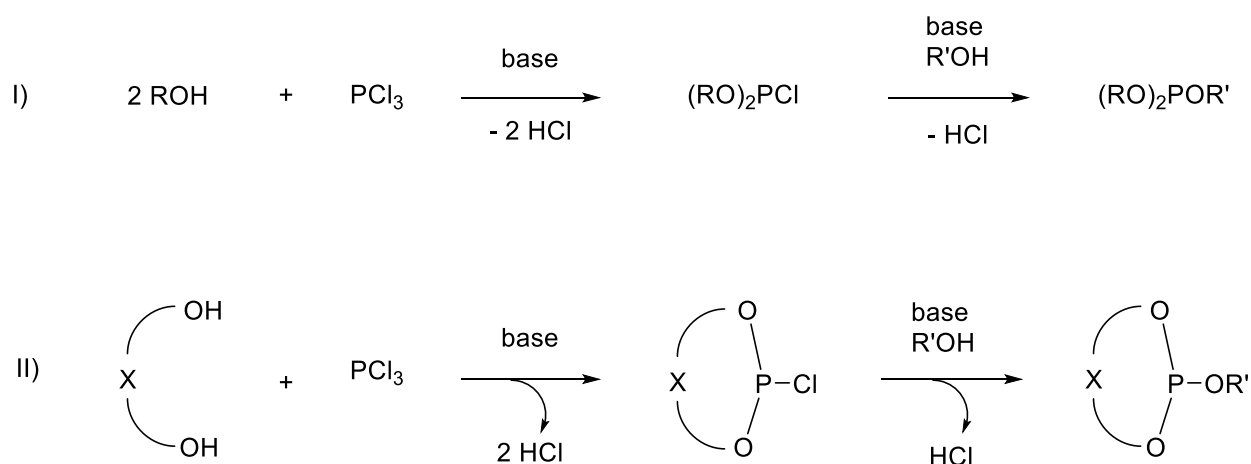
Scheme 8: General routes for the synthesis of phosphites.

When the synthesis with PCl_3 is applied, the use of a base (ammonia, trialkylamines or nitrogen containing heterocycles) is recommended. Trapping of the HCl does not only shift the equilibrium of the reaction towards the desired product but also inhibits the reaction of phosphites with HCl to the corresponding dialkyl hydrogen phosphites.

It is also possible to synthesize nonsymmetrically substituted phosphites of the structure $P(OR_2)OR'$ by subsequent reaction procedures as shown in Scheme 9.³⁵ For small scale reactions usually nonpolar solvents like THF or toluene are used. For large-scale reactions, solvents may not be required. During the reaction of diols and phosphorus trichloride, monochlorophosphorus diesters, also referred as phosphorochloridites, are usually formed, as these benefit from enhanced stability by the ring structure. Subsequently, these can be treated with monoalcohols as shown in Scheme 9, II.⁴⁹ This procedure can be applied successfully when the ring size of the synthesized cyclic phosphite consists of five to eight atoms.⁴⁶ Sometimes, it is advantageous to enhance the nucleophilicity of the alcohol. For this purpose it can be treated with organolithium compounds to convert them into the corresponding Li-salts.⁵⁰

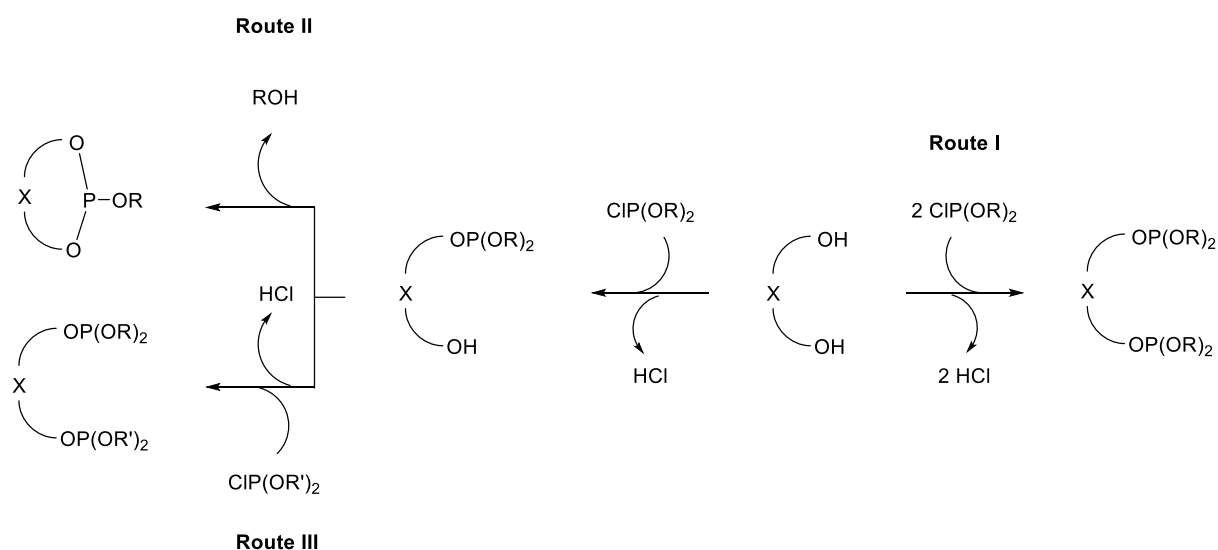
1 Introduction

1.1 Hydroformylation



Scheme 9: Synthesis of nonsymmetrically substituted phosphites.

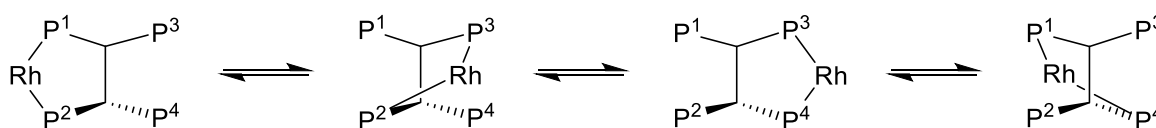
Starting from the previously reported synthesis of nonsymmetric phosphites also the synthesis of symmetric⁴³ and nonsymmetric bidentate or polydentate phosphites is possible.^{10,51,52} A common problem in the synthesis of nonsymmetric phosphites from two diols (as it would occur if the second alcohol R'OH in Scheme 9, example II would also be a diol) is the formation of a cyclic phosphite as well as a monoester (Scheme 10, Route I and Route II). When the steric construction of the backbone allows the formation of both products, two compounds may be produced. This can lead to a hard-to-separate mixture which requires additional purification steps and eventually reduces the yield of the desired product.³⁶ Otherwise, this synthesis procedure can also be employed to synthesize nonsymmetric potentially bidentate phosphites (Scheme 10, Route III).⁵³ Similarly, based on polyols, potentially polydentate coordinating ligands are also accessible.⁵⁴⁻⁵⁶



Scheme 10: Synthesis of symmetric and nonsymmetric potentially bidentate phosphites.

1.1.4 Potentially polydentate coordinating ligands in hydroformylation

Polydentate ligands can inherit several positive properties to the catalytic system. The stability of rhodium complexes with bi- and polydentate ligands can benefit from the chelate effects as it is statistically less likely to dissociate all phosphorus groups at the same time. Zhang *et al.* argued that tetradentate ligands can show enhanced chelating abilities due to multiple chelating modes which might increase the local phosphorus concentration around the metal center (Scheme 11).⁵⁷ If one phosphorus group dissociates from the metal center, two other phosphorus moieties can rearrange and thus restore the catalytically active state. This kind of “enhanced multidentarity” is demonstrated to enhance the ligand to stabilize catalytic systems and improve their longevity in transition-metal-catalyzed coupling reactions.^{58–62} Additionally, these ligands lead to higher concentrations of the desired catalytic species mentioned in chapter 1.1.2 due to the presence of multiple chelating modes. The rhodium center can be coordinated in four different manners by the same ligand (Scheme 11).⁶³ Unfortunately, up to now no real proof of this behavior has been given in the literature.



Scheme 11: Enhanced chelating ability of a tetraphosphine ligand through multiple chelating modes and increased local phosphorus concentration at the metal center.

Moreover, sterically hindered P-ligands favor the formation of linear aldehydes. The previously (Chapter 1.1.3) mentioned bidentate BIPHEPHOS was one of the first ligands designed for this purpose followed by many other examples.^{43,45} There are also several tri- or tetradentate ligands reported in the literature that inherit excellent *n*-regioselectivities of up to 99 % (two examples are shown in Figure 3).^{8,57,63–65} Furthermore, these polydentate ligands give the described superior results at exceptionally low ligand/metal ratios. This fact is also an important benefit of polydentate ligands as usually a huge excess of ligand is used, which in turn leads to higher production costs. The economic efficiency of an industrial process can be significantly increased if a lower ligand concentration is required. Moreover, the use of more complicated and therefore more expensive ligands could therefore gain more interest.

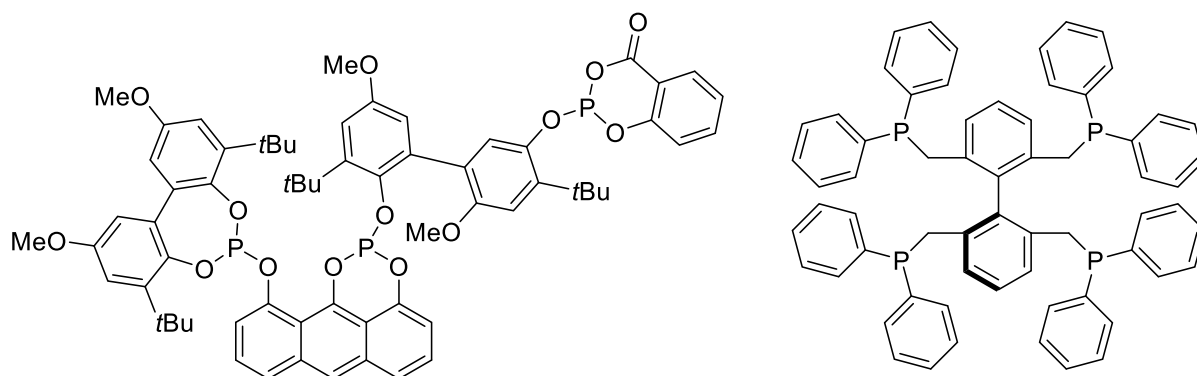


Figure 3: Structures of a tridentate phosphite by Börner and a tetradentate phosphine by Zhang.

1.1.4.1 PNP-ligands in hydroformylation

A special case of potentially tridentate ligands are PNP-ligands which contain one potentially coordinating nitrogen in the backbone of the structure and two additional phosphorus groups.

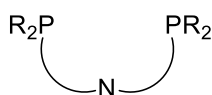
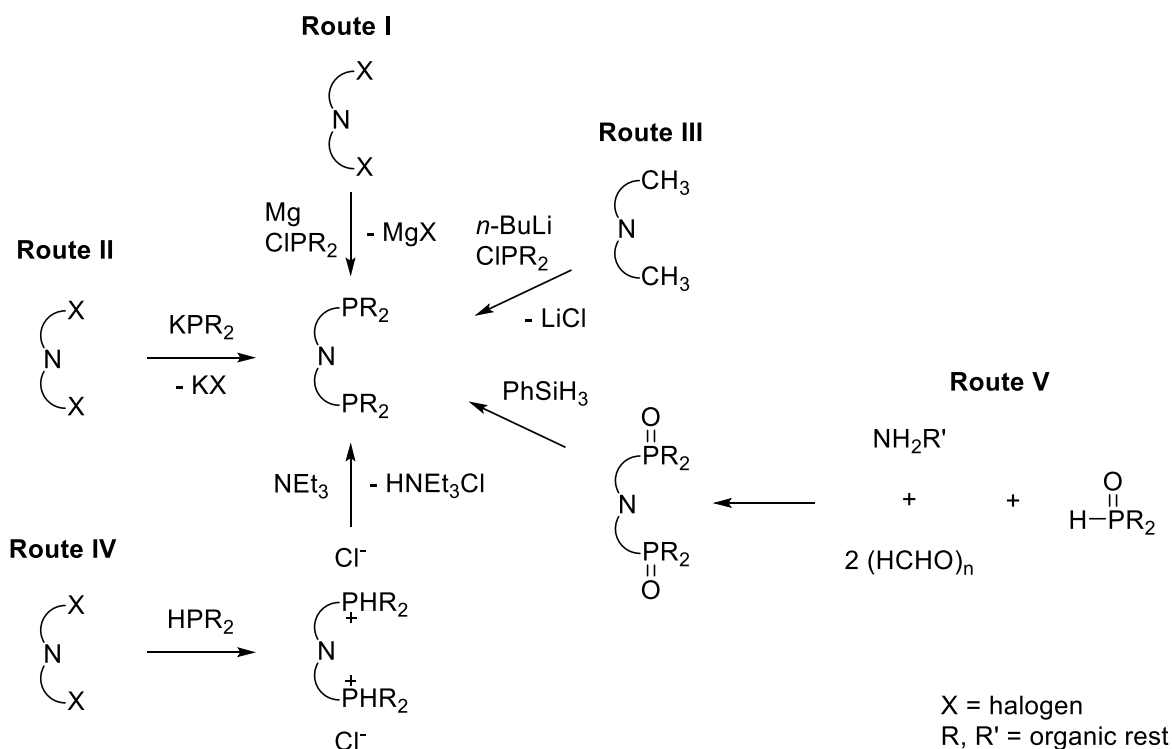


Figure 4: Systematic structure of PNP-ligands.

PNP-ligands with a phosphine group containing aryl or alkyl groups are generally synthesized by one of the following four routes (Scheme 12). The first methodology uses magnesium and halophosphines in a Grignard type reaction. In this case the halogen from the phosphorus precursor is displaced by the organometallic compound.⁶⁶⁻⁶⁸ Route II employs a strong base such as potassium *tert*-butoxide to deprotonate the secondary phosphine. The generated phosphide reacts in a second step with a dihalogenated dialkyl or diaryl amine.^{68,69} Alternatively, also sodium phosphide can be used.⁷⁰ For the third route an activated methyl derivative is first deprotonated with an organolithium compound. Afterwards a halophosphine is added.^{71,72} Route IV showcases the addition of a secondary phosphine to the halogenated backbone followed by selective deprotonation with triethylamine.⁷³ Only recently, Keglevich reported a microwave assisted Kabachnik-Fields reaction to synthesize PNP-ligands from primary amines, paraformaldehyde and secondary phosphines (Route V).⁷⁴

Several structures are available as options for the backbone. It may contain nitrogenous heterocycles (e. g. pyridine, pyrrole or triazole) or secondary or tertiary amines. The latter are frequently protected throughout the whole synthesis.

1 Introduction
1.1 Hydroformylation



Scheme 12: Synthesis routes for PNP-phosphine ligands.

There are currently only a few reports in the literature concerning the use of PNP-pincer ligands in hydroformylation. Different from other tri- or tetradentate ligands, pincer ligands can bind to three adjacent coplanar sites of the metal center.^{75,76} Additionally, their backbone is relatively smaller.⁷⁷ Chen and co-workers described the rhodium-catalyzed hydroformylation of cyclohexene, 2,5-norbornadiene (NBD) and dicyclopentadiene (DCPD) using four PNP-pincer ligands with pyridine backbone (Figure 5).⁷⁷ They were able to achieve conversions of cyclohexene of up to 97 % with ligand L1. For the more sterically demanding NBD even conversions up to 99.9 % were reported. It was also possible to obtain a 97 % yield of the di-aldehyde with ligands L1 and L2 which is one of the best results reported up to now.^{78,79} Another superior regioselectivity was achieved by the assistance of ligand L4 which gave only the mono-aldehyde and no detectable di-aldehyde at all. Unfortunately, the conversion in this case reached only 21 %. The hydroformylation of DCPD was performed in a similarly successful manner with conversions by up to 99.9 % and yields of the di-aldehyde by up to 93 %.

1 Introduction

1.1 Hydroformylation

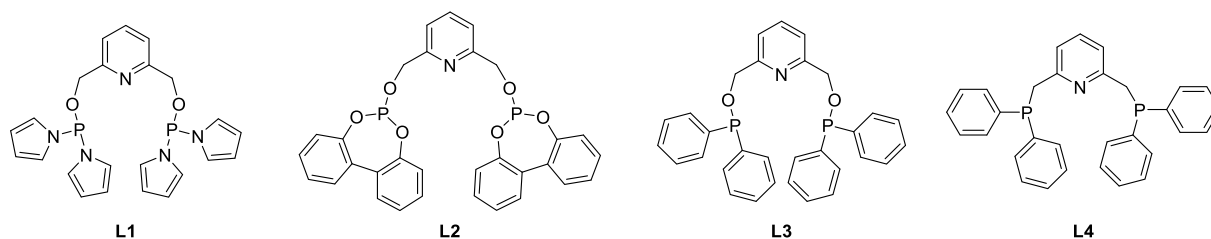
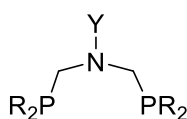


Figure 5: PNP-pincer ligands used for hydroformylation by Chen.

Furthermore, the group of Keglevich reported the platinum-catalyzed hydroformylation of styrene using PNP-pincer ligands with amine backbone (Figure 6) synthesized by a microwave assisted method.⁷⁴ These ligands showed good activities and chemoselectivities with conversion to the corresponding aldehydes by up to 79 %. Moreover, they induced high regioselectivity. In this case the substituents at the phosphine moieties seem to have an impact on the activity of the catalyst as the ligand with benzyl substituent showed lower conversions than the 4-MeC₆H₄-substituted analogue paired with similar chemoselectivities. Conversely the substituent at the amine backbone had no remarkable effect.



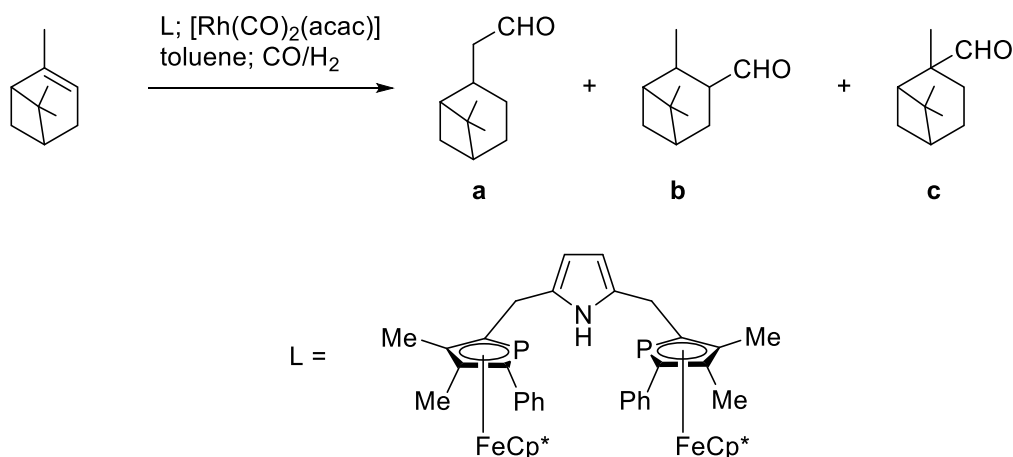
Y = *n*-Bu, cyclo-Hex, Bn
R = Bn, 4-MeC₆H₄

Figure 6: PNP-pincer ligands used for hydroformylation by Keglevich.

An interesting new type of PNP-pincer ligands was described by Mathey *et al.* containing a pyrrole backbone decorated with phosphabenzene units.⁸⁰ The ligand was tested in the rhodium-catalyzed hydroformylation of α -pinene (Scheme 13) and mainly produced the terminal aldehyde with a yield of 49 % and a ratio of a:b:c of 21.8:4.3:1.

1 Introduction

1.1 Hydroformylation



Scheme 13: PNP-pincer ligand by Mathey and application thereof in the hydroformylation of α -pinene.

1.1.4.2 Triphosphorus ligands in hydroformylation

The use of hemilabile coordinating polyphosphorus ligands represents an interesting concept for the hydroformylation of olefins. Surprisingly, compared to bi- and tetraphosphorus ligands, only a few examples of triphosphorus ligands were reported. As already mentioned in chapter 1.1.4, polydentate ligands are characterized by improved chelating properties which eventually result in a higher regioselectivity of the catalytic system.⁵⁷

One of the earlier investigations of triphosphorus ligands in hydroformylation was published by Taniguchi and co-workers in 1988 as they investigated rhodium complexes with $\text{MeC}(\text{CH}_2\text{PPh}_2)_3$ ("triphos") in hydrogenation and hydroformylation.⁸¹ In this study they compared activity and regioselectivity of the tridentate ligand with the monodentate coordinating triphenylphosphine in the hydroformylation of 1-hexene. The tridentate ligand showed a lower activity (and no activity at both low temperature and low pressure), but the *l/b*-ratio was higher compared to those obtained with the monodentate ligand. Very similar results were reported by the research group of Caulton two years later.⁸²

Just recently in 2018 Baricelli and co-workers investigated the hydroformylation of limonene by comparing the monodentate triphenylphosphine, the bidentate dppe and the previously mentioned triphos. They claimed to be the first research group to investigate the hydroformylation of terpenes with a triphosphine ligand. In this case no significant difference in regioselectivity was observed as all three catalytic systems provided the desired limonenal in around 95 % yield, yet the activity of the bi- and tridentate system was significantly lower compared with that realized by the assistance of the monodentate ligand. The authors proposed that the catalytic mechanism proceeds according to a mechanism similar to those with 1-hexene as substrate. In this case, the catalytically active species is a hydrido carbonyl complex containing two phosphorus atoms coordinated at the rhodium center in an equatorial fashion.⁸³

1 Introduction

1.1 Hydroformylation

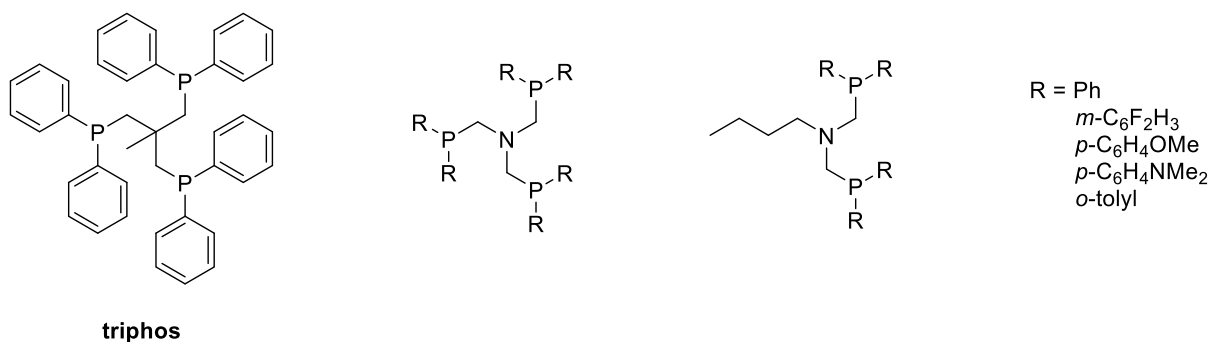


Figure 7: Investigated bi- and triphosphine ligands.

Furthermore, in 2018 the group of Nozaki compared triphos and newly designed nitrogen centered bi- and tridentate ligands in the branched-selective hydroformylation of rather reactive alkenes (1-hexene, allylbenzene, allyl cyanide and 3-butenol) as substrate. They observed significantly higher activities induced by the new ligands compared to triphos. They also noted a divergent reactivity of the bi- and triphosphines at low loading and low pressures. Whereas triphosphines afforded mainly branched aldehydes, the diphosphine did not. However, excellent *b*-selectivity could only be maintained at the expense of low activity.⁸⁴

Another example in this specific field concerns two new tridentate phosphorus structures, which were tested in the hydroformylation of terminal and internal alkenes by Zhang and co-workers. They developed a tridentate analogue to Bisbi (Figure 8) that showed slightly better *l*-selectivity in the hydroformylation of 1-octene, 1-hexene and 2-octene compared to the parent ligand.⁸⁵ Moreover, a butene mixture was oxygenated with high *l*-selectivities of up to 96.8 % and turn over frequencies. The newly synthesized Tribi also induced higher *l*-selectivity in the hydroformylation of 1-octene than the monodentate triphenylphosphine. Moreover, a triphosphoramidite ligand was synthesized which exhibited excellent *l*-selectivities (up to 99.8 %) in the hydroformylation of 1-octene and 1-hexene and also very high regioselectivities in the isomerization/hydroformylation of 2-octene (98 %).⁸⁶ This result is similar to that obtained with the tetradentate analogue and superior to that of the bidentate analogue. Additionally, catalysts of the triphosphoramidite exhibited good regioselectivities in the hydroformylation of styrene.

1 Introduction

1.2 Hydrolysis of phosphites

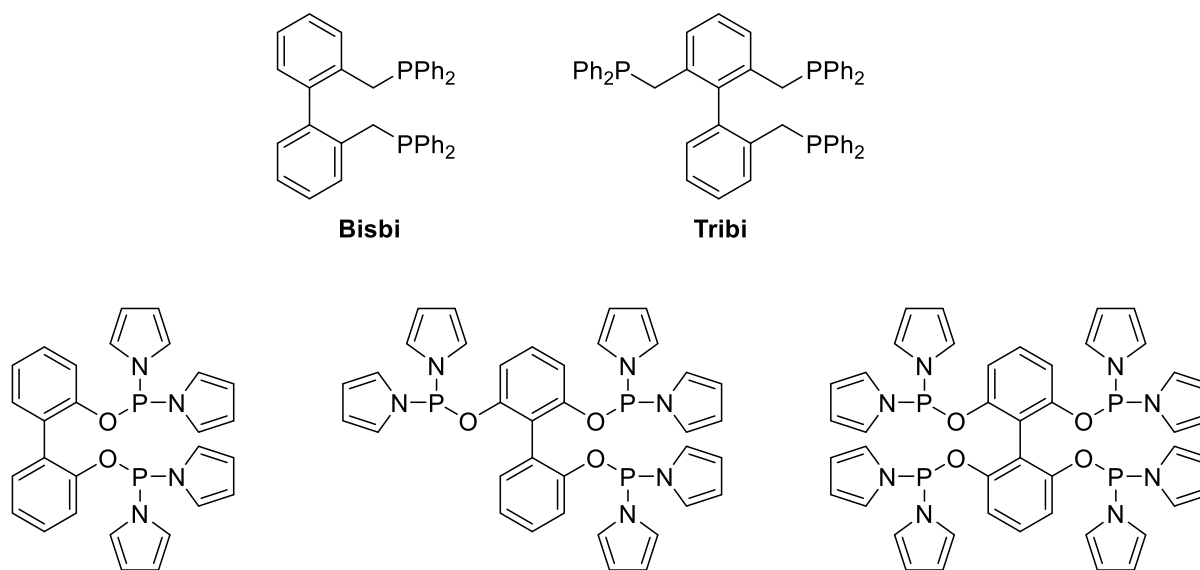


Figure 8: Structures of Bisbi, Tribi and selected phosphoramidites.

1.2 Hydrolysis of phosphites

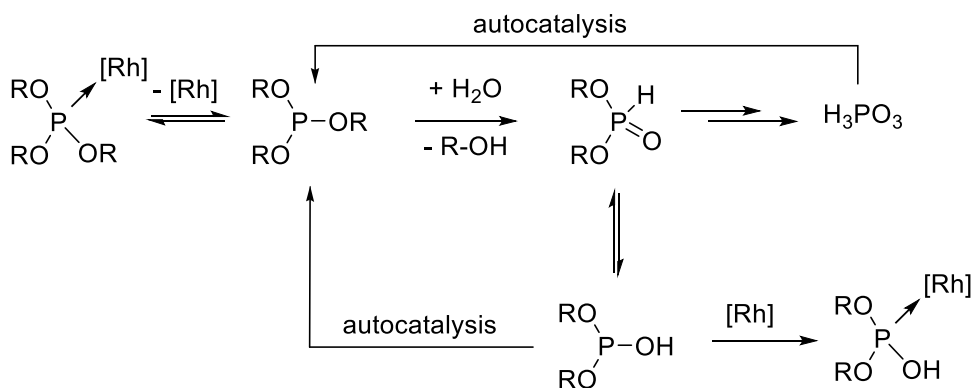
A catalyst is a chemical compound that increases the rate of a reaction by providing an alternative reaction pathway with lower activation energy compared to the non-catalyzed mechanism without being consumed. Therefore, it is assumed, in theory, that it is fully regenerated after each catalytic cycle and can continue to act repeatedly. Because of this virtue, in general only very small amounts of catalyst are required. However, in practice, the catalyst is always subjected to alterations, for example, due to degradation reaction with the components present in the catalytic system (e.g. starting products, (side)products, solvents and impurities), which in turn results in a decrease in the concentration of the catalyst. This may consequently affect activity and/or selectivity.⁸⁷ Especially organic ligands, which are used in homogeneous catalysis and form the catalytically active species together with a metal, are prone to those alterations.

Whereas phosphines are susceptible to oxidation and P-C bond activation, phosphites and similar P-O bond-containing compounds are mostly instable towards hydrolysis.^{7,87,88} Due to the reaction with water, pentavalent species are formed which cannot coordinate to the metal center because they lack a free electron pair. As a result, unmodified metal carbonyl complexes emerge, which are less active, selective, and, in the worst case, cause a loss of the precious metal by formation of catalytically inactive clusters, followed by metal deposition.⁸⁸ However, since the pentavalent form of the phosphoric acid diester is in tautomeric equilibrium with a trivalent form, coordination of the degradation products to the metal center is possible (Scheme 14). When all aryloxy or alkoxy groups are gradually substituted, phosphorous acid remains as the final product.

1 Introduction

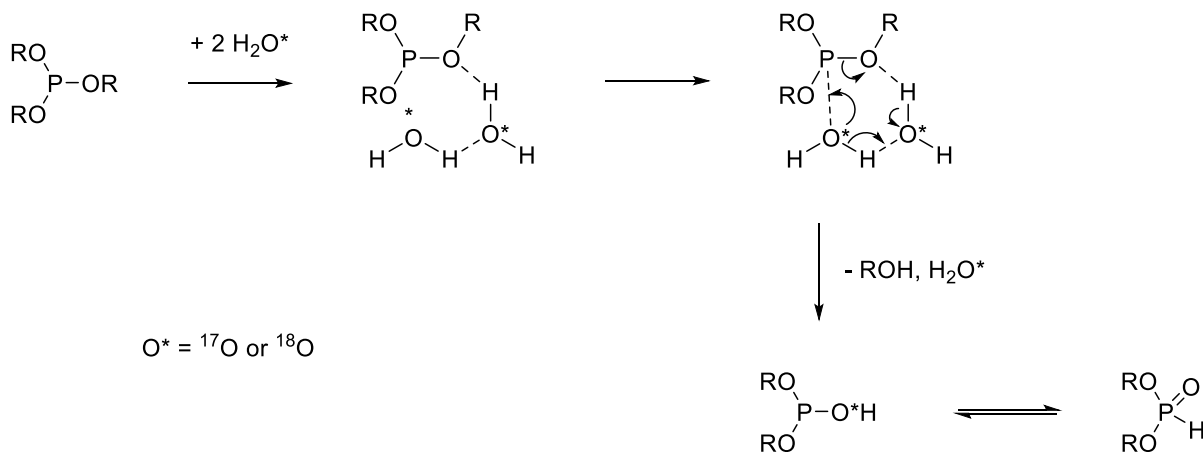
1.2 Hydrolysis of phosphites

The acid will then catalyze with acidic organic phosphorus intermediates (phosphoric acid esters) the hydrolysis and lead to the autocatalyzed decomposition of the ligand.⁸⁹



Scheme 14: Degradation of phosphites by (autocatalytic) hydrolysis.

The exact hydrolysis mechanism was investigated by utilization of NMR experiments with ¹⁷O- and ¹⁸O-labeled water. The results provided evidence that a P-O- and not a C-O-bond is cleaved, as the alcohol that was released from the reaction did not contain the labeled oxygen.⁸⁹



Scheme 15: Mechanism of the hydrolysis of phosphites.

The hydrolytic stability of phosphites is an important issue in industrial processes, because water will inevitably be formed during hydroformylation as a byproduct of the aldol condensation of the product aldehydes. Therefore, the study of their behavior towards water is crucial for the design of new ligands, as well as for adjusting proper reaction conditions. Of course, measures against hydrolysis should not affect the catalytic properties of the ligand. In the literature, some phosphites are described which combine all the desired properties. Prominent examples are the

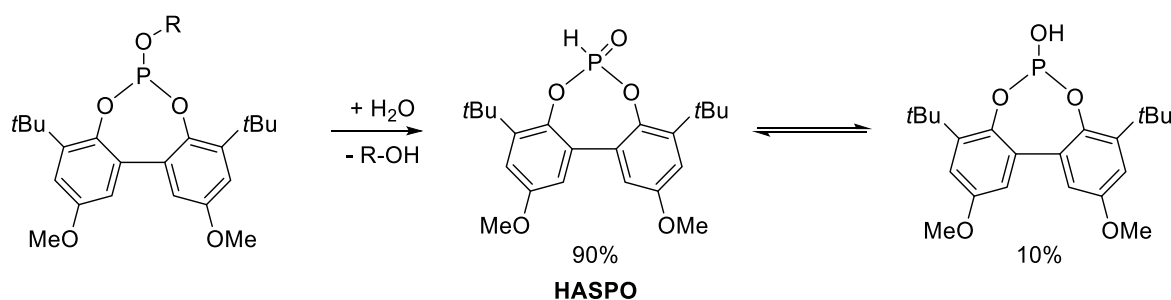
1 Introduction

1.2 Hydrolysis of phosphites

phosphites Alkanox® and BIPHEPHOS, both of which were already mentioned in chapter 1.1.3. These two phosphites are decorated with several *tert*-butyl groups. Due to the large number of different substituents, the unique effect of a single group on stability and catalytic properties does not become clear. Therefore, especially dedicated studies are highly requested.

To date, only a very limited number of investigations concerning the hydrolysis of phosphites have been reported in the literature. One remarkable study was reported by van Leeuwen and co-workers several years ago, where they utilized a simple heteroatom-substituted phosphine oxide (HP(O)Ph₂), often referred to as a HASPO, in platinum-catalyzed hydroformylation. The results suggested that the catalytic impact of such degradation products should not be underestimated.⁹⁰

In a previous study from the group of Börner it was also reported that *O,O'*-3,3'-di-*tert*-butyl-5,5'-dimethoxy-1,1'-biphenyl-2,2'-diylphosphonate, which is a hydrolysis product of several industrially used mono- and bidentate ligands, can coordinate to rhodium(I) in its trivalent form (Scheme 16).^{88,91,92} Several mono- and di-nuclear rhodium complexes were formed. These catalysts modified by HASPO exhibited increased activity and *n*-regioselectivity in the hydroformylation of 1-octene and *n*-octenes compared to the unmodified ("naked") rhodium. Additionally, five secondary aryl-substituted phosphine oxides with different steric and electronic properties were synthesized and their coordination behavior investigated.⁹¹ Furthermore, their performance in the hydroformylation of cyclohexene and 1-octene was investigated, proving that they form active hydroformylation catalysts.⁹²



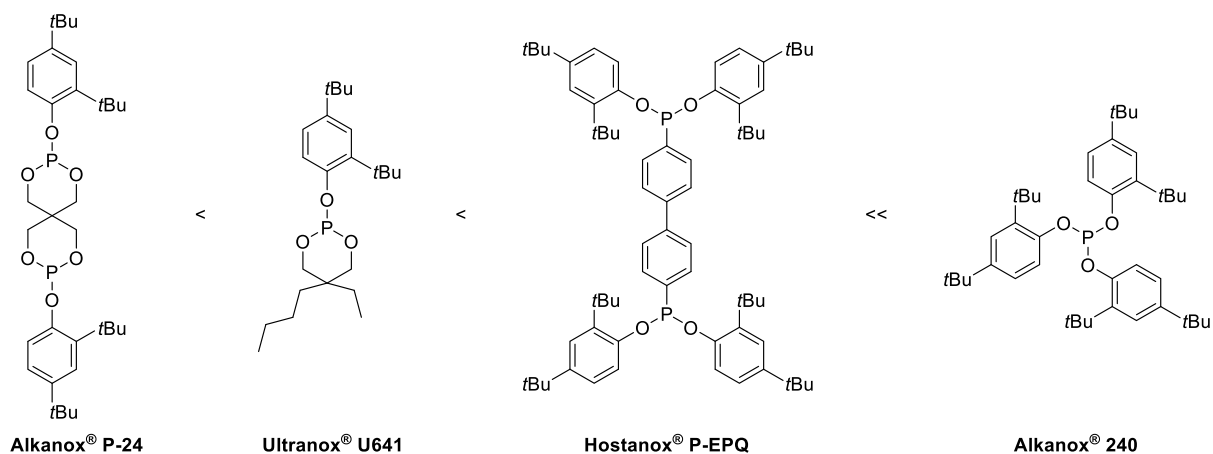
Scheme 16: Degradation of *O,O'*-3,3'-di-*tert*-butyl-5,5'-dimethoxy-1,1'-biphenyl-2,2'-diylphosphonate and its tautomeric equilibrium between pentavalent and trivalent structure.

Studies addressing the stabilizing and destabilizing effects of substituents on the stability of phosphites are even rarer. Since very different analytic methods and reaction conditions have been applied, the comparison of results reported in the literature is almost impossible. For example, the hydrolysis stability of several bulky phosphites bearing *tert*-butyl groups (e.g. Alkanox® P-24, Ultrinox® U641, Sandostab P-EPQ (now Hostonox® P-EPQ®) and Alkanox® 240), which are used in polymer chemistry as antioxidants, was investigated by the research group of

1 Introduction

1.2 Hydrolysis of phosphites

Edge.⁹³ In this case the hydrolysis rates were measured at 60 °C in a saturated NaCl solution. Alkanox® P-24 was fully hydrolyzed after 7 h, Ultranox® U641 after 18 h, Sandostab P-EPQ (now Hostanox® P-EPQ) after 90 h, and Alkanox® 240 showed no sign of hydrolysis after 400 h (Scheme 17).

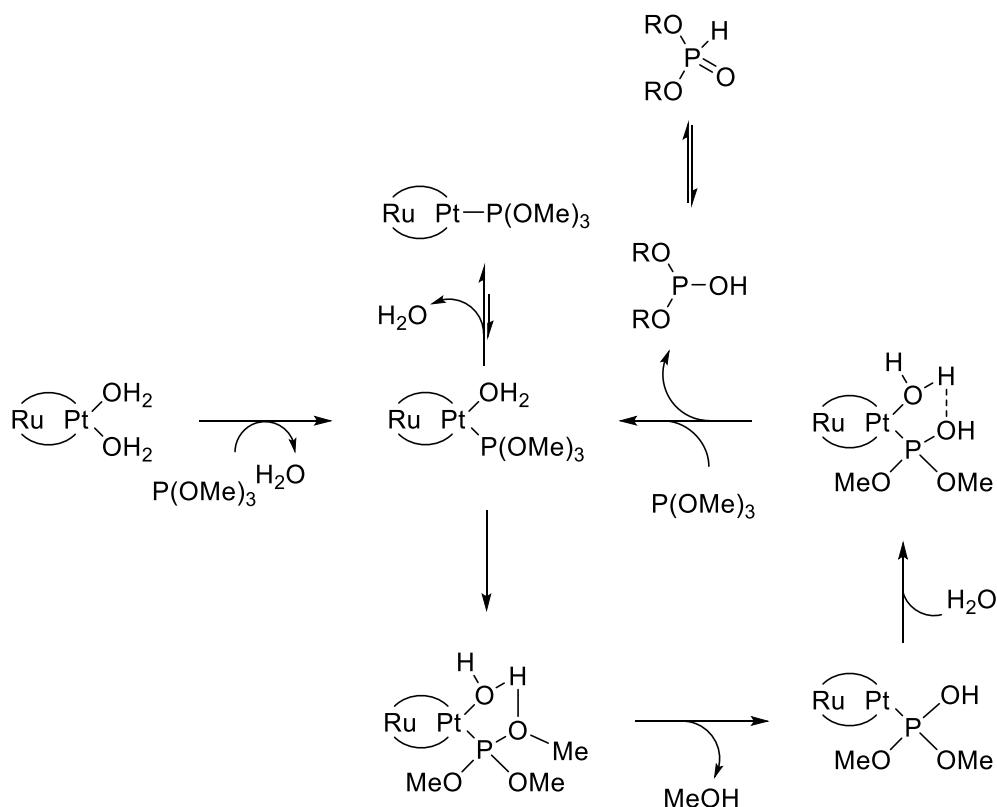


Scheme 17: Hydrolysis stability of bulky phosphites.

Recently, Oberhauser and Manca reported on the catalytic hydrolysis of aromatic and aliphatic tertiary phosphites by cationic phosphametalocene-based platinum(II) aqua complexes under neutral reaction conditions.⁹⁴ Evidence was given that the selective cleavage of a P-O bond occurs in the coordination sphere of the platinum(II) due to the transfer of a water molecule to the phosphite (Scheme 18). The results also showed a clear difference in the reaction rate of the hydrolysis between aromatic and aliphatic phosphites, with the aromatic structures exhibiting a significantly slower decomposition rate.

1 Introduction

1.2 Hydrolysis of phosphites



Scheme 18: Proposed catalytic cycle for the phosphite hydrolysis reaction in the coordination sphere of platinum(II).

In 2016, again the group of Börner studied the hydrolysis of a nonsymmetric bidentate phosphite and its both monophosphite constituents, respectively (Figure 9).⁹⁵ The concerned nonsymmetric bidentate ligand was characterized by a biphenolphosphite and an acylphosphite moiety. In this study, the biphenolphosphite unit was proven to be of a magnitude more stable towards the hydrolysis than the acylphosphite unit, which decomposed rapidly to salicylic acid and phosphorous acid.

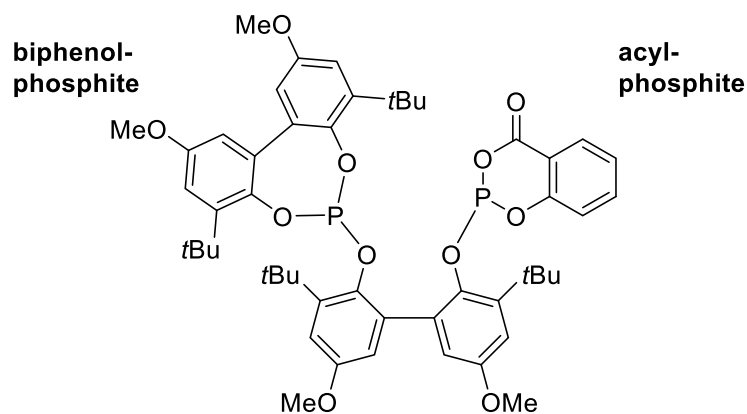


Figure 9: Structure of the investigated nonsymmetric bisphosphite.

1 Introduction

1.2 Hydrolysis of phosphites

In addition, the influence of different substituents on the acylphosphite moiety on the hydrolytic stability was elucidated using *in situ* NMR spectroscopical methods. In principle, organic substituents with electron donating or accepting properties alter the Lewis-basicity of phosphorus and oxygen. The rate of hydrolysis can also be controlled by introduction of sterically demanding bulky substituents which cause kinetic inhibition. Noteworthy, bulky and electron donating groups (e.g. *tert*-butyl or methoxy) improve the stability, whereas electron withdrawing substituents, such as chlorine, have a destabilizing effect (Figure 10).

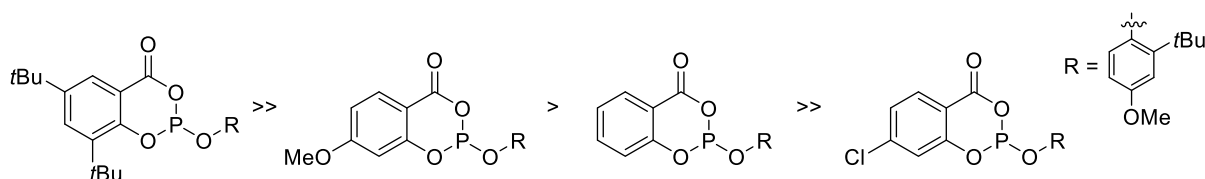
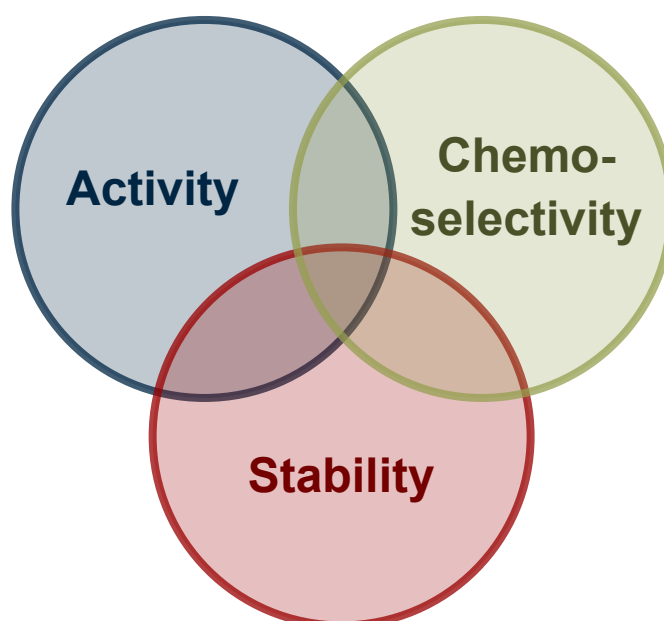


Figure 10: Effect of substituents on the hydrolysis stability of an acylphosphite.

2 Aim of investigations

Even after over 80 years of scientific research in the field of hydroformylation, the reliance of properties, such as activity, chemoselectivity and stability, on the structure of the catalyst is not yet sufficiently understood. To further elucidate this topic, the influences of different substitution patterns and denticity of organic ligands on the hydroformylation properties of the resulting catalysts were investigated in order to correlate these features with the overall performance in catalytic reactions.



We hypothesized that different substituents on phosphorus directly or in more distant positions can significantly influence hydroformylation properties and stability. In addition, the use of several coordinating groups could probably also have a major impact on the aforementioned properties.

Therefore, to better understand these influences, the following tasks have been dealt with in the context of this thesis: Several potentially mono- and bidentate phosphites with different substitution patterns should be synthesized. Unsubstituted biphenolphosphite and benzopinacolphosphite were chosen because they exhibited superior catalysis properties in previous investigations.⁹⁶⁻⁹⁸ The influence of various substituents on the hydroformylation performance and hydrolysis stability should be investigated independently from other structural alterations. Furthermore, several PNP-pincer ligands with different substituents on the phosphine

2 Aim of investigations

moieties should be synthesized and subsequently tested concerning their catalytic properties. Also, a potentially tridentate sterically hindered phosphine should be tested in the catalytic reaction using supplementary the statistical tool of Factorial Design to optimize the yield and regioselectivity of the reaction.

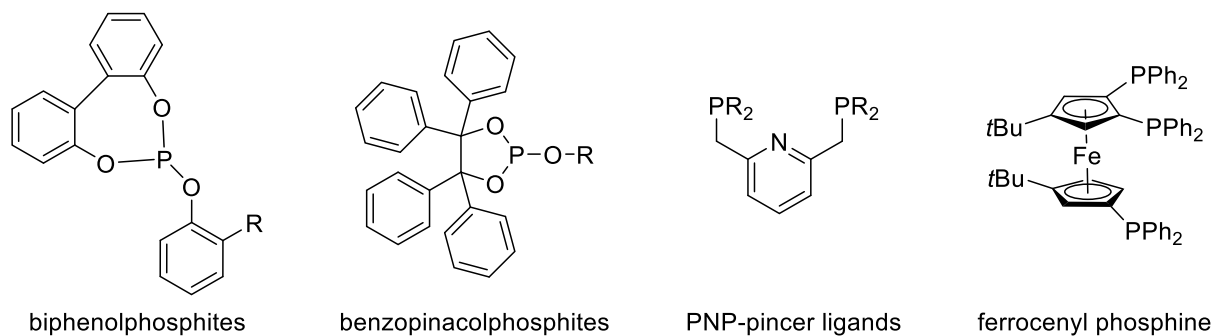


Figure 11: Investigated structures.

3 Results and discussion

3.1 Investigations of substituent effects of mono- and bidentate phosphites on hydroformylation performance and hydrolysis stability

3 Results and discussion

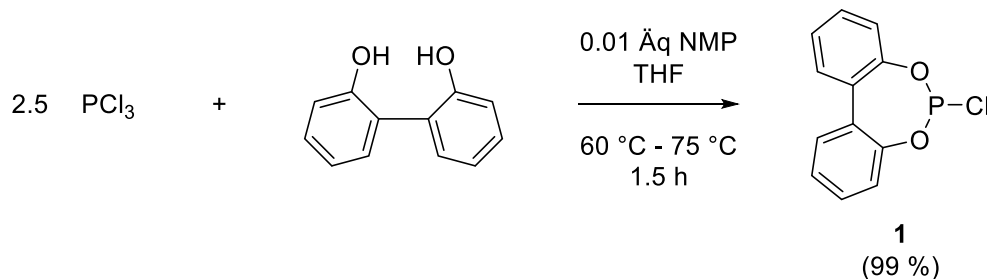
3.1 Investigations of substituent effects of mono- and bidentate phosphites on hydroformylation performance and hydrolysis stability

3.1.1 Biphenolphosphites

3.1.1.1 Synthesis

To investigate the influence of different substitution patterns on mono- and bidentate phosphites seven ligands with biphenol moiety were synthesized, containing substituents in *ortho*- and *meta*-position to the aryl phosphite group. Moreover, the influence of a free hydroxyl groups and varying OH-protection groups were examined.

First biphenolphosphorchloridite **1**, as chemical building block for the synthesis of the phosphites, was synthesized adapting a synthesis procedure developed in our research group.⁹⁹ For this 2,2'-biphenol was treated with an excess of phosphorus trichloride in the presence of *N*-methyl-2-pyrrolidone (NMP) at 60 °C (Scheme 19).

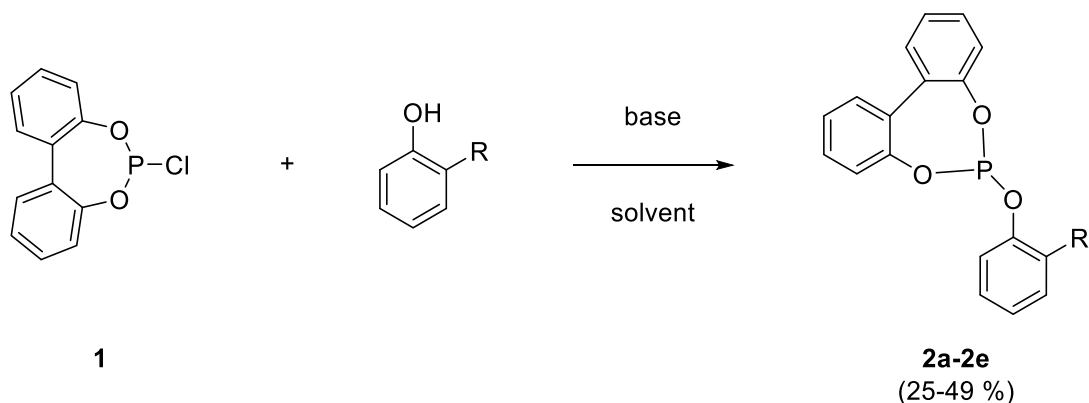


Scheme 19: Synthesis of a biphenolphosphorchloridite.

As reference, to study the impact of the different substituents, the simple and completely unsubstituted biphenolphosphite **2a** was synthesized from the previously produced 6-chloro-dibenzo[*d,f*][1,3,2]dioxaphosphepine (**1**) and phenol using triethylamine as supporting base. Furthermore, a phosphite using an *ortho*-phenyl substituted phenol was prepared (**2b**). The reaction equation can be found in Scheme 20 and detailed information is gathered in Table 1.

3 Results and discussion

3.1 Investigations of substituent effects of mono- and bidentate phosphites on hydroformylation performance and hydrolysis stability



Scheme 20: General synthesis of biphenolphosphites.

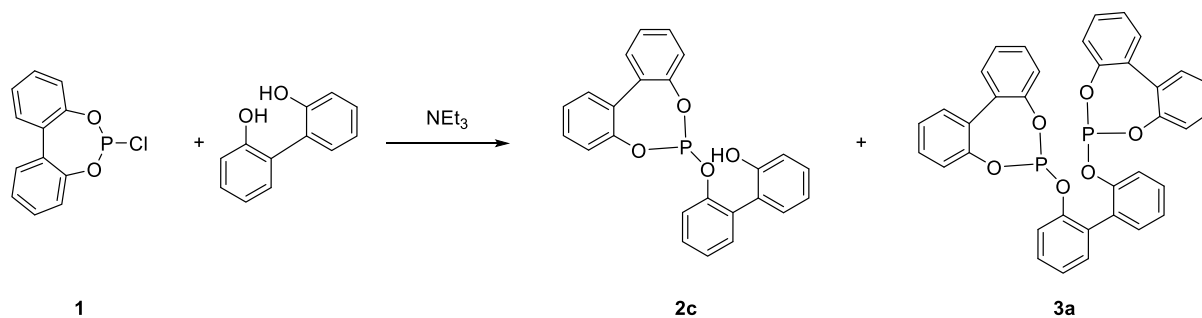
Table 1: Reaction conditions and yields of monophosphites synthesized.

| Phosphite | -R | Base | Solvent | Temperature [°C] | Yield [%] |
|-----------|----|------------------|---------|------------------|-----------|
| 2a | -H | NEt ₃ | toluene | -20 | 26 |
| 2b | | NEt ₃ | THF | -20 | 49 |
| 2c | | <i>n</i> -BuLi | THF | -30 | 38 |
| 2d | | NEt ₃ | toluene | -20 | 41 |
| 2e | | NEt ₃ | THF | -20 | 25 |

Furthermore, phosphite **2c** bearing a free hydroxyl group was assembled. As starting product again 2,2'-biphenol was used. In this case triethylamine did not prove to be a suitable base. The reaction of 6-chloro-dibenzo[*d,f*][1,3,2]dioxaphosphine and one equivalent 2,2'-biphenol led to a mixture of phosphorus containing compounds with the symmetric bisphosphite **3a** as main product (Scheme 21). Only the selective deprotonation of one hydroxyl group of 2,2'-biphenol with *n*-BuLi and the resulting formation of the corresponding lithium salt with subsequent addition of the phosphorchloridite **1** led to significant production of the desired monophosphite **2c**.

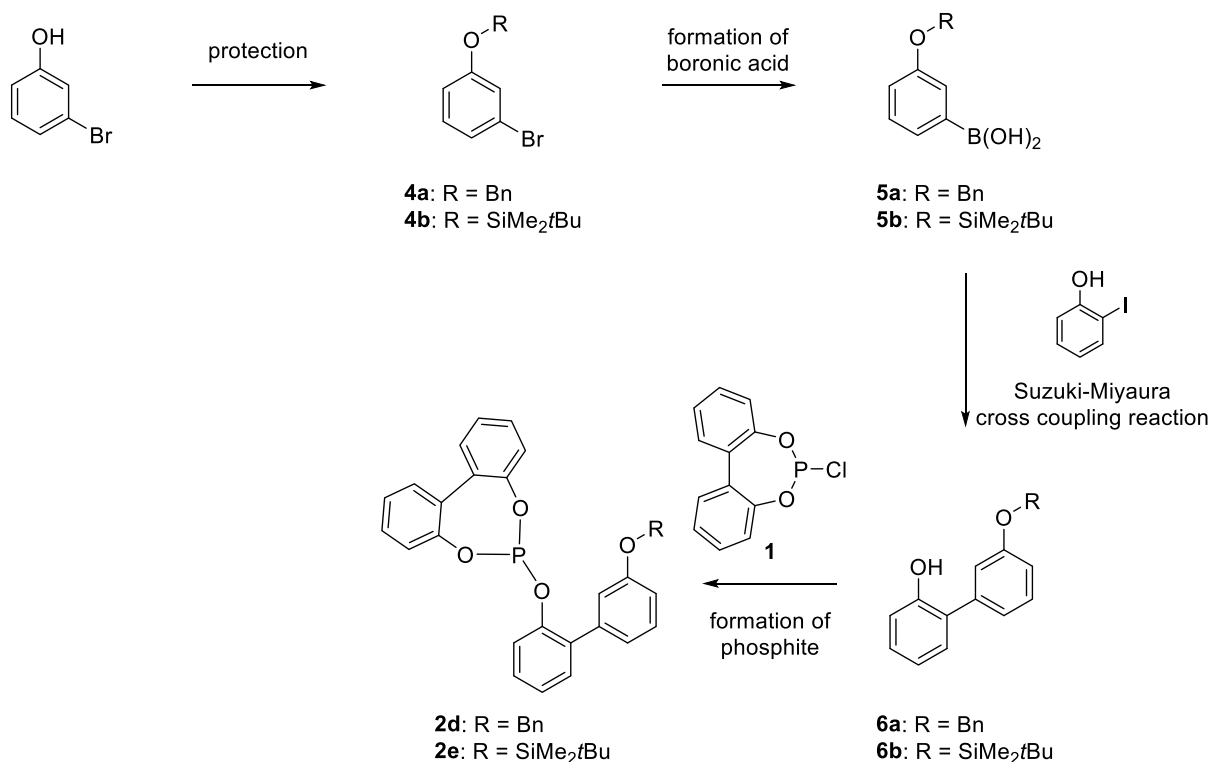
3 Results and discussion

3.1 Investigations of substituent effects of mono- and bidentate phosphites on hydroformylation performance and hydrolysis stability



Scheme 21: Synthesis of **2c** in the presence of triethylamine.

To receive two monophosphites with differently protected hydroxyl groups several reaction steps were necessary to obtain the sophisticated nonsymmetric biphenol building block which are further described in Scheme 22. In the first step, the free hydroxyl group of the bromophenol was protected. According to the literature two protocols for the synthesis of the building blocks **4a**¹⁰⁰ and **4b**¹⁰¹ were applied. For the following step, the conversion of bromine into a boronic acid moiety, literature procedures were adapted as well to synthesize **5a** and **5b**.^{102,103}



Scheme 22: Reaction scheme for the synthesis of the hydroxyl protected phosphites **2d** and **2e**.

3 Results and discussion

3.1 Investigations of substituent effects of mono- and bidentate phosphites on hydroformylation performance and hydrolysis stability

The *O*-protected biphenols **6a** and **6b**, which are required as building blocks for the final phosphite were synthesized by the Suzuki–Miyaura cross coupling reaction. The reaction conditions were taken from a literature procedure for the coupling of two phenols to symmetric and nonsymmetric biphenols.¹⁰⁴ Table 2 depicts the optimization protocol for both compounds. For the benzyl protected biphenol **6a** the reaction conditions of entry 2 were chosen due to time efficiency. In case of the *O*-*tert*-butyldimethylsilyl protected compound **6b** the reaction conditions of entry 7 afforded the best yield with 69 %.

Table 2: Optimization of Suzuki–Miyaura coupling reactions for the synthesis of the protected biphenols **6a** and **6b**.

| Entry | Protecting group | Pd/C [mol%] | Solvent | Temperature [°C] | Time [h] | Yield [%] |
|-------|-----------------------|-------------|------------------|------------------|----------|-----------|
| 1 | Bn | 2 | H ₂ O | 80 | 48 | 13 |
| 2 | Bn | 5 | H ₂ O | 100 | 48 | 54 |
| 3 | Bn | 5 | H ₂ O | 100 | 24 | 53 |
| 4 | SiMe ₂ tBu | 5 | H ₂ O | 70 | 18 | 49 |
| 5 | SiMe ₂ tBu | 5 | isopropanol | 70 | 18 | 48 |
| 6 | SiMe ₂ tBu | 5 | acetonitrile | 70 | 18 | 0 |
| 7 | SiMe ₂ tBu | 5 | 1,4-dioxane | 70 | 18 | 69 |
| 8 | SiMe ₂ tBu | 5 | H ₂ O | 90 | 18 | 25 |
| 9 | SiMe ₂ tBu | 5 | 1,4-dioxane | 90 | 18 | 10 |

Afterwards the free hydroxyl group was coupled with the biphenolphosphorchloridite **1**, as already described, to form the final phosphites **2d** and **2e** in moderate yields (Table 1).

Moreover, the two bidentate phosphites **3a** and **3b** with biphenol moiety, which were already synthesized in previous studies,¹⁰⁵ were resynthesized for the purpose of this thesis (Figure 12). Compound **3a** is an analogue to BIPHEPHOS, which was already mentioned in the previous chapters 1.1.3, 1.1.4 and 1.2. This compound possesses a symmetric 2,2'-biphenol in the backbone which links two phosphite moieties. In contrast, **3b** consists of a nonsymmetric 2,3'-biphenol backbone, which was generated by Suzuki–Miyaura cross coupling.¹⁰⁴

3 Results and discussion

3.1 Investigations of substituent effects of mono- and bidentate phosphites on hydroformylation performance and hydrolysis stability

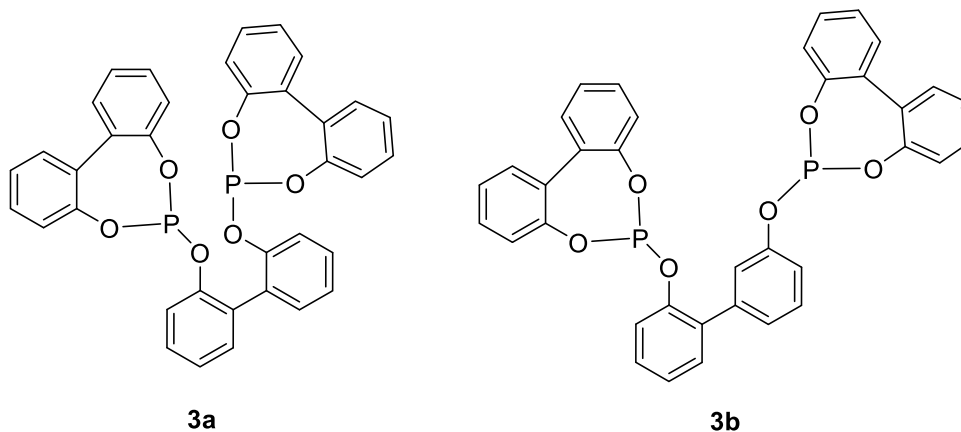


Figure 12: Structures of the bidentate phosphites 3a and 3b.

3.1.1.2 Hydroformylation experiments

Afterwards, all new ligands were tested in the rhodium-catalyzed hydroformylation and evaluated individually in hydrolysis experiments. To investigate the activity and *n*-selectivity of the monodentate and bidentate biphenolphosphites, hydroformylation experiments were performed using *n*-octenes — a technical relevant mixture of isomeric octenes — as a model substrate. The hydroformylation experiments were performed in a 16 ml stainless steel autoclave manufactured by HEL Group (Figure 13).

3 Results and discussion

3.1 Investigations of substituent effects of mono- and bidentate phosphites on hydroformylation performance and hydrolysis stability



Figure 13: The 16 ml autoclave manufactured by HEL Group.

The highest yields of aldehydes with over 90 % were achieved with rhodium complexes of ligands **2a**, **2c**, **2d** and **3a** whereas the complexes bearing the bidentate BIPHEPHOS analogue **3a** showed the best yield with 95 %. Interestingly **3a** induced under the same reaction conditions also a good *n*-selectivity with 48.0 % (Table 3, entry 16). Higher *n*-selectivities were accompanied by significantly lower activities. It is worth mentioning that **3a** gave these high activity and *n*-selectivity at a relatively low P/Rh ratio. When a higher P/Rh ratio was applied, the aldehyde yield dropped significantly. All catalysts of new monodentate phosphite ligands led to similar activities and *n*-selectivities. Among the catalysts with monodentate phosphites only a rhodium complex based on **2e**, containing an *O*-*tert*-butyldimethylsilyl group, did not show any hydroformylation activity at all. This phosphite even seems to have an inhibiting effect. Moreover, the potentially bidentate ligand **3b**, gave lower aldehyde yields than all other phosphites except for **2e**. Also, in this case, similar to the hydroformylation with **3a**, the highest activity was again achieved at relatively low P/Rh ratio. Experiments with higher P/Rh ratio showed lower yields but high *n*-selectivities.

3 Results and discussion

3.1 Investigations of substituent effects of mono- and bidentate phosphites on hydroformylation performance and hydrolysis stability

Table 3: Hydroformylation^a of *n*-octenes^b with biphenolphosphites.

| Entry | Ligand | P/Rh | Yield of Aldehydes ^c [%] | <i>n</i> -Selectivity ^c [%] |
|-------|-----------|------|--|--|
| 1 | 2a | 2 | 88 | 31.0 |
| 2 | | 4 | 93 | 29.5 |
| 3 | | 8 | 93 | 20.3 |
| 4 | 2b | 2 | 88 | 33.2 |
| 5 | | 4 | 85 | 28.9 |
| 6 | | 8 | 52 | 29.6 |
| 7 | 2c | 2 | 87 | 44.0 |
| 8 | | 4 | 89 | 43.0 |
| 9 | | 8 | 92 | 37.8 |
| 10 | 2d | 2 | 93 | 32.2 |
| 11 | | 4 | 89 | 32.4 |
| 12 | | 8 | 75 | 28.9 |
| 13 | 2e | 2 | 0 | - |
| 14 | | 4 | 1 | - |
| 15 | | 8 | 0 | - |
| 16 | 3a | 2 | 95 | 48.0 |
| 17 | | 4 | 65 | 38.9 |
| 18 | | 8 | 5 | 68.3 |
| 19 | 3b | 2 | 35 | 43.4 |
| 20 | | 4 | 6 | 61.6 |
| 21 | | 8 | 3 | 78.3 |

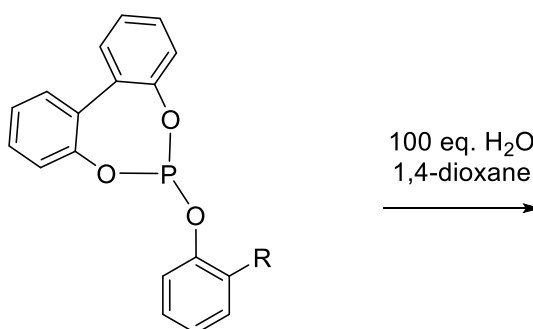
^a[Rh] = 1.0×10⁻³ mol·L⁻¹; T = 120 °C; *p* = 20 bar; *t* = 4 h; solvent: toluene; S/Rh = 2000. ^b3.3% 1-octene, 48.4% *Z/E*-2-octene, 29.2% *Z/E*-3-octene, 16.4% *Z/E*-4-octene, 2.1% skeletal C8-olefinic isomers, 0.6% *n*-octane. ^cDetermined by GC with toluene as internal standard.

3 Results and discussion

3.1 Investigations of substituent effects of mono- and bidentate phosphites on hydroformylation performance and hydrolysis stability

3.1.1.3 Hydrolysis experiments

To test the synthesized phosphites towards their stability against water, a definite amount of phosphite was dissolved in 1,4-dioxane to gain a 0.049 M solution. Afterwards 100 equivalents of deoxygenized water were added. The general protocol is shown in Scheme 23.



Scheme 23: Hydrolysis conditions for biphenolphosphites.

The use of a high excess of 100 equivalents of water opens up the possibility of applying pseudo-first-order kinetics to determine the reaction constant and half-life of the reaction. A pseudo-first-order can be assumed when one reagent is present in large excess and therefore stays approximately at a constant concentration during the reaction. The kinetic can be described by equation (1).

$$-\frac{d[A]}{dt} = k \cdot [A] \quad (1)$$

If the concentrations of starting product A or of a final product are plotted against time t , an exponential curve results. A logarithmic plot, on the other hand, provides a linear correlation for the decrease of the concentration of the starting compound. The exemplary plots of **3a** are shown in Figure 14.

3 Results and discussion

3.1 Investigations of substituent effects of mono- and bidentate phosphites on hydroformylation performance and hydrolysis stability

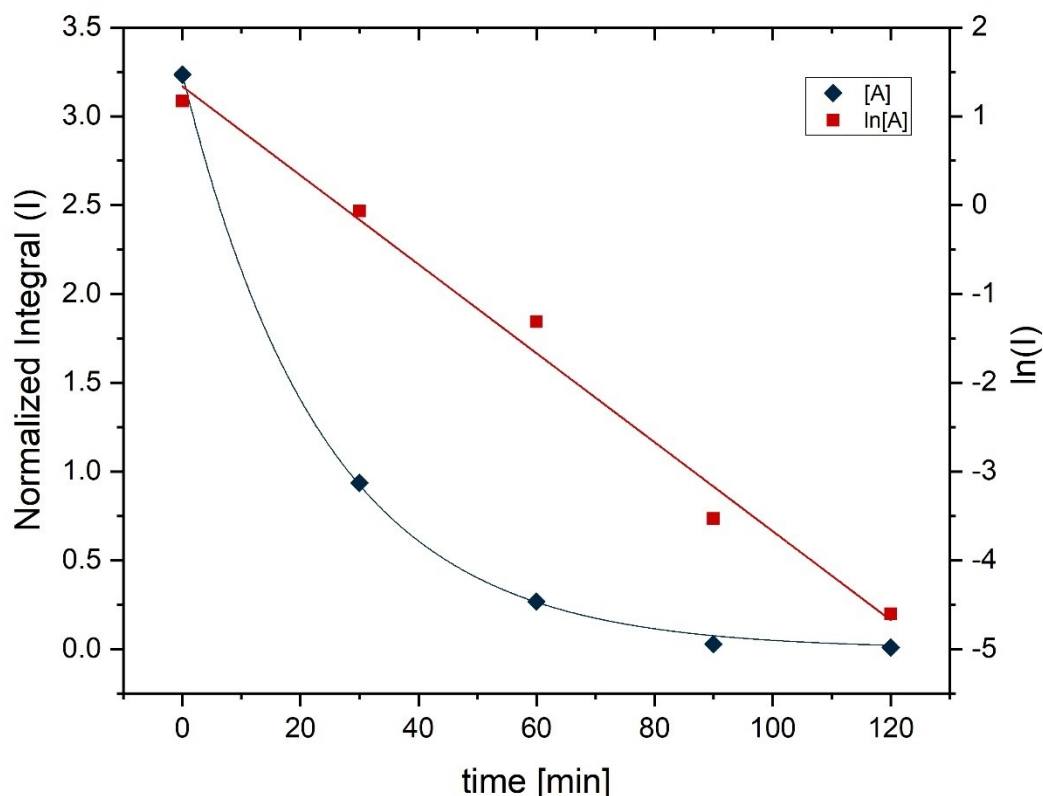


Figure 14: Direct and logarithmized plots of the concentration profile of 3a during hydrolysis. Conditions: $[L] = 0.049 \text{ mol}\cdot\text{L}^{-1}$; $\text{H}_2\text{O}/L = 100$; $T = 90 \text{ }^\circ\text{C}$; solvent: 1,4-dioxane.

To determine the half-life of the phosphites, the rate constant k_{obs} is needed, which can be derived from the equations of the plotted concentration profiles. The half-life of a pseudo-first-order reaction can be calculated using equation (2).

$$t_{1/2} = \frac{\ln(2)}{k} \quad (2)$$

The half-life could not be obtained for all decomposition experiments as some phosphites decomposed too quickly, whereby not sufficient data points existed to determine the rate constant. Moreover, other phosphites did not decompose at all, and some experimental data did not show the behavior of first-order reactions. Therefore, besides the half-life, the complete decomposition time of the phosphites was also determined.

3 Results and discussion

3.1 Investigations of substituent effects of mono- and bidentate phosphites on hydroformylation performance and hydrolysis stability

The hydrolysis of the phosphites was studied at room temperature to obtain sufficient differentiation (Table 4) and at 90 °C to simulate common conditions for hydroformylation reactions (Table 5). The hydrolysis of biphenolphosphites showed very divergent results. The lowest hydrolysis stability was noted for **2c** and **2d**. Both decomposed in less than eight hours at room temperature which is why not enough data points for the determination of the rate constant could be measured (Table 4, entries 3 and 5). The highest stability was observed for **2e** and **3b**. Both showed half-life times of over 1200 hours at room temperature and over 10 hours at 90 °C (Table 4 and Table 5, both entries 5 and 7).

Table 4: Hydrolysis^a of biphenolphosphites at room temperature.

| Entry | Ligand | k_{obs}^b [10^{-4} min^{-1}] | $t_{1/2}^b$ [h] | Complete Decomposition ^c [h] |
|-------|-----------|---|-----------------|---|
| 1 | 2a | 0.435 | 265.7 | 2140 |
| 2 | 2b | 0.423 | 273.2 | 1858 |
| 3 | 2c | - | - | 8 |
| 4 | 2d | - | - | 4 |
| 5 | 2e | 0.096 | 1203.5 | 2985 |
| 6 | 3a | 0.988 | 116.9 | - |
| 7 | 3b | 0.088 | 1309.8 | - |

^a[L] = 0.049 mol·L⁻¹; H₂O/L = 100; T = room temperature; solvent: 1,4-dioxane. ^bDetermined by quantitative ³¹P NMR based on pseudo-first-order rate constant, derived from exponential curve fitting of decomposition versus time. ^cDetermined by ³¹P NMR.

3 Results and discussion

3.1 Investigations of substituent effects of mono- and bidentate phosphites on hydroformylation performance and hydrolysis stability

Table 5: Hydrolysis^a of biphenolphosphites at 90 °C.

| Entry | Ligand | k_{obs}^b [10^{-3} min^{-1}] | $t_{1/2}^b$ [h] | Complete Decomposition ^c [h] |
|-------|-----------|---|-------------------|---|
| 1 | 2a | 0.697 ^d | 16.6 ^d | 7.0 |
| 2 | 2b | 7.156 | 1.6 | 8.0 |
| 3 | 2c | - | - | 0.0 |
| 5 | 2d | - | - | 0.0 |
| 6 | 2e | 0.633 ^d | 18.2 ^d | 11.5 |
| 4 | 3a | 3070.000 | 0.0 | 2.0 |
| 7 | 3b | 64.200 | 0.2 | 10.5 |

^a[L] = 0.049 mol·L⁻¹; H₂O/L = 100; T = 90 °C; solvent: 1,4-dioxane. ^bDetermined by quantitative ³¹P NMR based on pseudo-first-order rate constant derived from exponential curve fitting of decomposition versus time. ^cDetermined by ³¹P NMR. ^dDetermined for the initial period of hydrolysis without autocatalysis. Onset of autocatalysis for **2a**: 2 h, **2e**: 6.5 h.

At 90 °C the decomposition rates of the phosphites **2a** and **2e** increased at a certain point, which may be rationalized by autocatalysis due to the increasing formation of acidic degradation products. Therefore, the reaction rate constant and half-life were determined only for the initial part of the reaction (2 h for **2a** and 6.5 h for **2e**). Afterwards the decomposition reaction accelerated significantly. The hydrolysis behavior of both phosphites is shown in Figure 15.

3 Results and discussion

3.1 Investigations of substituent effects of mono- and bidentate phosphites on hydroformylation performance and hydrolysis stability

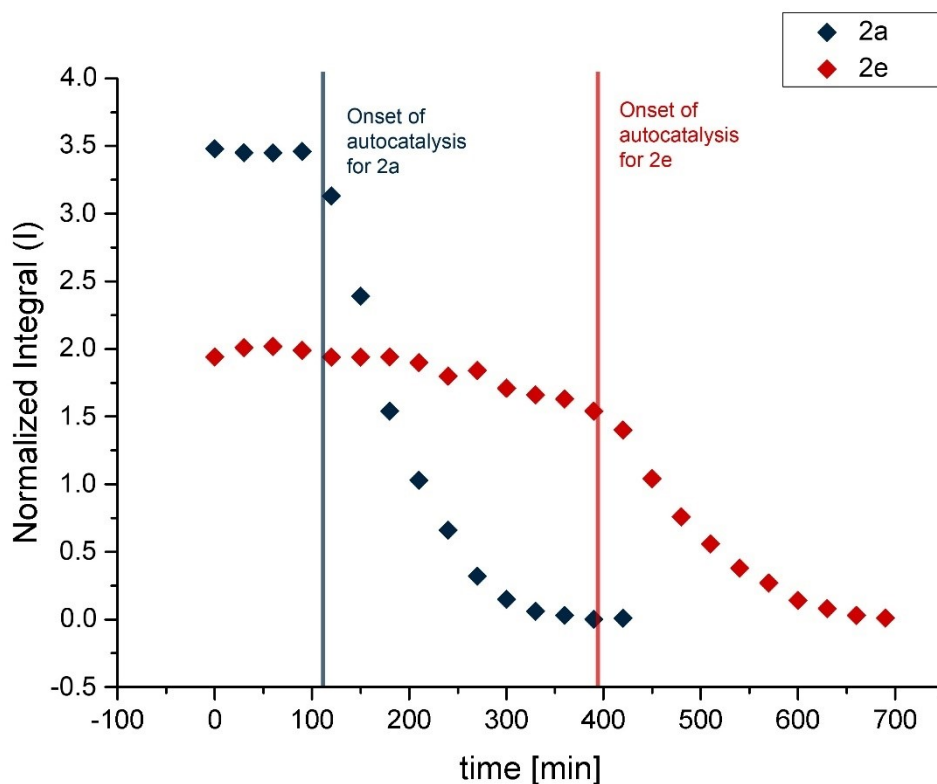


Figure 15: Hydrolysis of 2a and 2e at 90 °C.

3.1.1.4 Conclusion

In conclusion, no clear trend in the hydroformylation properties with respects to the substitution patterns on the aryl phosphite backbone in the application of the newly synthesized biphenolphosphites can be derived. It is worth mentioning that an *O*-silyl group (ligand **2e**), apparently possesses inhibiting properties. This might be explained with a desilylation of the hydroxyl group. This is particularly worth mentioning because phosphites with silyl groups have already been synthesized and tested in hydroformylation in our research group.¹⁰⁶ In these experiments no inhibiting properties were noticed. It should be kept in mind that in the previous study a triisopropylsilyl group (TIPS) was used whereas in this work the slightly more labile *tert*-butyldimethylsilyl group (TBS) was applied. Just for descriptive reasons, it should be mentioned that the TIPS group showed a 22 times slower cleavage rate under acidic conditions and 54 times slower cleavage rate under basic conditions than the *tert*-butyldimethylsilyl group (TBS) for the example of *para*-cresols.¹⁰⁷

3 Results and discussion

3.1 Investigations of substituent effects of mono- and bidentate phosphites on hydroformylation performance and hydrolysis stability

Moreover, catalysts based on phosphites **2a**, **2b**, **2c** and **3a** display similar hydroformylation properties. Only **3a** generated a higher *n*-selectivity. Furthermore, the rhodium complex of **3b** owned poor activity but significantly better *n*-selectivity especially compared to the complexes with monodentate phosphites.

The hydrolysis experiments with biphenolphosphites with different substituents show some interesting tendencies: these can also be seen in Figure 16. The completely unsubstituted phosphite **2a** and the sparsely substituted phosphite **2b** can be considered as a reference for the other substitution patterns of symmetric and nonsymmetric biphenolphosphites.

On the one hand, two structures with rather low hydroformylation activity exhibited the highest stability (**2e** and **3b**). Both possess a nonsymmetric biphenol moiety. On the other hand, structures with hydroxyl group in *ortho*-position of the biphenol backbone are characterized by a very low hydrolysis stability (**2c** and **3a**). Since these structural motifs are very common in ligand design the results are preeminent. Usually, industrially used ligands contain sterically demanding aryl substituents close to the said hydroxyl groups, which may be extremely beneficial for the overall hydrolysis stability.

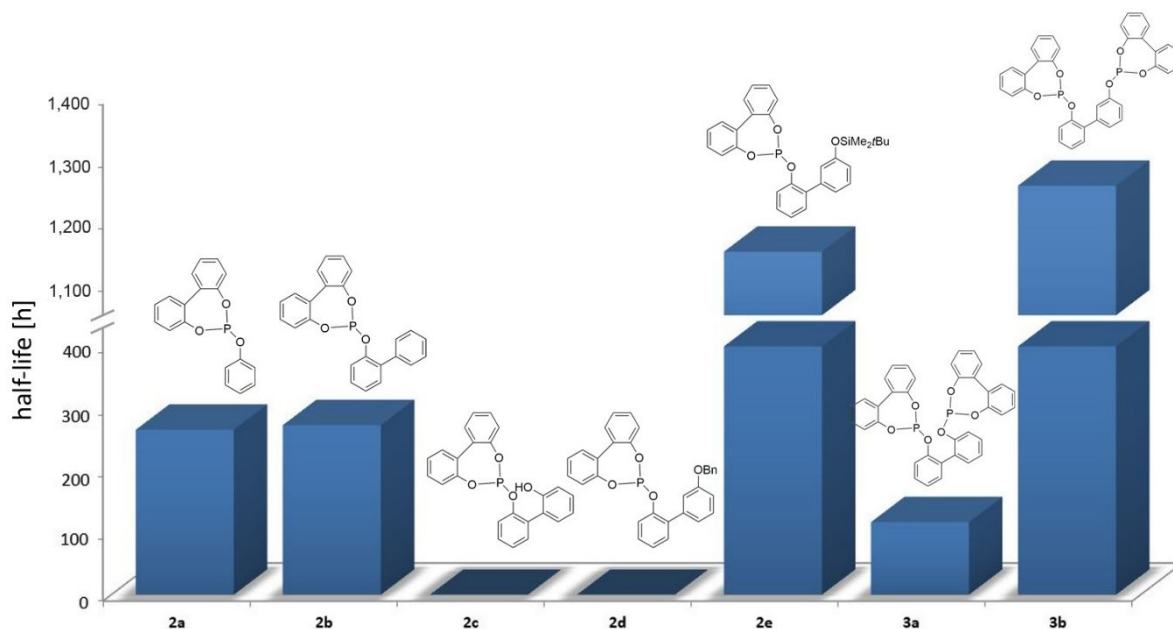


Figure 16: Half-life times of biphenolphosphites at room temperature.

3 Results and discussion

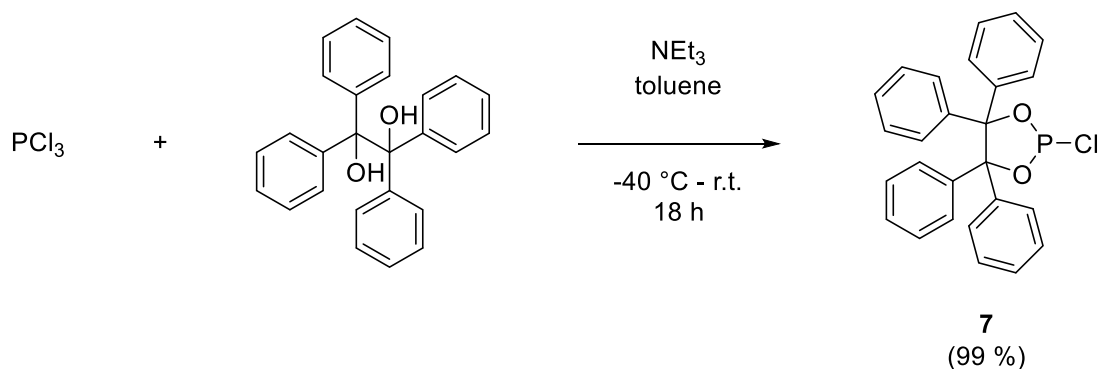
3.1 Investigations of substituent effects of mono- and bidentate phosphites on hydroformylation performance and hydrolysis stability

3.1.2 Benzopinacolphosphites

3.1.2.1 Synthesis

In the context of this study, besides the previously described biphenolphosphites, 12 monodentate benzopinacolphosphites with varying substituents were prepared to investigate the influence of different substituents in *ortho*-, *meta*- and *para*-position on the aryl phosphite group. Precisely the effect of phenyl substituents, condensed ring systems and *tert*-butyl substituents was studied. Several phosphites with benzopinacol structure have already been synthesized and tested in hydroformylation previously.^{96–98,108,109} Some of these synthesis protocols were adapted for this thesis.¹¹⁰

First, the required phosphorchloridite **7** was synthesized by reaction of phosphorus trichloride and benzopinacol in the presence of triethylamine as HCl scavenger (Scheme 24).¹⁰

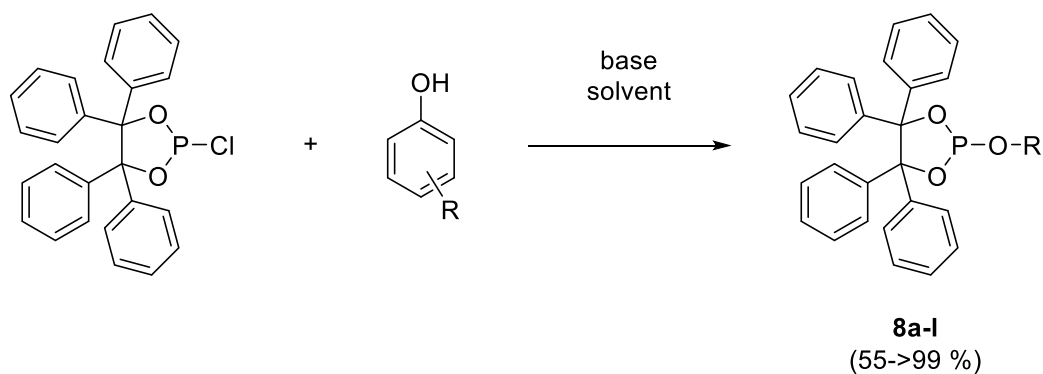


Scheme 24: Synthesis of phosphorchloridite **7** with benzopinacol moiety.

Afterwards the product was treated with the relevant substituted phenol in the presence of triethylamine as supporting base. Alternatively, the phenol was first deprotonated with *n*-BuLi to form the lithium salt, which was subsequently reacted with the phosphorchloridite **7** (Scheme 25). Precise reaction conditions and yields are described in Table 6.

3 Results and discussion

3.1 Investigations of substituent effects of mono- and bidentate phosphites on hydroformylation performance and hydrolysis stability



Scheme 25: Synthesis of benzopinacol phosphites 8a-l.

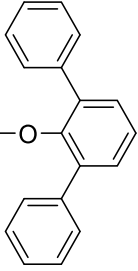
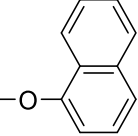
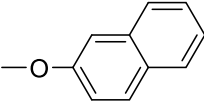
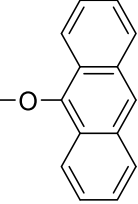

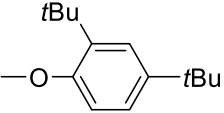
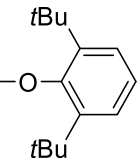
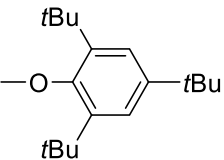
The low reaction temperatures usually serve to slow down the formation of HCl so that it is only present in low concentrations in the reaction solution before it reacts with triethylamine to form the corresponding ammonium salt. Higher concentrations of HCl could lead to degradation of the phosphite. Moreover, the formation of the ammonium salt formed from evolving HCl shifts the reaction equilibrium further towards the phosphite. It was observed that phenyl substituted phenols only needed the relatively weak base, triethylamine, for deprotonation. Phenols with more than one *tert*-butyl groups, or condensed aromatic ring systems, usually required the application of the stronger base *n*-butyllithium. Otherwise the reaction was much more unselective, and the work-up was massively hampered.

Table 6: Reaction conditions and yields of the benzopinacol phosphites.

| Phosphite | -O-R | Base | Solvent | Temperature [°C] | Yield [%] |
|-----------|------|------------------|---------|------------------|-----------|
| 8a | | NEt ₃ | toluene | 20 | 63 |
| 8b | | NEt ₃ | toluene | -20 | 76 |
| 8c | | NEt ₃ | toluene | 20 | 68 |
| 8d | | NEt ₃ | toluene | 20 | 83 |

3 Results and discussion

3.1 Investigations of substituent effects of mono- and bidentate phosphites on hydroformylation performance and hydrolysis stability

| | | | | | |
|-----------|---|------------------|---------|-----|-----|
| 8e |  | NEt ₃ | toluene | -20 | 87 |
| 8f |  | <i>n</i> -BuLi | THF | -20 | 77 |
| 8g |  | <i>n</i> -BuLi | THF | -20 | >99 |
| 8h |  | <i>n</i> -BuLi | THF | -20 | 73 |
| 8i |  | NEt ₃ | toluene | 20 | 93 |
| 8j |  | <i>n</i> -BuLi | THF | -20 | 55 |
| 8k |  | <i>n</i> -BuLi | THF | 0 | 71 |
| 8l |  | <i>n</i> -BuLi | THF | 0 | 55 |

Crystals suitable for X-ray crystal structure analysis were obtained by Muhammad Sharif in our research group, for the two benzopinacolphosphites **8a** and **8c**, which can be seen in Figure 17 and Figure 18, respectively.¹¹ The comparison of both structures reveals that a phenyl substituent in the *meta*-position does not significantly influence the length of the central P–O bonds.

3 Results and discussion

3.1 Investigations of substituent effects of mono- and bidentate phosphites on hydroformylation performance and hydrolysis stability

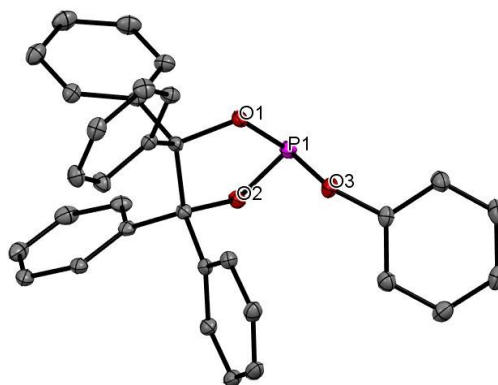


Figure 17: Molecular structure of 8a in the solid state. Displacement ellipsoids correspond to 30 % probability. Hydrogen atoms are omitted for clarity. Selected bond lengths [Å] and angles [°]: P1-O1 1.6275(9), P1-O2 1.6223(9), P1-O3 1.6403(9); O2-P1-O1 94.20(4), O2-P1-O3 106.71(5), O1-P1-O3 94.53(5).

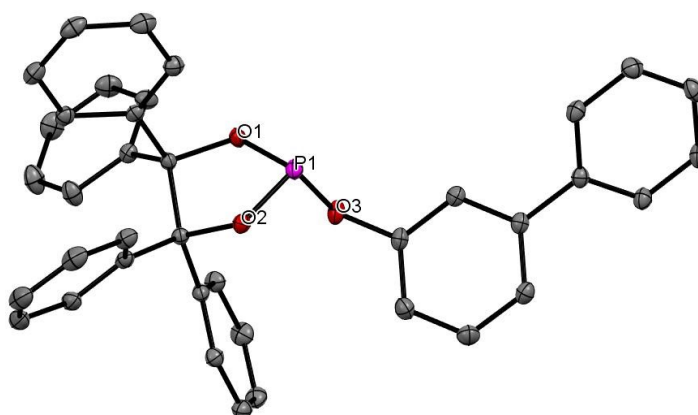


Figure 18: Molecular structure of 8c in the solid state. Displacement ellipsoids correspond to 30 % probability. Hydrogen atoms are omitted for clarity. Selected bond lengths [Å] and angles [°]: P1-O1 1.6292(9), P1-O2 1.6189(9), P1-O3 1.6397(9); O2-P1-O1 94.10(4), O2-P1-O3 105.61(5), O1-P1-O3 95.53(5).

3.1.2.2 Hydroformylation experiments

Catalysts of the benzopinacolphosphites were investigated concerning their activity, chemoselectivity and stability as well.

To investigate these issues again *n*-octenes were used as a model substrate. For the benzopinacolphosphites as ligands, the rate constant k_{obs} of the conversion was determined as a different autoclave equipped with a gas flow meter was available for the following experiments. Whenever possible it was defined by exponential curve fitting of the measured gas consumption during the reaction. As already mentioned for the hydrolysis experiments in chapter 3.1.1.2,

3 Results and discussion

3.1 Investigations of substituent effects of mono- and bidentate phosphites on hydroformylation performance and hydrolysis stability

pseudo-first-order kinetics can be applied because of the vast excess of synthesis gas. The entries 1-12 and 17 of Table 7 were taken from a recent manuscript of the work group and added here for comparison.¹¹²

Table 7: Hydroformylation^a of *n*-octenes^b with benzopinacolphosphites.

| Entry | Ligand | T [°C] | Yield of Aldehydes ^c [%] | <i>n</i> -Selectivity ^c [%] | <i>k</i> _{obs} ^d [min ⁻¹] |
|-------|-----------|--------|-------------------------------------|--|---|
| 1 | 8a | 120 | 40 | 19.4 | - |
| 2 | 8b | 120 | 99 | 17.6 | 0.223 |
| 3 | 8c | 120 | 9 | 32.1 | - |
| 4 | 8d | 120 | 3 | 40.8 | - |
| 5 | 8e | 120 | 97 | 18.9 | 0.266 |
| 6 | 8f | 120 | 82 | 18.0 | - |
| 7 | | 110 | 98 | 26.5 | 0.067 |
| 8 | 8g | 120 | 71 | 15.9 | - |
| 9 | | 110 | 94 | 21.5 | 0.064 |
| 10 | 8h | 120 | 57 | 22.2 | - |
| 11 | | 110 | 97 | 15.6 | 0.304 |
| 12 | | 100 | 90 | 10.7 | - |
| 14 | 8i | 120 | 91 | 15.0 | 0.116 |
| 15 | 8j | 120 | 96 | 17.0 | 0.284 |
| 16 | 8k | 120 | 93 | 29.7 | 0.067 |
| 17 | 8l | 120 | 18 | 33.6 | - |

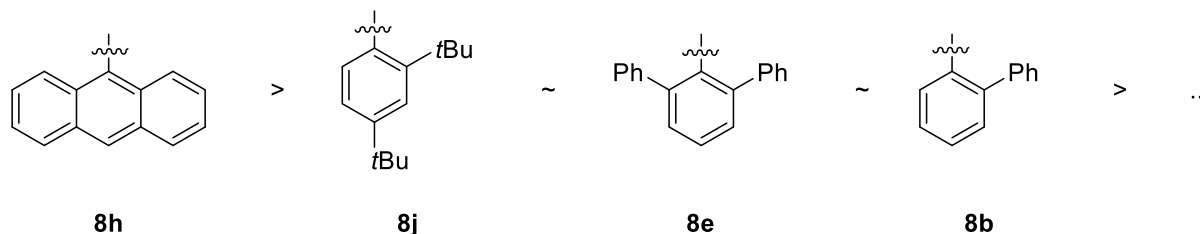
^a[Rh] = 1.0×10⁻³ mol·L⁻¹; *p* = 50 bar; *t* = 4 h; solvent: toluene; *S*/*Rh* = 2200. ^b3.3% 1-octene, 48.4% *Z/E*-2-octene, 29.2% *Z/E*-3-octene, 16.4% *Z/E*-4-octene, 2.1% skeletal C8-olefinic isomers, 0.6% *n*-octane. ^cDetermined by GC with toluene as internal standard. ^dPseudo-first-order rate constant derived from exponential curve fitting of gas consumption versus time.

The highest yields after four hours reaction time were achieved for the reaction with phosphites **8b**, **8e**, **8f** and **8h** with over 97 % (Table 7, entries 2, 5, 7 and 11). Taking into account the rate constant *k*_{obs}, ligands **8b**, **8e**, **8h** and **8j** induced the highest activity (Table 7, entries 2, 5, 11, and 15). Generally, substituents in *ortho*-position, especially phenyl substituents and condensed aromatic ring systems, allow the achievement of high activity. However, *tert*-butyl groups (**8j**,

3 Results and discussion

3.1 Investigations of substituent effects of mono- and bidentate phosphites on hydroformylation performance and hydrolysis stability

Table 7, entry 15) may also contribute beneficially to the activity. The following general tendency can be derived (Scheme 26).



Scheme 26: The order of activity in hydroformylation in dependence on position and nature of substituents.

All *n*-selectivities were within a range of 10.7% and 40.8%. Noteworthy however, the highest *n*-selectivities were associated with relatively low yields and activities. The highest *n*-selectivity (29.7%) paired with reasonable activity (93%, 0.067 min⁻¹) was obtained with **8k** as ligand (Table 7, entry 16). Furthermore, the catalyst based on ligand **8f** exhibited comparable properties with an *n*-selectivity of 26.5 %, a yield of 93 % and a rate constant k_{obs} of 0.067 min⁻¹. Phosphites **8g** and **8h**, with condensed aromatic structures, induced slightly better *n*-selectivities than the parent phenyl substituted structure. Phenyl substituents in *ortho*-position and *tert*-butyl substituents in *para*-position lowered the regioselectivity.

It can be concluded that the tendencies for yield and *n*-selectivity in dependence of the reaction temperature are not the same for each ligand. For **8f** (Table 7, entries 6 and 7) and **8g** (entries 8 and 9), the decrease in temperature led to an increase in the yield of aldehyde as well as in *n*-selectivity. In contrast, the same manipulation in the reaction with **8h** only gave an increase in yield while dropping the temperature from 120 °C to 110 °C. A further decrease to 100 °C did not affect the yield, but the *n*-selectivity eroded with the decreasing temperature in this particular case.

3.1.2.3 Hydrolysis experiments

To test their stability against water, a definite amount of phosphite was dissolved in 1,4-dioxane in order to obtain a 0.049 M solution and afterwards 100 equivalents of deoxygenized water were added as already described for the biphenolphosphites in chapter 3.1.1.3. Hydrolysis was investigated at room temperature and at 90 °C. All results are listed in Table 8 and Table 9.

The exemplary plots of the concentration profile in unaltered and logarithmized form of **8a** are shown in Figure 19.

3 Results and discussion

3.1 Investigations of substituent effects of mono- and bidentate phosphites on hydroformylation performance and hydrolysis stability

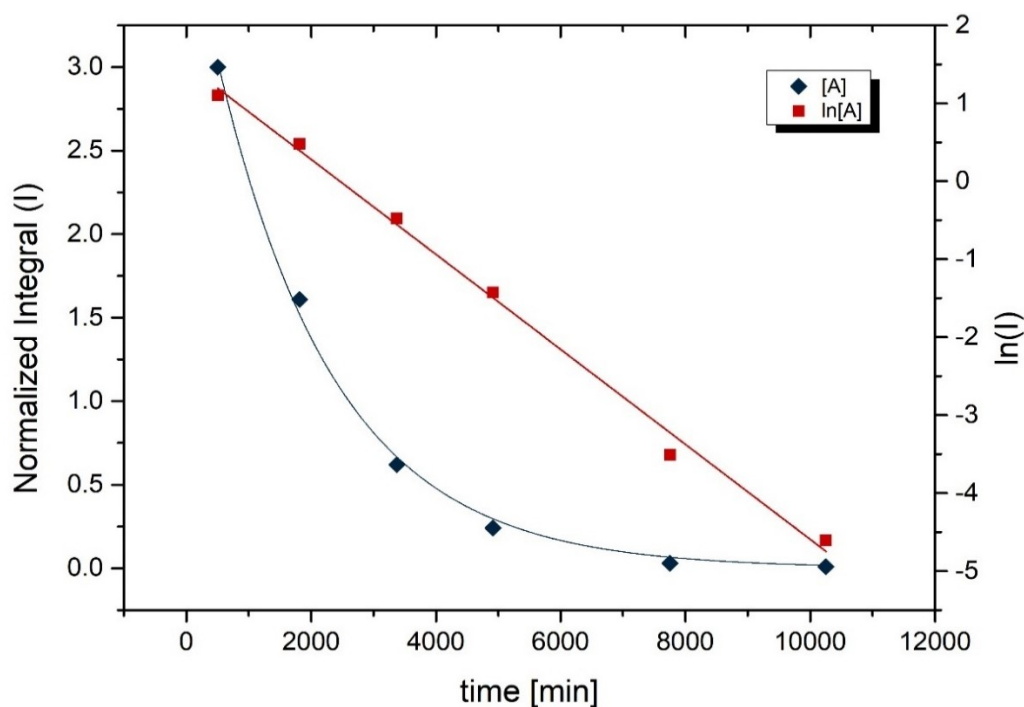


Figure 19: Direct and logarithmized plots of the concentration profile of **8a** during hydrolysis. Conditions: $[L] = 0.049 \text{ mol}\cdot\text{L}^{-1}$; $\text{H}_2\text{O}/L = 100$; $T = \text{room temperature}$; solvent: 1,4-dioxane.

Table 8: Hydrolysis^a of benzopinacolphosphites at room temperature.

| Entry | Ligand | k_{obs}^b [10^{-4} min^{-1}] | $t_{1/2}^b$ [h] | Complete Decomposition ^c [h] |
|-------|-----------|---|---------------------|---|
| 1 | 8a | 6.093 | 19.0 | 171 |
| 2 | 8b | 2.583 | 44.7 | 503 |
| 3 | 8c | 6.584 | 17.5 | 179 |
| 4 | 8d | - | - | 122 |
| 5 | 8e | - | - | 3626 |
| 6 | 8f | 0.015 ^d | 7944.5 ^d | 3145 |
| 7 | 8g | 0.028 ^d | 4139.5 ^d | 1495 |
| 8 | 8h | 0.383 | 301.7 | 2259 |
| 9 | 8i | - | - | 47 |
| 10 | 8j | 1.226 | 94.2 | 755 |
| 11 | 8k | - | - | >10740 |
| 12 | 8l | - | - | >10740 |

^a $[L] = 0.049 \text{ mol}\cdot\text{L}^{-1}$; $\text{H}_2\text{O}/L = 100$; $T = \text{room temperature}$; solvent: 1,4-dioxane. ^bDetermined by quantitative ³¹P NMR based on pseudo-first-order rate constant derived from exponential curve fitting of decomposition versus time. ^cDetermined by ³¹P NMR. ^dDetermined for the initial period of hydrolysis without autocatalysis. Onset of autocatalysis for **8f**: 1930 h, **8g**: 930 h.

3 Results and discussion

3.1 Investigations of substituent effects of mono- and bidentate phosphites on hydroformylation performance and hydrolysis stability

Table 9: Hydrolysis^a of benzopinacolphosphites at 90 °C.

| Entry | Ligand | k_{obs}^b [10^{-3} min^{-1}] | $t_{1/2}^b$ [h] | Complete Decomposition ^c [h] |
|-------|-----------|---|-------------------|---|
| 1 | 8a | 131.435 | 0.1 | 1.0 |
| 2 | 8b | 63.802 | 0.2 | 2.0 |
| 3 | 8c | 92.091 | 0.1 | 1.0 |
| 4 | 8d | 245.329 | 0.05 | 1.0 |
| 5 | 8e | 0.363 ^d | 31.8 ^d | 13.5 |
| 6 | 8f | 0.404 ^d | 28.6 ^d | 10.0 |
| 7 | 8g | 6.020 ^d | 1.9 ^d | 3.0 |
| 8 | 8h | 0.019 | 0.6 | 3.5 |
| 9 | 8i | - | - | 0.5 |
| 10 | 8j | 0.068 | 0.2 | 2.5 |
| 11 | 8k | - | - | >225.0 |
| 12 | 8l | - | - | >225.0 |

^a[L] = 0.049 mol·L⁻¹; H₂O/L = 100; T = 90 °C; solvent: 1,4-dioxane. ^bDetermined by quantitative ³¹P NMR based on pseudo-first-order rate constant derived from exponential curve fitting of decomposition versus time. ^cDetermined by ³¹P NMR. ^dDetermined for the initial period of hydrolysis without autocatalysis. Onset of autocatalysis for **8e**: 8.5 h, **8f**: 5.5 h, **8g**: 1.5 h.

In the hydrolysis experiments, some similar trends were observed at room temperature as well as at 90 °C. While **8k** and **8l** were astonishingly stable, **8d** and **8i** decomposed rapidly. Therefore, no rate constant for these phosphites could be derived. Furthermore, not all benzopinacolphosphites exhibited an exponential decomposition behavior throughout the whole reaction time. The decomposition rates of **8e**, **8f** and **8g** increased to a certain point, which can be rationalized with progressing autocatalysis due to the formation of acidic degradation products. The relevant hydrolysis behavior at 90 °C is shown in Figure 20.

3 Results and discussion

3.1 Investigations of substituent effects of mono- and bidentate phosphites on hydroformylation performance and hydrolysis stability

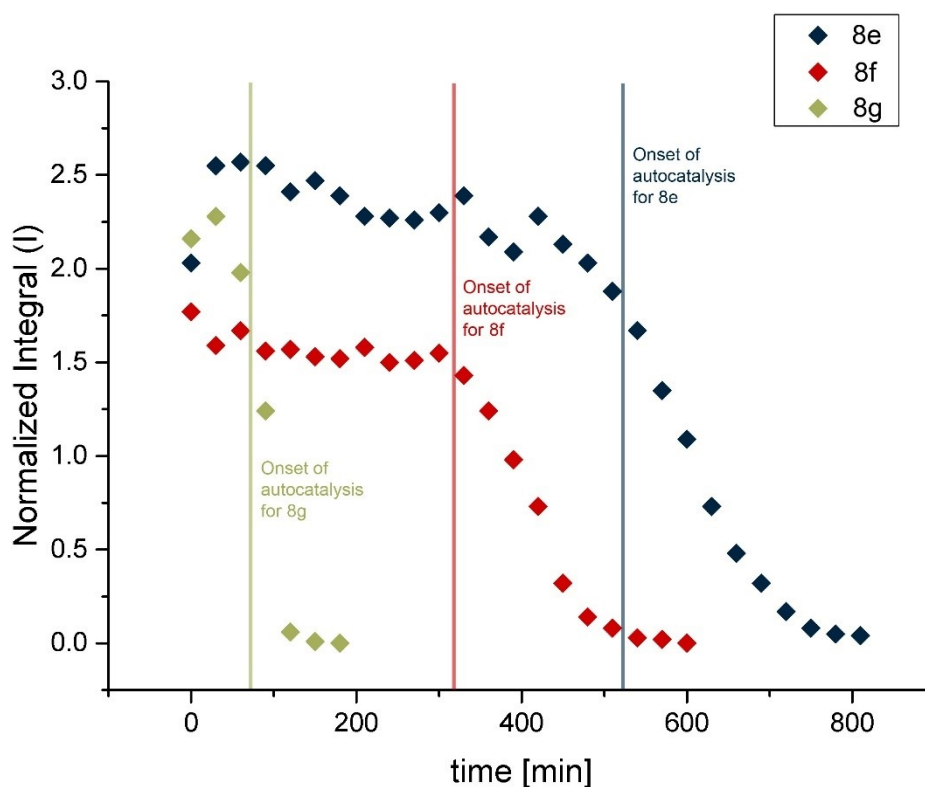


Figure 20: Hydrolysis of 8f, 8g and 8h at 90 °C.

It is significant that sterically demanding aryl substituents in *ortho*-position to the phosphorus moiety increase the hydrolysis stability to an exceptional level. The extremely high stability of phosphites **8k** and **8l** at room temperature bearing *tert*-butyl groups in *ortho*-position should be particularly emphasized. Furthermore, **8e**, **8f** and **8h**, which either possess phenyl substituents or condensed aromatic rings in *ortho*-position to the phosphite group belong to the most robust structures. In contrast, phosphites with substituents in the *para*-position can be considered as slightly more labile towards hydrolysis than the unsubstituted parent structure (**8a**). The latter exhibited a decomposition time over 60 times shorter at room temperature, and over 225 times shorter at 90 °C, than the most stable phosphites (**8k** and **8l**).

3 Results and discussion

3.1 Investigations of substituent effects of mono- and bidentate phosphites on hydroformylation performance and hydrolysis stability

3.1.2.4 Conclusion

A series of monophosphites with substituted benzopinacol backbone were synthesized and tested as ligands in the rhodium-catalyzed hydroformylation of *n*-octenes. Among these ligands, phosphites with a single aryl substituent in the *ortho*-position of the phosphorus moiety exhibited especially high activities and yields of the desired aldehyde. This was observed for structures bearing phenyl groups as well as for those with *tert*-butyl groups. Surprisingly, phosphites **8c** and **8d**, both containing a phenyl group, in the first case in *meta*- and in the second case in *para*-position, can be considered as ineligible for the hydroformylation of *n*-octenes — at least under our reaction conditions. The same holds for **8l**, where the phenyl ring is decorated with three *tert*-butyl groups. For **8c** and **8d**, this failure can be rationalized by their low stability, which leads to catalytically unreactive species (Figure 21). The catalyst derived from phosphite **8l** might be inactive because of the large steric hindrance exerted by the three *tert*-butyl substituents. Probably, this substitution pattern inhibits the coordination of the phosphorus to rhodium. Generally, *tert*-butyl groups in *ortho*-position stabilize the ligand towards hydrolysis. This is in full agreement with former results, where bulky *ortho*-alkyl substituents were incorporated, e.g., in the prominent monophosphite Alkanox[®] or the diphosphite Biphephos (*vide supra*).

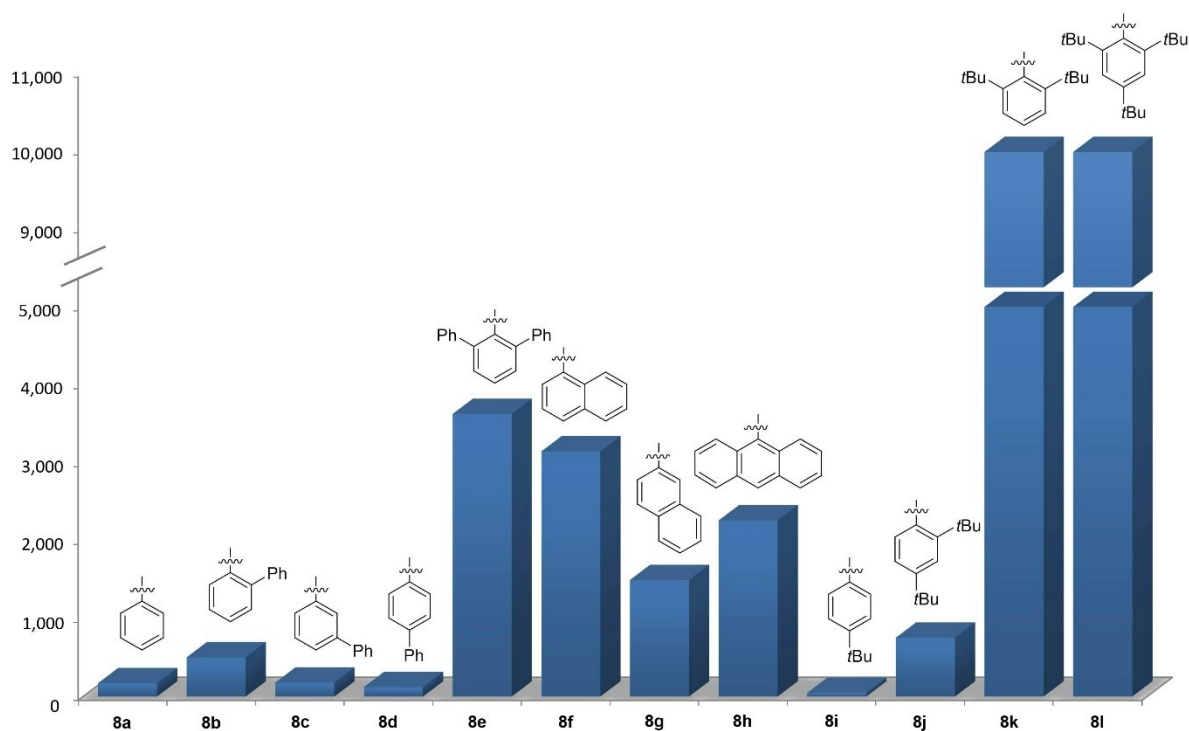


Figure 21: Complete decomposition times of biphenolphosphites at room temperature.

3 Results and discussion

3.1 Investigations of substituent effects of mono- and bidentate phosphites on hydroformylation performance and hydrolysis stability

In terms of regioselectivity, the catalysts of those ligands that induced low activities usually exhibited high *n*-selectivities (Figure 22). The highest *n*-selectivities paired with aldehyde yields over 20 % were produced by assistance of **8f**, **8h** and **8k** which are all characterized by sterically demanding structures. Another very sterically demanding phosphite (**8e**) displayed a high activity, but mediocre *n*-selectivity. This result must arise from the fast reaction with the non-isomerized internal olefins. In general, our study gives evidence that a compromise must be found, where the catalytic and stabilizing properties of ligands have to be matched.

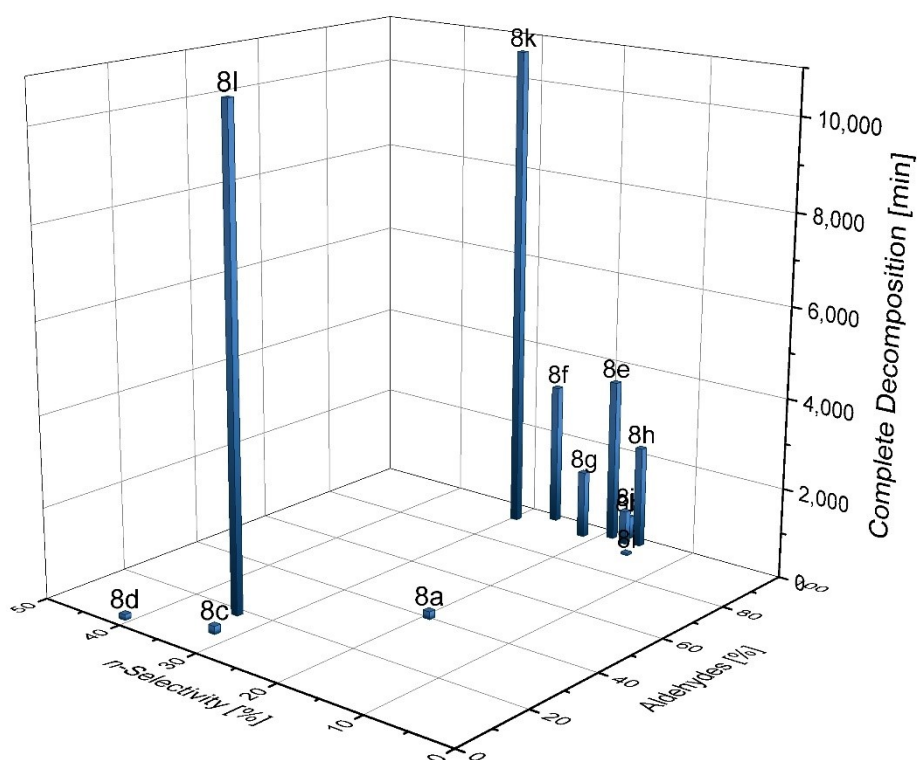


Figure 22: 3D-plot of aldehyde yield and *n*-selectivity under optimized reaction conditions and the complete decomposition at room temperature.

3 Results and discussion

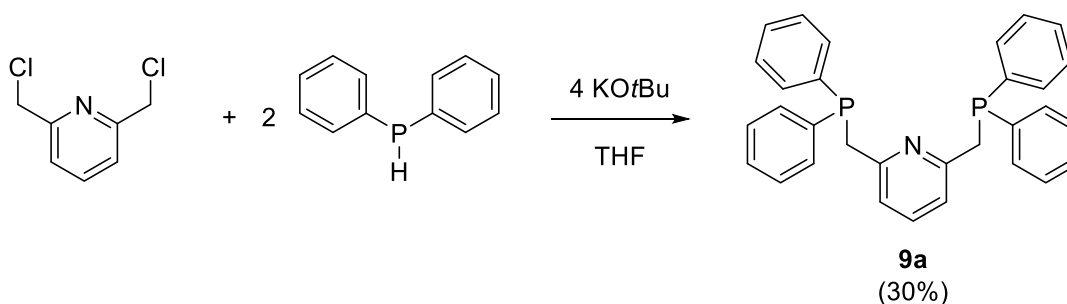
3.2 Investigations of hemilabile potentially tridentate coordinating PNP-ligands

3.2 Investigations of hemilabile potentially tridentate coordinating PNP-ligands

3.2.1 Synthesis of PNP-ligands

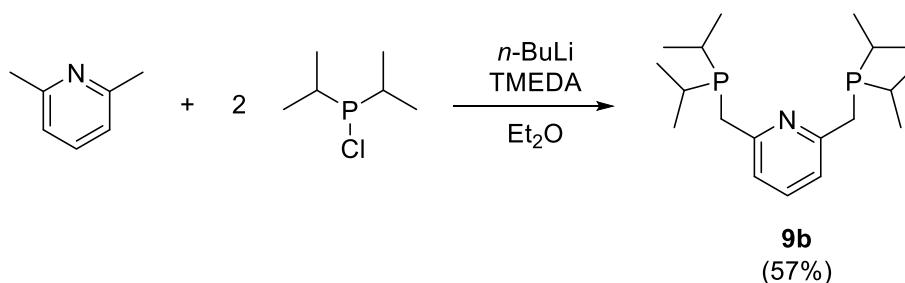
As previously described (chapter 1.1.4.1) the application of potentially tridentate PNP-ligands in hydroformylation reactions was not intensively studied up to now. To gain some more insights two pyridine-based phosphine ligands were synthesized during the work for this thesis.

Two protocols were found in the literature. The ligand with phenyl substituents on the phosphorus was assembled from diphenylphosphine, which was treated with potassium *tert*-butylate. After deprotonation of the phosphine, 2,6-bis(chloromethyl)pyridine was added to form the potentially tridentate coordinating ligand **9a** (Scheme 27).⁶⁹



Scheme 27: Synthesis of PNP^{Ph}(9a).

Another diphosphine equipped with *iso*-propyl groups was synthesized from 2,6-dimethylpyridine. First 2,6-dimethylpyridine was deprotonated with *n*-butyllithium and tetramethylethylenediamine (TMEDA). Afterwards chlorodiisopropylphosphine was added and the pure final product **9b** was received after distillation as a yellow oil.⁷²



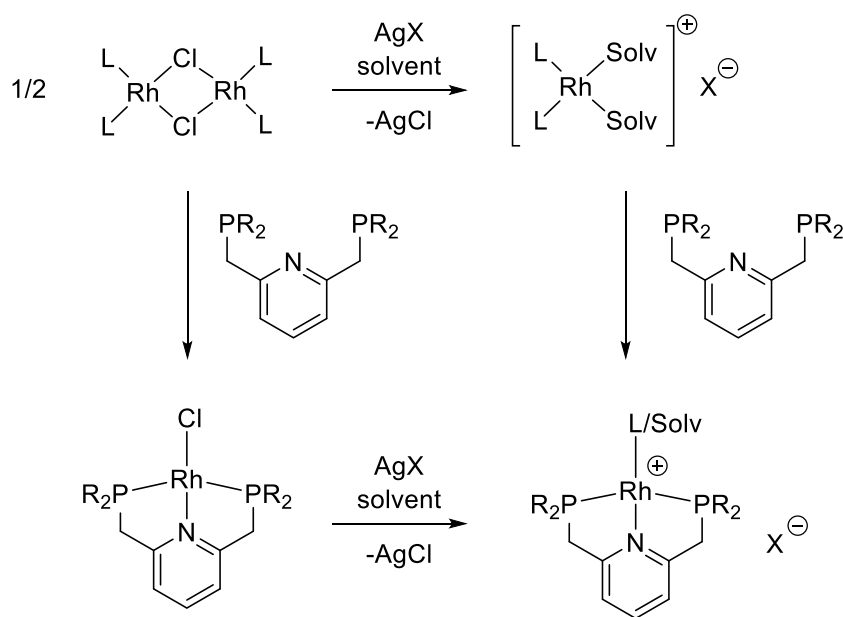
Scheme 28: Synthesis of PNP^{Pr}(9b).

3 Results and discussion

3.2 Investigations of hemilabile potentially tridentate coordinating PNP-ligands

3.2.2 Synthesis of cationic and neutral rhodium complexes

Starting from these two ligands several attempts to synthesize cationic rhodium complexes were made. In general, there are two options to construct the desired complexes. The first way proceeds via a solvated cationic rhodium complex which reacts with the PNP-ligand in a subsequent reaction step (Scheme 29).¹¹³⁻¹¹⁷ In a second version, a rhodium precursor reacts first with the PNP-ligand and afterwards chloride is abstracted from the complex and exchanged with a non-coordinating anion.¹¹⁸



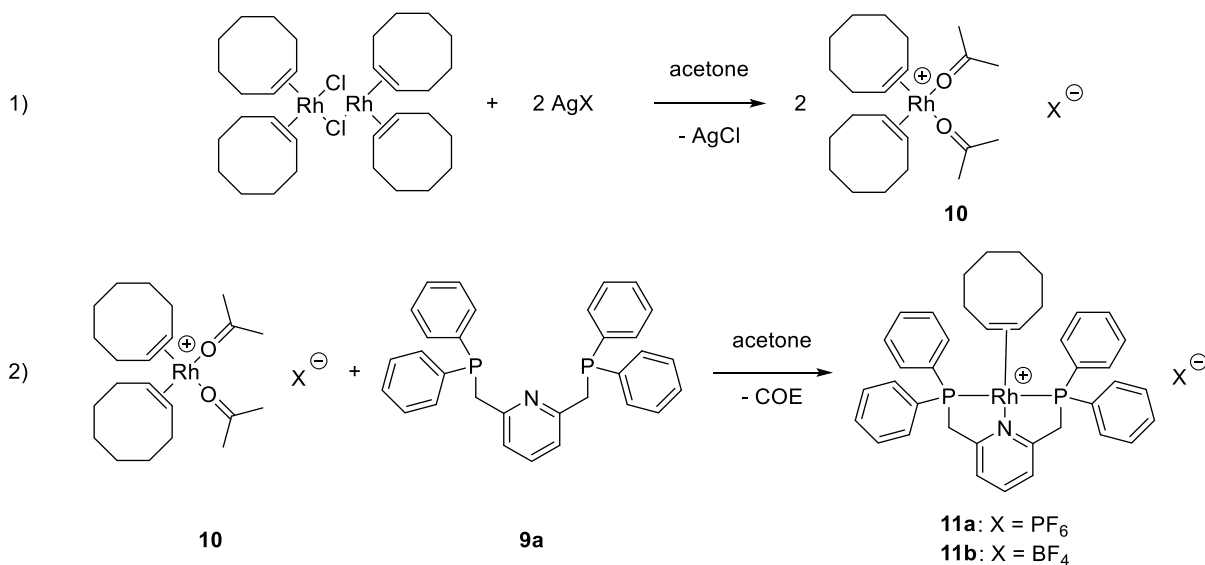
Scheme 29: Routes for the synthesis of cationic rhodium complexes.

During our studies multiple attempts were made to synthesize the cationic $[\text{Rh}(\text{PNP}^{\text{Ph}})(\text{COE})]^+$ ion using varying reaction conditions and anions. Starting from chlorobis(cyclooctene)rhodium dimer the respective solvated cationic rhodium complex **10** was obtained as an intermediate (Scheme 30, reaction 1). Afterwards the resulting silver chloride was removed by filtration and **10** was treated with a PNP-ligand (reaction 2).

The first attempt using THF as the solvent was not successful because THF polymerized. Acetone proved to be a better solvent for the reaction.

3 Results and discussion

3.2 Investigations of hemilabile potentially tridentate coordinating PNP-ligands



Scheme 30: Synthesis of [Rh(PNP^{Ph})(COE)]X.

In this case a mixture of mainly two components was received (Figure 23, a). After several purification steps (precipitating the side-product by adding diethyl ether to a concentrated acetone solution of the mixture) the purified complex (b) and an isolated side-product (c) were received. The final yield of the pure complex **11a** (9 %) was too low to perform subsequent reactions.

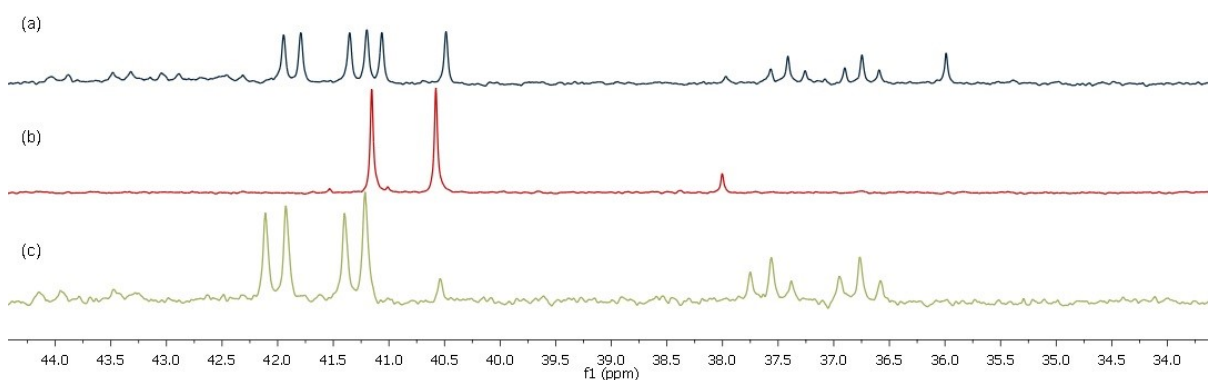


Figure 23: ³¹P NMR spectra of the reaction mixture (a), the purified desired complex (b) and the dimer side-product (c).

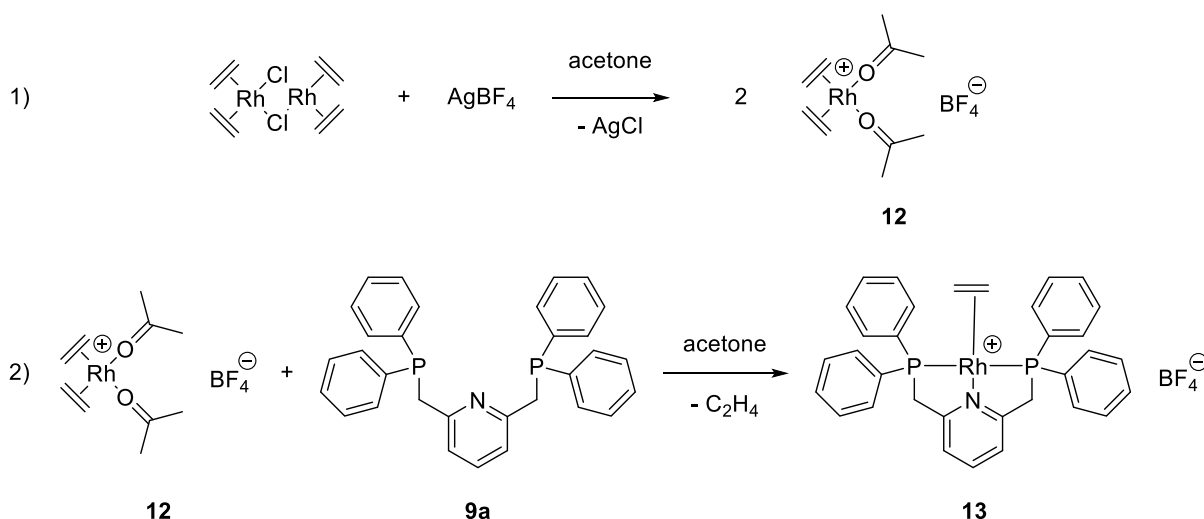
To achieve lower amounts of byproduct, a change of silver salt was considered. Taube *et al.* reported significantly higher amounts of byproduct when using PF₆⁻ as anion for a similar complex, compared to the preparations using BF₄⁻ and OTf salts.¹¹⁶ Keeping this in mind, we tried the reaction with AgBF₄. Unfortunately, no significant improvement in the proportions of the

3 Results and discussion

3.2 Investigations of hemilabile potentially tridentate coordinating PNP-ligands

desired complex to the byproduct compared to the reaction with AgPF_6 was achieved. The mixture still remained hard to separate and the BF_4^- complex **11b** could not be isolated in pure form.

After several trials with the cyclooctene complex another attempt, following a literature procedure, was tested. For this the less bulky ethylene complex $[\text{Rh}(\text{PNP}^{\text{Ph}})(\text{C}_2\text{H}_4)]\text{BF}_4$ (**13**) was approved (Scheme 31).¹¹⁶ The quantitative ^{31}P NMR spectrum of the reaction solution indicated 75 % conversion to the desired complex. The amount of byproduct was significantly lower than that with the cyclooctene counterpart. Unfortunately, the desired complex revealed rather instable in solution. Decomposition took place very quickly when it was not kept under an atmosphere of ethylene. Therefore, further attempts using this complex were cancelled.

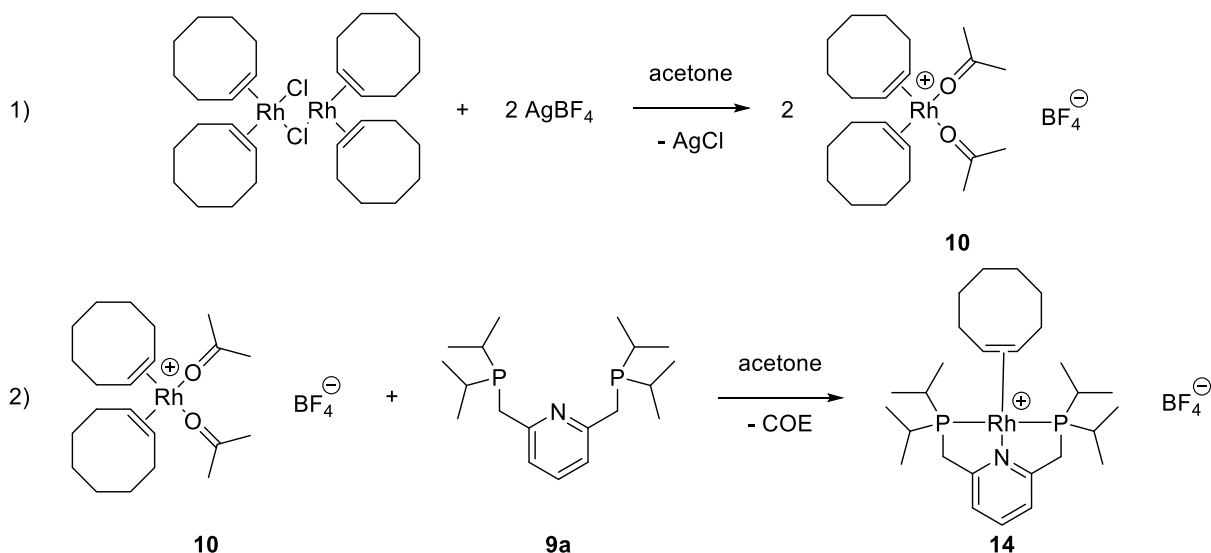


Scheme 31: Synthesis of $[\text{Rh}(\text{PNP}^{\text{Ph}})(\text{C}_2\text{H}_4)]\text{BF}_4$ (**13**).

Taking in mind the results with the sterically demanding phenyl substituents at the phosphorus, also synthesis attempts were carried out using the less sterically demanding *iso*-propyl substituted ligand.¹¹⁷ In this case large amounts of a hitherto unknown byproduct were obtained. Quantitative ^{31}P NMR spectrum indicated a ratio of 15:85 complex:byproduct. Unfortunately, the desired complex could not be purified.

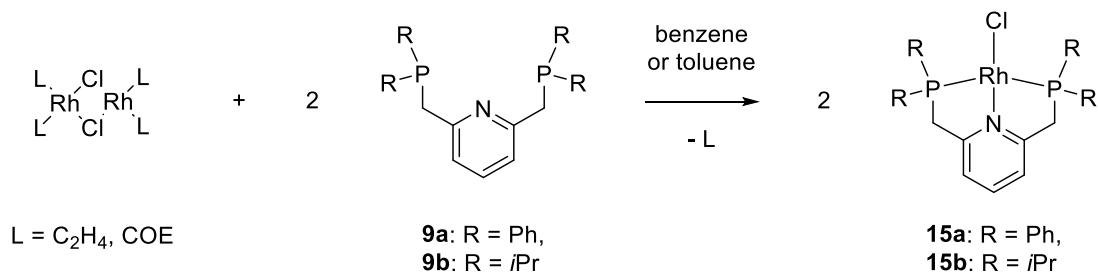
3 Results and discussion

3.2 Investigations of hemilabile potentially tridentate coordinating PNP-ligands



Scheme 32: Synthesis of $[\text{Rh}(\text{PNP}^{\text{iPr}})(\text{COE})]\text{BF}_4$ (**14**).

Furthermore, the synthesis of cationic rhodium complexes was attempted via a second option, which was also mentioned in Scheme 29. For this, the chlorinated complexes of the two selected ligands were synthesized by adapting literature methodologies (Scheme 33).



Scheme 33: Synthesis of $\text{Rh}(\text{PNP})\text{Cl}$ (**15**).

Based on the phenyl substituted ligand the chlorinated rhodium complex **15a** was synthesized following a protocol by Sacco.¹¹⁸ Chlorobis(ethylene)rhodium dimer and 2,6-bis[(diphenylphosphino)methyl]pyridine (**9a**) were dissolved in 1.5 ml and 4 ml benzene, respectively. Afterwards the ligand solution was slowly added to the solution of the rhodium cyclooctene complex. After stirring, and filtrating the cloudy solution, the desired complex was obtained with 58% yield.

Also the chlorinated rhodium complex with the *iso*-propyl substituted PNP-ligand **15b** was prepared following a literature procedure.¹¹⁹ The chlorobis(cyclooctene)rhodium dimer and 2,6-bis[(di-*iso*-propylphosphino)methyl]pyridine (**9b**) were separately dissolved in toluene. The

3 Results and discussion

3.2 Investigations of hemilabile potentially tridentate coordinating PNP-ligands

solution of the ligand was added to the rhodium complex afterwards. After stirring for 30 minutes and filtration of the cloudy solution the desired complex was obtained with 69 % yield.

To validate the geometry of the obtained chloro complexes, **15b** was crystallized from a saturated toluene solution, which was layered with heptane. In the X-ray structural analysis, the rhodium center is embedded in a square planar arrangement of four ligating atoms. Overall, an almost planar structure (excluding the *iso*-propyl groups) can be observed. As can be seen in the second picture of Figure 24, the plane of the phosphine groups is slightly tilted compared to the plane of the pyridine ring. The torsion angle of the phosphorus P1 to the carbon C3 of the pyridine ring has been determined to be -11.6° . It can be expected that during the hydroformylation reaction the equatorial–equatorial coordination of the two phosphorus groups stays intact.

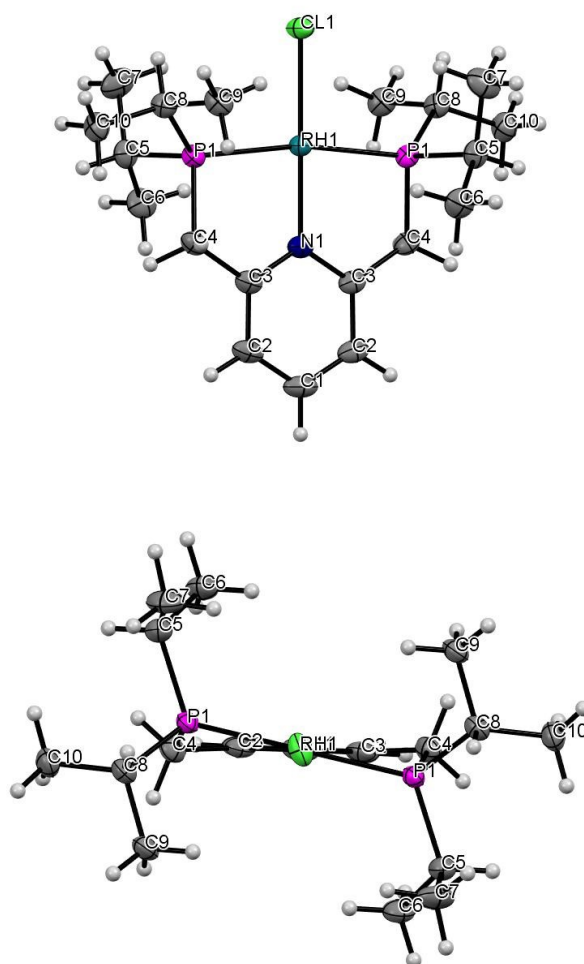


Figure 24: Molecular structure of Rh(PNP^{iPr})Cl-complex (15b) in the solid state from two different angles. Displacement ellipsoids correspond to 30 % probability. Selected interatomic distances [Å]: P1-Rh1, 2.2389(4); Cl1-Rh1, 2.3481(5); N1-Rh1, 2.0212(18). Selected angles [°]: P1-Rh-Cl1, 95.428(10); Cl1-Rh1-N1, 180.000; P1-Rh1-P1, 169.14(2); N1-Rh1-P1, 84.572(10). Selected torsion angles [°]: P1-Rh1-N1-C3, -11.63(11).

3 Results and discussion

3.2 Investigations of hemilabile potentially tridentate coordinating PNP-ligands

In a second step, the chloro complex was treated with a silver salt to get the anticipated cationic rhodium complex. An attempt was made with the previously reported phenyl substituted complex. This complex reacted with silver tetrafluoroborate in the presence of acetonitrile. We speculate that the advantageous donor properties of acetonitrile should stabilize the resulting cationic rhodium complex. Unfortunately, the ^{31}P NMR spectrum showed signals of a mixture of several phosphorus compounds. None of them fitted the anticipated doublet signal.

3.2.3 Hydroformylation experiments with PNP-complexes

The two new chloro complexes were tested in the hydroformylation. Substrate 1-octene was used instead of the isomeric mixture of *n*-octenes. 1-Octene represents a common model substrate in hydroformylation as it is easy to handle and widely available through petroleum refinery. All results are collected in Table 10.

Table 10: Hydroformylation^a of 1-octene with PNP-complexes.

| Entry | Complex | <i>p</i> [bar] | <i>T</i> [°C] | Yield of Aldehydes ^b [%] | <i>n</i> -Selectivity ^b [%] | Yield of Hydrogenation product ^b [%] |
|-------|------------|----------------|---------------|-------------------------------------|--|---|
| 1 | 15a | 20 | 100 | 10.8 | 53.1 | 30.4 |
| 2 | 15a | 20 | 120 | 3.9 | 51.2 | 33.6 |
| 3 | 15a | 50 | 100 | 87.8 | 37.7 | 3.4 |
| 4 | 15a | 50 | 120 | 44.5 | 44.6 | 16.2 |
| 5 | 15b | 20 | 100 | 11.8 | 52.6 | 26.0 |
| 6 | 15b | 20 | 120 | 4.3 | 56.9 | 33.4 |
| 7 | 15b | 50 | 100 | 53.7 | 51.7 | 13.6 |
| 8 | 15b | 50 | 120 | 86.9 | 35.3 | 3.9 |

^a[Rh] = $1,0 \cdot 10^{-3}$ mol·L⁻¹; t = 4 h; solvent: toluene; S/Rh = 2000. ^bDetermined by GC with toluene as internal standard.

As can be seen in Figure 25, the yields of aldehyde for the phenyl substituted complex as well as for the *iso*-propyl substituted complex were significantly lower at 20 bar than at 50 bar syngas pressure. At 20 bar, the yield of **15a** and **15b** at 100 °C and 120 °C were at similar levels, with around 11 % and 4 %, respectively (Table 10, entries 1 and 2). Moreover, the yields at 100 °C were for both complexes slightly higher than at 120 °C.

3 Results and discussion

3.2 Investigations of hemilabile potentially tridentate coordinating PNP-ligands

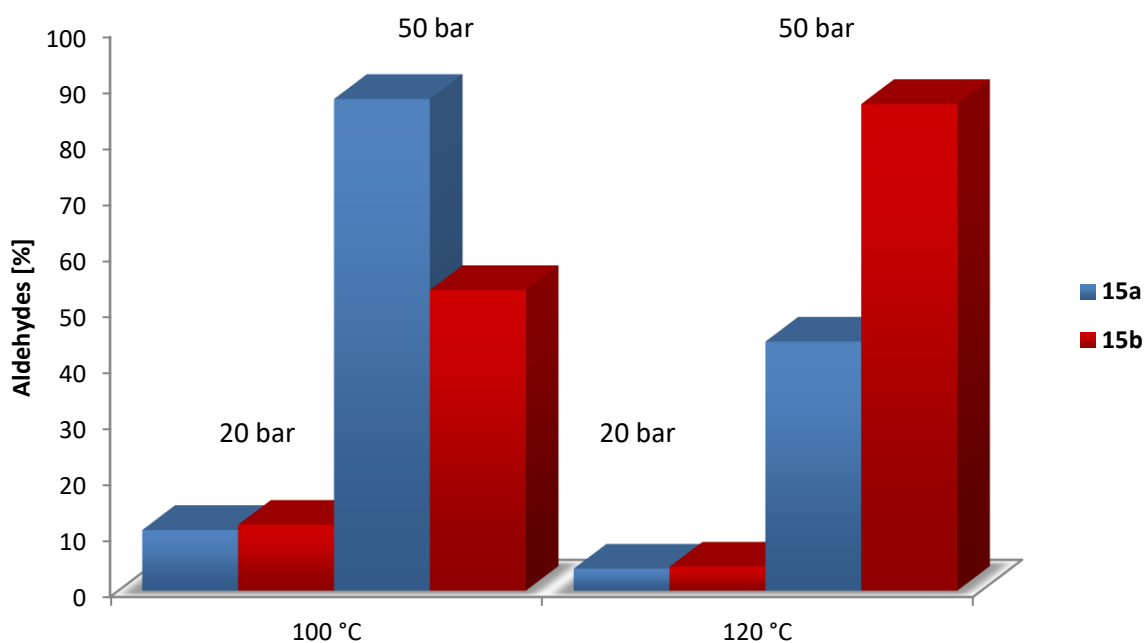


Figure 25: Yields of aldehydes obtained with complexes **15a** and **15b** at different reaction conditions.

At 50 bar, both complexes showed a different behavior. With complex **15a** the yield of aldehyde at 100 °C was significantly higher than at 120 °C while with complex **15b** the reversed trend was observed. The highest yield for **15a** was obtained at 100 °C and 50 bar (Table 10, entry 3) whereas the highest yield for **15b** was achieved at 120 °C and 50 bar (entry 4). Additionally, the volumetric syngas uptakes at different pressures were investigated for the hydroformylation reactions using **15a** (Figure 26 and Figure 27). It stands out that the uptake at both pressures was at 120 °C considerably lower than at a reaction temperature of 100 °C. This result might be rationalized by a lower stability of the phenyl substituted complex under these harsher reaction conditions leading to a loss of hydroformylation activity. With complex **15b**, this behavior could not be observed as the yield was higher at 120 °C than at 100 °C.

3 Results and discussion

3.2 Investigations of hemilabile potentially tridentate coordinating PNP-ligands

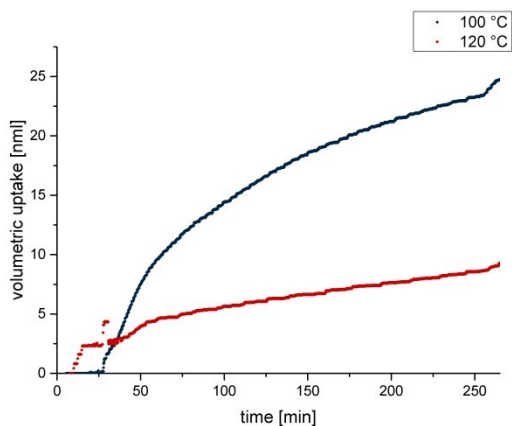


Figure 26: Volumetric uptake of syngas during the hydroformylation with **15a** at 20 bar.

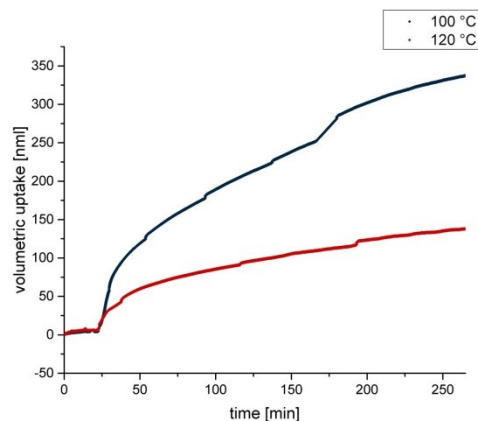


Figure 27: Volumetric uptake of syngas during the hydroformylation with **15a** at 50 bar.

Also, the GC spectra of some hydroformylation reactions indicated the formation of reasonable amounts of the hydrogenation product *n*-octane. The proportion was especially high for the conversions at 20 bar syngas pressure, both for **15a** and **15b** (see Table 10). Exemplarily the GC spectrum of **15a** at 20 bar and 100 °C is shown in Figure 28. In contrast, at a pressure of 50 bar a significantly lower ratio of hydrogenation product was found. Moreover, in the experiments with **15a** at 50 bar and 120 °C (entry 4) and with **15b** at 50 bar and 100 °C (entry 7) the amount of alkane was higher compared to the experiments were the same syngas pressure but another temperature was applied. The high degree of side reaction in the experiment at 20 bar explains why the formation of the desired aldehyde was relatively poor at low syngas pressure.

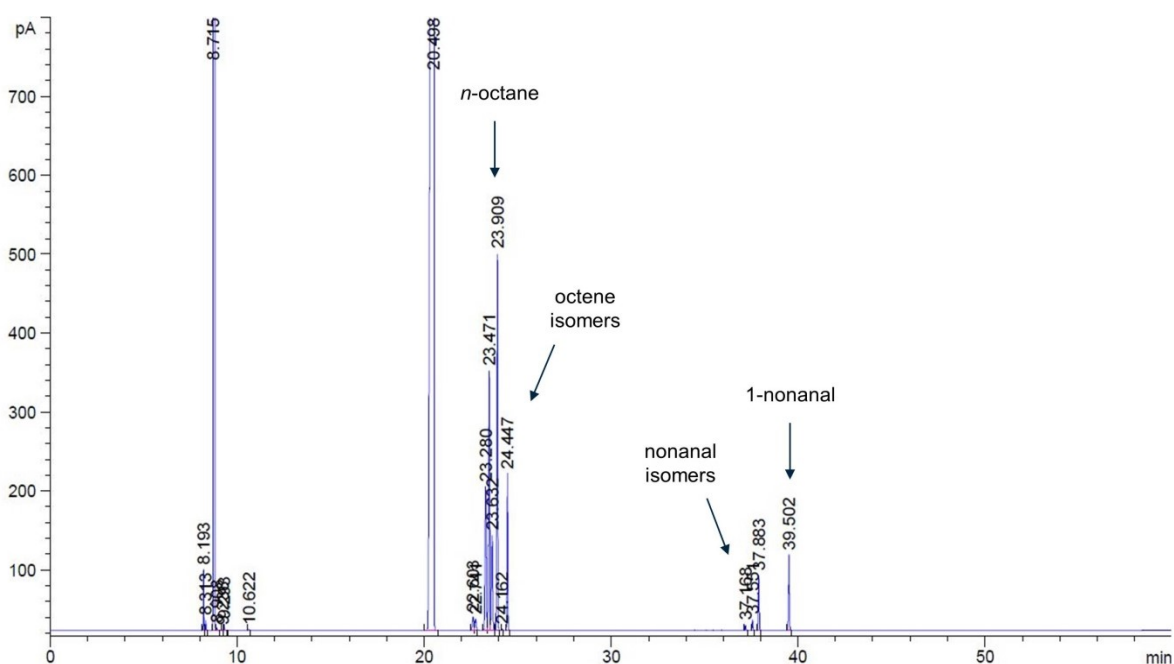


Figure 28: GC spectrum of the hydroformylation reaction with **15a** at 20 bar and 100 °C.

3 Results and discussion

3.2 Investigations of hemilabile potentially tridentate coordinating PNP-ligands

As shown in Figure 29 the *n*-selectivity of the conversion was in most cases around 50 %. Deviating from this general observation are two experiments: With complex **15a** at 100 °C and 50 bar and also with complex **15b** at 120 °C and 50 bar the *n*-selectivity decreased to 37.7 % and 35.3 %, respectively (Table 10, entries 3 and 8). In the corresponding GC spectra (Figure 30 and Figure 31), four signals can be observed in the area of the nonanal isomers (between 35 and 40 min), which indicates the formation of all four possible isomers. This implies the isomerization of the double bond of the starting 1-octene as otherwise only two isomers of nonanal would be possible. On the basis of these findings, the low *n*-selectivity of these conversions can be explained by vigorous double bond isomerization. Therefore, lower amounts of the terminal alkene are available, which is crucial for the formation of the *n*-aldehyde.

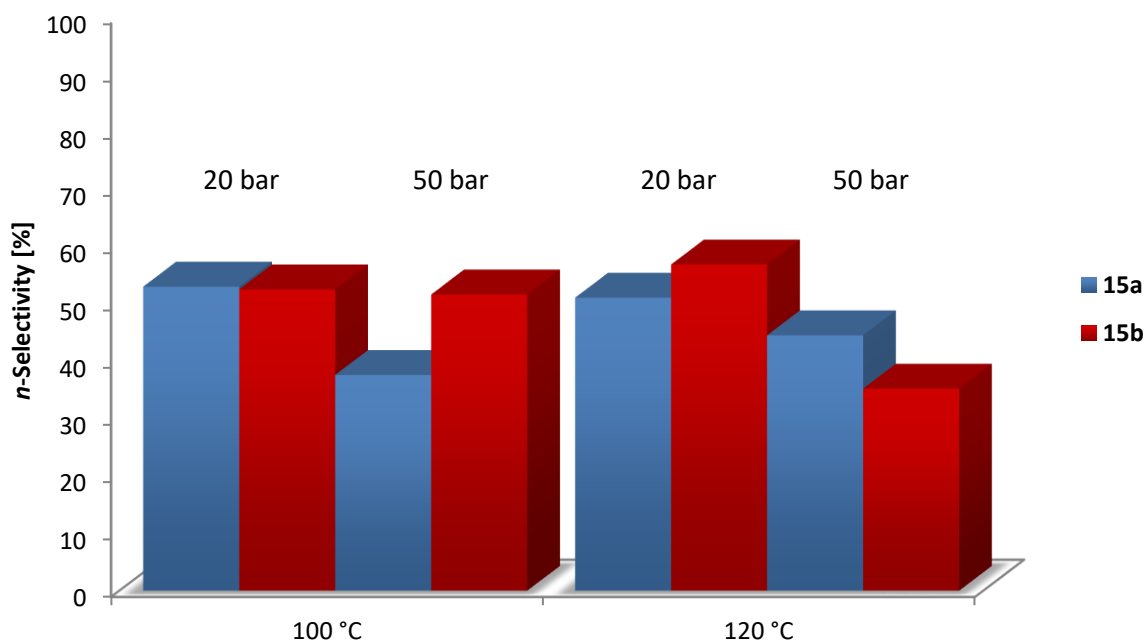


Figure 29: *n*-Selectivities of the hydroformylation of 1-octene with 15a and 15b at different reaction conditions.

3 Results and discussion

3.2 Investigations of hemilabile potentially tridentate coordinating PNP-ligands

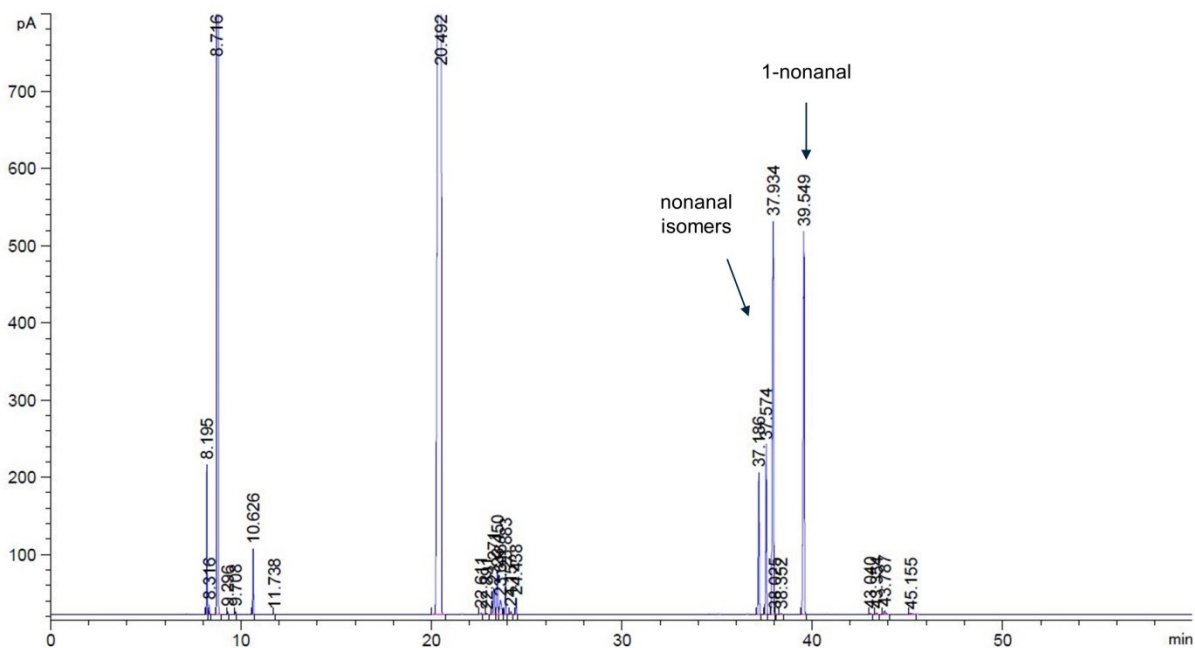


Figure 30: GC spectrum for the hydroformylation reaction with 15a at 50 bar and 100 °C.

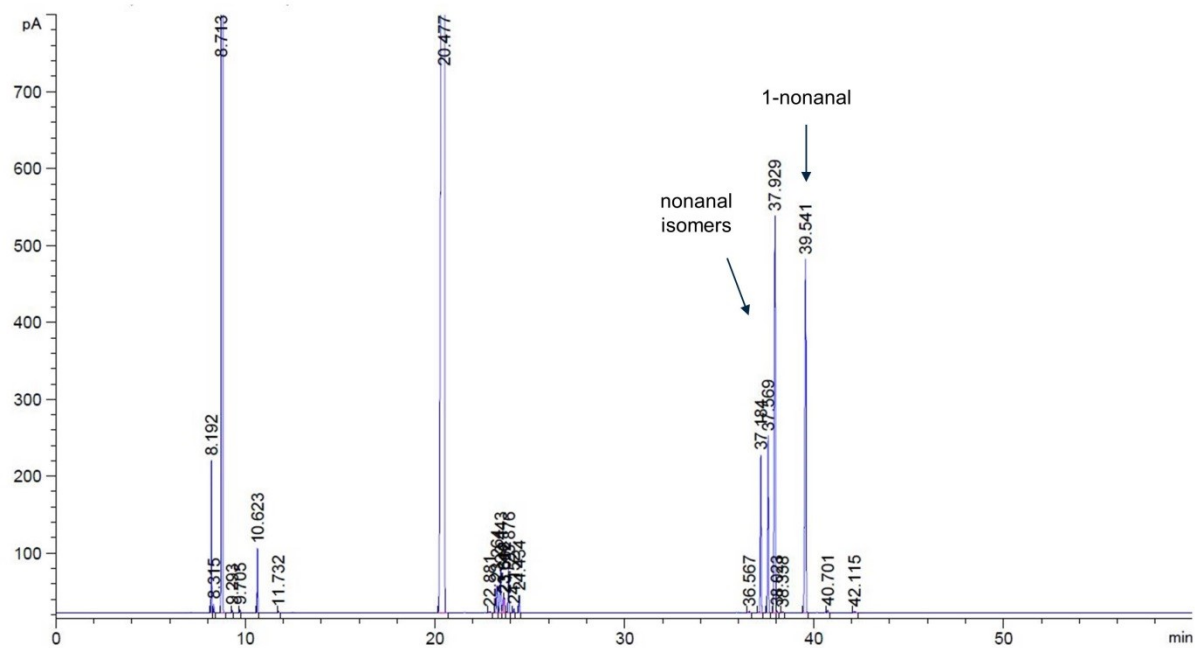


Figure 31: GC spectrum of the hydroformylation reaction with 15b at 50 bar and 120 °C.

3.2.4 Conclusion

In conclusion, the following similarities and differences between the two differently substituted pincer ligands were observed. On one hand, both catalysts **15a** and **15b** allow significantly higher yields of aldehyde at 50 bar syngas pressure than at 20 bar. At 20 bar high yields of the hydrogenation byproducts were observed for both complexes. On the other hand, the highest yield of aldehyde for the phenyl substituted complex **15a** was achieved at 50 bar and 100 °C with 87.8 %. In contrast superior yield for the *iso*-propyl substituted complex **15b** was noted at 50 bar and 120 °C with 86.9 %. With both complexes high yields were accompanied by low *n*-selectivities of 37.7 % for **15a** and 35.3 % for **15b**. These results can be rationalized by extended double bond isomerization. For all other experiments *n*-selectivities were around 50 %.

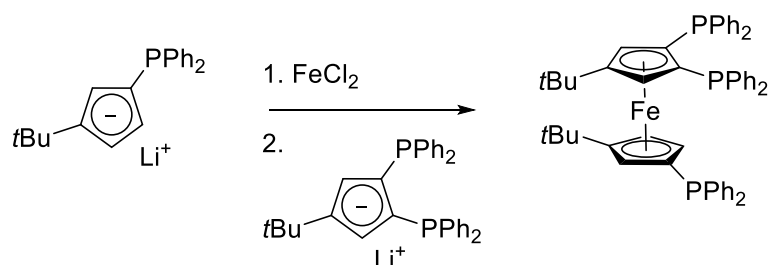
Overall, the PNP-pincer complexes, which were tested in the framework of this study, did not fulfil the anticipated positive hydroformylation properties even though aldehyde yields of over 80 % were achieved. It is especially disadvantageous that the presented complexes either show a significant ratio of side reaction or initiate a strong double bond isomerization.

3 Results and discussion

3.3 Investigation of a potentially tridentate coordinating ferrocenyl ligand

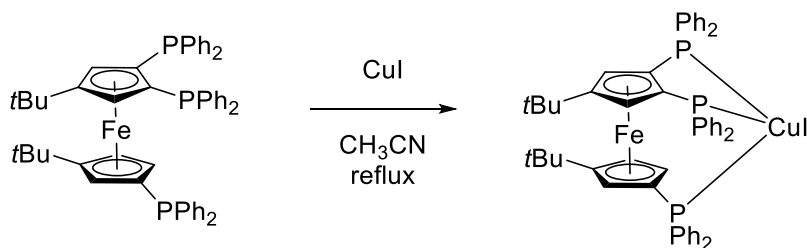
3.3 Investigation of a potentially tridentate coordinating ferrocenyl ligand

For the third topic of this thesis a potentially tridentate ferrocenyl ligand was investigated with respect to its hydroformylation properties. As an exemplary ligand the phenyl substituted 1,1',2-tris(diphenylphosphino)-3',4-di-*tert*-butylferrocene, also referred to as HiersoPHOS-2, was studied in detail. The ligand was first synthesized by the research group of Hierso in the attempt of developing several sterically hindered ferrocene backbone-based polydentate phosphine ligands without the need of an ansa-bridge.¹²⁰ Therefore, two *tert*-butyl groups were incorporated in the backbone of the structure with the aim that all three phosphine moieties point in the same direction. The triphosphine is usually synthesized by reacting alkali metal salts of adequately substituted cyclopentadienyl (cp) rings with iron dichloride, as described in Scheme 34.



Scheme 34: Synthesis procedure of HiersoPHOS-2.

The triphosphine and some analogues were already studied concerning coordination properties to copper and palladium as well as their behavior in CH-activation and palladium-catalyzed coupling reactions.¹²¹⁻¹²³ It was found that HiersoPHOS-2 coordinates in a tridentate fashion to copper salts, as depicted in Scheme 35.¹²¹



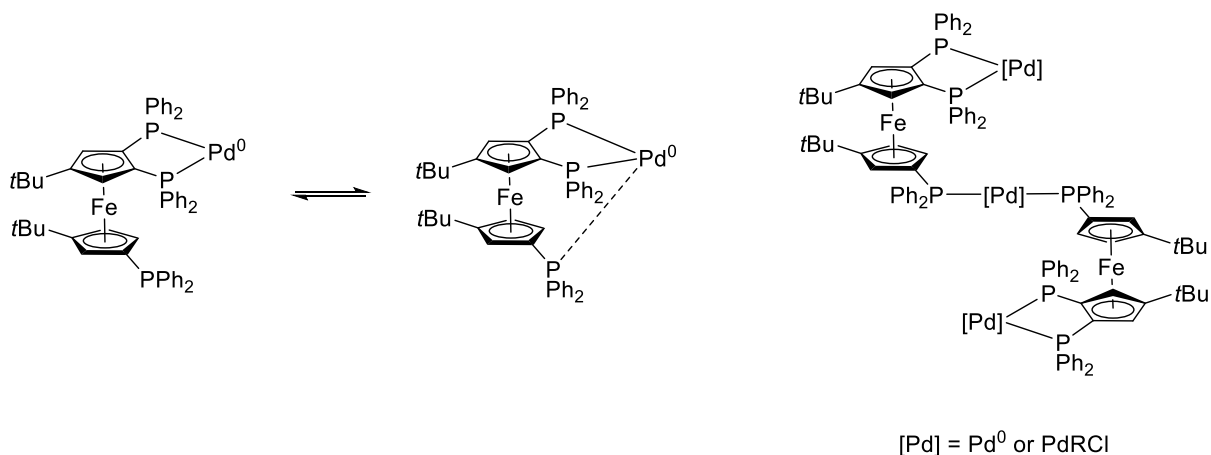
Scheme 35: Coordination mode of HiersoPHOS-2 to copper iodide.

In contrast, the ligand coordinates to palladium in a more sophisticated manner. Studies of Hierso and co-workers indicate that one palladium center is coordinated to the two phosphine moieties of the upper cp-ring. The remaining phosphine of the lower cp-ring is bound to another palladium

3 Results and discussion

3.3 Investigation of a potentially tridentate coordinating ferrocenyl ligand

atom in a monodentate fashion simultaneously bridging two ligands resulting in multimetallic complexes (Scheme 36).¹²¹ Moreover, due to the catalytic properties and their comparison to similar ferrocenyl ligands with varying number of coordinating groups, a coordination of all three phosphorus groups in a tridentate manner can be assumed during the catalytic cycle.¹²⁴



Scheme 36: Coordination mode of HiersoPHOS-2 to palladium.

Also, a stabilizing effect of the polydentate ligand on Pd⁰-species was described, resulting in slower oxidative addition of arylhalogenides but higher turnover numbers. Furthermore, this stabilizing effect led to the need of significantly lower amounts of ligand compared to a structurally related diphosphine.¹²⁴ In further investigations in palladium-catalyzed coupling reactions a superior behavior, compared to several analogous ferrocenyl ligands, was observed at remarkably low catalyst loadings.^{122,123}

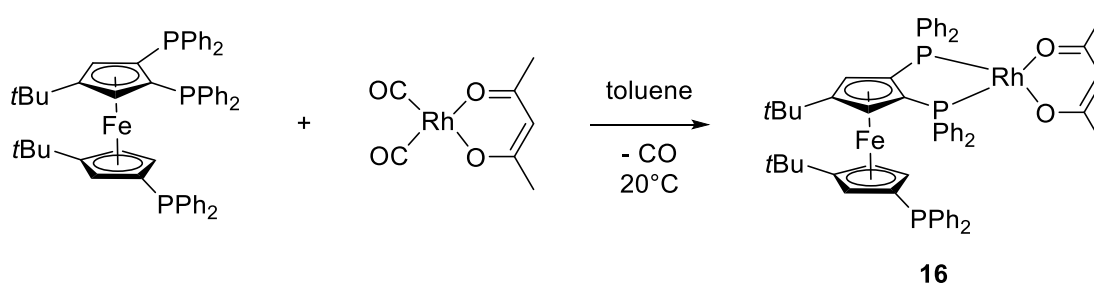
In virtue of the mentioned positive properties of this ligand, the application in hydroformylation and the coordinating behavior to rhodium were interesting.

3.3.1 Investigation of the complexation behavior of HiersoPHOS-2 to rhodium

In consideration of the results presented above, the complexation behavior of HiersoPHOS-2 to rhodium was studied. First of all, HiersoPHOS-2 was reacted with the rhodium precursor (acetylacetonato)dicarbonylrhodium(I) (Scheme 37).

3 Results and discussion

3.3 Investigation of a potentially tridentate coordinating ferrocenyl ligand



Scheme 37: Synthesis of the rhodium complex 16 with HiersoPHOS-2.

The ^{31}P NMR spectra of the uncoordinated ligand prior to the reaction (a) and the ligand after the coordination to rhodium (b) gave the signal pattern depicted in Figure 32. One singlet signal at $\delta = -19.7$ ppm is observed in both spectra. This resonance can be assigned to the single phosphorus atom of the lower cyclopentadienyl ring. Since no coupling with rhodium is observed, it can be assumed that this phosphorus atom does not coordinate to the metal. In the spectrum of the triphosphine before the reaction (a) two doublet signals at $\delta = -24.4$ ppm and $\delta = -23.7$ ppm are visible: these can be assigned to the two phosphorus atoms of the upper cyclopentadienyl ring. The doublet is generated by vicinal coupling of the two chemically but not magnetically equivalent phosphorus atoms through the aromatic structure. In the spectrum after the reaction with the rhodium precursor these signals shifted significantly to $\delta = 54.2$ ppm and $\delta = 55.8$ ppm, respectively. The two doublets became two doublets of doublets because of the coupling of both phosphorus atoms with the rhodium. Overall, the second spectrum (b), recorded at 25°C , gives proof for the coordination of rhodium only to two of the three phosphine groups, as shown in Scheme 37.

3 Results and discussion

3.3 Investigation of a potentially tridentate coordinating ferrocenyl ligand

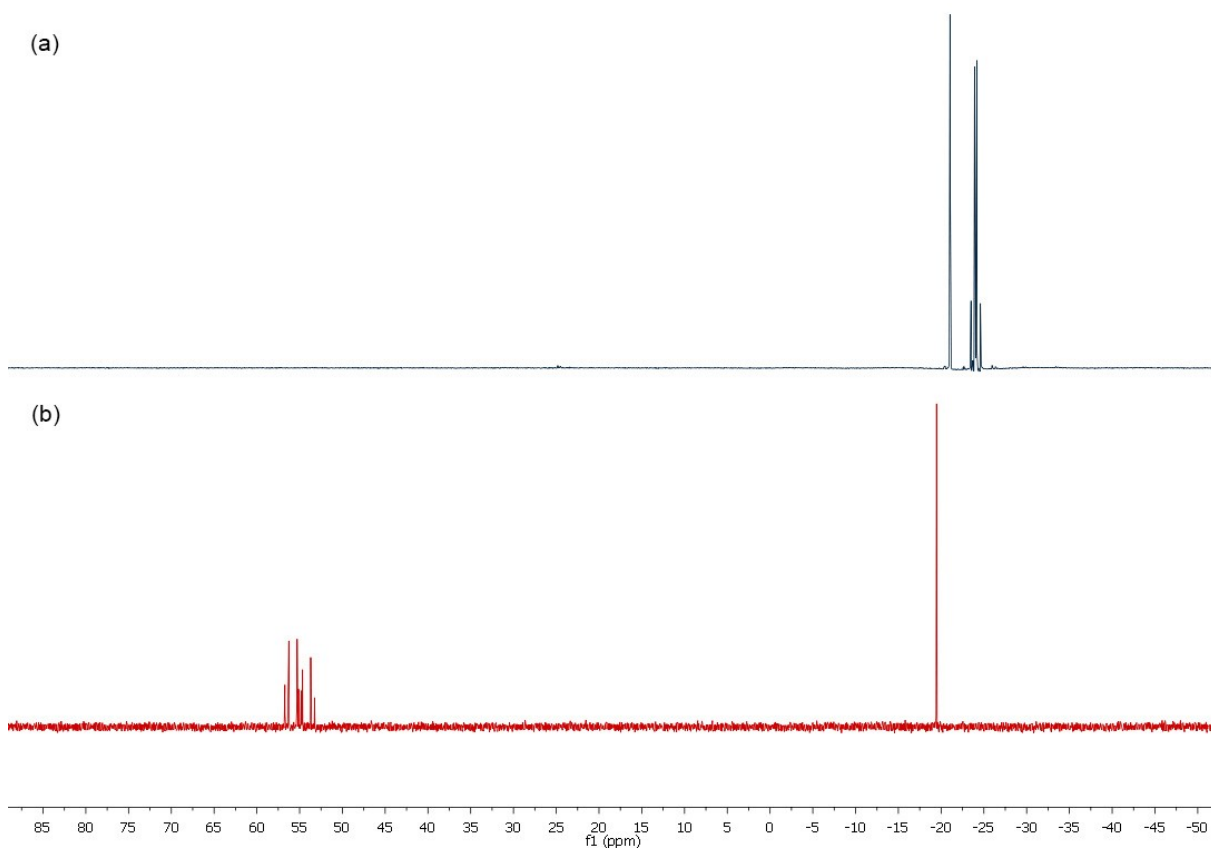


Figure 32: ^{31}P NMR spectra of HiersoPHOS-2 (a) and of the rhodium acetylacetonato complex (b).

As the coordination of the third phosphine to rhodium might be hindered by the sterically demanding groups in the backbone of the structure, it was investigated if it can coordinate at higher temperatures. Therefore, the NMR sample was heated and measured at nine temperatures in the range from 25 °C to 100 °C. These higher temperatures are especially interesting as these are common reaction conditions for hydroformylation reactions. All spectra can be seen in Figure 33.

Unfortunately, even at 100 °C no coupling of the isolated phosphorus group to rhodium and therefore no coordination of this group to the metal center was observed. It can be assumed that the potentially tridentate ligand HiersoPHOS-2 indeed only coordinates as a bidentate ligand to rhodium.

3 Results and discussion

3.3 Investigation of a potentially tridentate coordinating ferrocenyl ligand

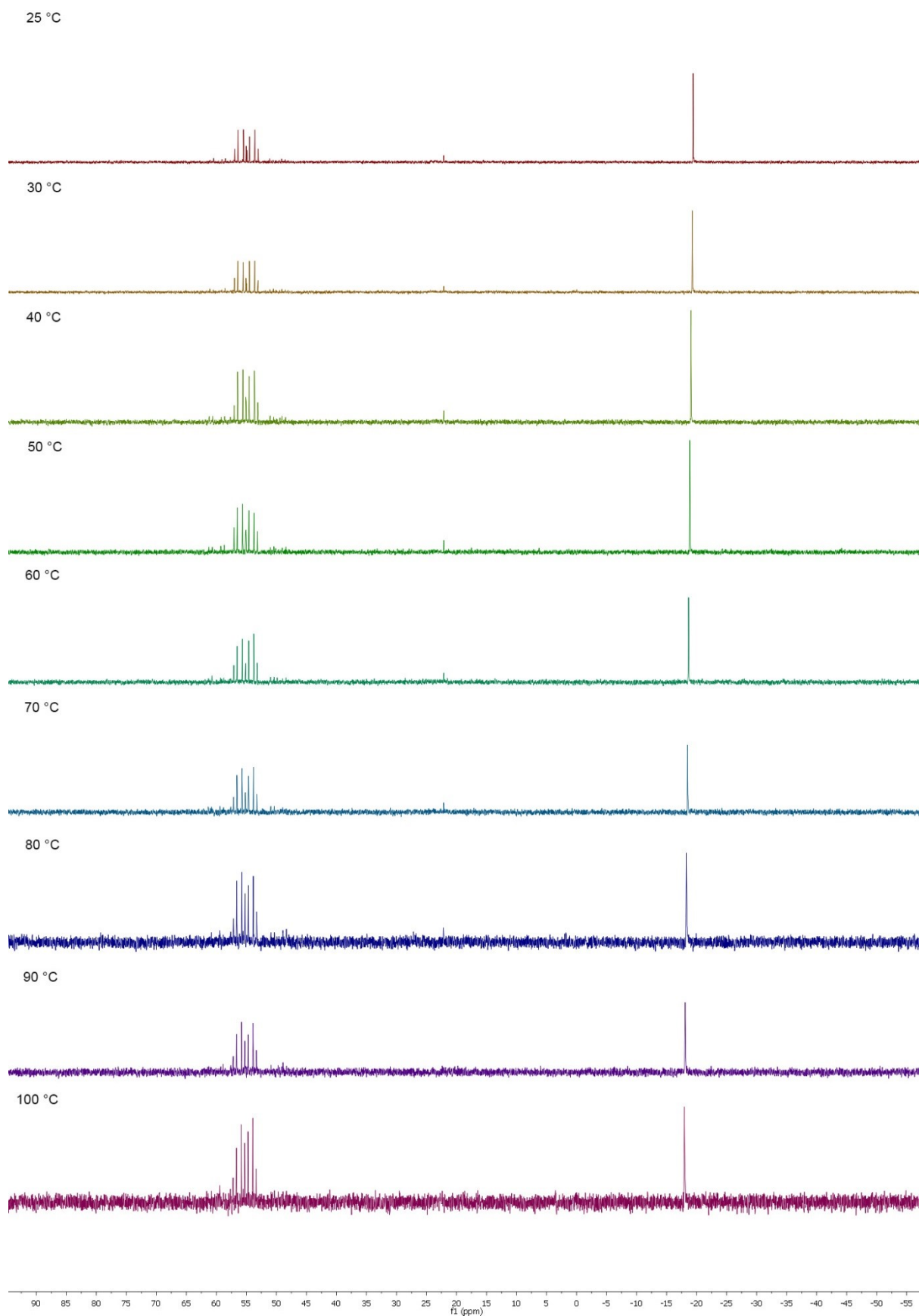


Figure 33: ^{31}P NMR spectra of the rhodium HiersoPHOS-2 complex at elevated temperatures.

3 Results and discussion

3.3 Investigation of a potentially tridentate coordinating ferrocenyl ligand

Furthermore, the reaction of HiersoPHOS-2 with the alternative rhodium precursor $[\text{Rh}(\text{COE})_2\text{Cl}]_2$ was investigated. The corresponding ^{31}P NMR spectra of the uncoordinated ligand (a) and the rhodium complex (b) are shown in Figure 34. Also, in this case the singlet at $\delta = -19.0$ ppm can be observed. But no corresponding resonance with coupling of phosphorus and rhodium are observable and the results are similar to those obtained with $\text{Rh}(\text{acac})(\text{CO})_2$.

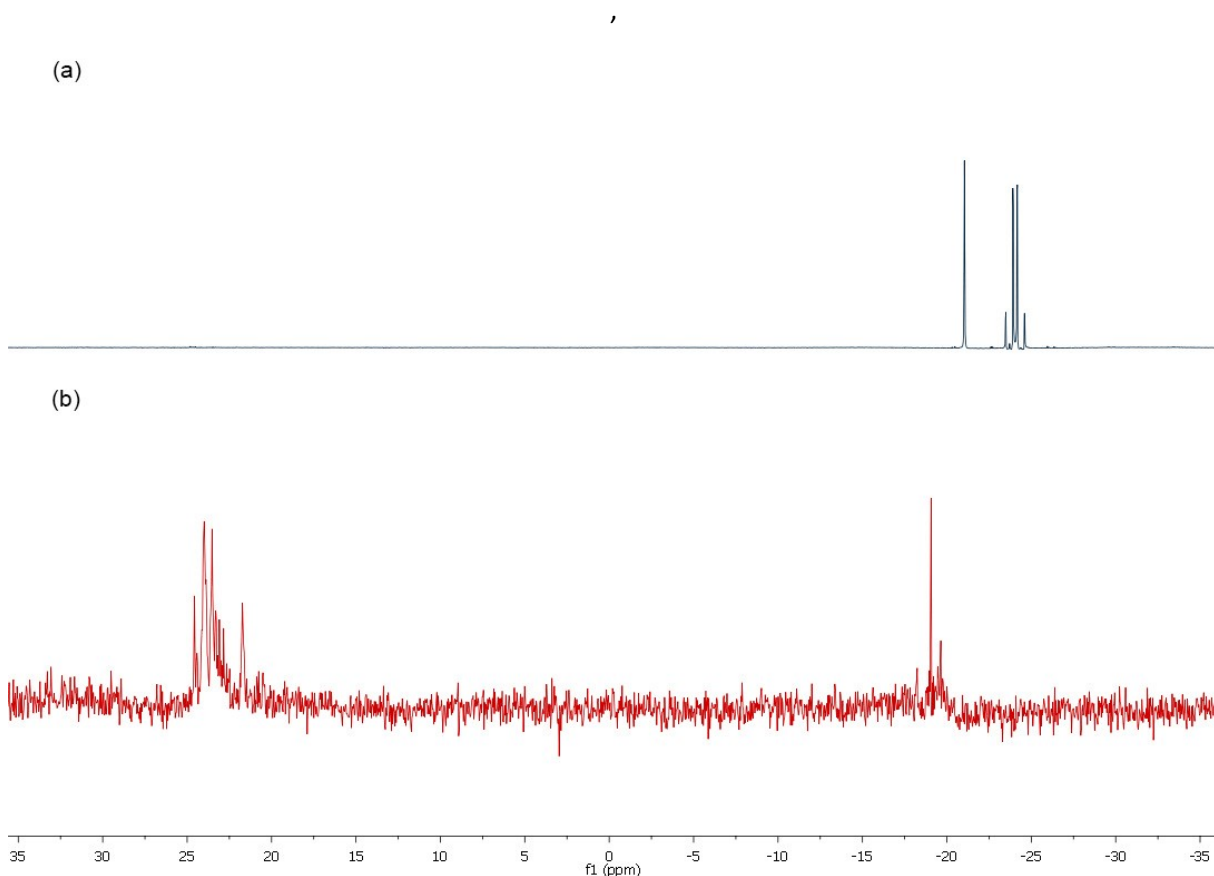


Figure 34: ^{31}P NMR spectra of HiersoPHOS-2 (a) and the corresponding rhodium complex with alternative rhodium precursor (b).

3 Results and discussion

3.3 Investigation of a potentially tridentate coordinating ferrocenyl ligand

3.3.2 Application of HiersoPhos-2 in hydroformylation

To evaluate the catalytic properties of HiersoPhos-2 it was tested in the rhodium-catalyzed hydroformylation of 1-octene. The experiments were performed in a 150 ml stainless steel autoclave manufactured by Premex Solutions GmbH (Figure 35).



Figure 35: 150 ml autoclave by Premex Solutions GmbH.

For the extensive study of the hydroformylation properties various parameters were altered, especially the ligand to rhodium ratio, as well as the syngas pressure and temperature. All results are collected in Table 11.

3 Results and discussion

3.3 Investigation of a potentially tridentate coordinating ferrocenyl ligand

Table 11: Hydroformylation^a of 1-octene with HiersoPHOS-2.

| Entry | P/Rh | <i>p</i> [bar] | <i>T</i> [°C] | Yield of Aldehyde ^b [%] | <i>n</i> -Selectivity ^b [%] | Yield of Hydrogenation product ^b [%] | <i>k</i> _{obs} ^c [min ⁻¹] |
|-------|------|----------------|---------------|------------------------------------|--|---|---|
| 1 | 2 | 20 | 120 | 21.0 | 67.1 | 40.9 | 0.055 |
| 2 | 3 | 20 | 120 | 70.4 | 62.4 | 6.0 | 0.012 |
| 3 | 6 | 20 | 120 | 5.0 | 70.9 | 15.6 | 0.004 |
| 4 | 3 | 20 | 80 | 14.3 | 92.7 | 0.3 | 0.001 |
| 5 | 3 | 20 | 100 | 38.8 | 82.0 | 4.2 | 0.005 |
| 6 | 3 | 20 | 140 | 65.1 | 54.1 | 3.1 | 0.007 |
| 7 | 3 | 10 | 80 | 13.5 | 86.8 | 2.8 | - |
| 8 | 3 | 10 | 120 | 71.3 | 62.1 | 2.0 | 0.014 |
| 9 | 3 | 50 | 80 | 11.3 | 94.7 | 1.0 | 0.001 |
| 10 | 3 | 50 | 120 | 46.2 | 80.5 | 3.8 | 0.005 |

^a[Rh] = 0.77×10⁻³ mol·L⁻¹; t = 4 h; solvent: toluene; S/Rh = 2200. ^bDetermined by GC with toluene as internal standard. ^cPseudo-first-order rate constant derived from exponential curve fitting of gas consumption versus time.

Concerning the ratio of phosphine groups and rhodium three different setups were tested ranging from a phosphorus to rhodium ratio of two to six. The results are displayed in Figure 38. The lowest ratio was chosen because of the previously mentioned multimetallic palladium complexes observed by Hierso in which one metal is bridging two ligands.¹²¹ Also, the previously described NMR experiments indicate the dominant formation of bidentate complexes. However, the implemented experiment (Table 11, entry 1) showed a comparably low yield of aldehyde. Meanwhile the rate constant of the reaction *k*_{obs} was very high compared to all other experiments. This is further supported by the gas consumption over time that does not decrease particularly, as can be seen in Figure 36. The reason for the low conversion to aldehydes could be a competitive gas consuming reaction and not the decomposition of the ligand or the catalytically active catalyst. It stands out that this conversion shows the highest amount of hydrogenation byproduct of all implemented experiments with 40.9 %. As the hydrogenation of olefins to alkanes is also a gas

3 Results and discussion

3.3 Investigation of a potentially tridentate coordinating ferrocenyl ligand

consuming side reaction, this could explain the comparably high reaction rate k_{obs} of the experiment combined with low conversions to aldehydes.

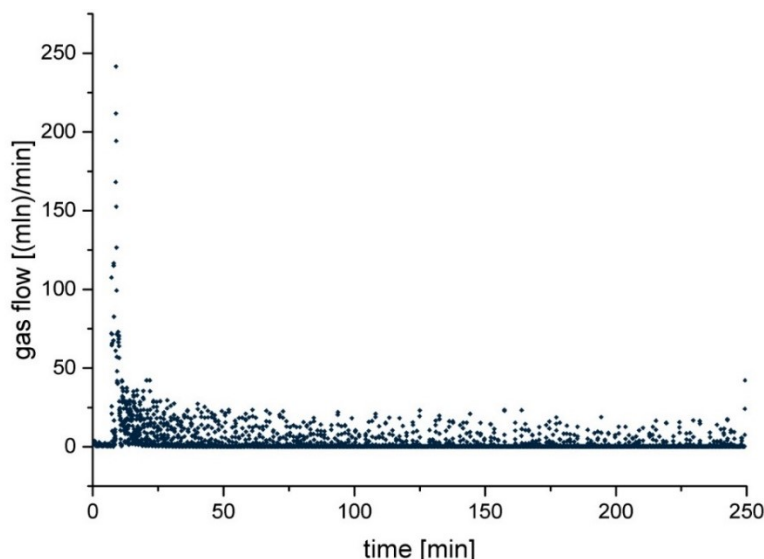


Figure 36: Gas consumption of the reaction with a P/Rh ratio of 2/1 at 120 °C and 20 bar (Table 11, entry 1).

Moreover, in the GC spectrum, which is shown in Figure 37, four signals in the area of the nonanal isomers were observed, similar to the hydroformylation results performed with PNP-complexes, which were described in chapter 3.2.3. This indicates the double bond isomerization of the used 1-octene, as this is necessary for the formation of the isomers 2-ethylheptanal and 2-propylhexanal.

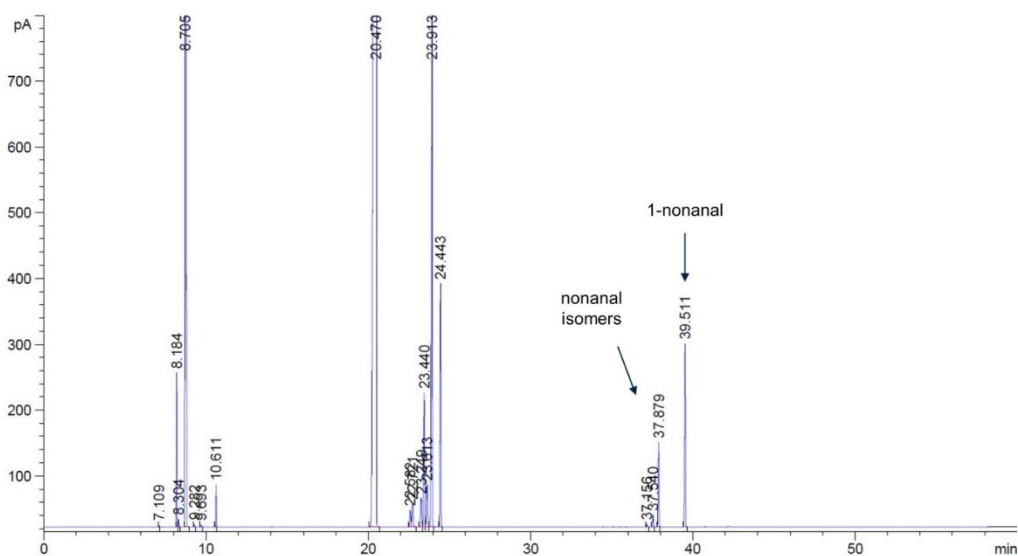


Figure 37: GC spectrum of the hydroformylation reaction at a phosphorus to rhodium ratio of 2/1, at 120 °C and 20 bar (Table 11, entry 1).

3 Results and discussion

3.3 Investigation of a potentially tridentate coordinating ferrocenyl ligand

The highest yield of aldehyde was observed by the use of three equivalent of phosphorus to rhodium whereas simultaneously the amount of hydrogenation byproduct decreased to 6.0 % (Table 11, entry 2). When the ratio of P/Rh was elevated to six the yield of aldehyde significantly dropped to only 5.0 % paired with a very low activity expressed by a rate constant k_{obs} of 0.004 min^{-1} (entry 3). This may be due to an inhibitory effect of the ligand as two ligands could possibly coordinate to the rhodium center in a bidentate manner. This would lead to the blocking of coordination positions at the metal center accompanied by the displacement of carbon monoxide under formation of a $[\text{RhHL}_4]$ complex. The latter does not promote the hydroformylation (compare chapter 1.1.2 Scheme 7). The formation of 15.6 % of hydrogenation product supports this hypothesis.

As shown in Figure 38 the n -selectivity of the conversion slightly dropped from 67.1 % to 62.4 % when the ratio of phosphorus to rhodium was increased from 2 to 3 whereas it rose again to 70.9 % at a ratio of 6. The behavior again confirms the observation from chapter 3.1.2.2 that high activity, in this case expressed by the aldehyde yield, is often accompanied by low n -selectivity.

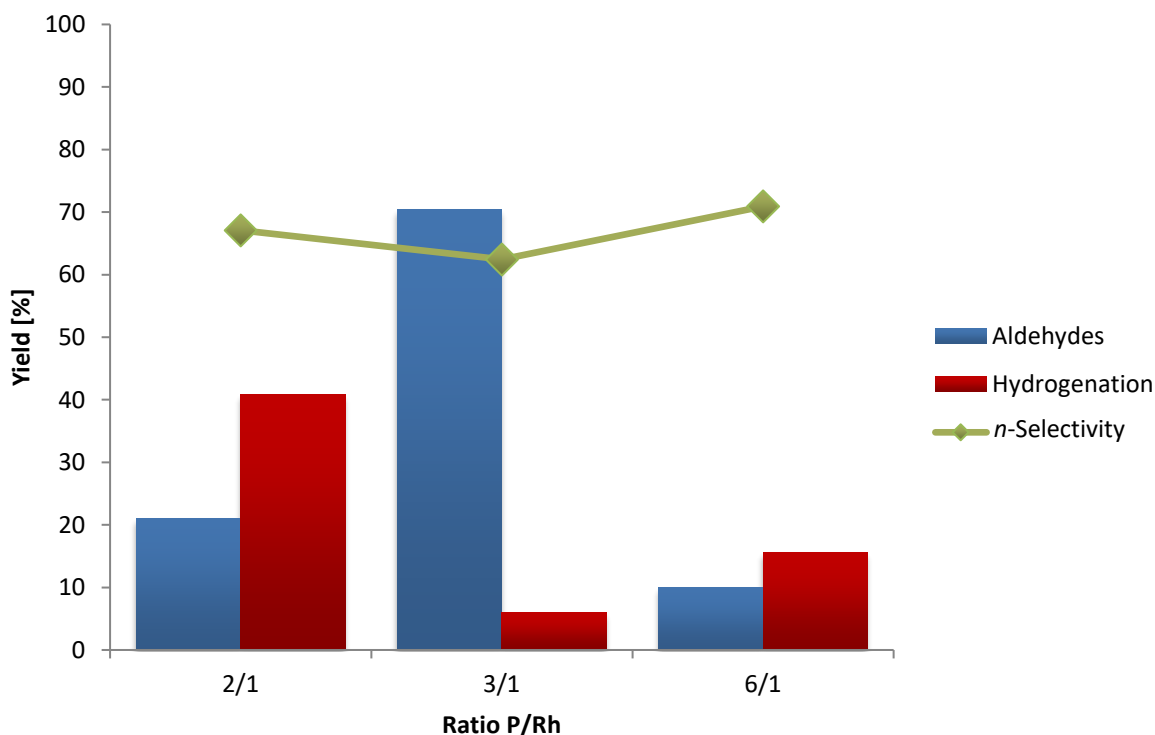


Figure 38: Yield of aldehydes, hydrogenation product and the n -selectivity at different ratios of P/Rh and a temperature of 120 °C and syngas pressure of 20 bar.

Because of the formerly described results, the ratio for all following experiments was set at a P/Rh ratio of 3/1. Subsequently, the temperature dependence of the conversion was investigated. As

3 Results and discussion

3.3 Investigation of a potentially tridentate coordinating ferrocenyl ligand

visualized in Figure 39 the aldehyde yield increased from 80 °C to 120 °C from a very poor yield of 14.3 % to a satisfactory yield of 70.4 % (Table 11, entries 2, 4 and 5). When the temperature was further elevated to 140 °C the yield stayed approximately the same with 65.1 % (Table 11, entry 6). The rate constant k_{obs} followed the same general trend in a slightly more pronounced way. At the same time the n -selectivity dropped from 92.7 % to 54.1 %, which again confirms the formerly mentioned correlation of activity and selectivity of the conversion.

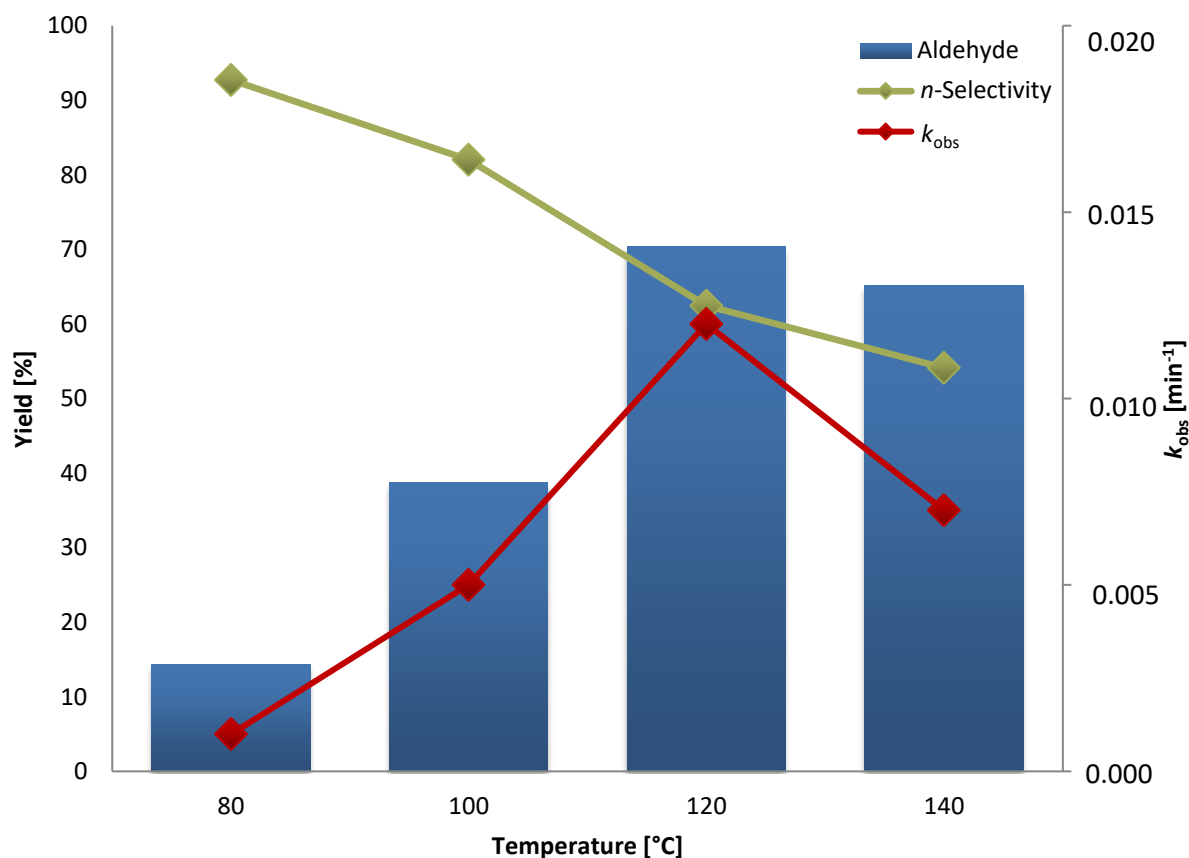


Figure 39: Yield of aldehydes and n -selectivity at varying reaction temperatures, P/Rh ratio of 3/1 and a syngas pressure of 20 bar.

As a third parameter the influence of the syngas pressure on the reaction was investigated. The visualized results of the yield and n -selectivity of the experiments are combined in Figure 40. As already covered in the paragraph before, it is a striking observation that the yield of aldehyde at 80 °C is lower than at 120 °C independent from the pressure. Moreover, it can be observed that the yield of aldehydes at a reaction temperature of 80 °C stayed approximately the same at varying syngas pressures but the n -selectivity increased from lower to higher pressures by up to 94.7 % (Table 11, entry 9).

3 Results and discussion

3.3 Investigation of a potentially tridentate coordinating ferrocenyl ligand

At 120 °C the yield of aldehyde was also almost the same, even when the syngas pressure was increased from 10 bar (71.3 %, entry 8) to 20 bar (70.4 %, entry 2). When the pressure was further elevated to 50 bar the yield decreased from 70.4 % to 46.2 % (entry 10). An increase of *n*-selectivity towards higher pressures, similar to the experiments at 80 °C, can also be observed at 120 °C. In this case the change from the lower pressures of 10 bar (62.1 %, entry 8) and 20 bar (62.4 %, entry 2) towards 50 bar was even more pronounced and led to a *n*-selectivity of 80.5 % (entry 10).

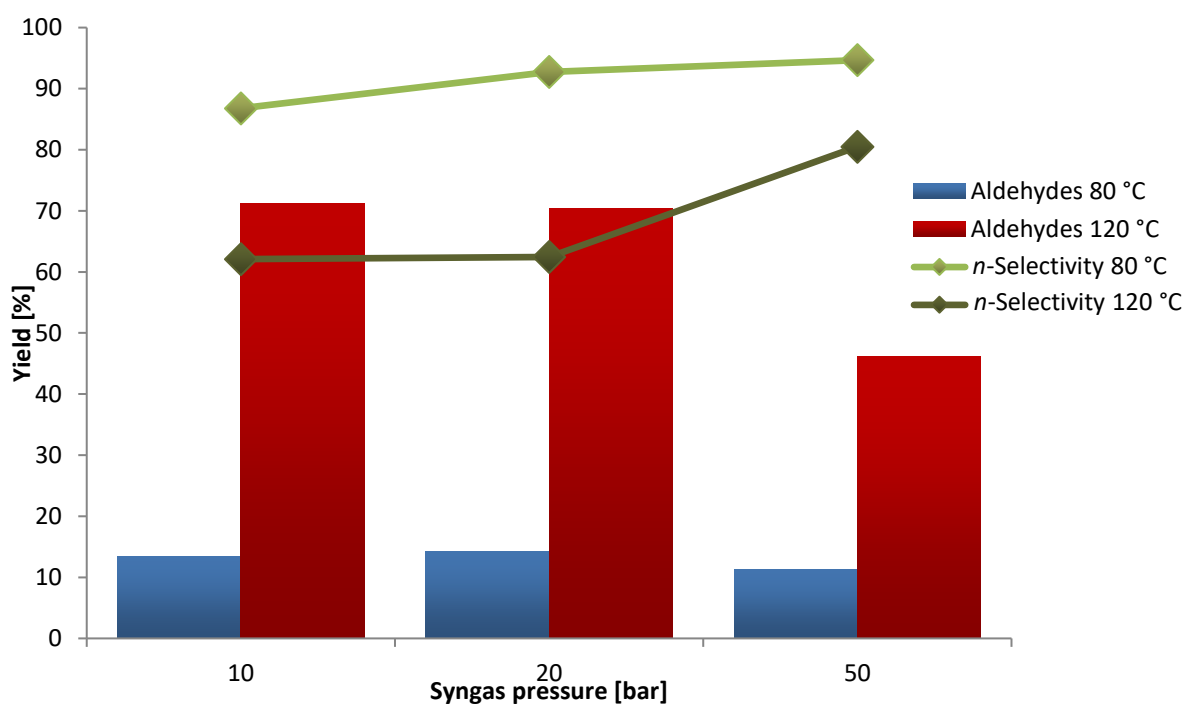


Figure 40: Yield of aldehydes and *n*-selectivity at varying syngas pressure, P/Rh ratio of 3/1 and at temperatures of 80 °C and 120 °C.

3.3.3 Factorial Design

In addition, the obtained results of the hydroformylation experiments were examined with the help of Factorial Design. By systematic change of the whole process or single reaction parameters this mathematical methodology is used to identify significant factors of a reaction, to rationalize their impact in the process, the way they interact and the prediction of optimal values for the process variables.¹²⁵ This kind of experimental design can be applied on several areas, such as chemistry,^{125,126} pharmaceutical industry,¹²⁷ as well as chemical and process engineering.¹²⁸

3 Results and discussion

3.3 Investigation of a potentially tridentate coordinating ferrocenyl ligand

In this thesis, a three-level two-factor 3^2 experimental design following standard methodology¹²⁵ was applied using pressure (p) and temperature (T) as variables for the optimization of aldehyde yield and regioselectivity. The general equation (3) was used:

$$y = a_0 + a_p p + a_T T + a_{pT} pT \quad (3)$$

where y denotes either the percentage of yield of aldehyde or the percentage of linear n -aldehyde obtained. Furthermore, a_0 describes an intercept of the equation, a_p and a_T represent linear terms representing each of the two parameters, whereas a_{pT} represents an interaction term of pressure and temperature.

3.3.3.1 Determination of the yield of the reaction

For the determination of the terms of equation (3) the results of selected hydroformylation experiments are listed down in Table 12, but can also be found in Table 11 in the previous chapter.

First the effect of the two parameters, pressure and temperature, on the yield of aldehyde from 1-octene was addressed by the modelling tool of Factorial Design. While the first four entries of Table 12 were essential for the determination of the equation terms, the last two entries 5 and 6 were needed for the test on significance of the parameters. The coding of -1, 0, +1 was assigned to the different levels of the observed parameter: -1 for the lowest level, 0 for the middle level and +1 for the highest level.

A lot of the work on significance goes back on the work of Student, whose true name was W. S. Gosset and who worked as a brewer for the Guinness' Brewery in Dublin, and later R. A. Fisher.^{125,129} In general, the term statistical significance means that the result is very unlikely to have occurred without the influence of a certain parameter.¹³⁰ In the framework of this thesis the significance of the parameters, temperature and pressure, was defined by a Student's t -test, which is a statistical hypothesis test. It can only be performed when there are more experimental data points than parameters in the model.

3 Results and discussion

3.3 Investigation of a potentially tridentate coordinating ferrocenyl ligand

Table 12: Selected results for the hydroformylation^a of 1-octene with obtained yield of aldehyde and coding according to Factorial Design.

| Entry | <i>p</i> [bar] | | <i>T</i> [°C] | | Yield of Aldehyde (<i>y</i>) ^b [%] |
|-------|----------------|------|---------------|------|--|
| | [bar] | code | [°C] | code | |
| 1 | 10 | -1 | 80 | -1 | 13.5 |
| 2 | 10 | -1 | 120 | +1 | 71.3 |
| 3 | 50 | +1 | 80 | -1 | 11.3 |
| 4 | 50 | +1 | 120 | +1 | 46.2 |
| 5 | 20 | 0 | 120 | +1 | 70.4 |
| 6 | 20 | 0 | 80 | -1 | 14.3 |

^a[Rh] = 0.77·10⁻³ mol·L⁻¹; t = 4 h; solvent: toluene; S/Rh = 2200; P/Rh = 3. ^bDetermined by GC with toluene as internal standard.

The needed design matrix *D*, as seen in Table 13, was formed wherein the rows refer to the chosen experiments and the columns refer to the terms of the equation.

Table 13: Design matrix *D* for the investigation concerning the yield of aldehyde.

| <i>a</i> ₀ | <i>a</i> _{<i>p</i>} | <i>a</i> _{<i>T</i>} | <i>a</i> _{<i>pT</i>} |
|-----------------------|------------------------------|------------------------------|-------------------------------|
| 1 | 10 | 80 | 800 |
| 1 | 10 | 120 | 1200 |
| 1 | 50 | 80 | 4000 |
| 1 | 50 | 120 | 6000 |
| 1 | 20 | 120 | 2400 |
| 1 | 20 | 80 | 1600 |

Proceeding from the data given in Table 13, the values of the terms can be derived with equation (4):

$$\mathbf{a} = (\mathbf{D}' \cdot \mathbf{D})^{-1} \cdot \mathbf{D}' \cdot \mathbf{y} \quad (4)$$

where *D'* refers to the transposed design matrix *D*.

3 Results and discussion

3.3 Investigation of a potentially tridentate coordinating ferrocenyl ligand

Also, the estimated values for \hat{y} can be determined by equation (5):

$$\hat{y} = D \cdot a \quad (5)$$

The obtained results for the values of the terms as well as the experimental (y) and estimated (\hat{y}) results for the yield of aldehyde of the reaction under altered reaction conditions are listed in Table 14.

Table 14: Values for a , experimental (y) and estimated (\hat{y}) results for the yield of aldehyde.

| Term | Value | y | \hat{y} |
|----------|----------|------|-----------|
| a_0 | -116.576 | 13.5 | 14.1 |
| a_p | 1.141 | 71.3 | 73.8 |
| a_T | 1.642 | 11.3 | 11.5 |
| a_{pT} | -0.015 | 46.2 | 47.0 |
| | | 70.4 | 67.1 |
| | | 14.3 | 13.5 |

For the determination of the terms, required for the Student's t -test, the coded design matrix D_c and the calculated matrix $(D_c' \cdot D_c)^{-1}$ are needed: they can be found in Table 15 and Table 16, respectively. The numbers in the diagonal of this matrix determine the variance v for each term so that, for example, $v_0 = 0.143$ represents the variance of a_0 .

Table 15: Coded design matrix D_c for the yield of aldehyde.

| a_0 | a_p | a_T | a_{pT} |
|-------|-------|-------|----------|
| 1 | -1 | -1 | +1 |
| 1 | -1 | +1 | -1 |
| 1 | +1 | -1 | -1 |
| 1 | +1 | +1 | +1 |
| 1 | 0 | +1 | 0 |
| 1 | 0 | -1 | 0 |

3 Results and discussion

3.3 Investigation of a potentially tridentate coordinating ferrocenyl ligand

Table 16: Matrix $(D_C' \cdot D_C)^{-1}$.

| | a_0 | a_p | a_T | a_{pT} |
|----------|--------------|--------------|--------------|--------------|
| a_0 | 0.167 | 0 | 0 | 0 |
| a_p | 0 | 0.250 | 0 | 0 |
| a_T | 0 | 0 | 0.167 | 0 |
| a_{pT} | 0 | 0 | 0 | 0.250 |

For the determination of the significance, the error sum of squares between the observed and the estimated results are also necessary. They were calculated using equation (6) and the data given in Table 14:

$$S_{resid} = \sum_{i=1}^I (y_i - \hat{y}_i)^2 = \mathbf{18.760.} \quad (6)$$

Afterwards the error sum of squares was divided by the degrees of freedom using equation (7):

$$s = \frac{S_{resid}}{N - P} = \mathbf{9.380} \quad (7)$$

wherein N refers to the number of experiments (in this case 6) and P refers to the number of terms or parameters (in this case 4). Therefore, the Student's t -test cannot be performed when the number of experiments equals the number of terms as this would result in 0 degrees of freedom.

Using the previously obtained data, t can be calculated for every coefficient a using equation (8):

$$t = a / \sqrt{sv} \quad (8)$$

wherein s refers to the error sum of squares and v is the variance for every term derived from the diagonal of the matrix shown in Table 16. The higher this ratio the more significant is the coefficient.

Finally, the statistical significance was obtained from a two-tailed t -distribution. In this case the probability values were determined using EXCEL function TDIST by entering the absolute values for t , the degrees of freedom and the number of sides (two in this case). All data used and obtained are collected in Table 17.

3 Results and discussion

3.3 Investigation of a potentially tridentate coordinating ferrocenyl ligand

Table 17: Values of t and significance.

| Term | Coded Value | ν | $\sqrt{s\nu}$ | t | Probability [%] |
|----------|-------------|-------|---------------|--------|-----------------|
| a_0 | 37.823 | 0.167 | 1.250 | 30.251 | >99.9 |
| a_p | -6.814 | 0.250 | 1.531 | -4.449 | 98.9 |
| a_T | 24.793 | 0.167 | 1.250 | 19.829 | >99.9 |
| a_{pT} | -5.724 | 0.250 | 1.531 | -3.738 | 98.0 |

The obtained results indicate that the pressure is significant for the yield of the reaction with a probability of 98.9 % and the temperature with a probability of over 99.9 %. Also, the interaction between pressure and temperature represented by a_{pT} indicates a high significance with a probability of 98.0 %. From these three parameters temperature possesses the highest absolute value for t indicating that it also has the highest impact on the yield of the aldehyde. The absolute values of t for pressure and the interaction of pressure and temperature are significantly lower than the value obtained for temperature.

Adding the uncoded values for the reaction terms, which are collected in Table 14, in equation (3) the following equation (9) for the linear model of the yield results:

$$y = -116.576 + 1.141 \cdot p + 1.642 \cdot T - 0.015 \cdot pT \quad (9)$$

To verify the precision of the model, two experimental results, which were not included in the generation of the model, were compared to the results obtained by using equation (9). For a pressure of 20 bar and a temperature of 100 °C the model predicts a yield of 40.3 %, which can be considered as a good agreement with the experimentally obtained result of 38.8 % (Table 11, entry 5). For reaction conditions with a pressure of 20 bar and a temperature of 140 °C, a yield of 93.9 % is predicted whereas the experiment only gave a yield of 65.1 % (Table 11, entry 6). This indicates that at higher temperatures an unknown effect, that was not taken into account during the generation of the model, plays a role. This shows that Factorial Design is a useful modeling tool for the prediction and optimization of chemical reaction but it should also be used carefully. Sometimes not all possible factors are taken into account while generating the model, and therefore deviations of the model from actual experimental results are possible.

Using equation (9), the response surface of the regioselectivity of the reaction was derived: this can be seen in Figure 41. It gives proof that the yield is strongly dependent of the reaction temperature. If the temperature is increased a higher yield is obtained. The model predicts that in the investigated range of up to 100 bar at least a temperature of 18 °C is required which gets even

3 Results and discussion

3.3 Investigation of a potentially tridentate coordinating ferrocenyl ligand

more obvious in the depiction of the 0 % yield line projected onto the pressure/temperature plane, as can be seen in Figure 42. Since our autoclave can only be used for pressures up to 50 bar, at this pressure, according to the model, temperatures of at least 67 °C must be applied to generate conversion.

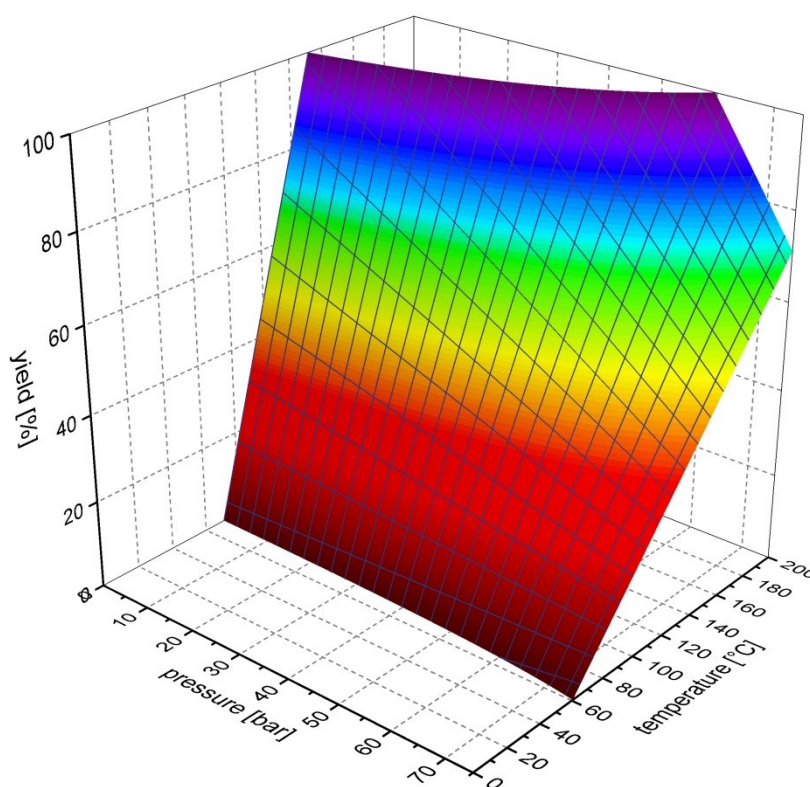


Figure 41: Three-dimensional representation of the response surface of yield derived from equation (9).

It is also noticeable that if the temperature is further increased, the yield is rising faster at lower pressures than at higher pressures. This behavior is also visible in Figure 43, which depicts the 100 % yield line projected onto the pressure/temperature plane. Also, in this representation it is visible that a yield of 100 % can only be achieved at temperatures beyond 130 °C independent from the applied pressure. Furthermore, it can be concluded that the higher the pressure, the higher the temperature must be in order to achieve a yield of 100 %. For example, at a pressure of 50 bar a temperature of 180 °C is needed. Also, for instance at a pressure of 20 bar a temperature of 144 °C is required to achieve complete conversion, according to the model. Very similar reaction conditions were already tested with a pressure of 20 bar and a temperature of 140 °C whereby only a conversion of 65.1 % was achieved experimentally. This observation underlines that at higher temperatures an unknown factor plays a role which was not included in the generation of the model. Such high temperatures usually lead to the degradation of the catalyst

3 Results and discussion

3.3 Investigation of a potentially tridentate coordinating ferrocenyl ligand

or the ligand, used to generate the catalytically active species. Therefore, it could be more useful to elongate the reaction time to achieve higher yields than increasing the temperature over 120 °C.

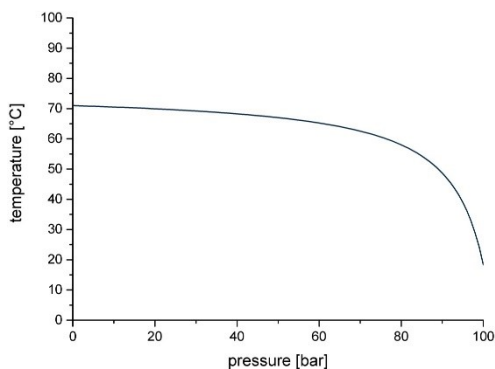


Figure 42: Projection of the yield of aldehyde = 0 % line onto the pressure/temperature plane.

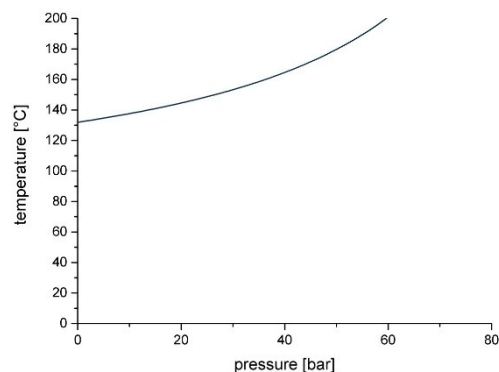


Figure 43: Projection of the yield of aldehyde = 100 % line onto the pressure/temperature plane.

By comparing the two diagrams Figure 42 and Figure 43 it is also striking that from 0 % yield to 100 % yield of aldehyde the general effect of the alteration of pressure on to the required temperature is inverted. This means that the projection for 0 % aldehyde yield the temperature can be lower at higher pressures. Meanwhile, the projection for an aldehyde yield of 100 % indicates that higher temperatures are required with increasing pressure to retain optimal yield.

3.3.3.2 Determination of the regioselectivity of the reaction

For the determination of the terms mentioned in the general equation (3) concerning the n -selectivity of the hydroformylation of 1-octene, the results of selected experiments and the corresponding coding are listed in Table 18.

3 Results and discussion

3.3 Investigation of a potentially tridentate coordinating ferrocenyl ligand

Table 18: Selected results for the hydroformylation^a of 1-octene with obtained *n*-selectivity and coding according to Factorial Design.

| Entry | <i>p</i> [bar] | | <i>T</i> [°C] | | <i>n</i> -Selectivity (<i>y</i>) ^b |
|-------|----------------|------|---------------|------|---|
| | [bar] | code | [°C] | code | [%] |
| 1 | 10 | -1 | 80 | -1 | 86.8 |
| 2 | 10 | -1 | 120 | +1 | 62.1 |
| 3 | 50 | +1 | 80 | -1 | 94.7 |
| 4 | 50 | +1 | 120 | +1 | 80.5 |
| 5 | 20 | 0 | 120 | +1 | 62.4 |
| 6 | 20 | 0 | 80 | -1 | 92.7 |
| 7 | 20 | 0 | 100 | 0 | 82.0 |

^a[Rh] = 0.77·10⁻³ mol·L⁻¹; t = 4 h; solvent: toluene; S/Rh = 2200; P/Rh = 3. ^bDetermined by GC with toluene as internal standard.

Again, the first step was the determination of the significance of the parameters pressure and temperature using a Student's *t*-test. The needed design matrix *D* can be seen in Table 19.

Table 19: Design matrix *D* for the investigation concerning the *n*-selectivity of the reaction.

| <i>a</i> ₀ | <i>a</i> _{<i>p</i>} | <i>a</i> _{<i>T</i>} | <i>a</i> _{<i>pT</i>} |
|-----------------------|------------------------------|------------------------------|-------------------------------|
| 1 | 10 | 80 | 800 |
| 1 | 10 | 120 | 1200 |
| 1 | 50 | 80 | 4000 |
| 1 | 50 | 120 | 6000 |
| 1 | 20 | 120 | 2400 |
| 1 | 20 | 80 | 1600 |
| 1 | 20 | 100 | 2000 |

Also from this data the value of the terms can be calculated using equation (4) and again the estimated values for \hat{y} were derived from equation (5). These results and the experimentally obtained results for the yield of aldehydes (*y*) can be found in Table 20.

3 Results and discussion

3.3 Investigation of a potentially tridentate coordinating ferrocenyl ligand

Table 20: Values for a , experimental (y) and estimated (\hat{y}) results for the n -selectivity.

| Term | Value | y | \hat{y} |
|----------|---------|------|-----------|
| a_0 | 149.708 | 86.8 | 89.4 |
| a_p | -0.461 | 62.1 | 61.6 |
| a_T | -0.773 | 94.7 | 95.6 |
| a_{pT} | 0.008 | 80.5 | 80.0 |
| | | 62.4 | 66.2 |
| | | 92.7 | 91.0 |
| | | 82.0 | 78.6 |

As already mentioned in the previous section, for the determination of the terms needed for the Student's t -test, the coded design matrix D_C and the calculated matrix $(D_C' \cdot D_C)^{-1}$ are required: they are written in Table 21 and Table 22, respectively.

Table 21: Coded design matrix D_C for the n -selectivity.

| a_0 | a_p | a_T | a_{pT} |
|-------|-------|-------|----------|
| 1 | -1 | -1 | +1 |
| 1 | -1 | +1 | -1 |
| 1 | +1 | -1 | -1 |
| 1 | +1 | +1 | +1 |
| 1 | 0 | +1 | 0 |
| 1 | 0 | -1 | 0 |
| 1 | 0 | 0 | 0 |

Table 22: Matrix $(D_C' \cdot D_C)^{-1}$.

| | a_0 | a_p | a_T | a_{pT} |
|----------|--------------|--------------|--------------|--------------|
| a_0 | 0.143 | 0 | 0 | 0 |
| a_p | 0 | 0.250 | 0 | 0 |
| a_T | 0 | 0 | 0.167 | 0 |
| a_{pT} | 0 | 0 | 0 | 0.250 |

3 Results and discussion

3.3 Investigation of a potentially tridentate coordinating ferrocenyl ligand

The error sum of squares between the observed and estimated results were again calculated by equation (6) and the data given in Table 20. The results can be found in equation (10):

$$S_{resid} = \sum_{i=1}^I (y_i - \hat{y}_i)^2 = 39.780. \quad (10)$$

Afterwards the error sum of squares is divided by the degrees of freedom using equation (11):

$$s = \frac{S_{resid}}{N-P} = 13.260. \quad (11)$$

In this case $N = 7$, as seven experiments were performed, and again four parameters P were considered in the general equation (3).

The values for t and the corresponding probability for the n -selectivity were determined in the same way as described in the previous section, and the results as well as the used values are collected in Table 23.

Table 23: Values of t and significance.

| Term | Coded Value | ν | $\sqrt{s\nu}$ | t | Probability [%] |
|----------|-------------|-------|---------------|-------|-----------------|
| a_0 | 80.330 | 0.143 | 1.376 | 58.36 | >99.9 |
| a_p | 6.320 | 0.250 | 1.821 | 3.57 | 96.0 |
| a_T | -11.359 | 0.167 | 1.487 | -7.64 | 99.5 |
| a_{pT} | 2.379 | 0.250 | 1.821 | 1.31 | 71.8 |

The results show that with a 96.0 % and 99.5 % probability, pressure and temperature have a significant influence on the regioselectivity of the reaction whereas the interaction of pressure and temperature is only significant with a 71.8 % probability. Also, the interaction has the lowest value of t , considering the absolute values. The absolute values indicate that the temperature has the highest impact on the regioselectivity of the reaction.

Proceeding from the general equation (3) and the values for the respective terms given in Table 20, the linear model can be derived with equation (12).

$$y = 149.708 - 0.461 \cdot p - 0.773 \cdot T + 0.008 \cdot pT \quad (12)$$

3 Results and discussion

3.3 Investigation of a potentially tridentate coordinating ferrocenyl ligand

To verify the precision of the model, an experimental result that was not used to generate the model was compared to the model's output for the specific conditions. It is found that the predicted regioselectivity of the reaction at 140 °C and 20 bar is 54.7 % while the experimental result at the same conditions is 54.1 % (as can be found in Table 11, entry 6). This can be considered as an excellent agreement of the calculated and experimental data.

Using equation (12), the response surface of the regioselectivity of the reaction was derived: it is displayed in Figure 44. It can be seen that low pressures as well as high temperatures lead to a low *n*-regioselectivity. This observation is supported by the projection of the 0 % *n*-selectivity line onto the pressure/temperature plane as can be seen in Figure 45. From this visualization it is possible to conclude, that 0 % *n*-selectivity and therefore a 100 % *b*-selectivity is achieved only at temperatures over 190 °C. As the used autoclave is approved for a maximum temperature of 150 °C the tested catalytic system can be discarded for the requirement of such conversions.

Furthermore, it is observed that higher pressures lead to higher *n*-selectivities even at temperatures over 100 °C. For example, at a pressure of 5 bar and a temperature of 100 °C a *n*-selectivity of 74 % is predicted whereas at 50 bar and the same temperature a *n*-selectivity of 89 % is predicted. Also, lower temperatures lead to a higher *n*-selectivity as well. When the pressure is kept at 25 bar while the temperature is altered from 100 °C to 150 °C, the *n*-selectivity decreases drastically from 81 % to 52 %.

3 Results and discussion

3.3 Investigation of a potentially tridentate coordinating ferrocenyl ligand

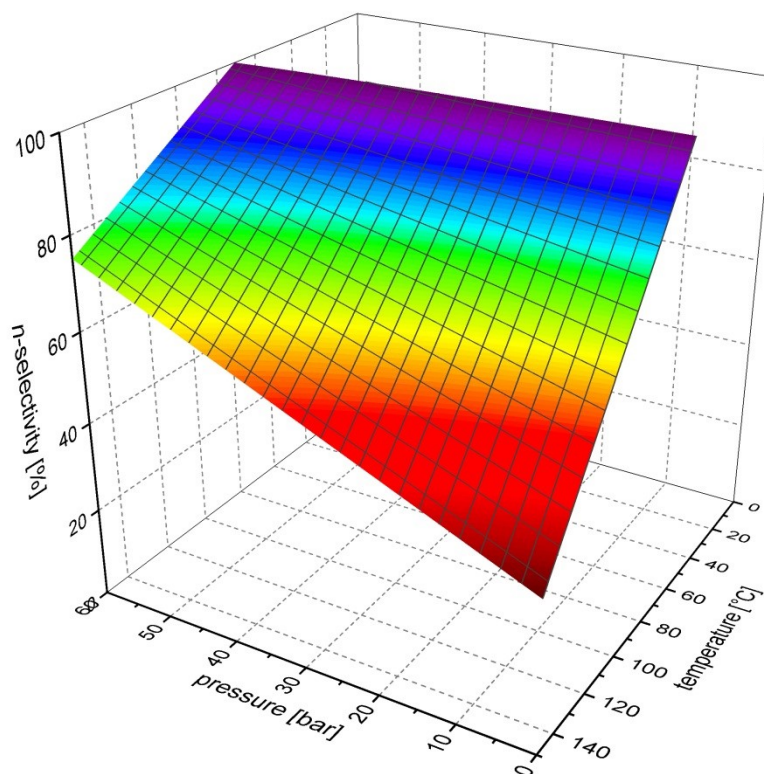


Figure 44: Three-dimensional representation of the response surface of regioselectivity derived from equation (12).

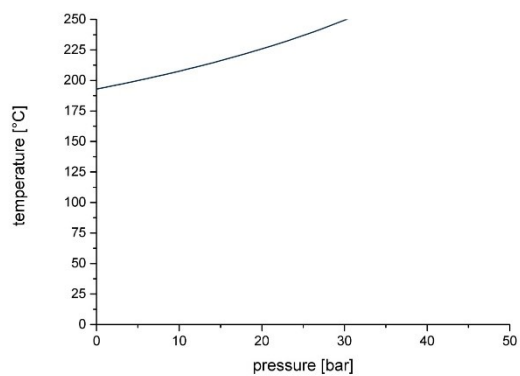


Figure 45: Projection of the n -selectivity = 0 % line onto the pressure/temperature plane.

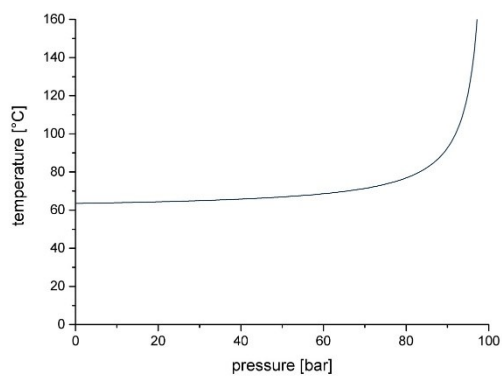


Figure 46: Projection of the n -selectivity = 100 % line onto the pressure/temperature plane.

3 Results and discussion

3.3 Investigation of a potentially tridentate coordinating ferrocenyl ligand

Equation (12) can also be used to predict the optimal conditions to achieve 100 % *n*-selectivity with 1-octene as substrate. Therefore, the equation was rewritten so that a relationship between temperature and pressure is achieved for the *n*-selectivity of 100 %. The relevant plot is shown in Figure 46. A prominent increase of the regioselectivity can therefore be obtained at very high pressures of over 90 bar. As our autoclave is only approved for pressures up to 50 bar these reaction conditions could not be tested. At a pressure of 10 bar a temperature of 64 °C and at 50 bar a temperature of 67 °C is required to realize the *n*-selectivity of 100 %. As the results of chapter 3.3.3.1 revealed, to obtain any conversion, at least a pressure of 50 bar and a temperature of 67 °C is required. These exact reaction conditions were not tested. Under these conditions the expected yield for a reaction time of four hours would be too low for a successful analysis. Instead, to increase the yield, the reaction time was prolonged from four hours to 24 hours. In the end, a syngas pressure of 50 bar, a temperature of 65 °C and a reaction time of 24 hours lead to a *n*-regioselectivity of 98.3 % paired with an overall aldehyde yield of 54.3 %. This is close to the estimated amount of 100 % *n*-regioselectivity predicted with the model especially considering the measurement error of the implemented quantification by GC analysis.

3.3.4 Conclusion

The following conclusions towards the complexation behavior and the hydroformylation properties of the potentially tridentate ferrocenyl ligand HiersoPHOS-2 can be made. In concern of the observed complexation behavior towards rhodium it can be stated that, according to the implemented NMR investigations, the ligand only coordinates in a bidentate and not in a tridentate manner to the metal center. Neither at room temperature nor at elevated temperatures of up to 100 °C coordination of the lone phosphine group located at the second cyclopentadiene ring was detected. From this complexation behavior, it has to be concluded that the ligand might also form the catalytically active species in a bidentate and not in a tridentate manner.

Furthermore, the hydroformylation properties in the conversion of 1-octene were investigated including the method of Factorial Design. Especially the effects of the ligand to rhodium ratio, as well as the alteration of syngas pressure and temperature, were investigated. The executed experiments led to the achievement of yields of aldehyde of up to 71.3 % and a *n*-regioselectivity of up to 98.3 %. By Factorial Design the influence of pressure and temperature were investigated further while reaction conditions for the achievement of 100 % yield and *n*-regioselectivity were predicted. In combination with Factorial Design, the significances of the parameters were also examined. The results pointed out that the alteration and especially the increase in temperature lead to higher yields while the application of a higher syngas pressure in combination with lower temperatures lead to a higher *n*-regioselectivity. Both observations were reinforced by the results

3 Results and discussion

3.3 Investigation of a potentially tridentate coordinating ferrocenyl ligand

obtained by the Student's *t*-test. Also, the interaction term of temperature and pressure was significant for the yield as well as for the regioselectivity. The influence was in both cases relatively small compared to the term for temperature and pressure alone. Even though it increased the accuracy of the resulting models as demonstrated by the excellent agreement of the models with experimental results that were not included in the generation of the models. In case of the optimization of the aldehyde yield the predicted results did not actually reach the achievement of a complete conversion within the chosen reaction time of four hours. Instead of an anticipated increase of yield at temperatures over 120 °C a decrease was observed. This behavior was not integrated in the generated model. Instead an elongation of the reaction time at lower temperatures could be beneficial. Moreover, a model was created to optimize the *n*-regioselectivity of the conversion. The results of high *n*-selectivities are unfortunately accompanied by low reaction rates and therefore low yields of aldehyde for the reaction time of four hours result. Therefore, an additional optimization experiment was performed at a longer reaction time of 24 hours leading to a *n*-regioselectivity of the investigated system at 50 bar and 65 °C of 98.3 %. This can be considered as an optimized result. It is satisfactory and close to the targeted 100 % regioselectivity, especially considering the measurement error of the GC analysis. Overall, the investigations using the statistical tool of Factorial Design can be considered as extremely useful in the optimization of hydroformylation reactions in particular and chemical reactions and technical processes in general. Although the optimization attempt of the aldehyde yield led to no satisfactory result as still unknown factors led to a decrease of yield at the predicted higher temperatures, the optimization of the *n*-regioselectivity can be considered as successful. Additionally, the model was comparatively easy to apply as it only consists of two reaction parameters. To improve the mathematical model more parameters could be included which would nevertheless also lead to a more complex procedure including a significantly higher number of experiments.

4 Concluding remarks

I want to conclude this thesis by discussing the influence of the ligand structure on the hydroformylation of olefins. The aim of this thesis was to investigate the influence of the structural alterations of phosphorus ligands on the activity, regioselectivity and the stability. Several mono- and bidentate phosphite ligands as well as potentially tridentate phosphine ligands were tested in hydroformylation reactions. Additionally, the phosphites were investigated by *in situ* NMR hydrolysis experiments.

The investigations with mono- and bidentate biphenolphosphites came to the results that, especially concerning the monodentate ligands, no clear trend in the hydroformylation properties was found. One phosphite was synthesized, which exhibited an inhibiting effect on the hydroformylation (**2e**) while all other monodentate phosphites induced high activity but poor *n*-selectivity. The highest *n*-selectivity was observed with a catalyst based on the bidentate BIPHEPHOS analogue **3a**. A comparable *n*-selectivity but with significantly lower activity was found for the unsymmetric diphosphite **3b**, which in turn was a considerably more stable. In general, the hydrolysis experiments showed that highly stable phosphites usually exhibited a significantly lower activity.

Furthermore, hydroformylation and hydrolysis experiments were performed with benzopinacolphosphites, which led to the result that phosphites with a single aryl substituent in the *ortho*-position of the phosphorus moiety exhibited especially high activities and yields of the desired aldehyde. These results were obtained for phenyl substituted as well as for *tert*-butyl substituted structures. It was especially observed that sterically demanding *tert*-butyl groups in *ortho*-position, as incorporated in the ligands **8k** and **8l**, stabilize the ligand towards hydrolysis. This is in full agreement with former results, where bulky *ortho*-alkyl substituents were incorporated, e.g., in the prominent monophosphite Alkanox® or the diphosphite BIPHEPHOS (*vide supra*). Unfortunately, phosphite **8l** exhibited an inferior activity in the hydroformylation experiments. This may be reasoned by the high steric demand of the three *tert*-butyl groups leading to a hindered coordination of the ligand to rhodium. In terms of regioselectivity, catalysts of those ligands that induced low activities usually exhibited high *n*-selectivities. Among the ligands inducing a yield of aldehyde over 20%, the highest regioselectivities were produced by means of the sterically demanding ligands **8f**, **8h** and **8k**. Another very sterically demanding phosphite (**8e**) allowed an excellent activity, but a mediocre *n*-selectivity. This effect must arise from the fast reaction with the non-isomerized internal alkenes. In general, our study gives evidence that a compromise must be found where the catalytic and stabilizing properties of ligands have to be matched.

4 Concluding remarks

In the second part of this thesis, two rhodium complexes based on two differently substituted phosphine pincer ligands were synthesized and tested concerning their hydroformylation properties. The crystal structure of **15b** confirmed the presumption that the three coordinating sites of the ligand coordinate in three adjacent coplanar sites to the metal center. Furthermore, at a pressure of 50 bar high conversions of up to 87 % yield of aldehyde were achieved. Especially at a lower pressure of 20 bar, the formation of aldehyde was accompanied by formation of significant amounts of hydrogenation products. Also, the *n*-regioselectivity of the catalytic systems can, for both complexes, be considered relatively low as the highest *n*-selectivity was 56.9 %. Overall, the anticipated positive catalytic properties of pincer ligands were not fulfilled with the investigated structures.

As a third topic of this thesis the potentially tridentate triphosphine ligand HiersoPHOS-2, containing a sterically demanding ferrocenyl backbone, was tested concerning its coordination behavior and properties in the hydroformylation of 1-octene. The NMR experiments indicated that the potentially tridentate ligand indeed coordinates in a bidentate manner to rhodium. For the investigation of activity and *n*-selectivity the effect of the ligand to rhodium ratio as well as the syngas pressure and temperature was examined. This led to the result that the optimal phosphorus to rhodium ratio is 3:1 which means that only one ligand coordinates to the metal center. A higher phosphorus to rhodium ratio did not prove to be beneficial. The mathematical tool of Factorial Design was deployed to further optimize the yield of aldehyde and the *n*-regioselectivity of the conversion. It was shown that the yield of aldehyde is massively dependent on the reaction temperature. However, the mathematical investigations also demonstrated that syngas pressure and interaction term of both parameters have a significant influence on both the yield and *n*-regioselectivity even though the influence was comparably low. Nevertheless, it increased the accuracy of the model, which was proven with the excellent fit of experimental results which were not included in the generation of the models. Unfortunately, the yield of aldehyde could not be optimized with the help of the generated model as the yield decreased at higher temperatures — a behavior that was not predicted by the calculated response surface. Besides the aldehyde yield, the *n*-regioselectivity of the hydroformylation of 1-octene was also optimized using Factorial Design, leading to an increase in the yield of *n*-aldehyde of up to 98.3 %, which can be considered as a successful optimization. These observations indicate that Factorial Design can be a very useful and easy optimization tool, but not all possible influences can be included in the model, which may lead to deviations of the actual practical results from the calculated and predicted results.

5 Appendix

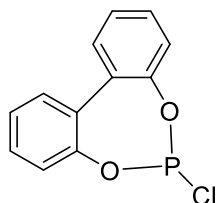
5.1 Experimental section

General Preparation

All reactions were carried out using standard Schlenk techniques under an atmosphere of argon (Linde AG). Commercial chemicals were purchased from Sigma-Aldrich Chemical Co., Tokyo Chemical Industry Co., Ltd., Acros Organics or abcr GmbH Deutschland. NMR spectra were recorded on a Bruker AVANCE 250 spectrometer (250 MHz for ^1H , 101 MHz for ^{31}P and 63 MHz for ^{13}C NMR), a Bruker AVANCE 300 spectrometer (300.13 MHz for ^1H , 121.5 MHz for ^{31}P and 75.5 MHz for ^{13}C NMR) or a Bruker AVANCE 500 spectrometer (500.13 MHz for ^1H and 125.8 Hz for ^{13}C NMR). Chemical shifts are given relative to TMS (^1H , ^{13}C) or phosphoric acid (^{31}P). Mass spectra were measured on Finnigan MAT 95-XP (Thermo Electron) or 1200/6210 (Agilent) facilities. IR-spectra were recorded on a Nicolet Magna-IR 550 spectrometer. Elemental analyses (C, H, P) were performed using a Leco 932 Analyzer and a Perkin Elmer Lambda 2 UV-Vis spectrophotometer. X-Ray crystallographic data were collected on a Bruker Kappa APEX II Duo diffractometer. The structures were solved by direct methods (SHELXS-97: Sheldrick, G. M. *Acta Cryst.* 2008, *A64*, 112.) and refined using full-matrix least-squares procedures on F^2 (SHELXL-2014: Sheldrick, G. M. *Acta Cryst.* 2015, *C71*, 3.).

The compounds 1-(benzyloxy)-3-bromobenzene (**4a**),¹⁰⁰ (3-bromophenoxy)(*tert*-butyl)dimethylsilane (**4b**),¹⁰¹ (3-(benzyloxy)phenyl)boronic acid (**5a**),^{102,103} (3-((*tert*-butyldimethylsilyl)oxy)phenyl)boronic acid (**5b**)^{102,103} and [1,1'-biphenyl]-2,3'-diol¹⁰⁴ were synthesized using literature procedures.

5.1.1 Synthesis procedures of phosphites with biphenol structure

6-Chloro-dibenzo[*d,f*][1,3,2]dioxaphosphepine (1):

To a solution of 1.3 ml phosphorus trichloride (14.38 mmol) in 5 ml THF 5.4 μ l *N*-methyl-2-pyrrolidone (0.06 mmol) were added. The solution was heated to 60 °C. At this temperature a solution of 1.04 g 2,2'-biphenol (5.58 mmol) in 5 ml THF was added dropwise. The reaction solution was heated to 75 °C for 90 min. Afterwards the solution was cooled to 50 °C and not reacted phosphorus trichloride and solvent was removed under reduced pressure. The raw product was dissolved again in 7.5 ml THF, filtered and the residue was washed with THF three times. The solvent was removed under reduced pressure yielding 1.38 g of a yellow oil (yield: 99 %).

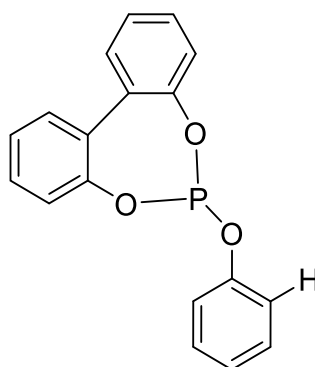
^1H NMR (300 MHz, CD_2Cl_2 , 298 K): δ = 7.55 (dd, $J_{\text{HH}} = 7.4$ Hz, $J_{\text{HH}} = 2.0$ Hz, 2H), 7.46 (td, $J_{\text{HH}} = 7.6$ Hz, $J_{\text{HH}} = 2.1$ Hz, 2H), 7.43 – 7.35 (m, 2H), 7.27 (dt, $J_{\text{HH}} = 7.7$ Hz, $J_{\text{HH}} = 1.2$ Hz, 2H) ppm.

^{13}C NMR (75 MHz, CD_2Cl_2 , 298 K): δ = 149.8 (d, $J_{\text{CP}} = 5.7$ Hz), 131.5 (d, $J_{\text{CP}} = 3.3$ Hz), 130.8 (d, $J_{\text{CP}} = 1.6$ Hz), 130.1, 127.0 (d, $J_{\text{CP}} = 1.4$ Hz), 122.7 (d, $J_{\text{CP}} = 2.2$ Hz) ppm.

^{31}P NMR (121 MHz, CD_2Cl_2 , 298 K): δ = 179.4 (s) ppm.

MS (EI, 70 eV): m/z = 252 (M^+ , 19), 250 (59), 232 (75), 216 (12), 215 (100), 169 (12), 168 (75), 139 (48), 84 (11), 38 (26), 36 (87), 35 (13).

HRMS (EI): Calculated for $\text{C}_{12}\text{H}_8\text{O}_2\text{ClP}$ (M^+) 249.99450, found 249.99436.

6-Phenoxydibenzo[*d,f*][1,3,2]dioxaphosphepine (2a):

To a solution of 1.84 g 6-chloro-dibenzo[*d,f*][1,3,2]dioxaphosphepine (**1**, 7.36 mmol) in 10 ml toluene a solution of 0.69 g phenol (7.33 mmol) and 3 ml triethylamine in 10 ml toluene was added at -20 °C. The solution was warmed to room temperature and stirred for another 18 h. Afterwards the solution was filtered and the residue was washed with toluene three times. Then the solvent was evaporated under reduced pressure. The residue was purified by column chromatography using dichloromethane/*n*-heptane = 1/19 as eluent yielding 0.59 g of a colorless oil (yield: 26 %).

¹H NMR (300 MHz, CD₂Cl₂, 298 K): δ = 7.43 (dd, *J*_{HH} = 7.5 Hz, *J*_{HH} = 1.9 Hz, 2H), 7.37 – 7.20 (m, 6H), 7.19 – 6.95 (m, 5H) ppm.

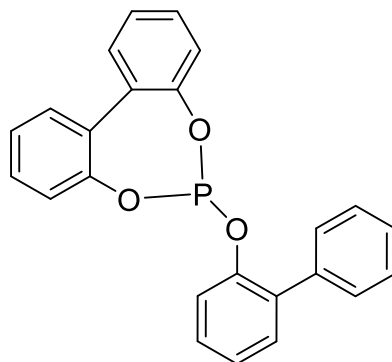
¹³C NMR (63 MHz, CD₂Cl₂, 298 K): δ = 152.2 (d, *J*_{CP} = 8.0 Hz), 149.5 (d, *J*_{CP} = 5.1 Hz), 131.7 (d, *J*_{CP} = 3.2 Hz), 130.6 (d, *J*_{CP} = 1.2 Hz), 130.4, 130.3, 129.9, 126.2, 125.0, 122.6, 121.1 (d, *J*_{CP} = 7.6 Hz) ppm.

³¹P NMR (121 MHz, CD₂Cl₂, 298 K): δ = 144.0 (s) ppm.

MS (EI, 70 eV): *m/z* = 308 (M⁺, 38), 307 (14), 228 (18), 216 (15), 215 (99), 169 (14), 168 (100), 140 (10), 139 (52), 93 (17), 77 (30), 65 (42), 63 (10), 51 (17), 39 (21).

HRMS (EI): Calculated for C₁₈H₁₃O₃P (M⁺) 308.05968, found 308.06012.

Elemental analysis (calc. for C₁₈H₁₃O₃P = 308.27 g/mol): C 68.04 (70.13), H 4.14 (4.25), P 11.07 (10.05) %.

6-([1,1'-Biphenyl]-2-yloxy)dibenzo[*d,f*][1,3,2]dioxaphosphepine (2b):

A solution of 0.63 g 2-phenylphenol (3.69 mmol) and 1.5 ml triethylamine (11.08 mmol, 1.12 g) in 7 ml THF was added dropwise to a solution of 0.93 g 6-chloro[*d,f*][1,3,2]dioxaphosphepine in 7 ml THF at -20 °C. Afterwards the reaction solution was stirred for 24 h at room temperature. The solvent was evaporated under reduced pressure and the residue was dissolved in toluene, filtrated and washed three times with toluene. The solvent was again evaporated under reduced pressure and the residue was purified by column chromatography using dichloromethane/*n*-heptane = 15/85 to yield 0.68 g of a colorless oil (yield: 49 %).

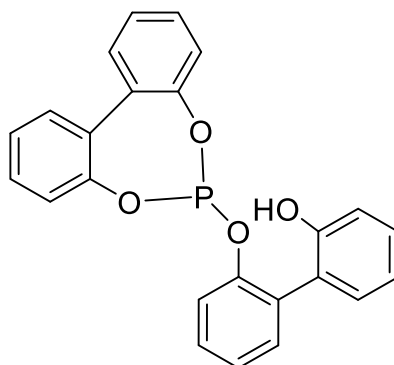
¹H NMR (300 MHz, CD₂Cl₂, 298 K): δ = 7.58–7.39 (m, 8H), 7.39–7.25 (m, 7H), 7.02 (ddd, ³J_{HH} = 7.4 Hz; ⁴J_{HH} = 2.1 Hz, ⁵J_{HH} = 1.1 Hz, 2H) ppm.

¹³C NMR (75 MHz, CD₂Cl₂, 298 K): δ = 149.5 (d, J_{CP} = 5.1 Hz), 149.3 (d, J_{CP} = 7.5 Hz), 138.3, 134.6 (d, J_{CP} = 3.2 Hz), 131.9, 131.6 (d, J_{CP} = 3.2 Hz), 130.5, 130.4, 129.8, 129.3, 128.8, 128.0, 126.0, 125.3, 122.6 (d, J_{CP} = 1.6 Hz), 121.5 (d, J_{CP} = 11.4 Hz) ppm.

³¹P NMR (121 MHz, CD₂Cl₂, 298 K): δ = 144.5 (s) ppm.

MS (EI): *m/z* (%) = 384 (M⁺, 99), 383 (M⁺-H, 100), 215 (100), 168 (99), 139 (57), 115 (37).

HRMS (ESI): Calculated for C₂₄H₁₈O₃P (M+H)⁺ 385.09881, found 385.09864. Calculated for C₂₄H₁₇O₃PNa (M+Na)⁺ 407.08075, found 407.08098.

2'-(Dibenzo[*d,f*][1,3,2]dioxaphosphepin-6-yloxy)-[1,1'-biphenyl]-2-ol (2c):

To a solution of 0.47 g 2,2'-biphenol (2.51 mmol) in 5 ml THF was added dropwise a solution of *n*-BuLi in hexane (1.6 M, 2.51 mmol) at -30 °C. The solution was stirred for 30 minutes at this temperature. Afterwards the solution was warmed to room temperature and a solution of 0.63 g 6-chloro-dibenzo[*d,f*][1,3,2]-dioxaphosphepine (**1**, 2.51 mmol) in 5 ml THF was added dropwise and the solution stirred for 18 h at room temperature. The solvent was evaporated under reduced pressure, the residue was dissolved in 10 ml toluene and filtrated. Afterwards the solvent was again evaporated under reduced pressure. The residue was dissolved in a small amount of dichloromethane and *n*-heptane was added to this solution until some precipitation was noticed. The solution was cooled overnight to 8 °C and was filtrated afterwards. The solid was dried *in vacuo* to yield 0.28 g of a slightly yellow solid (yield: 28 %).

¹H NMR (300 MHz, dioxane-*d*₈, 298 K): δ = 7.17-7.34 (m, 7H), 7.04-7.17 (m, 4H), 6.86-6.93 (m, 1H), 6.74-6.86 (m, 5H) ppm.

¹³C NMR (63 MHz, dioxane-*d*₈, 298 K): δ = 156.9, 150.0 (d, *J*_{CP} = 2.27 Hz), 132.1, 132.0, 131.3, 130.6, 129.9, 129.7, 129.2, 128.7, 128.0, 126.1, 125.9, 125.0, 122.9, 120.0, 118.1 ppm.

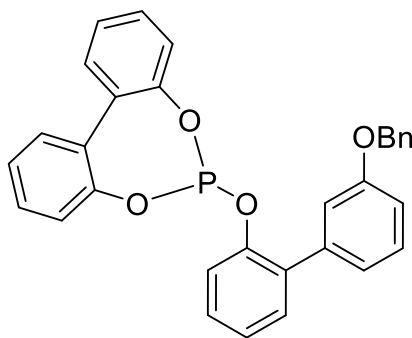
³¹P NMR (121 MHz, dioxane-*d*₈, 298 K): δ = 144.7 (s) ppm.

MS (EI, 70 eV): *m/z* (%) = 416 (M⁺+O, 36), 400 (M⁺, 9), 383 (100), 232, (41), 215 (73), 186 (60), 168 (96), 139 (46).

HRMS (ESI): Calculated for C₂₄H₁₈O₄P (M+H)⁺ 401.09372, found 401.09374. Calculated for C₂₄H₁₇O₄PNa (M+Na)⁺ 423.07567, found 423.07587.

Elemental analysis (calc. for C₂₄H₁₇O₄P = 400.36 g/mol): C 72.52 (72.00), H 4.29 (4.28) %.

IR (ATR, cm⁻¹) $\tilde{\nu}$ = 3058 (OH).

6-((3'-(Benzyloxy)-[1,1'-biphenyl]-2-yl)oxy)dibenzo[*d,f*][1,3,2]dioxaphosphepine (2d):

A solution of 0.15 g 3'-(benzyloxy)[1,1'-biphenyl]-2-ol (**6a**, 0.54 mmol) and 0.22 mol triethylamine (0.16 g, 1.62 mmol) in 7 ml toluene was added to a stirred solution of 0.14 g 6-chloro-dibenzo[*d,f*][1,3,2]-dioxaphosphepine (0.50 mmol) in 5 ml toluene at -20 °C. The solution was stirred for 60 h at room temperature. Afterwards the solution was filtered and the residue was washed with toluene three times. Then the solvent was evaporated under reduced pressure. The residue was purified by column chromatography using dichloromethane/*n*-heptane = 3/7 as eluent yielding 0.12 g as a colorless oil (yield: 49 %).

^1H NMR (250 MHz, CD_2Cl_2 , 298 K): δ = 7.26-7.50 (m, 16H), 7.15-7.19 (m, 1H), 7.07-7.13 (m, 1H), 6.97-7.06 (m, 3H), 5.02 (s, 2H, CH_2) ppm.

^{13}C NMR (63 MHz, CD_2Cl_2 , 298 K): δ = 159.0, 149.2 (d, J_{CP} = 5.05 Hz), 149.0 (d, J_{CP} = 7.91 Hz), 139.3, 137.5, 131.5, 131.3 (d, J_{CP} = 3.33 Hz), 130.6 (d, J_{CP} = 1.37 Hz), 130.2 (d, J_{CP} = 1.26 Hz), 129.6, 129.1, 128.7, 128.2, 127.9, 125.7 (d, J_{CP} = 0.92 Hz), 125.0 (d, J_{CP} = 0.80 Hz), 122.7, 122.3 (d, J_{CP} = 1.61 Hz), 121.4, 121.2, 116.5, 114.4, 70.3 ppm.

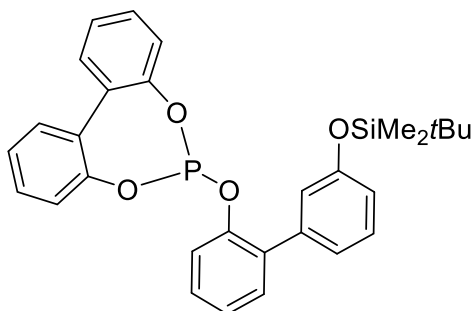
^{31}P NMR (101 MHz, CD_2Cl_2 , 298 K): δ = 144.7 (s) ppm.

MS (EI, 70 eV): m/z = 490 (M^+ , 2), 498 ($\text{M}-\text{H}^+$, 3), 400 (26), 399 (100), 371 (3), 215 (10), 168 (31), 139 (10), 92 (4), 91 (56), 65 (6).

HRMS (ESI): Calculated for $\text{C}_{31}\text{H}_{24}\text{O}_4\text{P}$ ($\text{M}+\text{H}$) $^+$ 491.14067, found 491.13992. Calculated for $\text{C}_{31}\text{H}_{23}\text{O}_4\text{PNa}$ ($\text{M}+\text{Na}$) $^+$ 513.12262, found 513.12164.

Elemental analysis (calc. for $\text{C}_{31}\text{H}_{23}\text{O}_4\text{P}$ = 490.49 g/mol): C, 77.68 (75.91); H, 4.52 (4.73) %.

6-((3'-((*tert*-Butyldimethylsilyl)oxy)-[1,1'-biphenyl]-2-yl)oxy)dibenzo[*d,f*][1,3,2]-dioxaphosphepine (2e):



To a solution of 0.81 g 6-chloro-dibenzo[*d,f*][1,3,2]-dioxaphosphepine (**1**, 3.03 mmol) in 10 ml THF was added dropwise a solution of 0.91 g 3'-((*tert*-butyldimethylsilyl)oxy)-[1,1'-biphenyl]-2-ol (**6b**, 3.03 mmol) and 1.3 ml triethylamine (9.08 mmol, 0.92 g) in 10 ml THF at a temperature of -20 °C. The reaction was stirred for 16 h at room temperature. Afterwards the solvent was evaporated under reduced pressure and the residue was dissolved in toluene, filtrated and washed three times with toluene. The solvent was evaporated again under reduced pressure. The product was purified by column chromatography using dichloromethane/*n*-heptane = 1/9 to yield 0.96 g of a colorless oil (yield: 62 %).

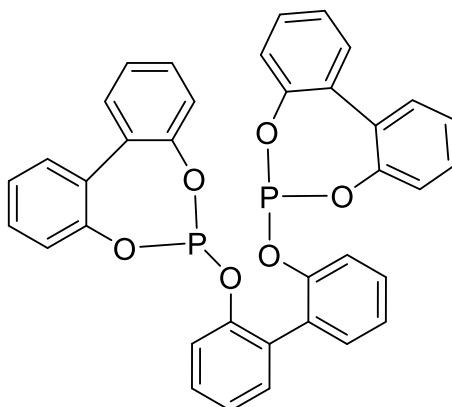
¹H NMR (63 MHz, CD₂Cl₂, 298 K): δ = 7.50 (d, *J*_{HH} = 2.1 Hz, 1H); 7.47 (d, *J*_{HH} = 2.2 Hz, 1H), 7.42 (dd, *J*_{HH} = 7.3 Hz, *J*_{HH} = 1.5 Hz, 1H), 7.39–7.24 (m, 8H), 7.10 (ddd, *J*_{HH} = 7.7 Hz, *J*_{HH} = 1.7 Hz, *J*_{HH} = 1.1 Hz, 1H), 7.07–7.04 (m, 1H), 7.04–7.02 (m, 1H), 7.01 (dd, *J*_{HH} = 2.4 Hz, *J*_{HH} = 1.7 Hz, 1H), 6.90 (ddd, *J*_{HH} = 8.1 Hz, *J*_{HH} = 2.5 Hz, *J*_{HH} = 1.1 Hz, 1H), 0.99 (s, 9H), 0.19 (s, 6H) ppm.

¹³C NMR (75 MHz, CD₂Cl₂, 298 K): δ = 156.1, 149.5 (d, *J*_{CP} = 5.2 Hz), 149.2 (d, *J*_{CP} = 7.4 Hz), 139.6, 134.5 (d, *J*_{CP} = 3.4 Hz), 131.8, 131.6 (d, *J*_{CP} = 3.2 Hz), 130.4 (d, *J*_{CP} = 1.4 Hz), 129.8, 129.7, 129.3, 126.0, 125.3, 123.5, 122.7 (d, *J*_{CP} = 1.6 Hz), 122.2, 121.7 (d, *J*_{CP} = 11.0 Hz), 119.7, 26.0, 18.7, -4.1 ppm.

³¹P NMR (121 MHz, CD₂Cl₂, 298 K): δ = 144.3 (s) ppm.

MS (EI, 70 eV): *m/z* (%) = 514 (M⁺, 43), 513 (M⁺-H, 49), 457 (83), 307 (65), 215 (100), 168 (86).

HRMS (EI): Calculated for C₃₀H₃₁O₄PSi (M⁺) 514.17237, found 514.17203.

2,2'-Bis(dibenzo[*d,f*][1,3,2]dioxaphosphepin-6-yloxy)-1,1'-biphenyl (3a):

A solution of 0.99 g 2,2'-biphenol (5.29 mmol) and 3 ml triethylamine (11.08 mmol, 1.12 g) in 7 ml THF was added dropwise to a solution of 2.65 g 6-chloro[*d,f*][1,3,2]dioxaphosphepine (**1**, 10.57 mmol) in 7 ml THF at -20 °C. Afterwards the reaction solution was stirred for 18 h at room temperature. The solvent was evaporated under reduced pressure and the residue was dissolved in toluene, filtrated and washed three times with toluene. The solvent was again evaporated under reduced pressure and the residue was purified by recrystallization from a mixture of dichloromethane and *n*-heptane to yield 1.09 g of a white powder (yield: 34 %).

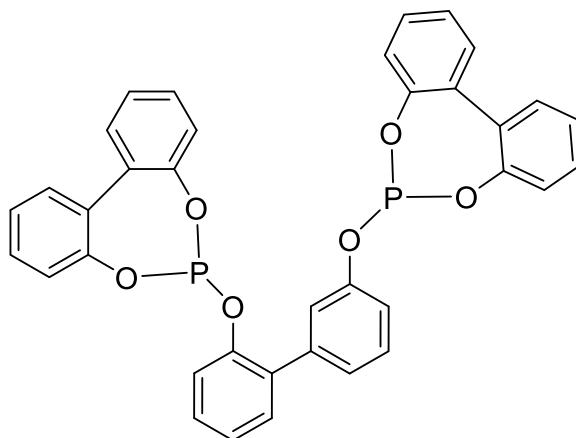
¹H NMR (300 MHz, CD₂Cl₂, 298 K): δ = 7.58 – 7.17 (m, 6H), 7.00 – 6.83 (m, 1H) ppm.

¹³C NMR (75 MHz, CD₂Cl₂, 298 K): δ = 150.3, 150.2, 150.2, 149.5, 149.5, 149.5, 132.8, 131.6, 130.9, 130.30, 129.8, 129.7, 125.9, 124.9, 122.6, 121.2, 121.1, 121.0 ppm.

³¹P NMR (121 MHz, CD₂Cl₂, 298 K): δ = 144.7 (s) ppm.

HRMS (ESI): Calculated for C₃₆H₂₅O₆P₂ (M+H)⁺ 615.11209, found 615.11203. Calculated for C₃₆H₂₄O₆P₂Na (M+Na)⁺ 637.09403, found 637.09394.

Elemental analysis (calc. for C₃₆H₂₄O₆P₂ = 614.52 g/mol): C, 70.85 (70.36); H, 4.41 (3.94); P, 9.34 (10.08) %.

6,6'-([1,1'-Biphenyl]-2,3'-diylbis(oxy))didibenzo[*d,f*][1,3,2]dioxaphosphepine (3b):

A solution of 0.10 g 2,3'-biphenol (0.56 mmol) in 4 ml THF and 0.3 ml triethylamine (0.23 g, 2.24 mmol) was added dropwise to a solution of 0.39 g 6-chloro-dibenzo[*d,f*][1,3,2]-dioxaphosphepine (**1**, 1.56 mmol) in 4 ml THF at -20 °C. The solution was stirred overnight at room temperature. Afterwards the solvent was evaporated under reduced pressure and the residue dissolved in 10 ml toluene, filtrated und washed three times with toluene. The solvent was evaporated again under reduced pressure. The leftover yellow oil was purified by column chromatography using dichloromethane/*n*-heptane = 3/7 to yield 0.10 g of a white solid (yield: 30 %).

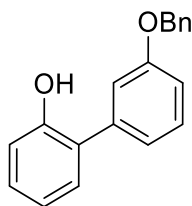
¹H NMR (300 MHz, CD₂Cl₂, 298 K): δ = 7.39-7.53 (m, 6H), 7.18-7.39 (m, 16H), 7.00-7.05 (m, 2H) ppm.

¹³C NMR (75 MHz, CD₂Cl₂, 298 K): δ = 151.8 (d, *J*_{CP} = 7.91 Hz), 149.2 (d, *J*_{CP} = 5.00 Hz), 149.2 (d, *J*_{CP} = 5.00 Hz), 149.0 (d, *J*_{CP} = 7.60 Hz), 139.9, (d, *J*_{CP} = 3.23 Hz), 133.3, 131.5, 131.4 (d, *J*_{CP} = 3.33 Hz), 131.3 (d, *J*_{CP} = 3.33 Hz), 130.3, 130.2, 129.9, 129.6, 129.4, 126.3, 125.8, 125.8, 125.1, 122.4, 122.3, 121.4, 121.2, 119.8, 119.6 ppm.

³¹P NMR (121 MHz, CD₂Cl₂, 298 K): δ = 144.3 (s), 144.0 (s) ppm.

HRMS (ESI): Calculated for C₃₆H₂₅O₆P₂ (M+H)⁺ 615.11209, found 615.11174. Calculated for C₃₆H₂₄O₆P₂Na (M+Na)⁺ 637.09403, found 637.09386.

Elemental analysis (calc. for C₃₆H₂₄O₆P₂ = 614.53 g/mol): C 71.07 (70.36), H 4.14 (3.94), P 12.20 (10.08) %.

3'-(Benzyloxy)[1,1'-biphenyl]-2-ol (6a):

0.22 g 2-Iodophenol (1.01 mmol) and 0.23 g [3-(benzyloxy)phenyl]boronic acid (**5a**, 1.01 mmol) were suspended in 10 ml water. To the suspension 0.05 g palladium on carbon (10 w%, 5 mol%) and 0.56 g potassium carbonate (4.05 mmol) were added and stirred for 24 h at 90 °C. Afterwards the suspension was cooled to ambient temperature and acidified by addition of aqueous HCl (2 M). It was extracted three times with ethyl acetate and the combined organic layers were washed with deionized water three times, dried and the solvent was removed *in vacuo*. The residue was purified by column chromatography on silica using *n*-heptane/dichloromethane = 2/8 as eluent yielding 0.15 g of a colorless oil (yield: 53 %).

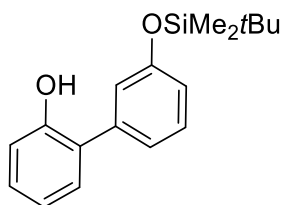
^1H NMR (300 MHz, CDCl_3 , 298 K) δ = 7.79 – 7.55 (m, 6H), 7.52 (m, 2H), 7.41 – 7.20 (m, 5H), 5.56 (s, 1H, OH), 5.39 (s, 2H, CH_2) ppm.

^{13}C NMR (75 MHz, CDCl_3 , 298 K) δ = 159.6, 152.5, 138.6, 136.9, 130.6, 130.2, 129.4, 128.8, 128.2, 128.0, 127.7, 121.6, 120.9, 116.0, 115.6, 114.7, 70.2 ppm.

MS (EI, 70 eV): m/z = 276 (M^+ , 24), 128 (9), 91 (100), 65 (10).

HRMS (EI): Calculated for $\text{C}_{19}\text{H}_{16}\text{O}_2$ (M^+) 276.11448, found 276.11444.

Elemental analysis (calc. for $\text{C}_{19}\text{H}_{16}\text{O}_2$ = 276.34 g/mol): C, 82.44 (82.58); H, 5.67 (5.84) %.

3'-((*tert*-Butyldimethylsilyl)oxy)-[1,1'-biphenyl]-2-ol (6b):

0.25 g 2-Iodophenol (1.14 mmol) and 0.29 g (3-((*tert*-butyldimethylsilyl)oxy)phenyl)boronic acid (**5b**, 1.14 mmol) were suspended in 10.3 ml 1,4-dioxane. To the suspension 0.06 g palladium on carbon (10 w%, 5 mol%) and 0.50 g potassium carbonate were added and stirred for 18 h at 70 °C. Afterwards the suspension was cooled to ambient temperature and quenched with deionized water. The mixture was filtered through a thin layer of silica, extracted three times with ethyl acetate and the combined organic layers were washed with deionized water three times, dried and the solvent was removed *in vacuo*. The residue was purified by column chromatography on silica using *n*-heptane/dichloromethane = 2/8 as eluent yielding 0.23 g of a colorless oil (yield: 69 %).

¹H NMR (300 MHz, CD₂Cl₂, 298 K): δ = 7.35 (t, *J*_{HH} = 7.8 Hz, 1H), 7.30 – 7.20 (m, 2H), 7.06 (ddd, *J*_{HH} = 7.6 Hz, *J*_{HH} = 1.6 Hz, *J*_{HH} = 1.0 Hz, 1H), 7.02 – 6.92 (m, 3H), 6.89 (ddd, *J*_{HH} = 8.1 Hz, *J*_{HH} = 2.5 Hz, *J*_{HH} = 1.0 Hz, 1H), 1.00 (s, 9H), 0.23 (s, 6H) ppm.

¹³C NMR (75 MHz, CD₂Cl₂, 298 K): δ = 157.0, 153.1, 139.1, 130.8, 130.7, 129.7, 128.5, 122.4, 121.4, 121.3, 120.1, 116.3, 26.0, 18.7, -4.1 ppm.

²⁹Si NMR (60 MHz, CD₂Cl₂, 298 K): δ = 21.49 ppm.

MS (EI, 70 eV): *m/z* (%) = 300 (M⁺, 16), 244 (11), 243 (40), 227 (15), 139 (16), 115 (18), 75 (74), 73 (11), 58 (17), 57 (100), 56 (20), 45 (16), 41 (50), 39 (12), 29 (17).

HRMS (EI): Calculated for C₁₈H₂₄O₂Si (M⁺) 300.15401, found 300.15485.

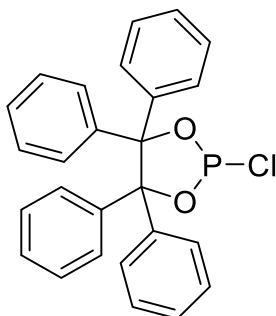
5.1.2 Hydroformylation with phosphites with biphenol structure

The hydroformylation experiments of phosphites with biphenol structure were performed in a 16 ml autoclave (HEL group, Hertfordshire, Great Britain) equipped with a gas inlet stirrer, a thermocouple, a pressure controller as well as a gas flow meter. A high-grade pure syngas (99.997 %; CO/H₂ = 1:1) was used, which was purchased from Linde AG. The composition of the technical octene mixture used as a substrate for the hydroformylation reaction was: 3.3 % 1-octene, 48.4 % *Z/E*-2-octene, 29.2 % *Z/E*-3-octene, 16.4 % *Z/E*-4-octene, 2.1 % skeletal C8-olefinic isomers, 0.6 % *n*-octane. Olefins were refluxed in an argon atmosphere over sodium metal and freshly distilled prior to use.

For the hydroformylation experiments the reaction solution was prepared under an atmosphere of argon. 0.002 g of Rh(acac)(CO)₂ and corresponding amount of ligand were dissolved in 8 ml of toluene. The mass of toluene was defined for GC analysis. Afterwards 1.80 g of *n*-octene (16 mmol) was added. The prepared reaction solutions were filled into the autoclave and purged with argon and syngas (Linde; H₂ (99.999 %):CO (99.997%) = 1:1) three times, respectively. Afterwards the stirred reaction solution was pressurized with 10 bar syngas and heated to the assigned temperature. After reaching the reaction temperature the pressure was elevated to 20 bar and the reaction was kept at constant pressure for 4 h. After this time the autoclave was cooled down to room temperature, the pressure was released and purged with argon. 0.5 ml of the reaction solution were diluted with 4 ml pentane and analyzed with gas chromatography (HP 5890 Series II plus, PONA, 50 m x 0,2 mm x 0,5 μm). The quantitative amount of remaining olefin and newly formed aldehyde were determined using toluene as internal standard.

5.1.3 Synthesis of phosphites with benzopinacol structure

2-Chloro-4,4,5,5-tetraphenyl-1,3,2-dioxaphospholane (7):



A stirred suspension of 6.50 g benzopinacol (17.74 mmol) in 105 ml THF was treated dropwise with a solution of 7.38 ml trimethylamine (53.21 mmol) in 15 ml THF. Afterwards a solution of 2.48 ml phosphorus trichloride (28.38 mmol) in 35 ml THF was added dropwise at $-40\text{ }^{\circ}\text{C}$. The reaction mixture was allowed to warm up slowly to room temperature, then stirred overnight and filtered. Volatiles were removed from the filtrate *in vacuo*. The obtained residue was dissolved in toluene (25 ml). After filtration, solvent was removed *in vacuo* and the solid product dried at 0.1 bar, $40\text{ }^{\circ}\text{C}$, for 5 h. Yield: 7.57 g (17.56 mmol, 99 %).

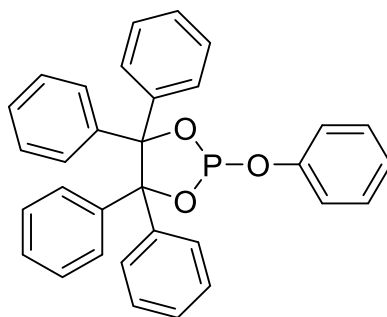
^1H NMR (300 MHz, CD_2Cl_2 , 298 K) δ = 6.97 – 7.03 (m, 4H), 7.05 – 7.12 (m, 4H), 7.14 – 7.31 (m, 8H), 7.48 – 7.60 (m, 4H) ppm.

^{13}C NMR (75 MHz, CD_2Cl_2 , 298 K) δ = 97.6 (d, J_{CP} = 8.5 Hz), 127.8, 128.1, 128.2, 128.6, 129.0 (d, J_{CP} = 3.8 Hz), 130.4, 141.4 (d, J_{CP} = 4.3 Hz), 141.7 ppm.

^{31}P NMR (121 MHz, CD_2Cl_2 , 298 K) δ = 173.0 (s) ppm.

MS (EI, 70 eV): m/z = 430 (M^+ , 1), 348 (12), 333 (45), 332 (100), 255 (15), 254 (17), 253 (25), 252 (18), 250 (11), 248 (29), 243 (10), 167 (13), 166 (84), 165 (83), 105 (18), 92 (40), 91 (67), 77 (13).

HRMS (EI): Calculated for $\text{C}_{26}\text{H}_{20}\text{O}_2\text{ClP}$ (M^+) 430.08840, found 430.08790.

2-Phenoxy-4,4',5,5'-tetraphenyl-1,3,2-dioxaphospholane (8a):

To a stirred suspension of 0.19 g phenol (1.98 mmol) in 5 ml toluene, 0.41 ml triethylamine (0.30 g, 2.97 mmol) was added dropwise. The reaction mixture was treated dropwise with a solution of 0.85 g 2-chloro-4,4,5,5-tetraphenyl-1,3,2-dioxaphospholane (**7**, 1.98 mmol) in 6 ml toluene at room temperature. The reaction mixture was stirred overnight and filtered. The filtrate was evaporated to dryness in vacuo. The residue obtained was dissolved in toluene (15 ml), the solution was filtered through a thin layer of silica and the solvent removed in vacuo and the solid product dried at 0.1 bar, 40 °C, for 5 h. Yield: 0.610 g (1.2 mmol, 63 %).

^1H NMR (250 MHz, CD_2Cl_2 , 298 K): δ = 6.69 – 6.78 (m, 2H), 7.05 – 7.25 (m, 19H), 7.50 – 7.62 (m, 4H) ppm.

^{13}C NMR (63 MHz, CD_2Cl_2 , 298 K): δ = 95.7 (d, J_{CP} = 7.9 Hz), 121.1 (d, J_{CP} = 8.1 Hz), 124.5, 127.6, 127.7, 127.8, 128.0, 129.3 (d, J_{CP} = 3.2 Hz), 130.1, 130.4, 142.5 (d, J_{CP} = 4.1 Hz), 143.2, 151.7 (d, J_{CP} = 8.5 Hz) ppm.

^{31}P NMR (121 MHz, CD_2Cl_2 , 298 K): δ = 139.5 (s) ppm.

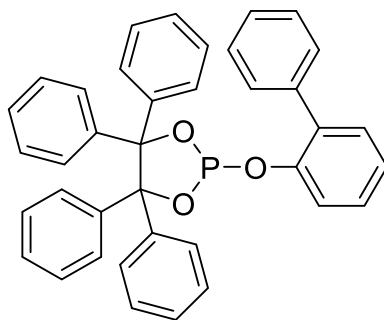
HRMS (ESI): Calculated for $\text{C}_{32}\text{H}_{26}\text{O}_3\text{P}$ ($\text{M}+\text{H}$) $^+$ 489.1614, found 489.1626.

Elemental analysis (calc. for $\text{C}_{32}\text{H}_{25}\text{O}_3\text{P}$ = 488.15 g/mol): C, 78.77 (78.68); H, 5.32 (5.16); P, 6.04 (6.34) %.

5 Appendix

Table 24: Crystallographic details of 8a.

| | |
|---|--|
| Chem. Formula | C ₃₂ H ₂₅ O ₃ P |
| Form. Wght. [g mol ⁻¹] | 488.15 |
| Color | Colorless |
| Cryst. system | Monoclinic |
| Space Group | <i>P</i> 2 ₁ / <i>n</i> |
| <i>a</i> [Å] | 14.9694 (4) |
| <i>b</i> [Å] | 9.5530 (2) |
| <i>c</i> [Å] | 18.7199 (5) |
| α [°] | 90 |
| β [°] | 112.7503 (6) |
| γ [°] | 90 |
| <i>V</i> [Å ³] | 2468.72 (11) |
| <i>Z</i> | 4 |
| ρ _{calc.} [g cm ⁻³] | 1.314 |
| μ [mm ⁻¹] | 0.144 |
| λ _{CuKα} [Å] | 0.71073 |
| <i>T</i> [K] | 150(2) |
| Reflections collected | 50826 |
| Independent reflections | 5970 |
| Reflections with <i>I</i> > 2 <i>s</i> (<i>I</i>) | 5184 |
| <i>R</i> _{int} | 0.0259 |
| <i>F</i> (000) | 1024 |
| <i>R</i> ₁ (R [<i>F</i> ² > 2 <i>s</i> (<i>F</i> ²)]) | 0.0355 |
| w <i>R</i> ₂ (<i>F</i> ²) | 0.0963 |
| Goodness-of-fit on <i>F</i> ² | 1.043 |
| Parameters | 325 |

2-([1,1'-Biphenyl]-2-yloxy)-4,4,5,5-tetraphenyl-1,3,2-dioxaphospholane (8b):

To a stirred suspension of 0.37 g 2-phenylphenol (2.204 mmol) in 6 ml toluene, 0.45 ml triethylamine (0.33 g, 3.31 mmol) was added dropwise at $-20\text{ }^{\circ}\text{C}$. The reaction mixture was treated dropwise with a cold solution of 0.95 g 2-chloro-4,4,5,5-tetraphenyl-1,3,2-dioxaphospholane (**7**, 2.204 mmol) in 6 ml toluene. The reaction mixture was stirred overnight and filtered. The filtrate was evaporated to dryness *in vacuo*. The residue obtained was dissolved in toluene (15 ml), the solution was filtered through a thin layer of silica, the solvent was removed *in vacuo* and the solid product dried at 0.1 bar, $40\text{ }^{\circ}\text{C}$, for 5 h. Yield: 0.944 g (1.67 mmol, 76 %).

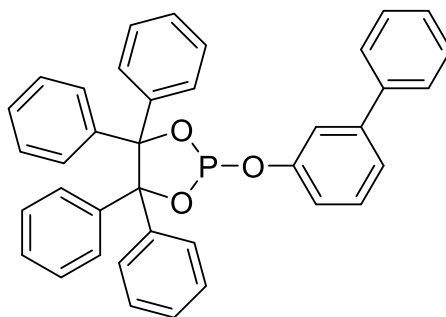
^1H NMR (300 MHz, CD_2Cl_2 , 298 K): δ = 6.9 – 7.1 (m, 11H), 7.1 – 7.3 (m, 7H), 7.3 – 7.4 (m, 7H), 7.4 – 7.5 (m, 4H) ppm.

^{13}C NMR (75 MHz, CD_2Cl_2 , 298 K): δ = 95.8 (d, J_{CP} = 8.3 Hz), 121.7 (d, J_{CP} = 12.5 Hz), 124.9, 127.6, 127.6, 127.7, 127.9, 128.6, 129.0, 129.2 (d, J_{CP} = 3.2 Hz), 130.3, 130.4, 131.5, 134.4 (d, J_{CP} = 3.1 Hz), 138.2, 142.5 (d, J_{CP} = 4.4 Hz), 143.0, 149.0 (d, J_{CP} = 9.0 Hz) ppm.

^{31}P NMR (121 MHz, CD_2Cl_2 , 298 K): δ = 138.6 ppm.

HRMS (ESI): Calculated for $\text{C}_{38}\text{H}_{30}\text{O}_3\text{P}$ ($\text{M}+\text{H}$) $^+$ 565.1927, found 565.1930.

Elemental analysis (calc. for $\text{C}_{38}\text{H}_{29}\text{O}_3\text{P}$ = 564,61 g/mol): C, 80.76 (80.84); H, 5.20 (5.18); P, 5.23 (5.49) %.

2-([1,1'-Biphenyl]-3-yloxy)-4,4,5,5-tetraphenyl-1,3,2-dioxaphospholane (8c):

To a stirred suspension of 0.37 g 3-phenylphenol (1.97 mmol) in 6 ml toluene, 0.41 ml triethylamine (0.30 g, 2.97 mmol) was added dropwise. The reaction mixture was treated dropwise with a solution of 0.85 g 2-chloro-4,4,5,5-tetraphenyl-1,3,2-dioxaphospholane (**7**, 1.97 mmol) in 6 ml toluene at room temperature. The reaction mixture was stirred overnight and filtered. The filtrate was evaporated to dryness *in vacuo*. The residue obtained was dissolved in toluene (15 ml), the solution was filtered through a thin layer of silica, the solvent was removed *in vacuo* and the solid product dried at 0.1 bar, 40 °C, for 5 h. Yield: 0.760 g (1.34 mmol, 68 %).

¹H NMR (300 MHz, CD₂Cl₂, 298 K): δ = 6.76-6.81 (m, 2H), 7.08-7.17 (m, 10H), 7.22-7.27 (m, 6H), 7.31-7.48 (m, 5H), 7.53-7.64 (m, 6H).

¹³C NMR (63 MHz, CD₂Cl₂, 298 K): δ = 95.9, (d, J_{CP} = 8.2 Hz), 114.9, 115.3, 119.5, 120.0, 120.1, 120.2, 120.3, 123.4, 126.0, 127.8, 127.9, 128.1, 128.2, 128.4, 128.9, 129.4, 129.5, 129.8, 130.6, 130.7, 140.9, 141.7, 142.6, 142.7, 143.4, 143.5, 152.3 (d, J_{CP} = 8.1 Hz) ppm.

³¹P NMR (121 MHz, CD₂Cl₂, 298 K): δ = 139.1 (s) ppm.

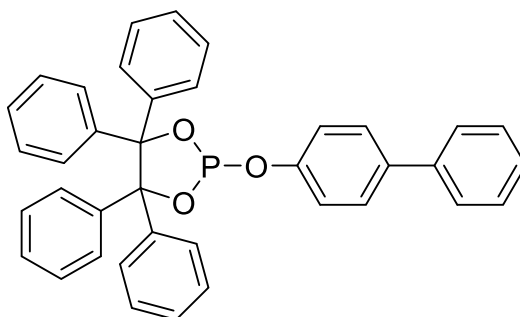
HRMS (ESI): Calculated for C₃₈H₃₀O₃P (M+H)⁺ 565.1927, found 565.1929.

Elemental analysis (calc. for C₃₈H₂₉O₃P = 564.61 g/mol): C, 80.75 (80.84); H, 5.04 (5.18); P, 5.34 (5.49) %.

5 Appendix

Table 25: Crystallographic details of 8c.

| | |
|---|--|
| Chem. Formula | C ₃₈ H ₂₉ O ₃ P |
| Form. Wght. [g mol ⁻¹] | 564.58 |
| Color | Colorless |
| Cryst. system | Monoclinic |
| Space Group | <i>P</i> 2 ₁ / <i>n</i> |
| <i>a</i> [Å] | 14.9935 (3) |
| <i>b</i> [Å] | 9.8857 (2) |
| <i>c</i> [Å] | 20.5571 (5) |
| α [°] | 90 |
| β [°] | 104.0748 (6) |
| γ [°] | 90 |
| <i>V</i> [Å ³] | 2955.52 (11) |
| <i>Z</i> | 4 |
| ρ _{calc.} [g cm ⁻³] | 1.269 |
| μ [mm ⁻¹] | 0.130 |
| λ _{CuKα} [Å] | 0.71073 |
| <i>T</i> [K] | 150(2) |
| Reflections collected | 60717 |
| Independent reflections | 7483 |
| Reflections with <i>I</i> > 2 <i>s</i> (<i>I</i>) | 6091 |
| <i>R</i> _{int} | 0.0310 |
| <i>F</i> (000) | 1184 |
| <i>R</i> ₁ (R [<i>F</i> ² > 2 <i>s</i> (<i>F</i> ²)]) | 0.0368 |
| w <i>R</i> ₂ (<i>F</i> ²) | 0.0984 |
| Goodness-of-fit on <i>F</i> ² | 1.027 |
| Parameters | 379 |

2-([1,1'-Biphenyl]-4-yloxy)-4,4,5,5-tetraphenyl-1,3,2-dioxaphospholane (8d):

To a stirred suspension of 0.37 g 4-phenylphenol (1.97 mmol) in 6 ml toluene, 0.41 ml triethylamine (0.30 g, 2.97 mmol) was added dropwise. The reaction mixture was treated dropwise with a solution of 0.85 g 2-chloro-4,4,5,5-tetraphenyl-1,3,2-dioxaphospholane (**7**, 1.97 mmol) in 6 ml toluene at room temperature. The reaction mixture was stirred overnight and filtered. The filtrate was evaporated to dryness *in vacuo*. The residue obtained was dissolved in toluene (15 ml), the solution was filtered through a thin layer of silica, the solvent removed *in vacuo* and the solid product dried at 0.1 bar, 40 °C, for 5 h. Yield: 0.930 g (1.64 mmol, 83 %).

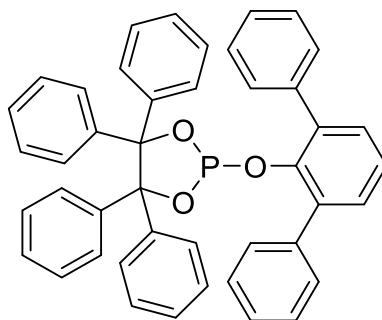
^1H NMR (300 MHz, CD_2Cl_2 , 298 K): δ = 6.82 (d, J_{HH} = 8.8 Hz, 1H), 7.03 – 7.28 (m, 18H), 7.28 – 7.64 (m, 10H) ppm.

^{13}C NMR (63 MHz, CD_2Cl_2 , 298 K): δ = 95.8 (d, J_{CP} = 8.0 Hz), 116.2, 121.4 (d, J_{CP} = 8.0 Hz), 127.4, 127.6, 127.7, 127.8, 128.0, 128.7, 129.3, 130.4, 140.9, 142.5 (d, J_{CP} = 4.1 Hz), 143.2, 151.2 (d, J_{CP} = 8.5 Hz) ppm.

^{31}P NMR (121 MHz, CD_2Cl_2 , 298 K): δ = 138.4 (s) ppm.

HRMS (ESI): Calculated for $\text{C}_{38}\text{H}_{30}\text{O}_3\text{P}$ ($\text{M}+\text{H}$) $^+$ 565.1927, found 565.1935.

Elemental analysis (calc. for $\text{C}_{38}\text{H}_{29}\text{O}_3\text{P}$ = 564.61 g/mol): C, 80.95 (80.84); H, 5.20 (5.18); P, 5.31 (5.49) %.

2-([1,1':3',1''-Terphenyl]-2'-yloxy)-4,4,5,5-tetraphenyl-1,3,2-dioxaphospholane (8e):

To a stirred suspension of 0.54 g 2,6-di-phenylphenol (2.204 mmol) in 6 ml toluene, 0.46 ml triethylamine (0.33 g, 3.31 mmol) was added dropwise at $-20\text{ }^{\circ}\text{C}$. The reaction mixture was treated dropwise with a cold solution of 0.95 g 2-chloro-4,4,5,5-tetraphenyl-1,3,2-dioxaphospholane (**7**, 2.204 mmol) in 6 ml toluene. The reaction mixture was stirred 24 h and filtered. The filtrate was evaporated to dryness *in vacuo*. The residue obtained was dissolved in toluene (15 ml), the solution was filtered through a thin layer of silica and the solvent removed *in vacuo* and the solid product dried at 0.1 bar, $40\text{ }^{\circ}\text{C}$, for 5 h. Yield: 1.113 g (1.74 mmol, 87 %).

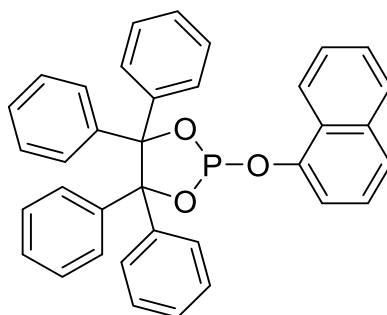
^1H NMR (300 MHz, CD_2Cl_2 , 298 K): δ = 6.93-7.17 (m, 9H), 7.28-7.48 (m, 20H), 7.53-7.59 (m, 2H), 7.65-7.69 (m, 2H).

^{13}C NMR (63 MHz, CD_2Cl_2 , 298 K): δ = 95.0 (d, J_{CP} = 8.4 Hz), 121.3, 125.1, 125.9, 127.5 (d, J_{CP} = 11.6 Hz), 127.6 (d, J_{CP} = 19.3 Hz), 128.0 (d, J_{CP} = 22.6 Hz), 128.8, 129.1 (d, J_{CP} = 3.4 Hz), 129.4, 129.9, 130.6, 130.9, 136.7 (d, J_{CP} = 5.1 Hz), 138.3, 138.7, 142.4 (d, J_{CP} = 4.8 Hz), 142.8, 147.2 (d, J_{CP} = 9.2 Hz), 150.1 ppm.

^{31}P NMR (121 MHz, CD_2Cl_2 , 298 K): δ = 144.8 (s) ppm.

HRMS (ESI): Calculated for $\text{C}_{44}\text{H}_{34}\text{O}_3\text{P}$ ($\text{M}+\text{H}$) $^+$ 641.2240, found 641.2244.

Elemental analysis (calc. for $\text{C}_{44}\text{H}_{33}\text{O}_3\text{P}$ = 640.72 g/mol): C, 81.91 (82.48); H, 5.33 (5.19); P, 4.94 (4.83) %.

2-(Naphthalen-1-yloxy)-4,4,5,5-tetraphenyl-1,3,2-dioxaphospholane (8f):

To a stirred suspension of 0.23 g 1-naphthol (1.60 mmol) in 4 ml THF, 5.00 ml *n*-BuLi (0.32 M, 1.60 mmol) in hexane was added dropwise at -20 °C, the mixture was stirred for 20 minutes, and warmed gently to room temperature. Then it was treated dropwise with a cold solution of 0.69 g 2-chloro-4,4,5,5-tetraphenyl-1,3,2-dioxaphospholane (**7**, 1.60 mmol) in 3 ml THF. The reaction mixture was stirred over night at room temperature. The filtrate was evaporated to dryness *in vacuo*. The residue obtained was dissolved in toluene (10 ml), the solution was filtered and the solvent removed *in vacuo*. The solid product was dried at 0.1 mbar, room temperature, for 5 h. Yield: 0.660 g (1.227 mmol, 77 %).

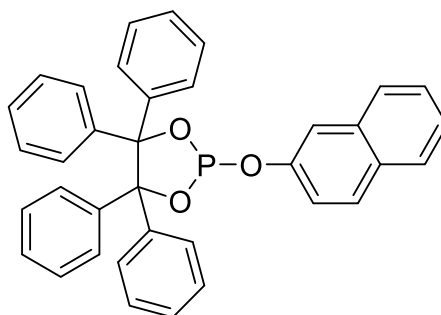
¹H NMR (300 MHz, CD₂Cl₂, 298 K): δ = 7.04 – 7.27 (m, 17H), 7.33 – 7.50 (m, 4H), 7.57 – 7.62 (m, 1H), 7.63 – 7.70 (m, 4H), 7.77 – 7.83 (m, 1H).

¹³C NMR (75 MHz, CD₂Cl₂, 298 K): δ = 96.0 (d, *J*_{CP} = 8.0 Hz), 115.2 (d, *J*_{CP} = 14.3 Hz), 123.0, 124.3, 126.2 (d, *J*_{CP} = 9.0 Hz), 127.0, 127.6, 127.7, 127.9, 128.0, 128.7, 129.3 (d, *J*_{CP} = 3.4 Hz), 129.6, 130.5, 135.3, 142.5 (d, *J*_{CP} = 4.2 Hz), 143.2, 148.1 (d, *J*_{CP} = 9.0 Hz).

³¹P NMR (121 MHz, CD₂Cl₂, 298 K): δ = 138.7 (s) ppm.

HRMS (ESI): Calculated for C₃₆H₂₇O₃PK (M+K)⁺ 577.13294, found 577.13377.

Elemental analysis (calc. for C₃₆H₂₇O₃P = 538.16 g/mol): C, 80.62 (80.35); H, 4.97 (4.98); P, 5.74 (5.75) %.

2-(Naphthalen-2-yloxy)-4,4,5,5-tetraphenyl-1,3,2-dioxaphospholane (8g):

To a stirred suspension of 0.23 g 2-naphthol (1.60 mmol) in 4 ml THF, 5.00 ml *n*-BuLi (0.32 M, 1.60 mmol) in hexane was added dropwise at -20 °C, the mixture was stirred for 20 minutes, and warmed gently to room temperature. Then it was treated dropwise with a cold solution of 0.69 g 2-chloro-4,4,5,5-tetraphenyl-1,3,2-dioxaphospholane (**7**, 1.60 mmol) in 3 ml THF. After 20 minutes the formation of precipitate (LiCl) was noticed. The reaction mixture was stirred overnight at room temperature. The filtrate was evaporated to dryness *in vacuo*. The residue obtained was dissolved in toluene (10 ml), the solution was filtered and the solvent removed *in vacuo*. The solid product was dried at 0.1 mbar, room temperature, for 5 h. Yield: 0.861 g (1.600 mmol, >99 %).

¹H NMR (300 MHz, CD₂Cl₂, 298 K): δ = 6.88 (dd, *J*_{HH} = 8.9 Hz, *J*_{HH} = 2.3 Hz, 1H), 7.05 – 7.30 (m, 17H), 7.37 – 7.51 (m, 2H), 7.57 – 7.65 (m, 4H), 7.73 (d, *J*_{HH} = 9.0 Hz, 2H), 7.79 (dd, *J*_{HH} = 8.4 Hz, *J*_{HH} = 1.3 Hz, 1H) ppm.

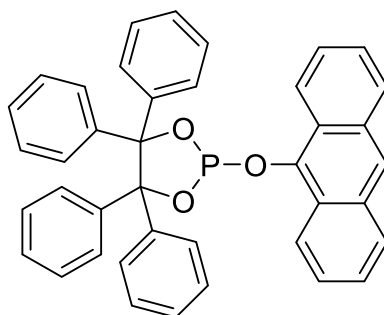
¹³C NMR (75 MHz, CD₂Cl₂, 298 K): δ = 95.8 (d, *J*_{CP} = 8.1 Hz), 116.5 – 117.0 (m), 121.8 (d, *J*_{CP} = 5.7 Hz), 125.4, 125.8, 127.1, 127.6, 127.7, 127.9, 128.0, 128.2, 128.7, 129.3 (d, *J*_{CP} = 3.2 Hz), 129.6, 130.1, 130.5, 131.0, 134.6, 142.5 (d, *J*_{CP} = 4.0 Hz), 143.2, 149.4 (d, *J*_{CP} = 8.3 Hz) ppm.

³¹P NMR (121 MHz, CD₂Cl₂, 298 K): δ = 138.1 (s) ppm.

HRMS (ESI): Calculated for C₃₆H₂₇O₃PK (M+K)⁺ 577.13294, found 577.13431.

Elemental analysis (calc. for C₃₆H₂₇O₃P = 538.16 g/mol): C, 80.57 (80.35); H, 4.95 (4.98); P, 5.77 (5.75) %.

2-(Anthracen-9-yloxy)-4,4,5,5-tetraphenyl-1,3,2-dioxaphospholane (8h):



To a stirred suspension of 0.32 g anthracen-9-ol (2.124 mmol) in 5 ml THF, 1.5 ml *n*-BuLi (1.6 M, 2.348 mmol) in hexane was added dropwise at -20°C . The orange mixture was stirred for 20 minutes, and warmed gently to room temperature. Then it was treated dropwise with a cold solution of 0.92 g 2-chloro-4,4,5,5-tetraphenyl-1,3,2-dioxaphospholane (**7**, 2.124 mmol) in 5 ml THF. The yellow reaction mixture was stirred over night at room temperature. The filtrate was evaporated to dryness *in vacuo*. The residue obtained was dissolved in toluene (10 ml), the solution was filtered and the solvent removed *in vacuo*. The solid product was dried at 0.1 mbar, 50°C and purified by column chromatography using dichloromethane/*n*-hexane = $\frac{1}{2}$ ($R_f = 0.5$). Yield: 0.554 g (0.942 mmol, 73 %).

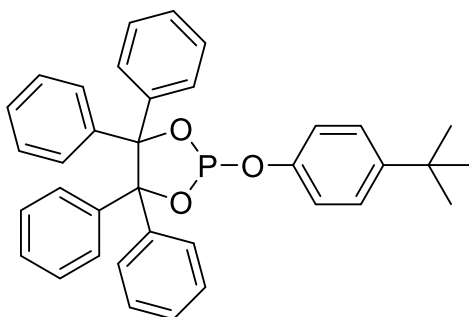
^1H NMR (300 MHz, CD_2Cl_2 , 298 K): $\delta = 7.01 - 7.18$ (m, 11H), 7.21 - 7.32 (m, 6H), 7.39 - 7.51 (m, 4H), 7.77 - 7.83 (m, 3H), 7.91 - 8.02 (m, 4H), 8.24 (s, 1H) ppm.

^{13}C NMR (75 MHz, CD_2Cl_2 , 298 K): $\delta = 96.3$ (d, $J_{\text{CP}} = 8.2$ Hz), 122.9 (d, $J_{\text{CP}} = 1.7$ Hz), 123.3 (d, $J_{\text{CP}} = 2.1$ Hz), 125.2 (d, $J_{\text{CP}} = 3.8$ Hz), 126.2 (d, $J_{\text{CP}} = 7.2$ Hz), 127.6, 127.7, 127.9, 128.0, 128.2 (d, $J_{\text{CP}} = 1.4$ Hz), 128.5, 128.6, 129.2 (d, $J_{\text{CP}} = 7.0$ Hz), 129.3, 129.4, 130.7, 132.6 (d, $J_{\text{CP}} = 1.3$ Hz), 133.3, 139.4, 142.3 (d, $J_{\text{CP}} = 4.4$ Hz), 143.2, 143.7 (d, $J_{\text{CP}} = 7.1$ Hz) ppm.

^{31}P NMR (121 MHz, CD_2Cl_2 , 298 K): $\delta = 144.1$ (s) ppm.

HRMS (ESI): Calculated for $\text{C}_{40}\text{H}_{30}\text{O}_3\text{P}$ ($\text{M}+\text{H}$) $^+$ 589.19326, found 589.19277.

Elemental analysis (calc. for $\text{C}_{40}\text{H}_{29}\text{O}_3\text{P}$ = 588.64 g/mol): C, 81.56 (81.62); H, 5.13 (4.97); P, 5.23 (5.26) %.

2-(4-(*tert*-Butyl)phenoxy)-4,4,5,5-tetraphenyl-1,3,2-dioxaphospholane (8i):

To a stirred suspension of 0.18 g 4-(*tert*-butyl)phenol (1.201 mmol) in 5 ml toluene, 0.41 ml triethylamine (0.301 g, 2.97 mmol) was added dropwise at room temperature. The reaction mixture was treated dropwise with a cold solution of 0.52 g 2-chloro-4,4,5,5-tetraphenyl-1,3,2-dioxaphospholane (**7**, 1.201 mmol) in 5 ml toluene. The reaction mixture was stirred 24 h at room temperature and filtered. The filtrate was evaporated to dryness *in vacuo*. The residue obtained was dissolved in toluene (15 ml), the solution was filtered through a thin layer of silica and the solvent removed *in vacuo* and the solid product dried at 0.1 bar, 40 °C, for 5 h. Yield: 0.610 g (1.12 mmol, 93 %).

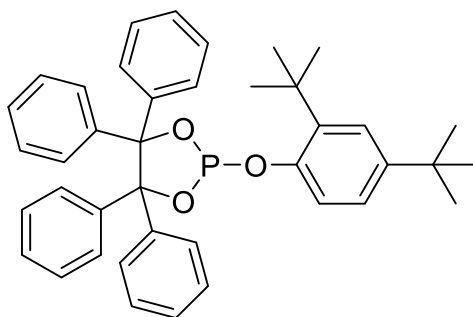
¹H NMR (500 MHz, CD₂Cl₂, 298 K): δ = 1.28 (s, 9H, 3CH₃), 6.63 – 6.67 (m, 2H), 7.03 – 7.13 (m, 10H), 7.18 – 7.27 (m, 8H), 7.53 – 7.59 (m, 4H) ppm.

¹³C NMR (75 MHz, CD₂Cl₂, 298 K): δ = 31.7 (3CH₃), 34.7, 95.7 (d, *J*_{CP} = 7.9 Hz), 120.6 (d, *J*_{CP} = 7.8 Hz), 127.0, 127.6, 127.7, 127.8, 127.9, 129.3 (d, *J*_{CP} = 3.3 Hz), 130.4, 142.6 (d, *J*_{CP} = 4.1 Hz), 143.3, 147.5 (d, *J*_{CP} = 1.4 Hz), 149.2 (d, *J*_{CP} = 8.6 Hz) ppm.

³¹P NMR (202 MHz, CD₂Cl₂, 298 K): δ = 138.8 (s) ppm.

HRMS (ESI): Calculated for C₃₆H₃₄O₃P (M+H)⁺ 545.2245, found 545.2247. Calculated for C₃₆H₃₃O₃PNa (M+Na)⁺ 567.2059, found 567.2064.

Elemental analysis (calc. for C₃₆H₃₃O₃P = 544.63 g/mol): C, 79.50 (79.39); H, 6.18 (6.11); P, 5.59 (5.69) %.

2-(2,4-di-*tert*-Butylphenoxy)-4,4,5,5-tetraphenyl-1,3,2-dioxaphospholane (8j):

To a stirred suspension of 0.54 g 2,4-di-*tert*-butylphenol (2.621 mmol) in 7 ml THF were added 1.92 ml of a solution of *n*-BuLi in hexane (1.6 M, 3.145 mmol) at -20 °C. The solution was stirred at -20 °C for 1 h and warmed to room temperature afterwards. A solution of 1.129 g 2-chloro-4,4,5,5-tetraphenyl-1,3,2-dioxaphospholane (**7**, 2.621 mmol) in 7 ml THF was added dropwise and the solution was stirred at room temperature for another 72 h. The solvent was evaporated *in vacuo* and the remaining residue was dissolved in toluene and filtered. The crude product was purified by column chromatography using dichloromethane/*n*-heptane = 5/95 to yield a white solid. Yield: 0.866 g (1.441 mmol, 55 %).

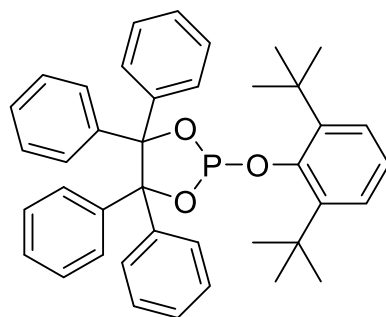
¹H NMR (250 MHz, CD₂Cl₂, 298 K): δ = 1.21 (s, 9H, 3CH₃), 1.29 (s, 9H, 3CH₃), 6.86 (d, *J*_{HH} = 8.2 Hz, 1H), 7.07 – 7.17 (m, 17H), 7.32 (d, *J*_{HH} = 2.5 Hz, 1H), 7.51 – 7.57 (m, 4H) ppm.

¹³C NMR (63 MHz, CD₂Cl₂, 298 K): δ = 30.4 (3CH₃), 31.8 (3CH₃), 35.0, 35.1, 95.8 (d, *J*_{CP} = 8.2 Hz), 121.0, 121.3, 124.1, 124.9, 127.6, 127.7, 127.8, 129.3 (d, *J*_{CP} = 3.4 Hz), 130.3, 140.7 (d, *J*_{CP} = 2.8 Hz), 142.7 (d, *J*_{CP} = 4.3 Hz), 143.2, 147.0, 148.5 (d, *J*_{CP} = 10.2 Hz) ppm.

³¹P NMR (101 MHz, CD₂Cl₂, 298 K): δ = 138.0 (s) ppm.

HRMS (ESI): Calculated for C₄₀H₄₂O₃P (M+H)⁺; 601,2866 found; 601.2866.

Elemental analysis (calc. for C₄₀H₄₁O₃P = 600.74 g/mol): C, 79.94 (79.97); H, 6.89 (6.88); P, 5.26 (5.16) %.

2-(2,6-di-*tert*-Butylphenoxy)-4,4,5,5-tetraphenyl-1,3,2-dioxaphospholane (8k):

To a stirred suspension of 0.41 g 2,6-di-*tert*-butylphenol (0.412 g, 2.00 mmol) in 5 ml THF, 1.00 ml *n*-BuLi (2.5 M, 2.50 mmol) in hexane was added dropwise at 0 °C. The mixture was stirred for 20 minutes, and warmed gently to room temperature. Then it was treated dropwise with a cold solution of 0.86 g 2-chloro-4,4,5,5-tetraphenyl-1,3,2-dioxaphospholane (**7**, 2.00 mmol) in 5 ml THF. The reaction mixture was stirred 24 h at room temperature and filtered. The filtrate was evaporated to dryness *in vacuo*. The residue obtained was dissolved in toluene (15 ml), the solution was filtered through a thin layer of silica and the solvent removed *in vacuo* and the solid product dried at 0.1 bar, 40 °C, for 5 h. Yield: 0.853 g (1.42 mmol, 71 %).

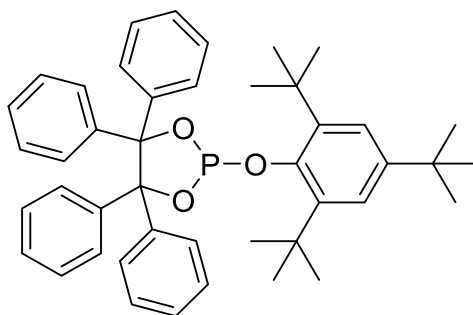
¹H NMR (300 MHz, CD₂Cl₂, 298 K): δ = 1.33 (s, 18H, 9CH₃), 6.94 – 7.13 (m, 11H), 7.14 – 7.21 (m, 6H), 7.30 (dd, *J*_{HH} = 8.0 Hz, *J*_{CP} = 1.7 Hz, 2H), 7.55 – 7.65 (m, 4H) ppm.

¹³C NMR (75 MHz, CD₂Cl₂, 298 K): δ = 96.2 (d, *J*_{CP} = 9.0 Hz), 124.2, 126.7, 127.5, 127.5, 127.8, 127.9, 128.2, 129.2 (d, *J*_{CP} = 4.3 Hz), 130.8, 131.7, 142.5 (d, *J*_{CP} = 4.9 Hz), 142.7, 144.3 (d, *J*_{CP} = 3.3 Hz), 150.8 (d, *J*_{CP} = 11.8 Hz) ppm.

³¹P NMR (121 MHz, CD₂Cl₂, 298 K): δ = 145.1 (s) ppm.

HRMS (ESI): Calculated for C₄₀H₄₂O₃P (M+H)⁺; 601.2856 found; 601.2866.

Elemental analysis (calc. for C₄₀H₄₁O₃P = 600.74 g/mol): C, 79.91 (79.97); H, 6.90 (6.88); P, 5.03 (5.16) %.

4,4,5,5-Tetraphenyl-2-(2,4,6-tri-*tert*-butylphenoxy)-1,3,2-dioxaphospholane (8l):

To a stirred suspension of 0.39 g 2,4,6-tri-*tert*-butylphenol (1.50 mmol) in 5 ml THF, 0.60 ml *n*-BuLi (2.5 M, 1.00 mmol) in hexane was added dropwise at 0 °C, mixture was stirred for 20 minutes, and warmed gently to room temperature. Then it was treated dropwise with a cold solution of 0.65 g 2-chloro-4,4,5,5-tetraphenyl-1,3,2-dioxaphospholane (**7**, 1.50 mmol) in 5 ml THF. The reaction mixture was stirred 24 h at room temperature and filtered. The filtrate was evaporated to dryness *in vacuo*. The residue obtained was dissolved in toluene (15 ml), the solution was filtered through a thin layer of silica and the solvent removed *in vacuo* and the solid product dried at 0.1 bar, 40 °C, for 5 h. Yield: 0.541 g (0.82 mmol, 55 %).

¹H NMR (500 MHz, CD₂Cl₂, 298 K): δ = 1.30 (s, 9H), 1.34 (s, 18H), 7.00 – 7.06 (m, 4H), 7.06 – 7.13 (m, 6H), 7.17 (dd, *J*_{HH} = 5.1 Hz, *J*_{HH} = 2.0 Hz, 5H), 7.33 (s, 3H), 7.57 – 7.65 (m, 4H) ppm.

¹³C NMR (126 MHz, CD₂Cl₂, 298 K): δ = 31.8 (3CH₃), 32.1 (d, *J*_{CP} = 3.8 Hz, (3CH₃)), 35.1, 96.2 (d, *J*_{CP} = 9.2 Hz), 123.8, 127.5 (d, *J*_{CP} = 6.1 Hz), 127.9 (d, *J*_{CP} = 12.1 Hz), 128.2, 129.2 (d, *J*_{CP} = 4.2 Hz), 130.9, 131.7, 142.5 (d, *J*_{CP} = 4.5 Hz), 142.8, 143.2 (d, *J*_{CP} = 3.3 Hz), 146.0, 148.3 (d, *J*_{CP} = 11.4 Hz) ppm.

³¹P NMR (121 MHz, CD₂Cl₂, 298 K): δ = 145.2 (s) ppm.

HRMS (ESI): Calculated for C₄₄H₅₀O₃P (M+H)⁺; 657.3492 found; 657.3492.

Elemental analysis (calc. for C₄₄H₄₉O₃P = 656.85 g/mol): C, 80.38 (80.46); H, 7.38 (7.52); P, 4.78 (4.72) %.

5.1.4 Hydroformylation with phosphites with benzopinacol structure

The hydroformylation experiments of phosphites with benzopinacol structure were performed in a 150 ml autoclave (Premex Solutions GmbH, Switzerland) equipped with a gas inlet stirrer, a thermocouple, a storage vessel allowing the addition of substrate under pressure applied, a Bronkhorst hitec® pressure controller as well as a Bronkhorst hitec® gas flow meter. The autoclave periphery allowed us to fill in and to remove any media and reagents under the exclusion of air. A high-grade pure syngas (99.997 %; CO/H₂ = 1:1) was used, which was purchased from Linde AG. The composition of the technical octene mixture used as a substrate for the hydroformylation reaction was: 3.3% 1-octene, 48.4% Z/E-2-octene, 29.2% Z/E-3-octene, 16.4% Z/E-4-octene, 2.1% skeletal C8-olefinic isomers, 0.6% *n*-octane. Olefins were refluxed in an argon atmosphere over sodium metal and freshly distilled prior to use.

For the hydroformylation experiments the reaction solution was prepared under an atmosphere of argon. The mass of toluene was defined for GC analysis. The stirred reaction solution was pressurized with 32 bar syngas and heated to the assigned temperature. After reaching the reaction temperature the pressure was elevated to 46 bar and the *n*-octene was added with a pressure of 54 bar. The reaction was kept at constant pressure of 50 bar for 4 h. The current gas flow was determined in a time cycle of three seconds simultaneously to the reaction process. The gas consumption curve thus obtained was used to determine the observed 1st order velocity constant k_{obs} . After the reaction time the autoclave was cooled down to room temperature, the pressure was released and purged with argon. 0.1 ml of the reaction solution were diluted with 1 ml pentane and analyzed with gas chromatography (HP 5890 Series II plus, PONA, 50 m x 0,2 mm x 0,5 µm). The quantitative amount of remaining olefin and newly formed aldehyde were determined using toluene as internal standard.

5.1.5 Hydrolysis of phosphites with biphenol and benzopinacol structure

NMR samples were filled in in an argon atmosphere with standard Schlenk-techniques. 1,4-dioxane was purchased from Acros Organics which is extremely dry and stored under argon protection. 1,4-Dioxane- d_8 was purchased from Deutero and distilled in an argon atmosphere prior to use. Tri-*n*-octylphosphine oxide and *p*-xylene- d_{10} were purchased from Sigma-Aldrich (St. Louis, MO, USA). The *in situ* ^{31}P NMR experiments were carried out in a sealed 9 inch, 5 mm NMR tube (Deutero) equipped with a sealed 12.5 m capillary (Sigma-Aldrich) of an inner diameter of 1 mm, which was filled with a 0.259 M solution of tri-*n*-octylphosphine oxide (TOPO) in *p*-xylene- d_{10} along with the sample solution as an external reference and the lock solvent. The samples were dissolved in 1,4-dioxane in a concentration of 0.049 M. Water was distilled in an argon atmosphere and added into the specimen before measurement. *In situ* NMR experiments were carried out on a Bruker AVANCE 300 III spectrometer at a Larmor frequency of 300 MHz for ^1H , 121 MHz for ^{31}P , and 75 MHz for ^{13}C NMR or a Bruker AVANCE 250 spectrometer at a Larmor frequency of 250 MHz for ^1H , 101 MHz for ^{31}P and 63 MHz for ^{13}C NMR. Quantitative ^{31}P spectra were acquired with a relaxation delay of 5 s and a scan number of 256, referenced by the chemical shift of TOPO set at 41 ppm, whose integral was set as 1.

5.1.5.1 Hydrolysis diagrams of biphenolphosphites

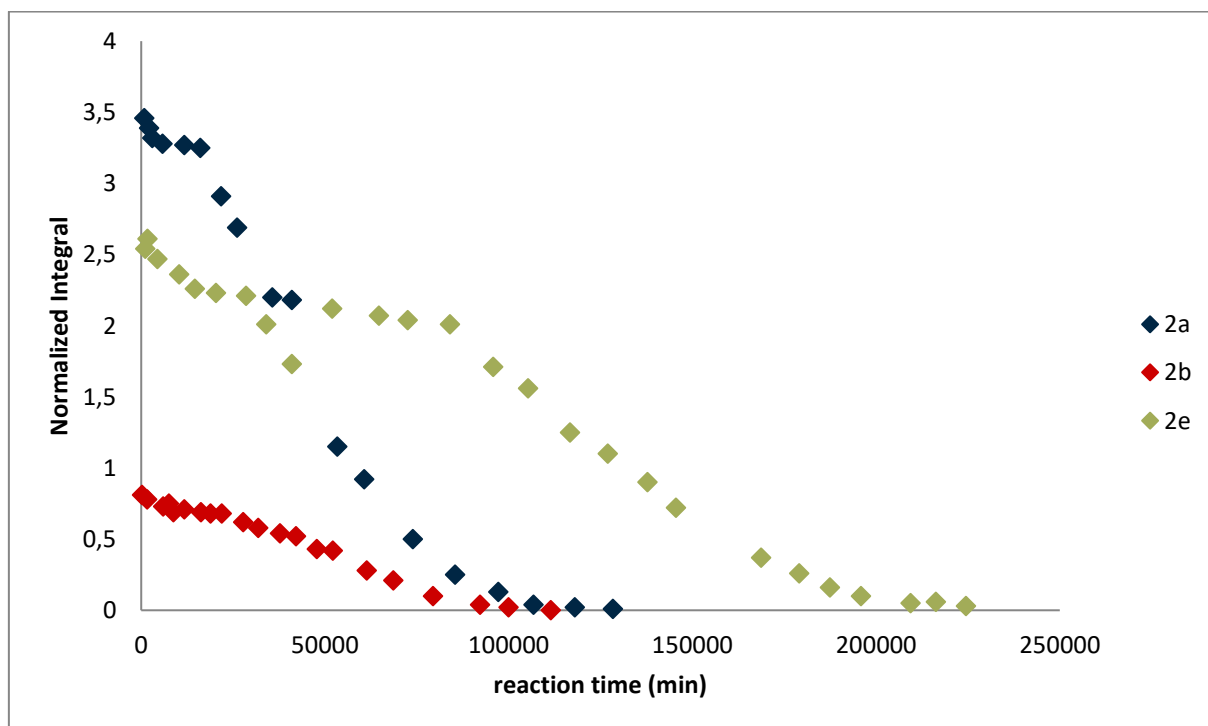


Figure A 1: Hydrolysis of 2a, 2b and 2e at room temperature.

5 Appendix

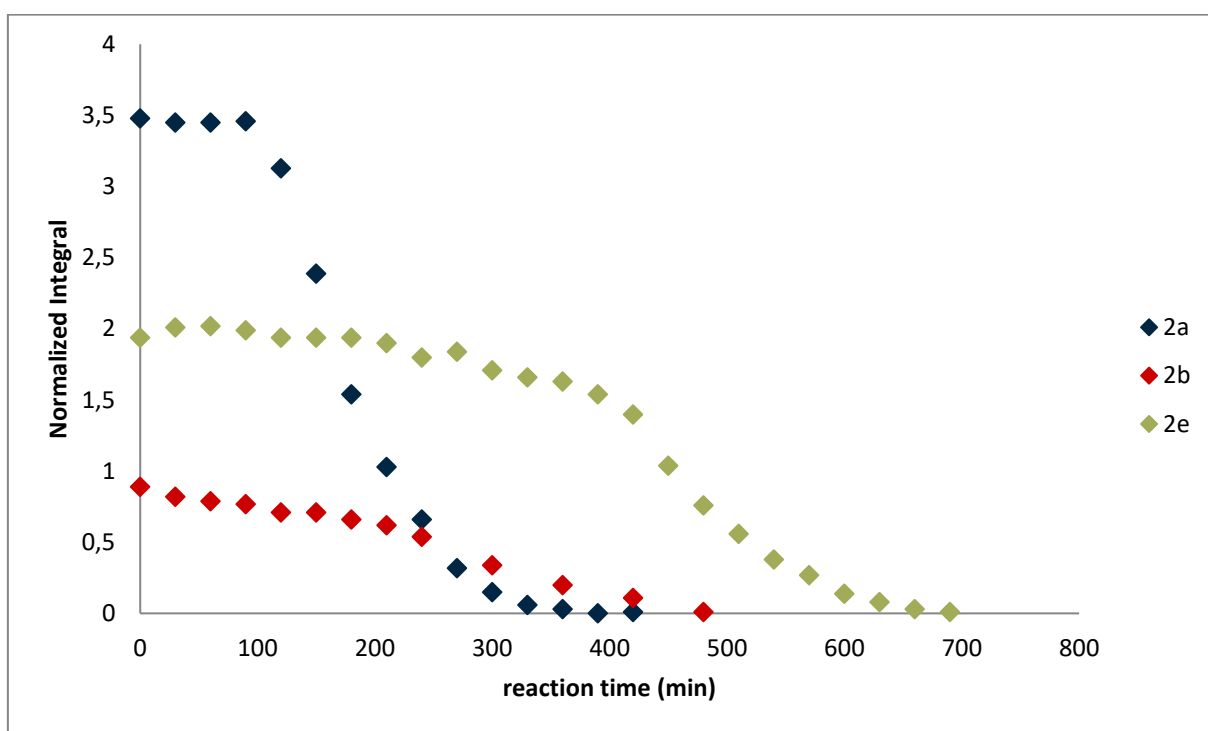


Figure A 2: Hydrolysis of 2a, 2b and 2e at 90 °C.

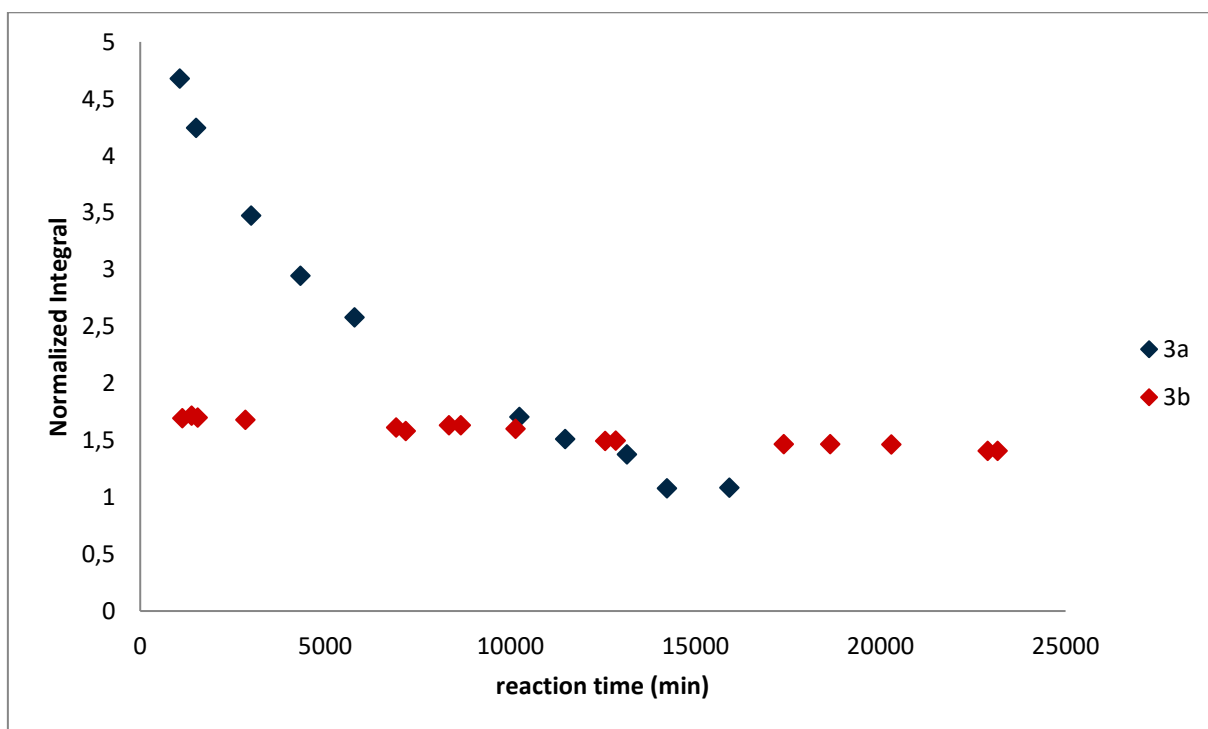


Figure A 3: Hydrolysis of 3a and 3b at room temperature.

5 Appendix

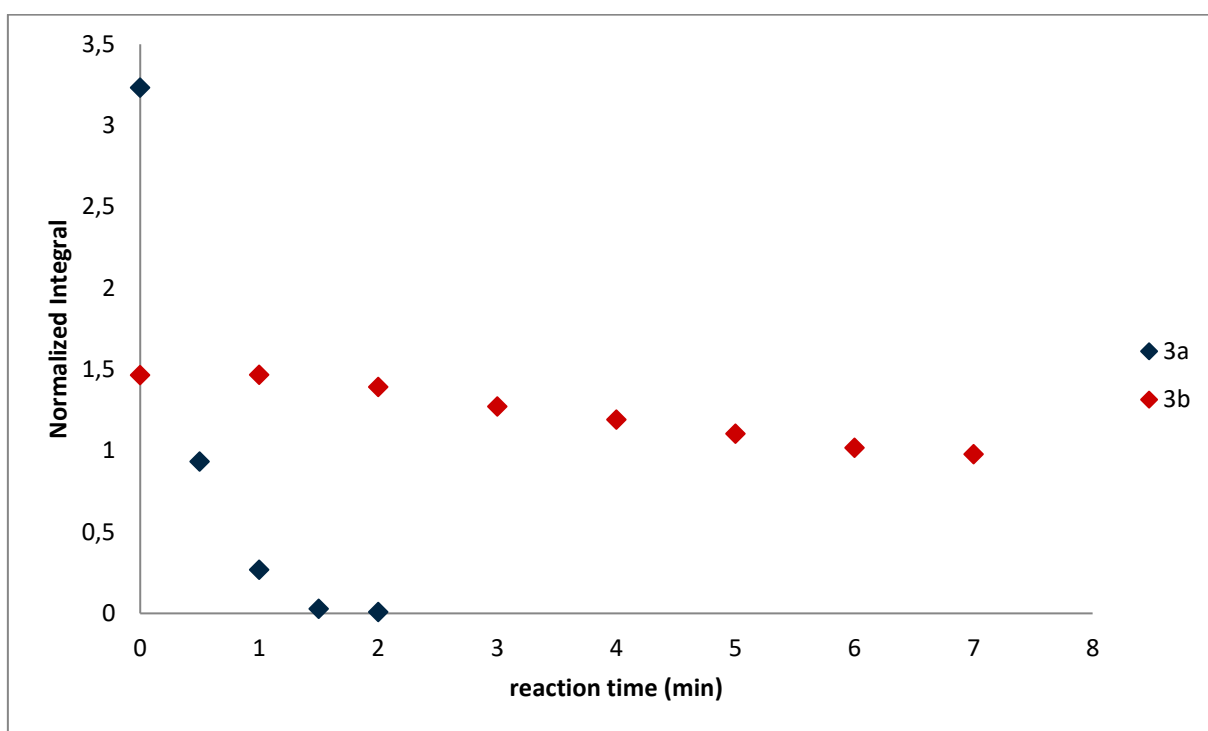


Figure A 4: Hydrolysis of 3a and 3b at 90 °C.

5.1.5.2 NMR spectra of hydrolysis reactions of biphenolphosphites

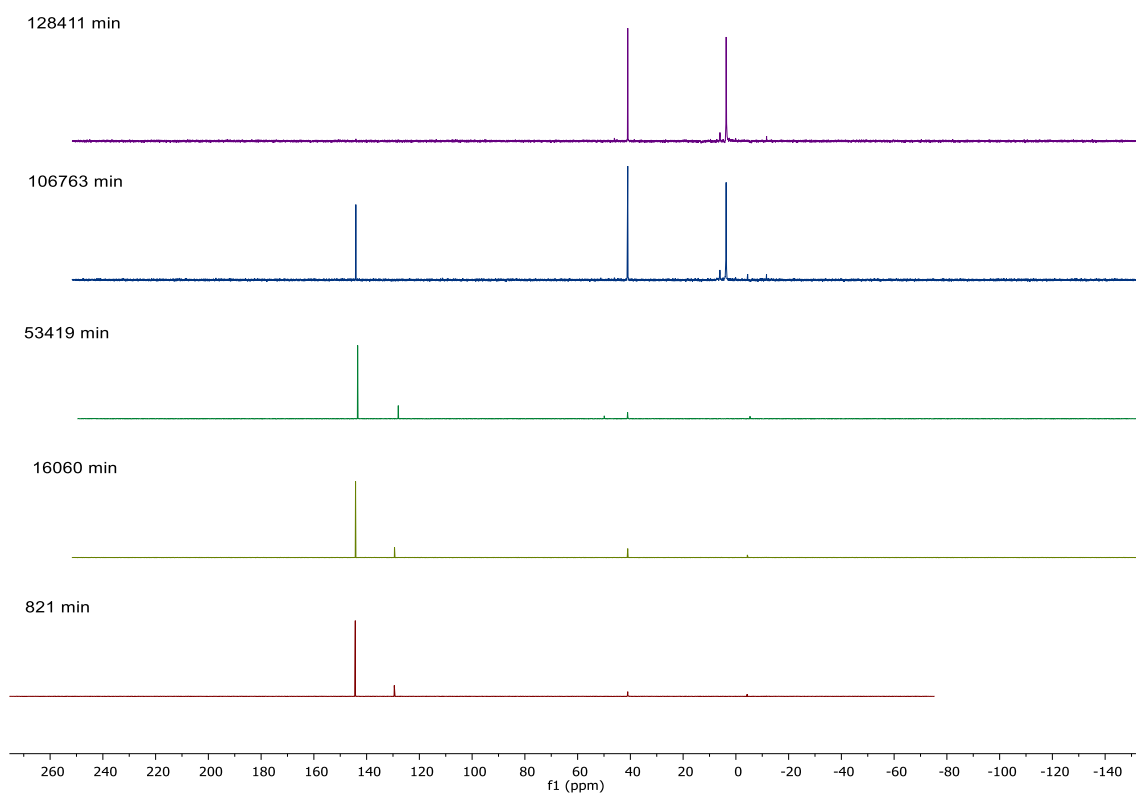


Figure A 5: NMR spectra of the hydrolysis of 2a at room temperature.

5 Appendix

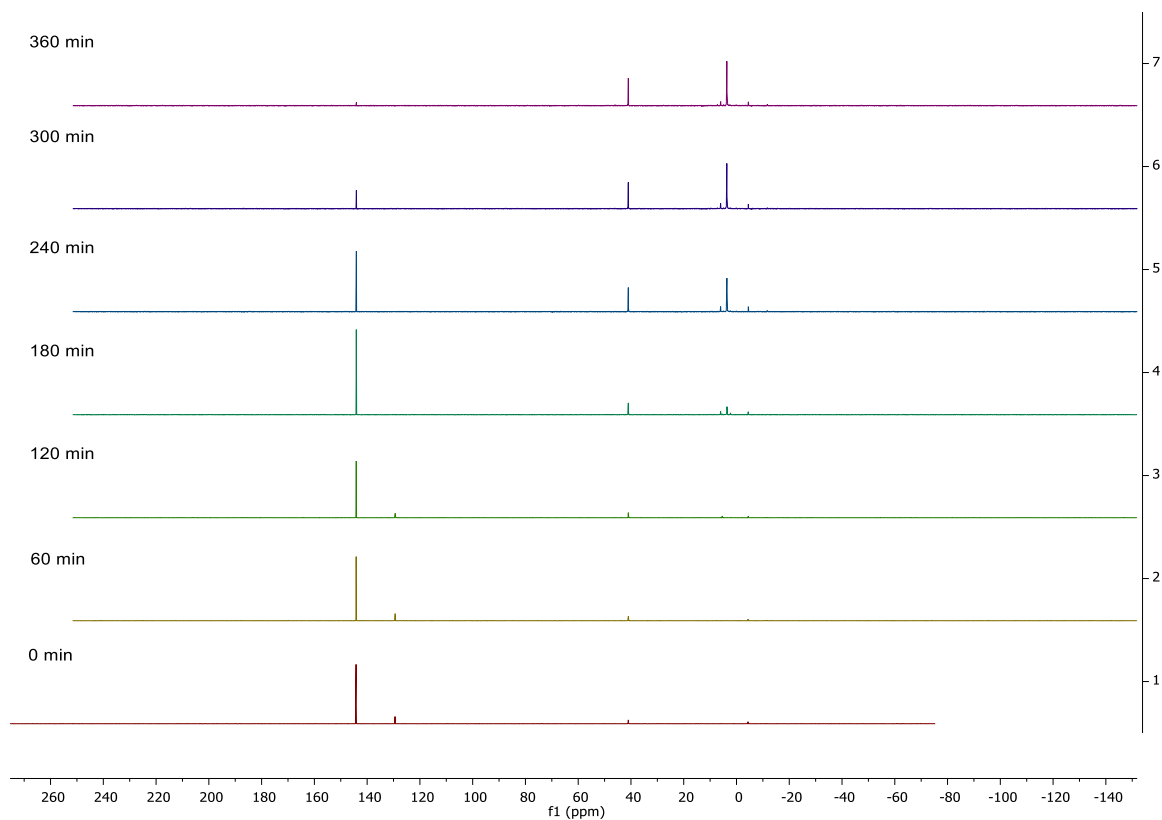


Figure A 6: NMR spectra of the hydrolysis of 2a at 90 °C.

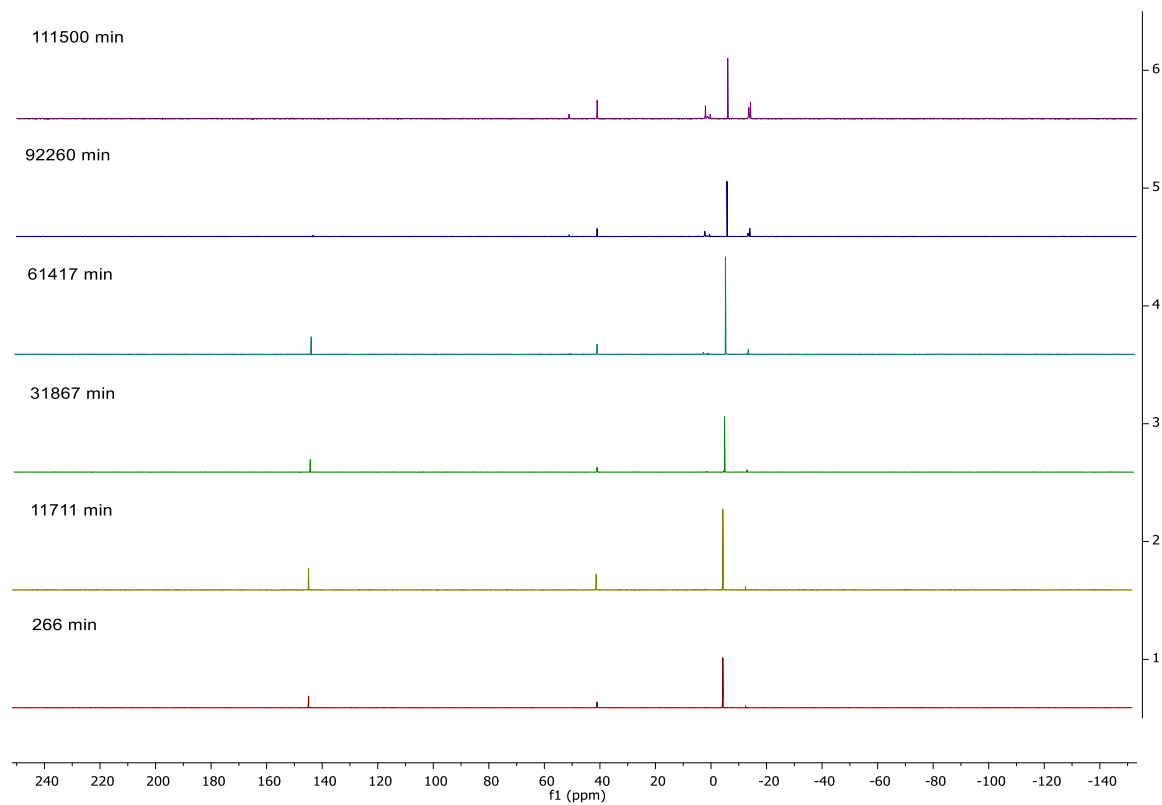


Figure A 7: NMR spectra of the hydrolysis of 2b at room temperature.

5 Appendix

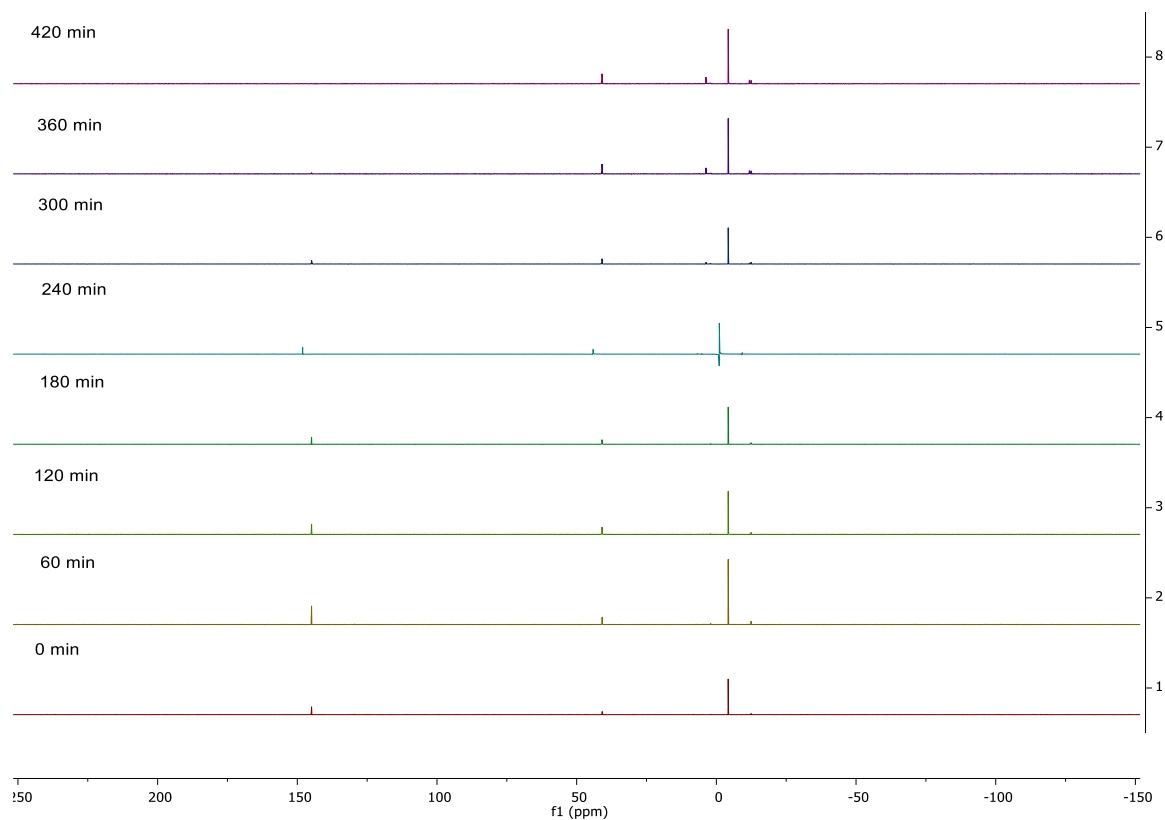


Figure A 8: NMR spectra of the hydrolysis of 2b at 90 °C.

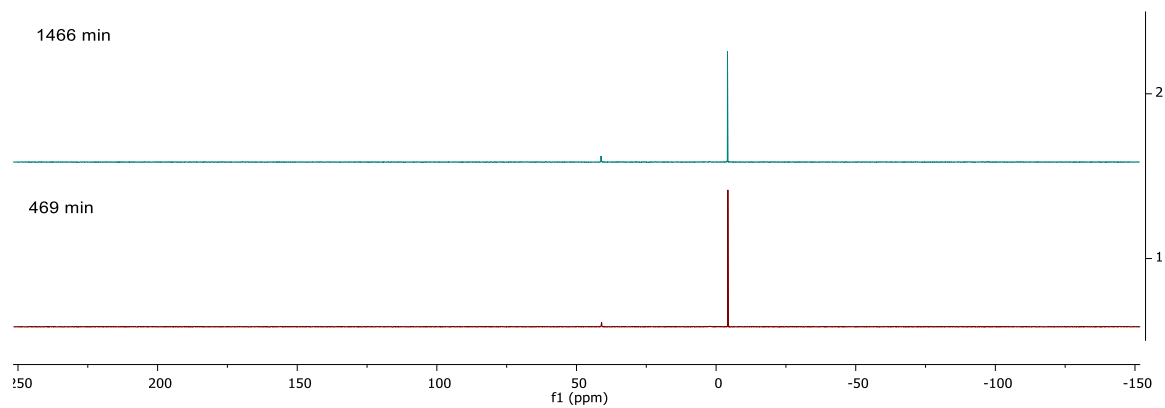


Figure A 9: NMR spectra of the hydrolysis of 2c at room temperature.

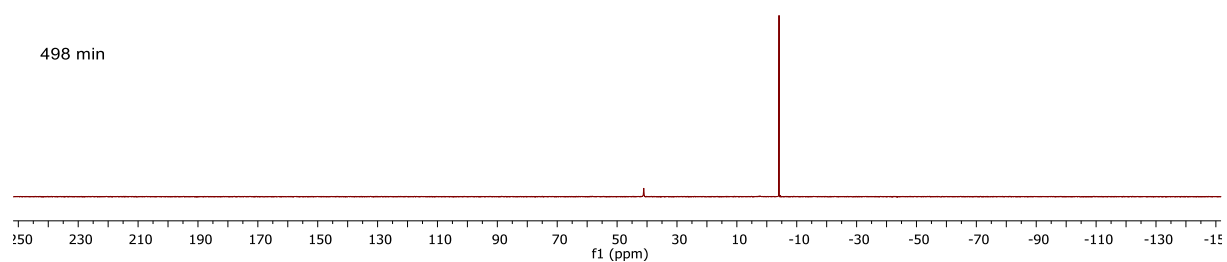


Figure A 10: NMR spectra of the hydrolysis of 2c at 90 °C.

5 Appendix

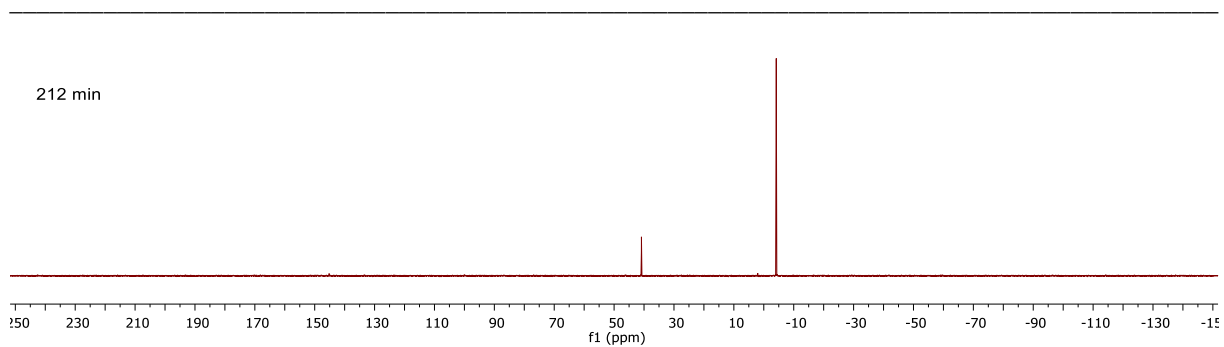


Figure A 11: NMR spectra of the hydrolysis of 2d at room temperature.

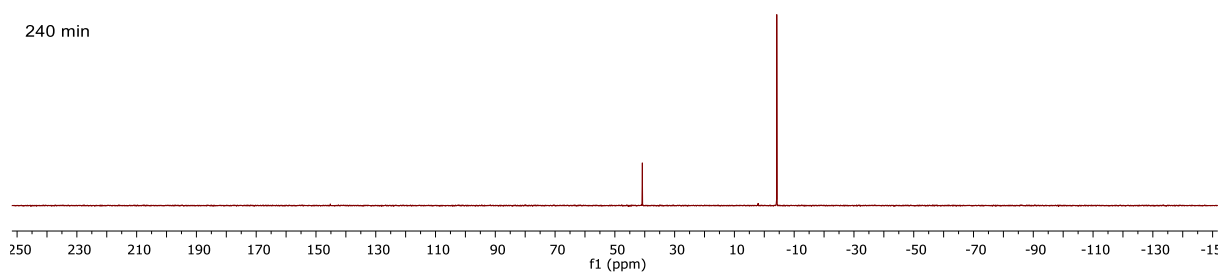


Figure A 12: NMR spectra of the hydrolysis of 2d at 90 °C.

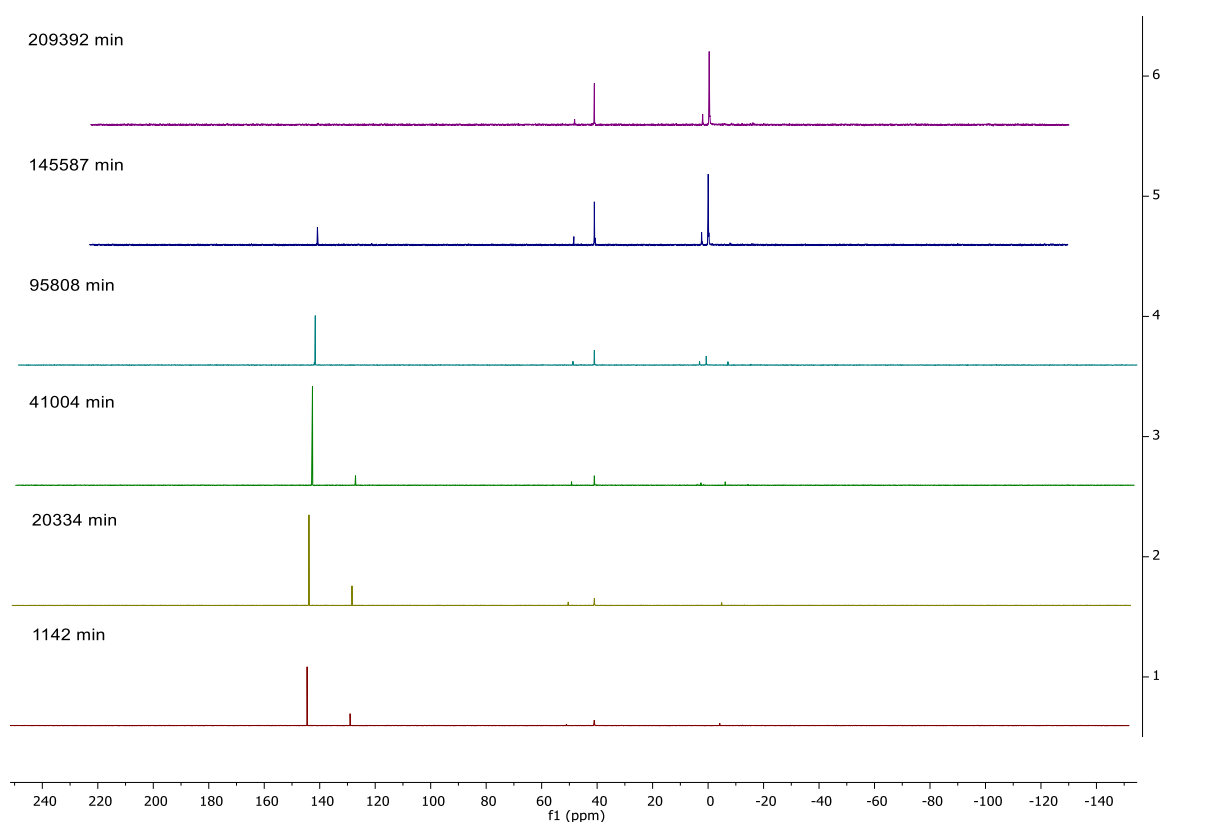


Figure A 13: NMR spectra of the hydrolysis of 2e at room temperature.

5 Appendix

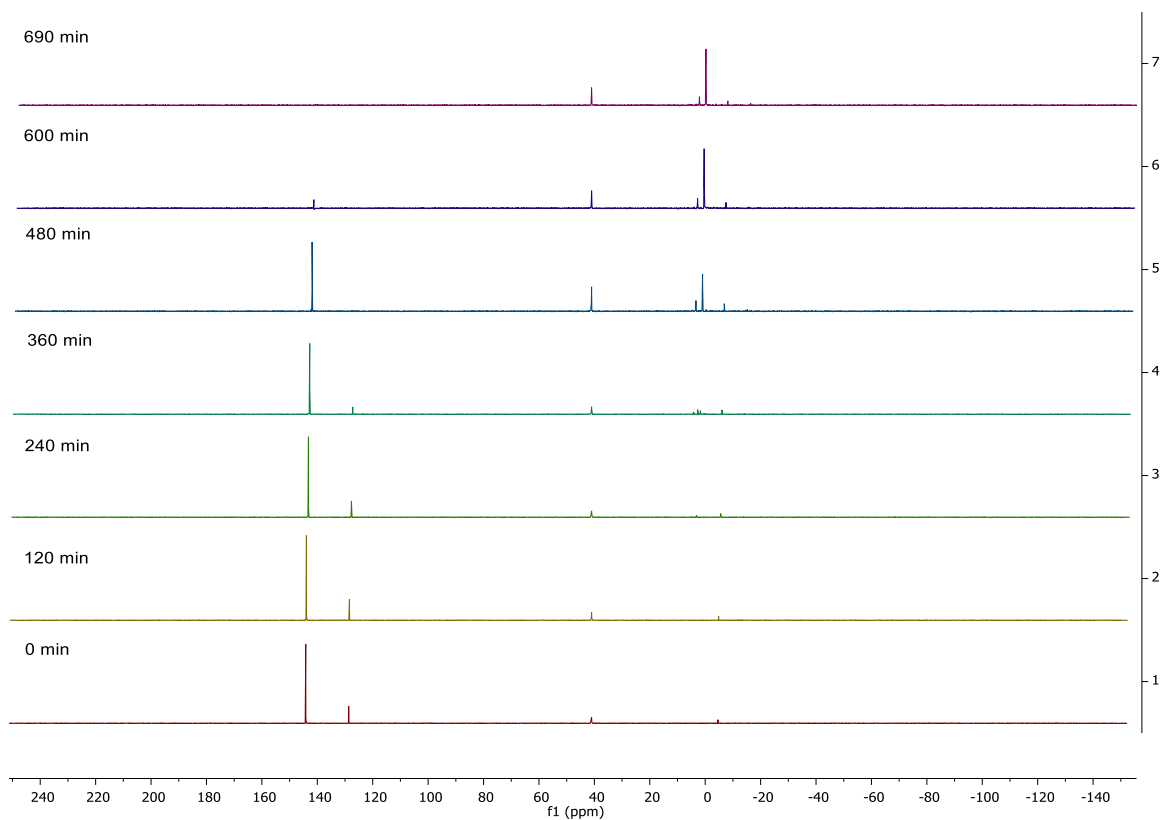


Figure A 14: NMR spectra of the hydrolysis of 2e at 90 °C.

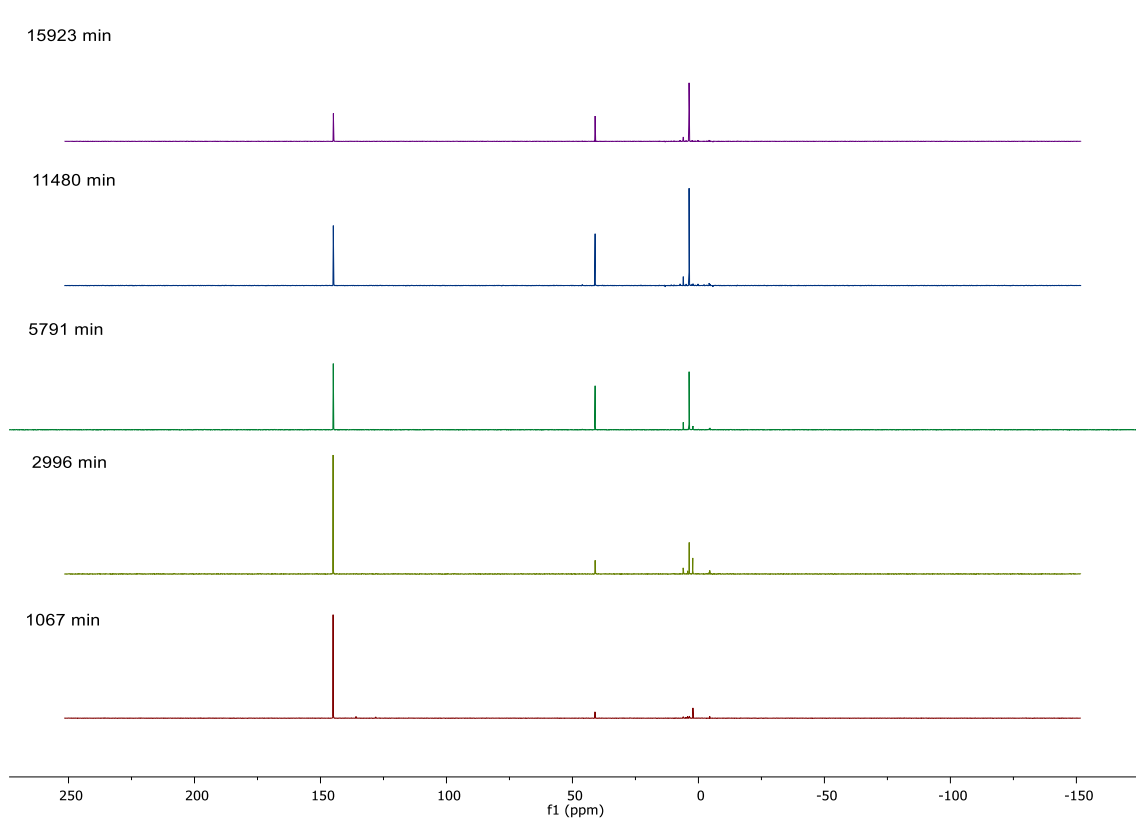


Figure A 15: NMR spectra of the hydrolysis of 3a at room temperature.

5 Appendix

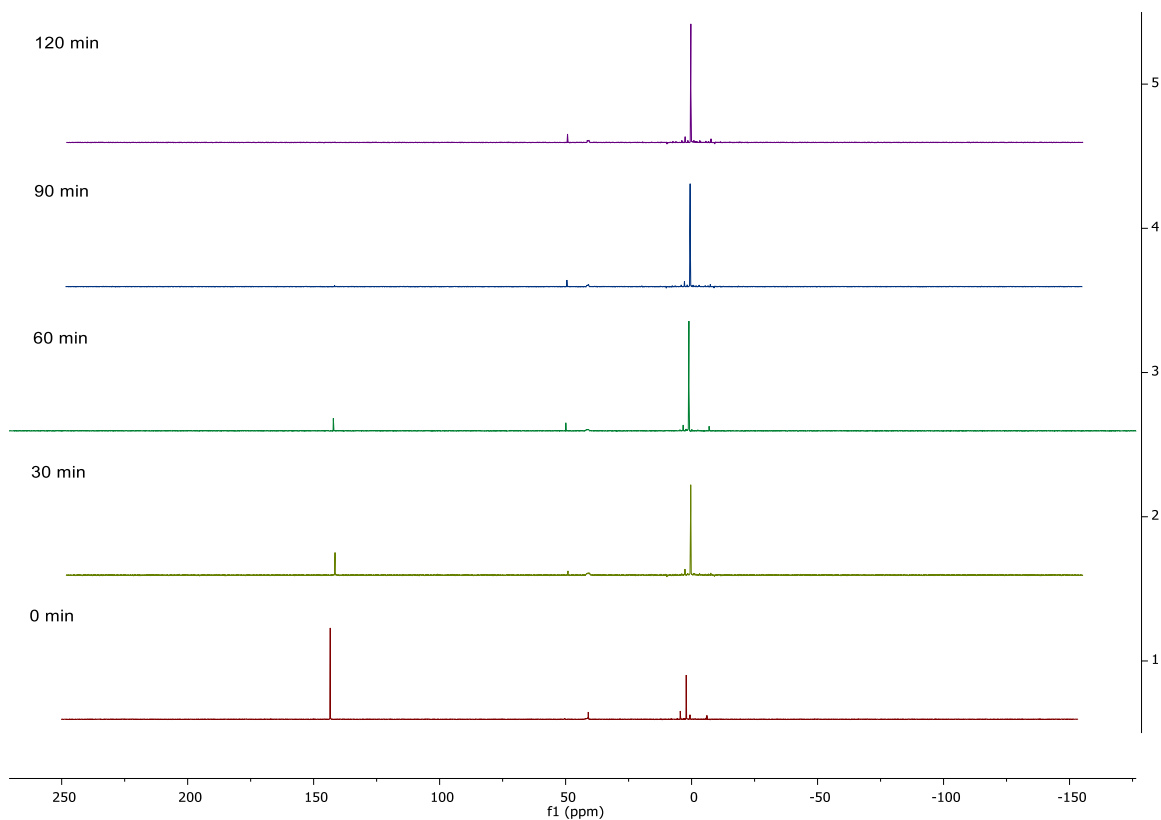


Figure A 16: NMR spectra of the hydrolysis of 3a at 90 °C.

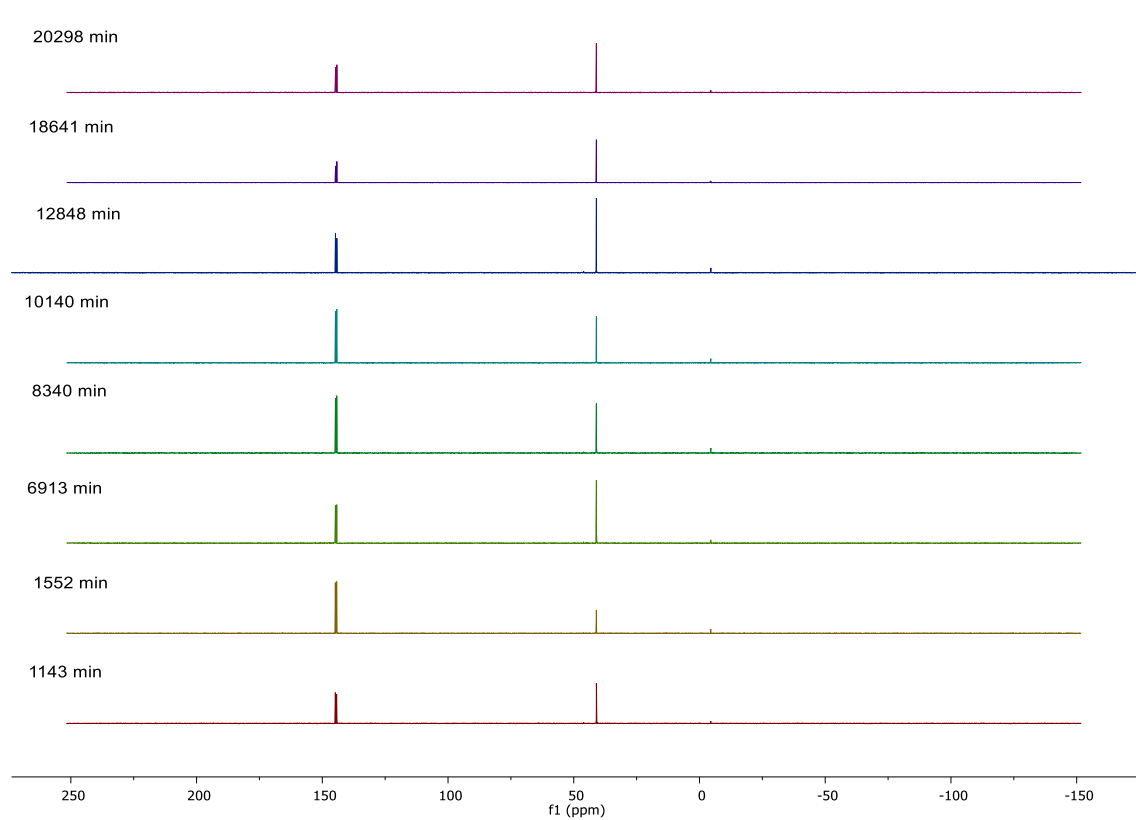


Figure A 17: NMR spectra of the hydrolysis of 3b at room temperature.

5 Appendix

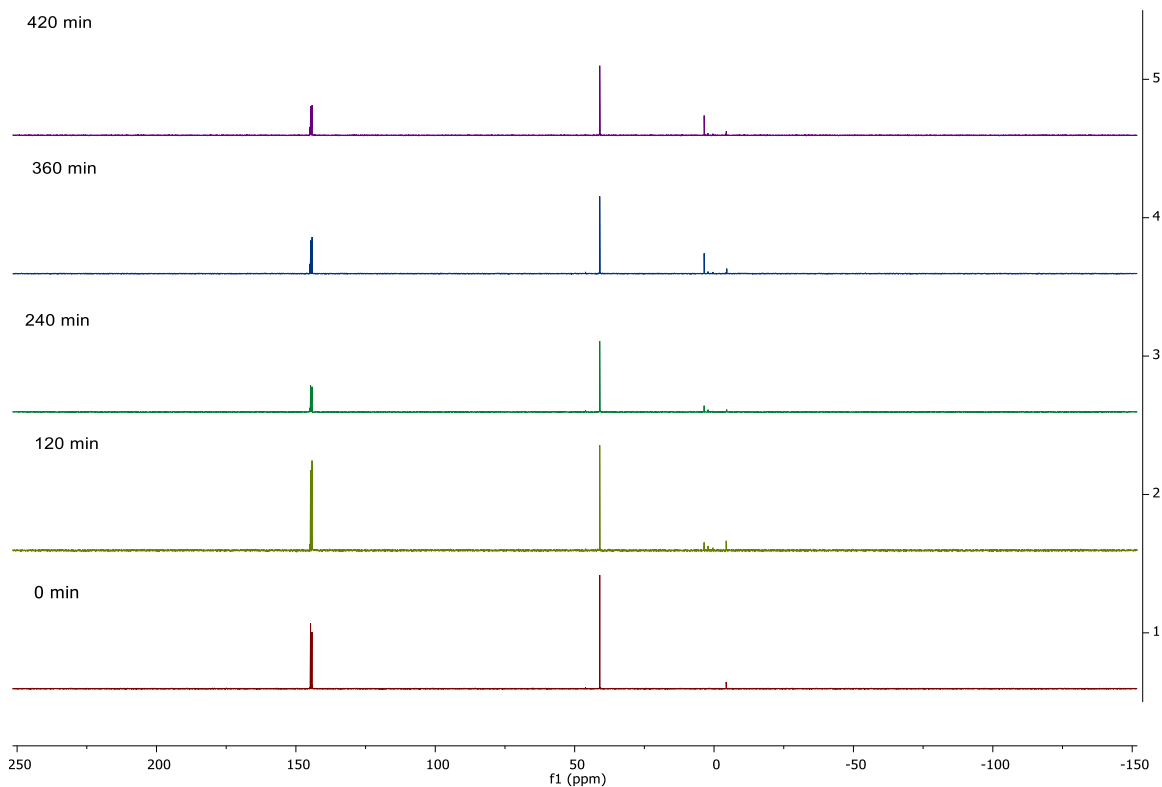


Figure A 18: NMR spectra of the hydrolysis of 3b at 90 °C.

5.1.5.3 Hydrolysis diagrams of benzopinacolphosphites

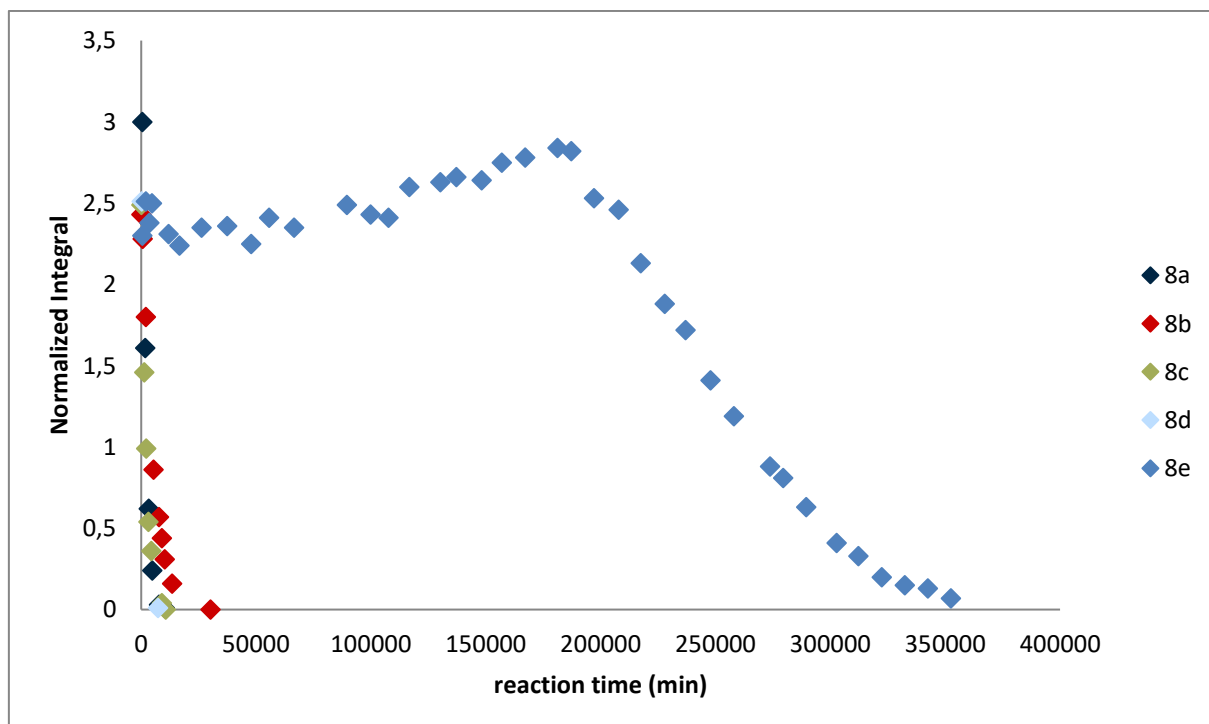


Figure A 19: Hydrolysis of 8a, 8b, 8c, 8d and 8e at room temperature.

5 Appendix

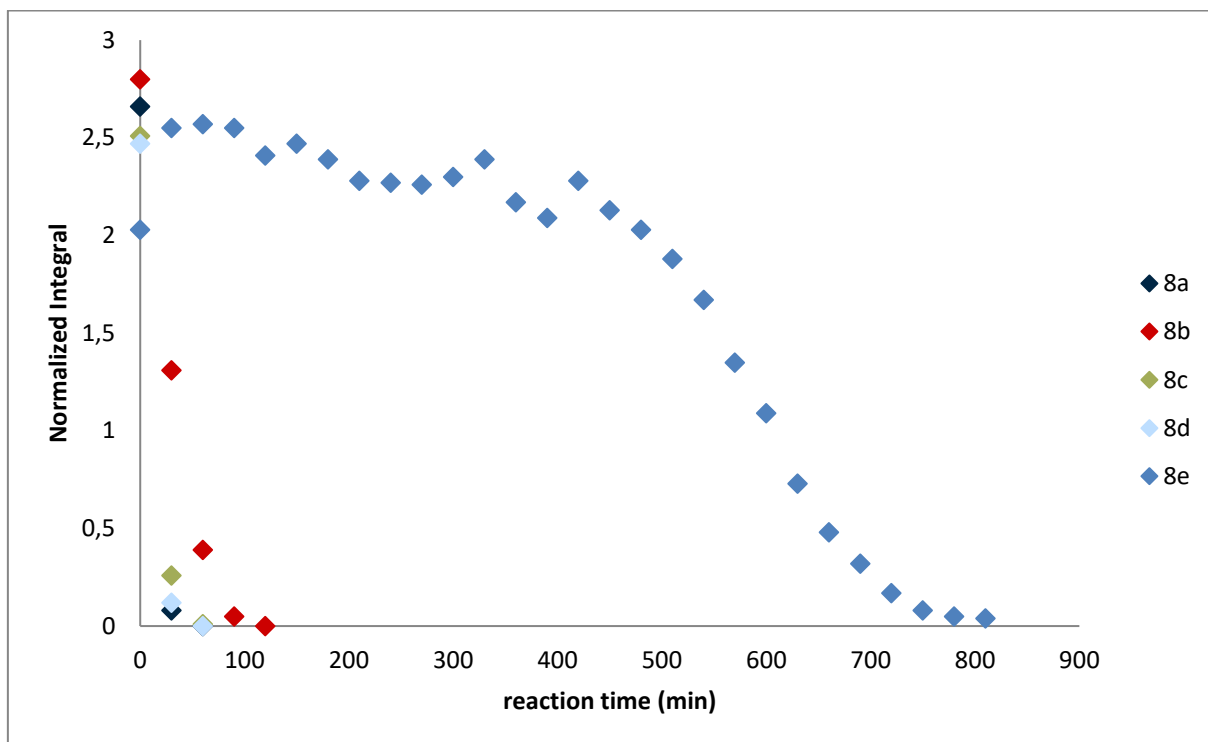


Figure A 20: Hydrolysis of 8a, 8b, 8c, 8d and 8e at 90 °C.

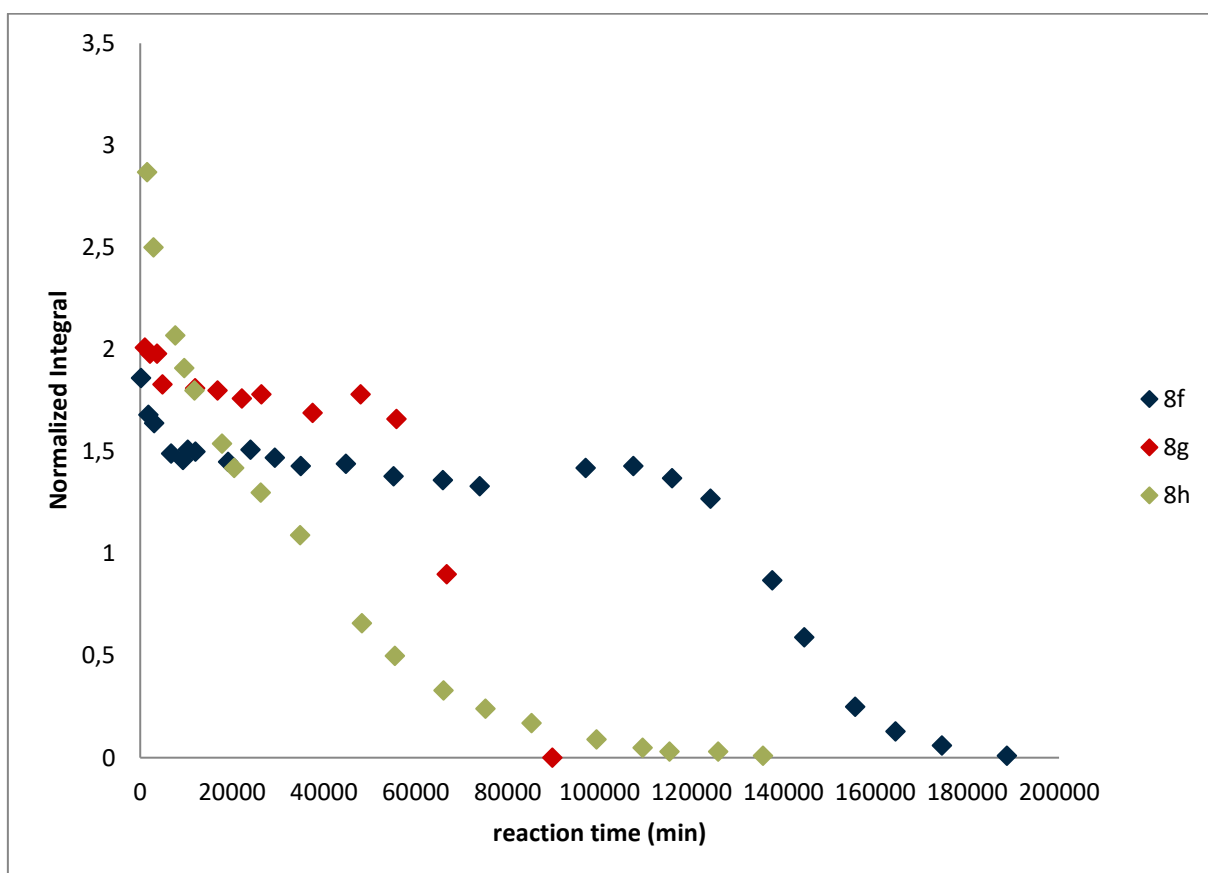


Figure A 21: Hydrolysis of 8f, 8g and 8h at room temperature.

5 Appendix

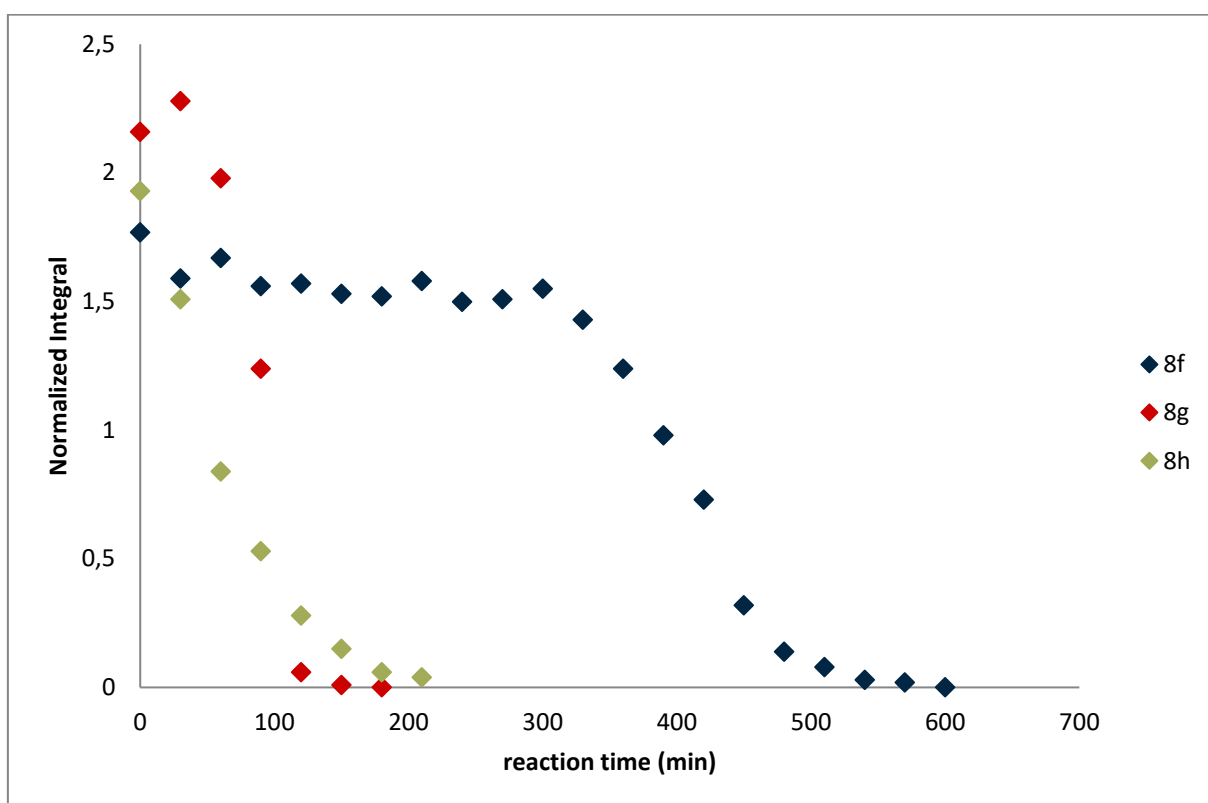


Figure A 22: Hydrolysis of 8f, 8g and 8h at 90 °C.

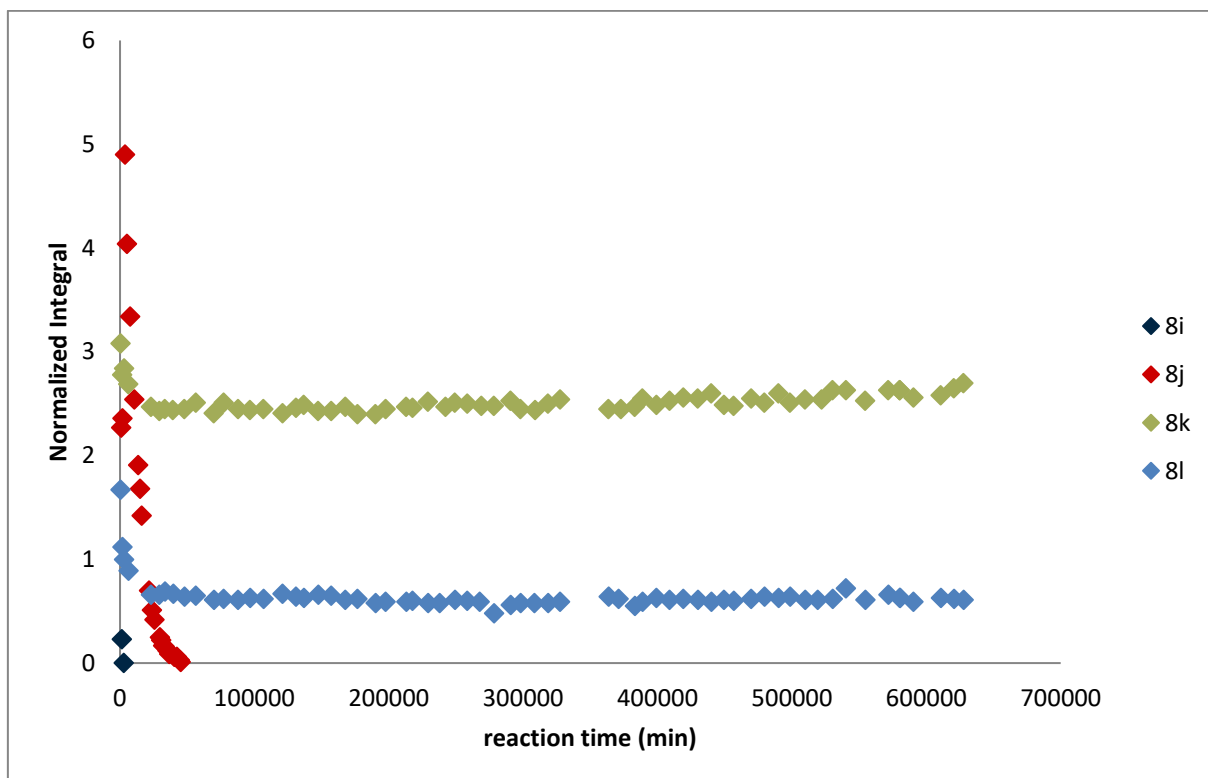


Figure A 23: Hydrolysis of 8i, 8j, 8k and 8l at room temperature.

5 Appendix

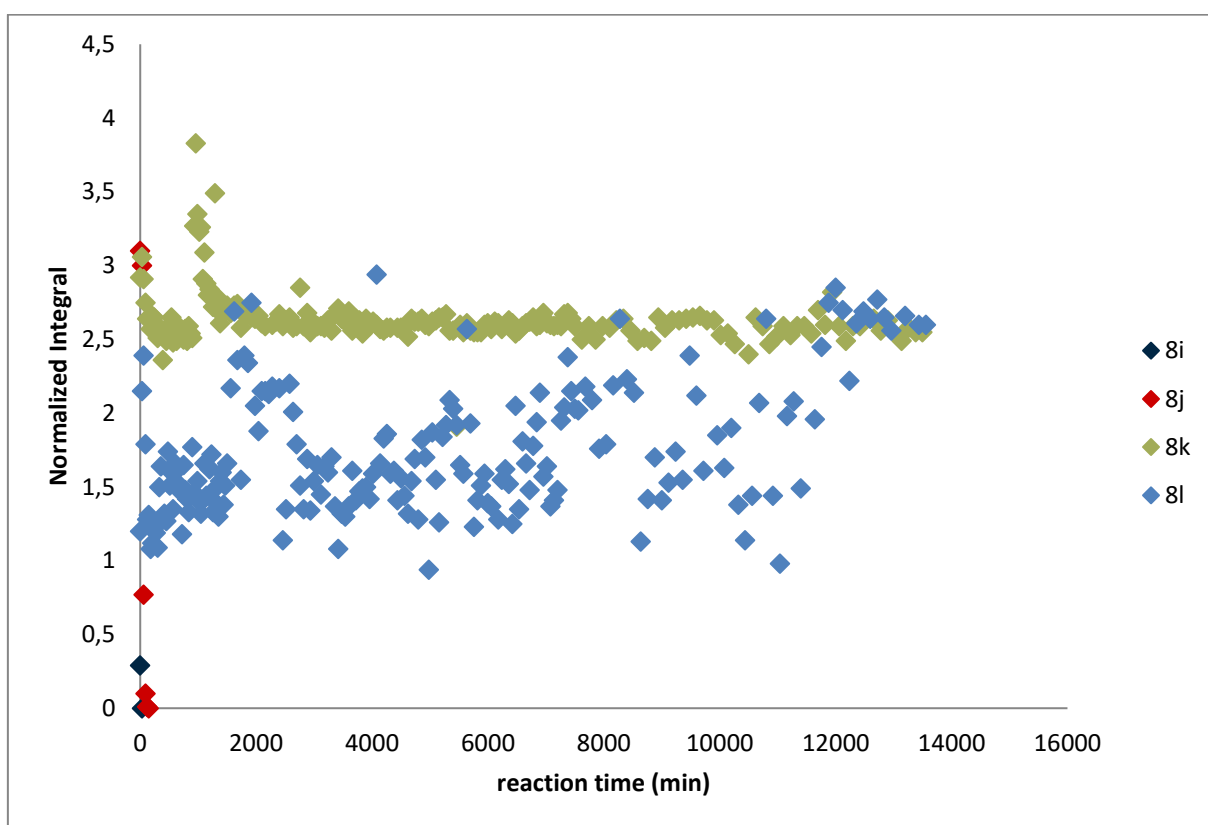


Figure A 24: Hydrolysis of 8i, 8j, 8k and 8l at 90 °C

5.1.5.4 NMR spectra of hydrolysis reactions of benzopinacolphosphites

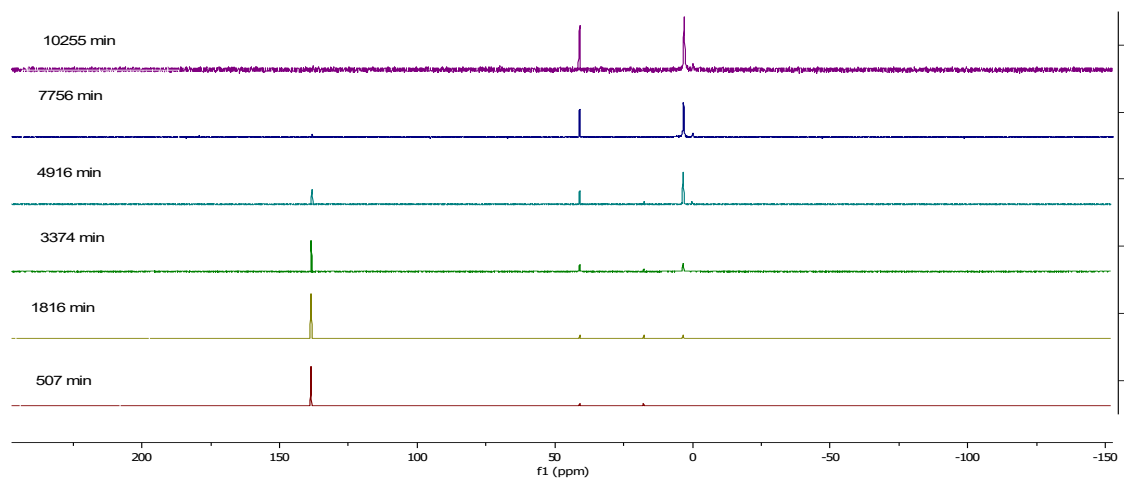


Figure A 25: NMR spectra of the hydrolysis of 8a at room temperature.

5 Appendix

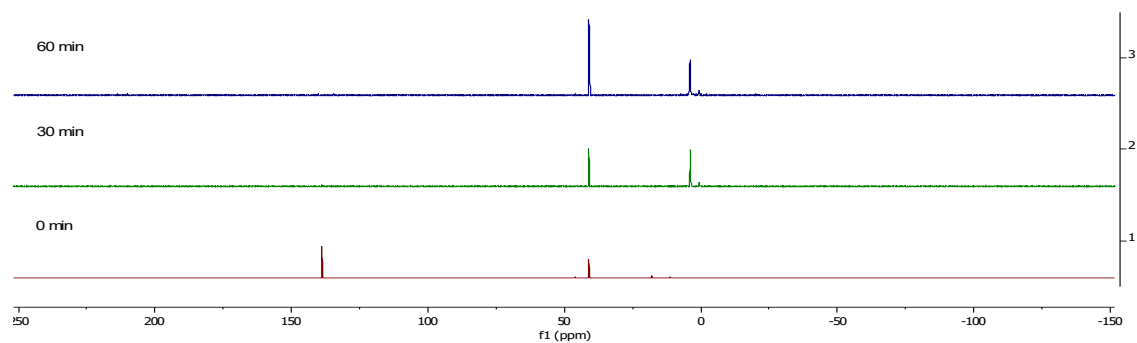


Figure A 26: NMR spectra of the hydrolysis of 8a at 90 °C.

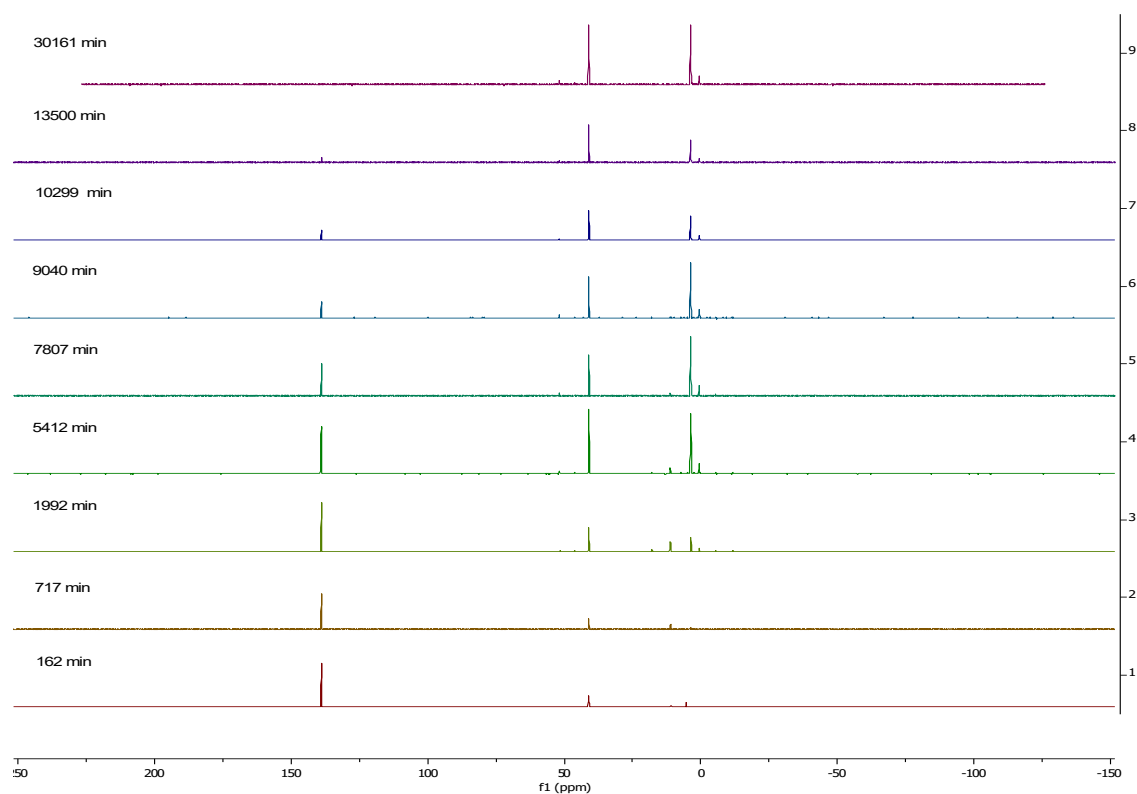


Figure A 27: NMR spectra of the hydrolysis of 8b at room temperature.

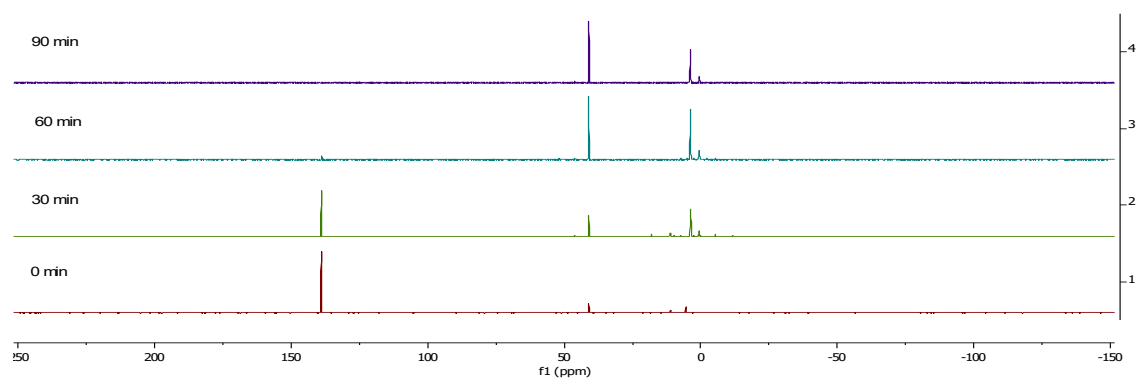


Figure A 28: NMR spectra of the hydrolysis of 8b at 90 °C.

5 Appendix

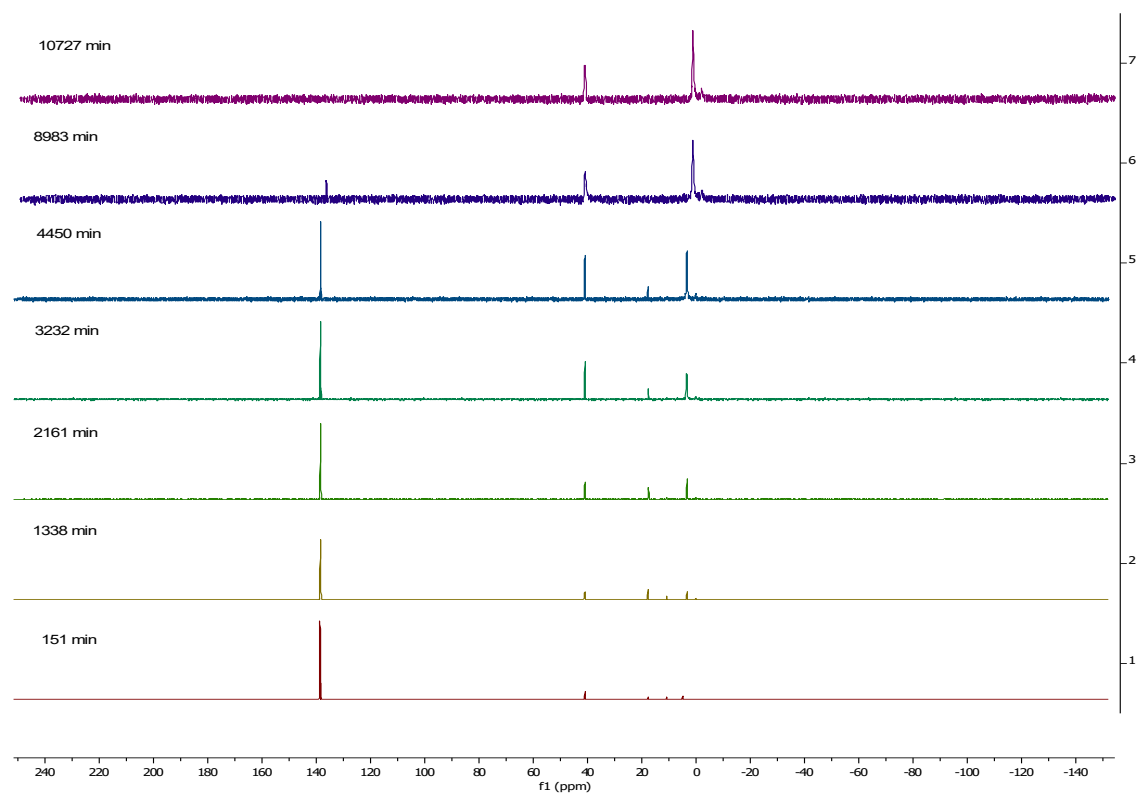


Figure A 29: NMR spectra of the hydrolysis of 8c at room temperature.

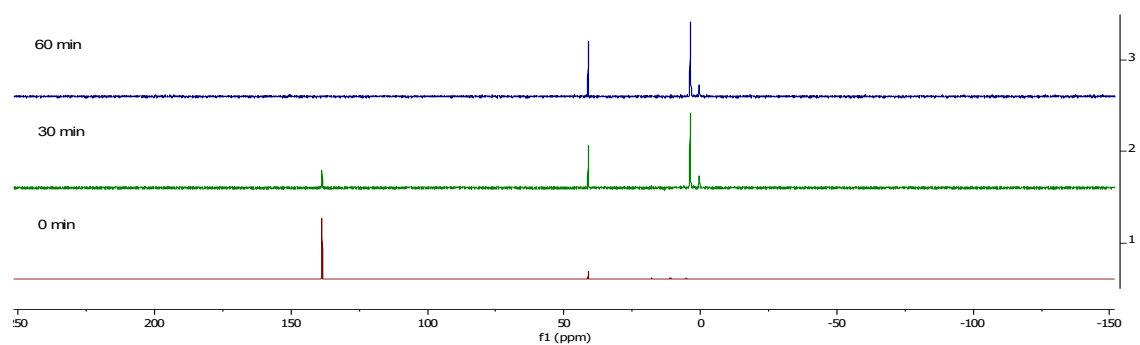


Figure A 30: NMR spectra of the hydrolysis of 8c at 90 °C.

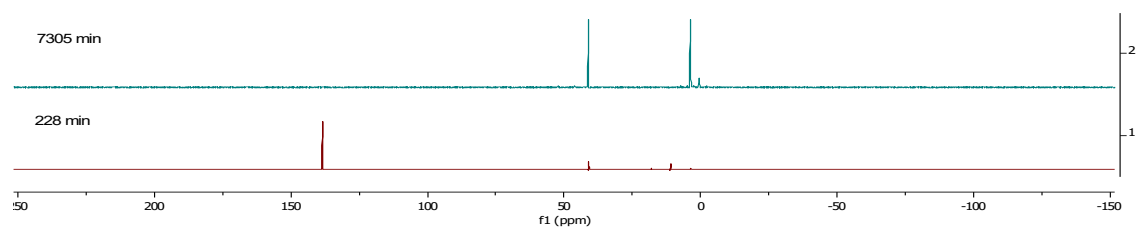


Figure A 31: NMR spectra of the hydrolysis of 8d at room temperature.

5 Appendix

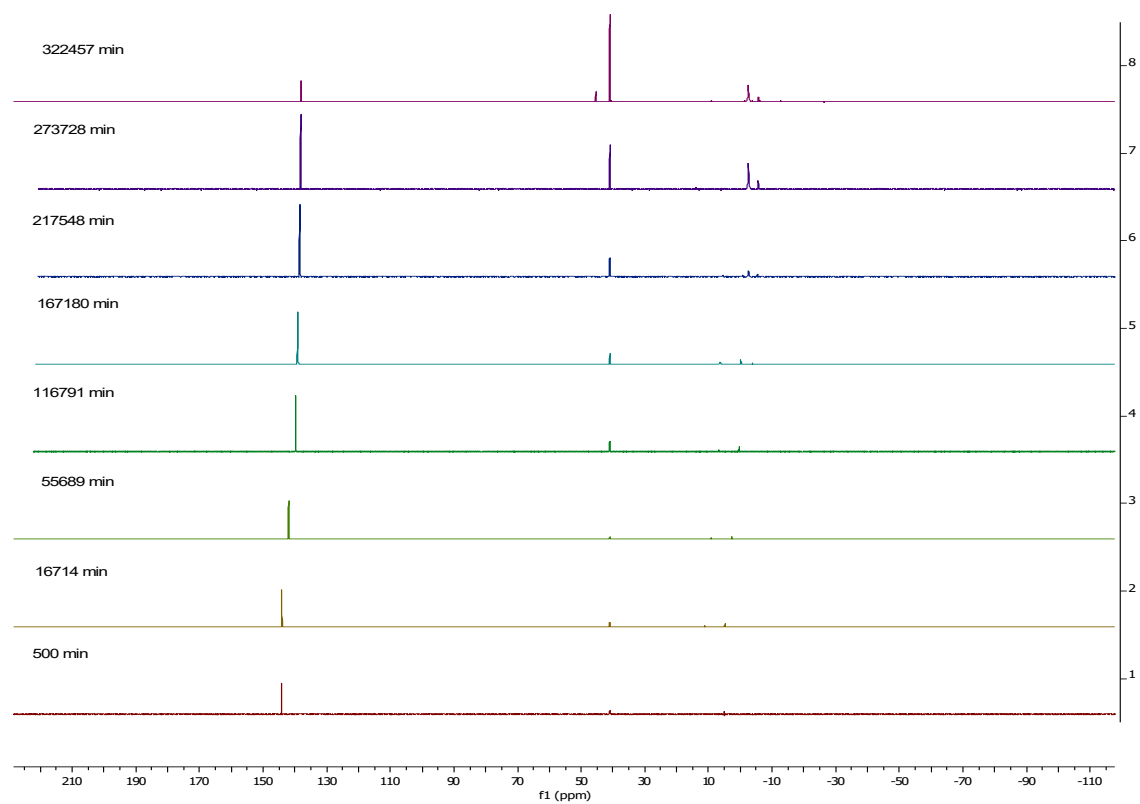


Figure A 32: NMR spectra of the hydrolysis of 8e at room temperature.

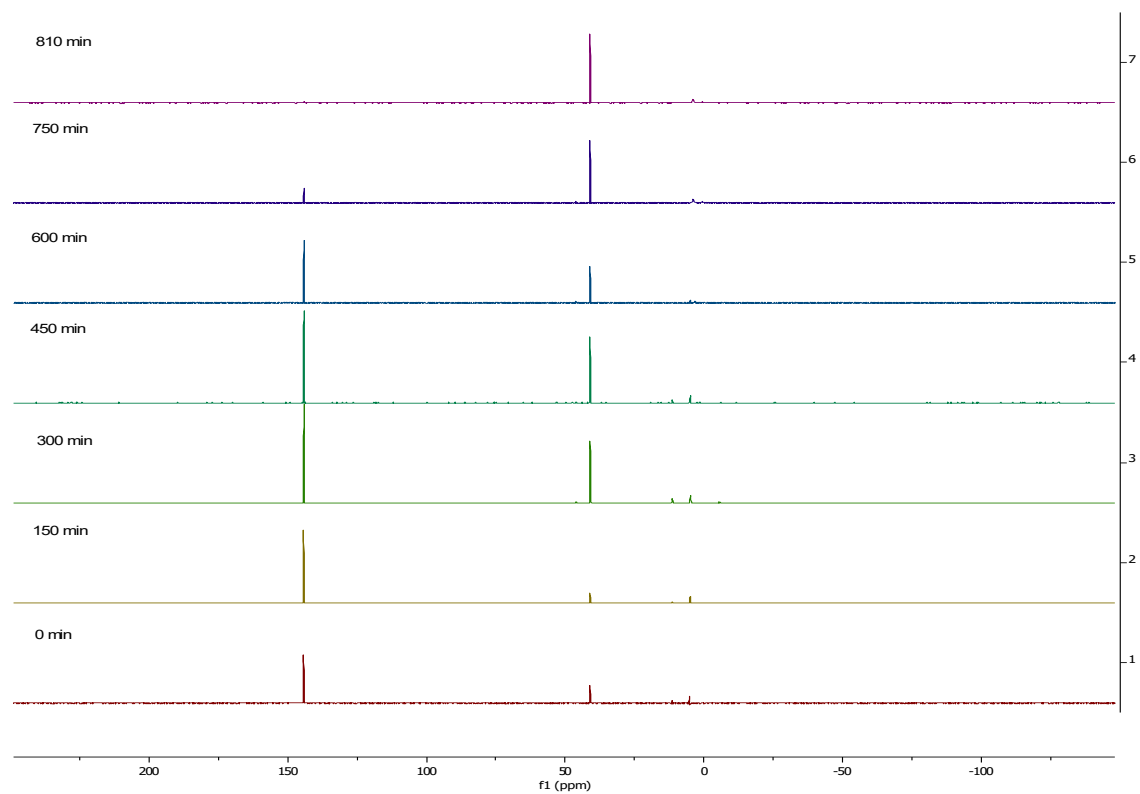


Figure A 33: NMR spectra of the hydrolysis of 8e at 90 °C.

5 Appendix

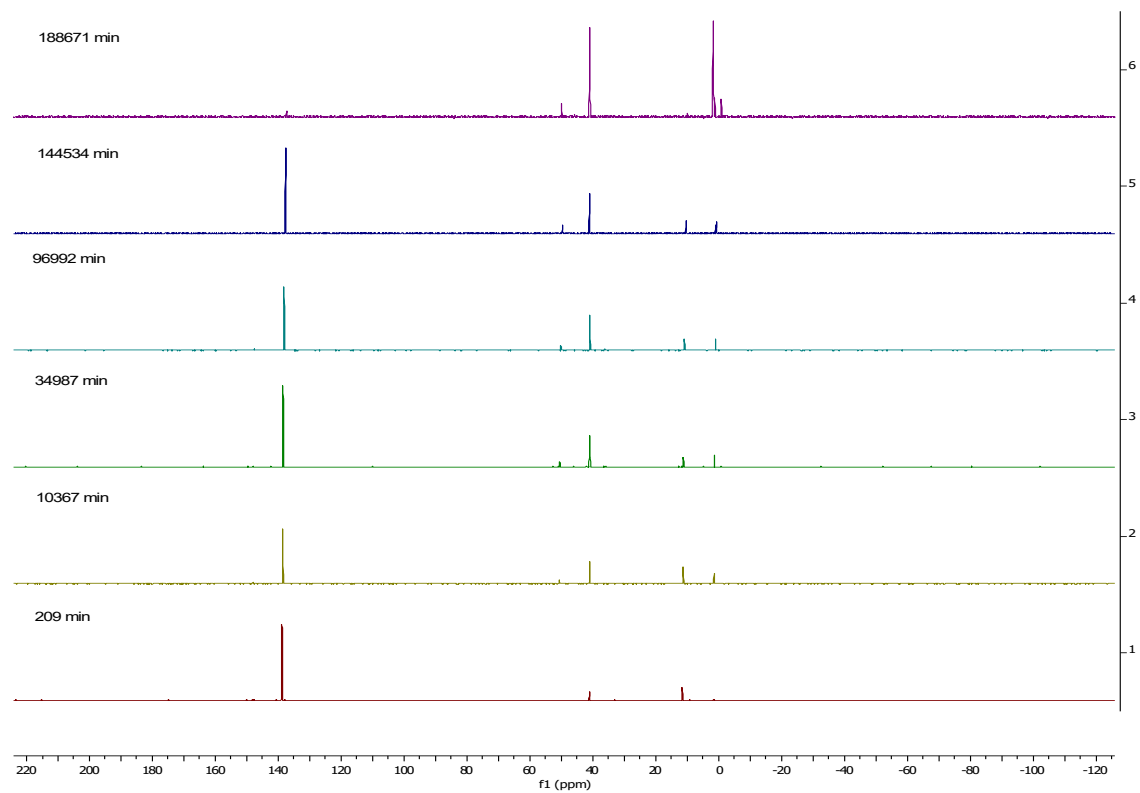


Figure A 34: NMR spectra of the hydrolysis of 8f at room temperature.

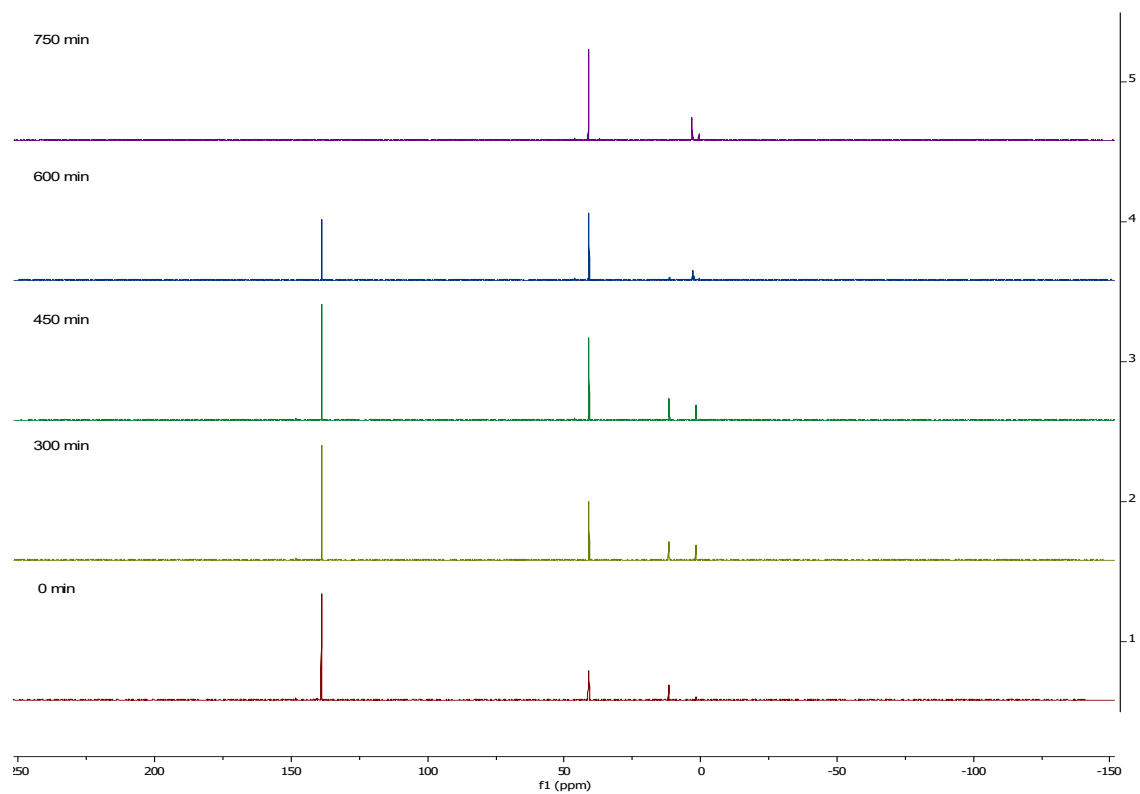


Figure A 35: NMR spectra of the hydrolysis of 8f at 90 °C.

5 Appendix

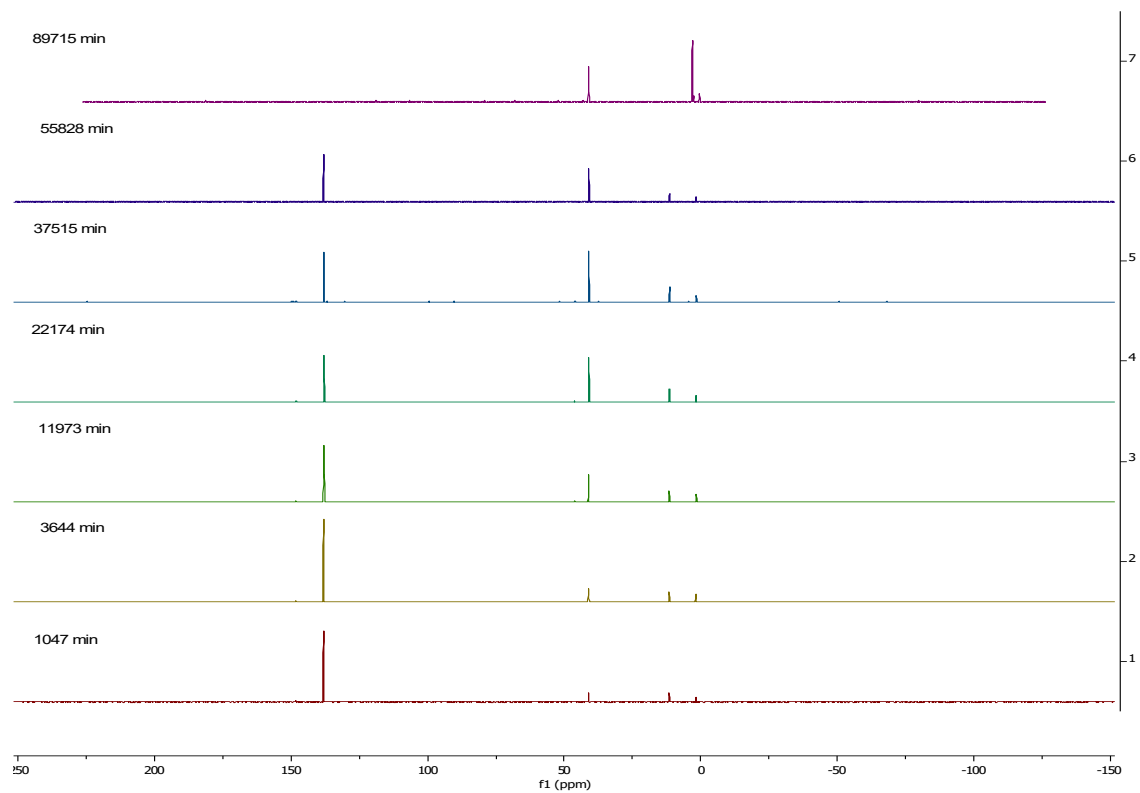


Figure A 36: NMR spectra of the hydrolysis of 8g at room temperature.

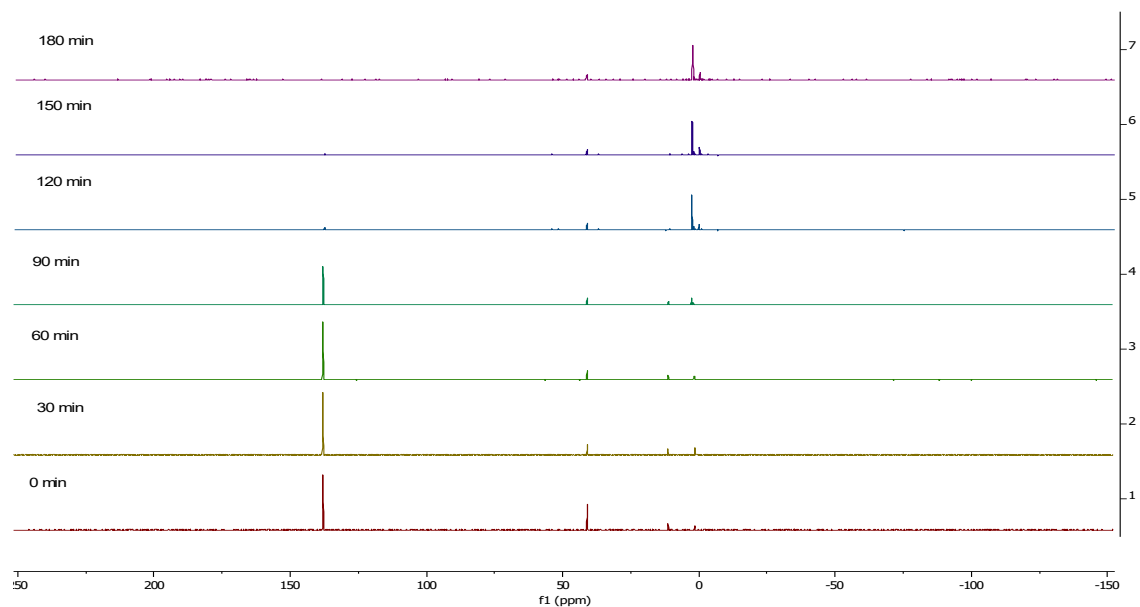


Figure A 37: NMR spectra of the hydrolysis of 8g at 90 °C.

5 Appendix

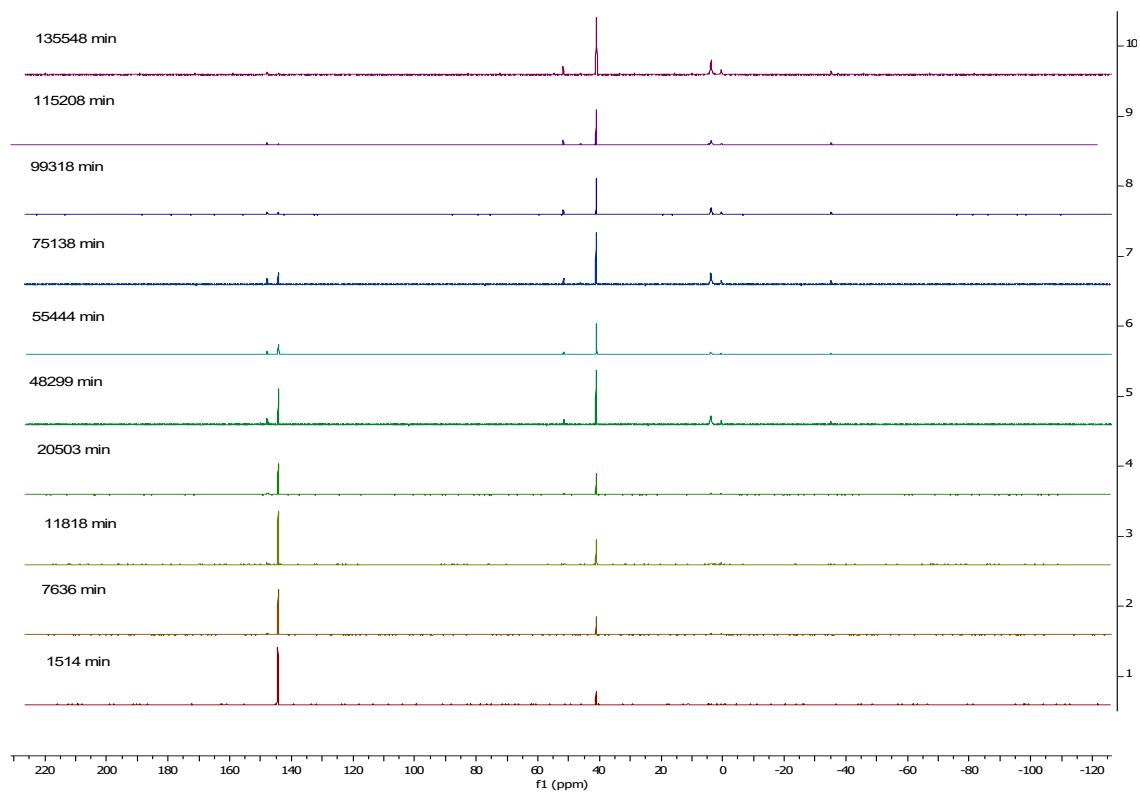


Figure A 38: NMR spectra of the hydrolysis of 8h at room temperature.

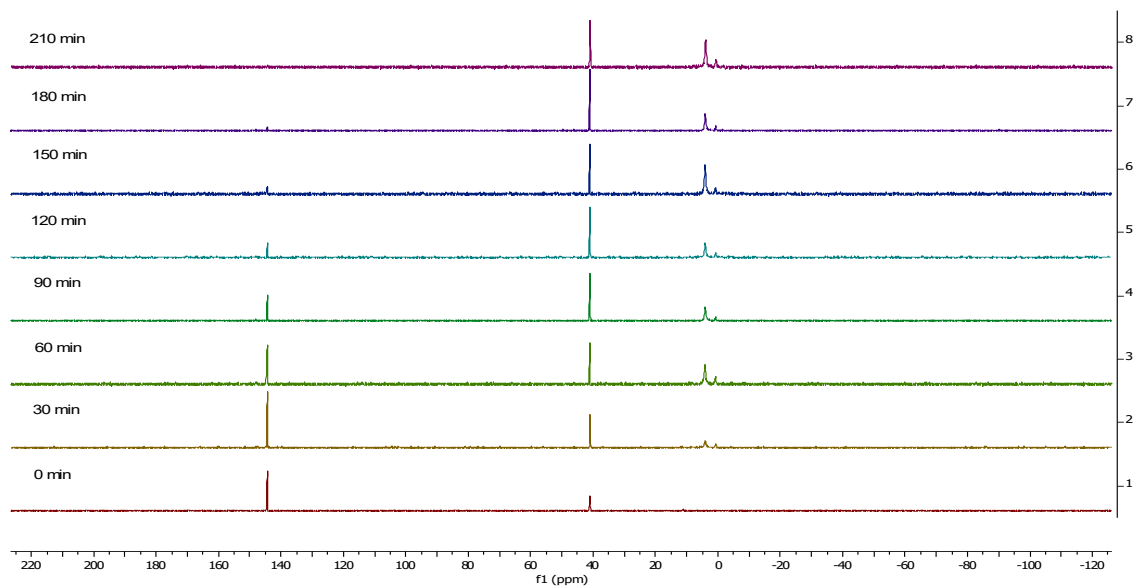


Figure A 39: NMR spectra of the hydrolysis of 8h at 90 °C.

5 Appendix

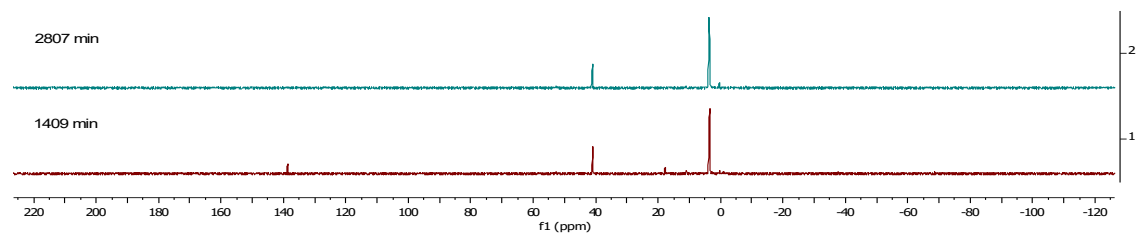


Figure A 40: NMR spectra of the hydrolysis of 8i at room temperature.

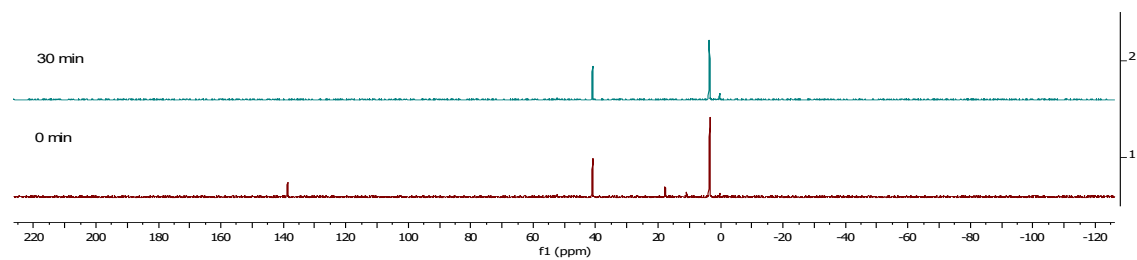


Figure A 41: NMR spectra of the hydrolysis of 8i at 90 °C.

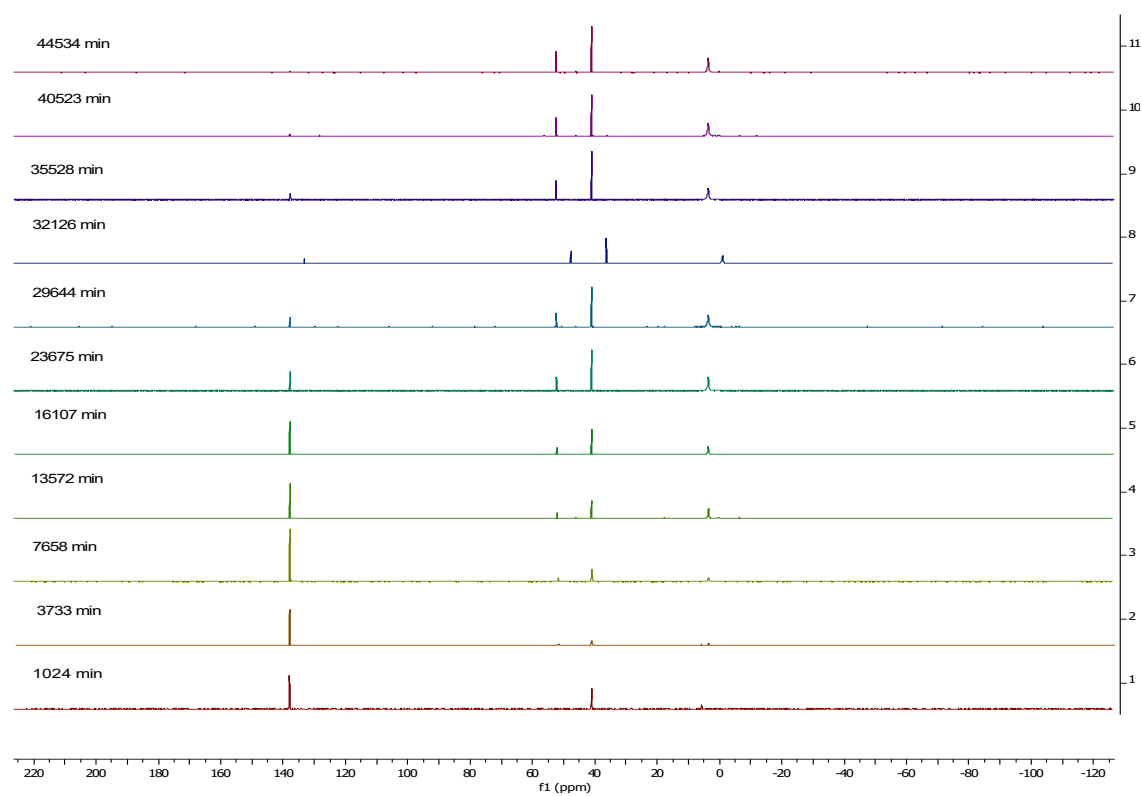


Figure A 42: NMR spectra of the hydrolysis of 8j at room temperature.

5 Appendix

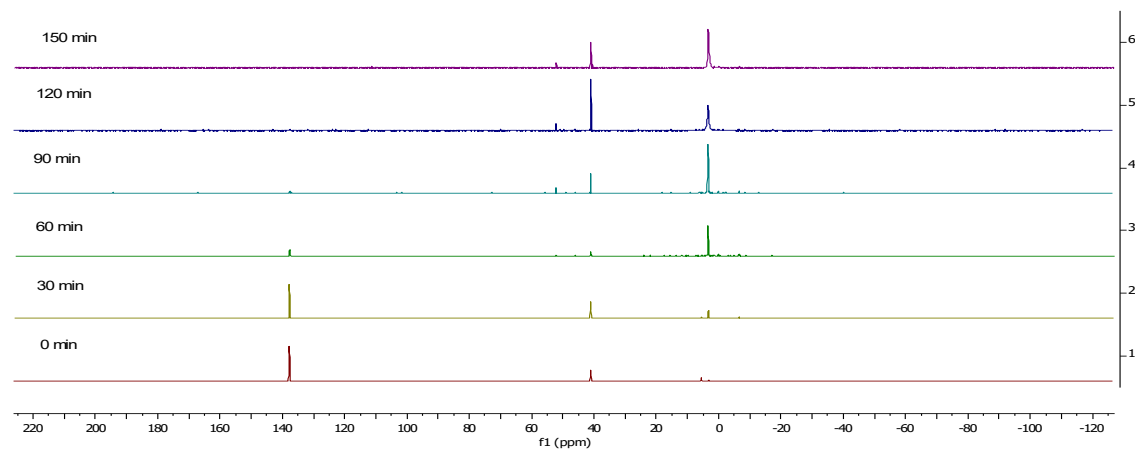


Figure A 43: NMR spectra of the hydrolysis of 8j at 90 °C.

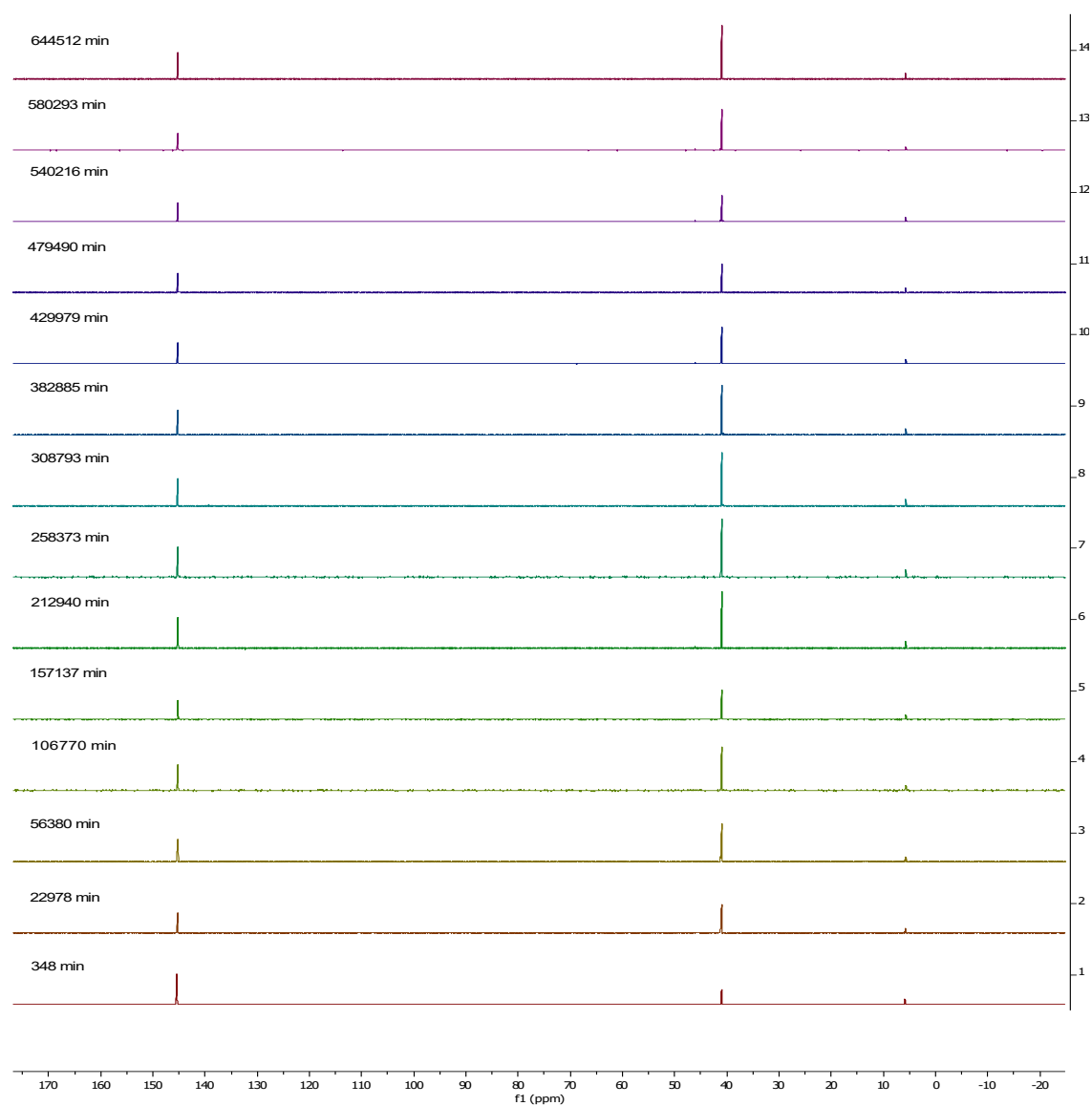


Figure A 44: NMR spectra of the hydrolysis of 8k at room temperature.

5 Appendix

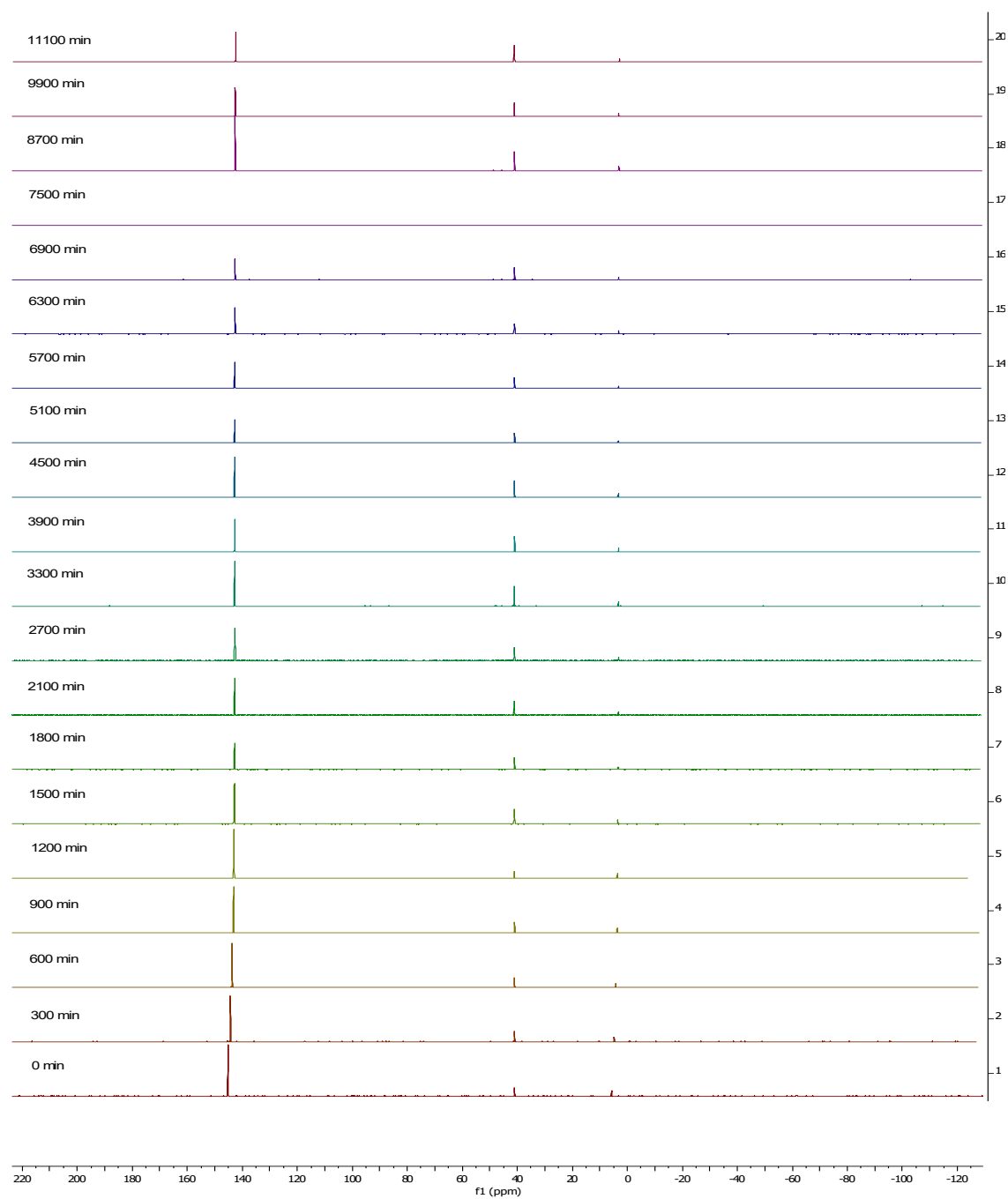


Figure A 45: NMR spectra of the hydrolysis of 8k at 90 °C.

5 Appendix

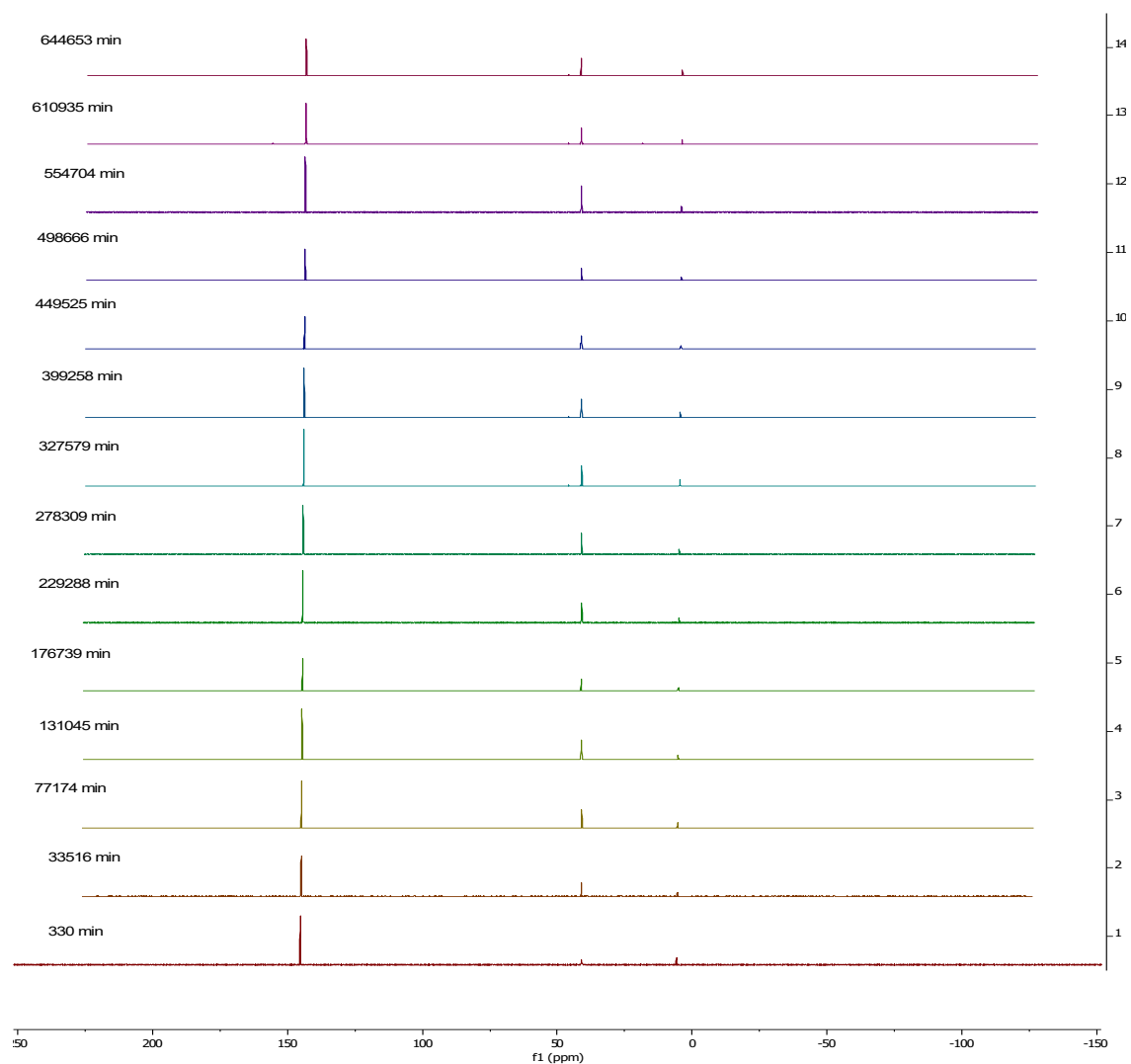


Figure A 46: NMR spectra of the hydrolysis of 8l at room temperature.

5 Appendix

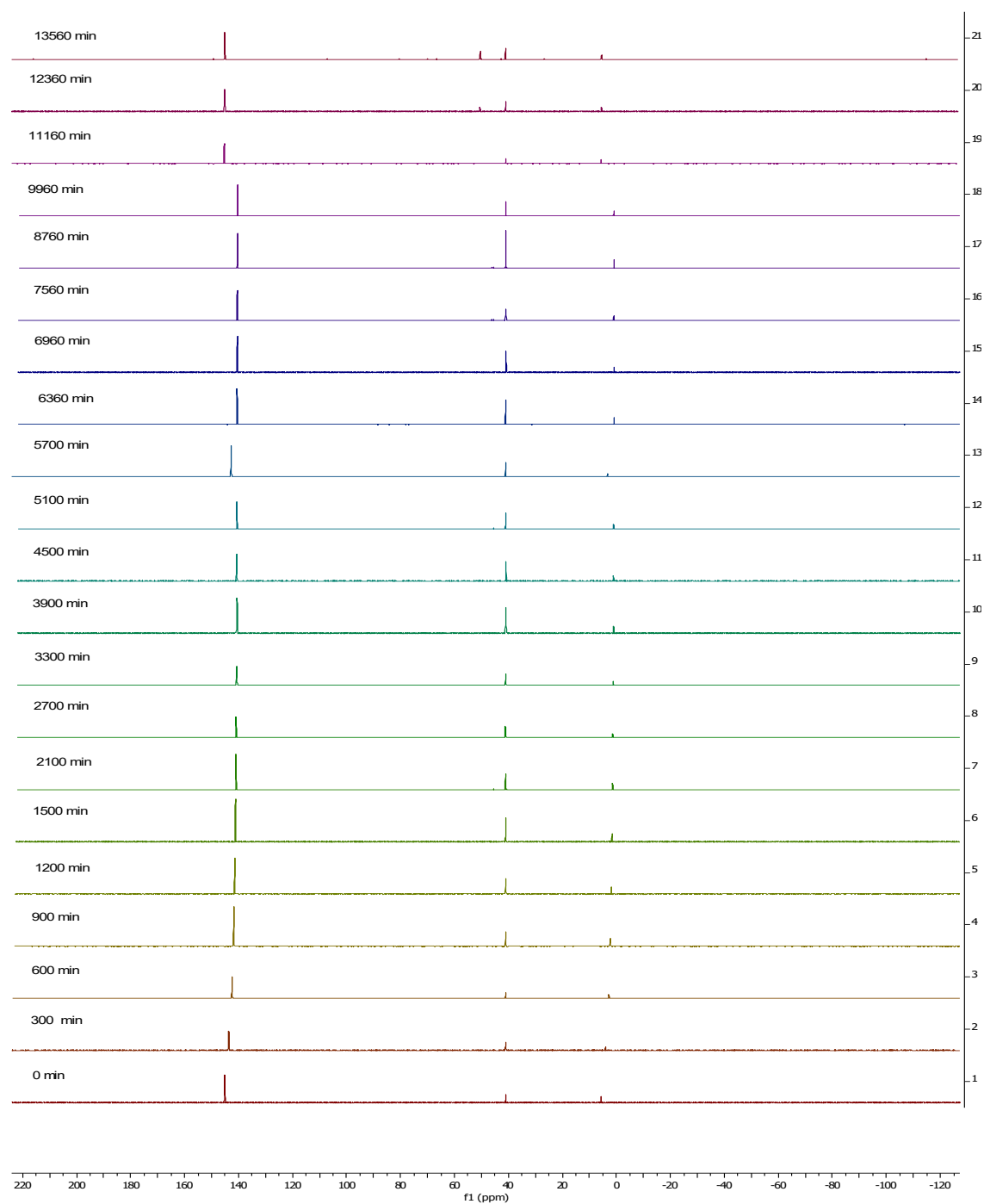
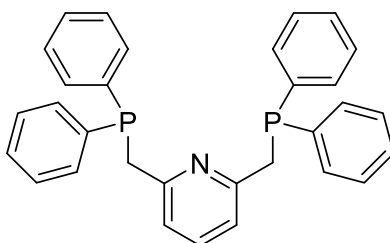


Figure A 47: NMR spectra of the hydrolysis of 8l at 90 °C.

5.1.6 Synthesis of PNP-ligands and -complexes

2,6-Bis[(diphenylphosphino)methyl]pyridine (9a):



To a stirred solution of 1.58 g diphenylphosphine (1.48 ml, 8.521 mmol) in 30 ml THF was added dropwise a solution of 1.91 g potassium *tert*-butoxide (17.042 mmol) in 20 ml THF at room temperature. The orange-red solution was cooled to 0 °C and 0.75 g 2,6-bis(chloromethyl)pyridine (4.260 mmol) was added as a solid. The solution was stirred for 18 h at room temperature and its color changed to yellow. The solvent was removed *in vacuo* and the precipitate was dissolved in dichloromethane and water. The water phase was extracted three times with dichloromethane and the combined organic phases were washed with water three times. Afterwards the organic layers were dried with sodium sulfate and the solvent was removed *in vacuo*. The pure product was crystallized from 10 ml dichloromethane and 60 ml methanol. The crystals were filtered and dried under reduced pressure to yield colorless crystals. Yield: 0.623 g (1.307 mmol, 30 %).

^1H NMR (300 MHz, CD_2Cl_2 , 298 K): δ = 3.58 (s, 4H, CH_2), 6.74 (dt, $J_{\text{HH}} = 7.8$ Hz, $J_{\text{HH}} = 1.3$ Hz, 2H, 3-Py), 7.24 (t, $J_{\text{HH}} = 7.7$ Hz, 1H, 4-Py), 7.30 (s, 12H, Ph), 7.38 – 7.50 (m, 8H, Ph) ppm.

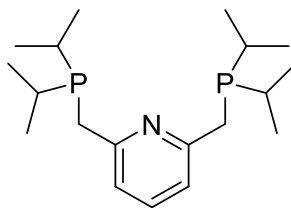
^{13}C NMR (75 MHz, CD_2Cl_2 , 298 K): δ = 39.1 (d, $J_{\text{CP}} = 16.5$ Hz), 121.4 (dd, $J_{\text{CP}} = 6.2$ Hz, $J_{\text{CP}} = 2.4$ Hz), 128.9 (d, $J_{\text{CP}} = 6.5$ Hz), 129.2, 133.5 (d, $J_{\text{CP}} = 19.1$ Hz), 136.6, 139.2 (d, $J_{\text{CP}} = 15.8$ Hz), 158.2 (d, $J_{\text{CP}} = 8.0$ Hz) ppm.

^{31}P NMR (121 MHz, CD_2Cl_2 , 298 K): δ = -11.2 (s) ppm.

MS (EI, 70 eV): m/z (%) = 476 (M^+ , 22), 475 (M^+ , 64), 398 (29), 293 (17), 291 (20), 290 (88), 288 (14), 213 (29), 212 (31), 185 (20), 184 (14), 183 (100), 181 (11) 180 (17), 152 (11), 107 (12).

HRMS (EI): Calculated for $\text{C}_{31}\text{H}_{27}\text{NP}_2$ (M^+) 475.16132, found 475.16128.

Elemental analysis (calc. for $\text{C}_{31}\text{H}_{27}\text{NP}_2 = 475.51$ g/mol): C, 78.30 (78.39); H, 5.63 (5.72); N, 2.90 (2.95); P, 13.05 (13.03) %.

2,6-Bis[(diisopropylphosphino)methyl]pyridine (9b):

To a stirred solution of 0.35 g 2,6-lutidine (0.38 ml, 3.277 mmol) and 1.03 ml TMEDA (0.80 g, 6.881 mmol) in 10 ml diethyl ether 4.30 ml *n*-butyllithium in *n*-hexane (1.6 M, 6.881 mmol) was added at 0 °C. The solution was warmed to room temperature and stirred for 4 h. 1.10 g chlorodiisopropylphosphine (1.16 ml, 1.10 g, 6.553 mmol) was dissolved in 10 ml diethyl ether and the dark red-brown solution of 2,6-lutidine, TMEDA and diethyl ether was added dropwise at -90 °C. The reaction solution was kept at -90 °C for 30 minutes and stirred at room temperature for another 18 h. The yellow cloudy solution was filtered and the solvent evaporated *in vacuo*. The crude product was purified by distillation (100 °C, 0.01 mbar) to yield a yellow oil. Yield: 0.626 g (1.844 mmol, 57 %).

¹H NMR (250 MHz, CD₂Cl₂, 298 K): δ = 0.96 – 1.13 (m, 24H, CH₃), 1.78 (heptd, *J*_{HH} = 7.0 Hz, *J*_{HH} = 1.8 Hz, 4H, CH(CH₃)₂), 2.91 (d, *J*_{HH} = 2.0 Hz, 4H, CH₂), 7.05 (d, *J*_{HH} = 7.7 Hz, 2H, 3-Py), 7.44 (t, *J*_{HH} = 7.7 Hz, 1H, 4-Py) ppm.

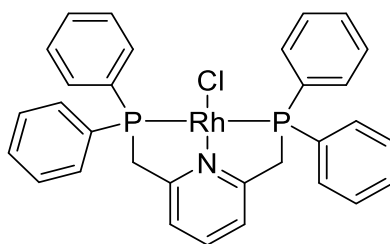
¹³C NMR (63 MHz, CD₂Cl₂, 298 K): δ = 19.5 (d, *J*_{CP} = 11.0 Hz, CH₃), 20.1 (d, *J*_{CP} = 14.7 Hz, CH₃), 24.1 (d, *J*_{CP} = 15.0 Hz, CH(CH₃)₂), 33.0 (d, *J*_{CP} = 22.2 Hz, CH₂), 120.8 (d, *J*_{CP} = 6.7 Hz, 3-Py), 136.5 (4-Py), 160.6 (d, *J*_{CP} = 8.7 Hz, 2-Py) ppm.

³¹P NMR (101 MHz, CD₂Cl₂, 298 K): δ = 11.8 (s) ppm.

MS (EI, 70 eV): *m/z* (%) = 339 (M⁺, 1), 297 (20), 296 (100), 224 (15), 223 (100), 168 (16), 138 (33), 137 (22), 136 (20), 107 (24), 106 (18), 43 (12).

HRMS (ESI): Calculated for C₁₉H₃₆NO₂P₂ (MO₂+H)⁺ 372.2221, found 372.2217. Calculated for C₁₉H₃₅NO₂NaP₂ (MO₂+Na)⁺ 394.2041, found 394.2035.

Elemental analysis (calc. for C₁₉H₃₅NP₂ = 339.44 g/mol): C, 66.66 (67.23); H, 10.57 (10.39); N, 3.73 (4.13); P, 18.16 (18.25) %.

[Rh(PNP^{Ph})Cl] (15a):

A solution of 0.10 g 2,6-bis[(diphenylphosphino)methyl]pyridine (**9a**, 0.205 mmol) in 4 ml toluene was added dropwise to a solution of 0.040 g $[\text{Rh}(\text{C}_2\text{H}_4)_2\text{Cl}]_2$ (0.102 mmol) in 4 ml toluene at room temperature. The orange-red cloudy solution was stirred for 18 h at room temperature and filtered afterwards. The solvent was evaporated *in vacuo* to yield a red solid. Yield: 0.033 g (0.054 mmol, 53 %).

^1H NMR (601 MHz, C_6D_6 , 298 K): δ = 3.21 (t, $J_{\text{HH}} = 4.2$ Hz, 4H, CH_2), 6.28 (d, $J_{\text{HH}} = 7.9$ Hz, 2H, 3-Py), 6.77 (t, $J_{\text{HH}} = 7.5$ Hz, 1H, 4-Py), 6.97 – 7.04 (m, 4H, Ph), 7.03 – 7.09 (m, 9H, Ph), 8.14 – 8.21 (m, 7H, Ph) ppm.

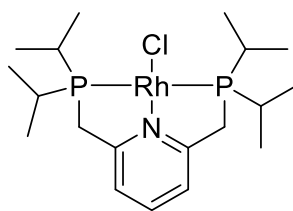
^{13}C NMR (75 MHz, $\text{THF-}d_8$, 298 K): δ = 41.11 (CH_2), 41.96 (CH_2), 123.43 (d, $J_{\text{CP}} = 3.1$ Hz), 128.99 (d, $J_{\text{CP}} = 4.9$ Hz), 129.18 (d, $J_{\text{CP}} = 11.8$ Hz), 129.85, 130.14, 132.05 (d, $J_{\text{CP}} = 2.6$ Hz), 132.23 (d, $J_{\text{CP}} = 9.3$ Hz), 134.08, 135.10, 136.41, 136.86 (t, $J_{\text{CP}} = 2.3$ Hz), 154.07 (d, $J_{\text{CP}} = 7.1$ Hz) ppm.

^{31}P NMR (243 MHz, C_6D_6 , 298 K): δ = 22.17 (d, $J_{\text{RhP}} = 150.5$ Hz) ppm.

HRMS (ESI): Calculated for $\text{C}_{31}\text{H}_{27}\text{ClNOP}_2\text{Rh}(\text{MO})^+$ 629.0311, found 629.0325.

5 Appendix

[Rh(PNP^{iPr})Cl] (**15b**):



A solution of 0.05 g 2,6-bis[(diisopropylphosphino)methyl]pyridine (**9b**, 0.134 mmol) in 2 ml toluene was added dropwise to a stirred solution of 0.05 g [Rh(COE)₂Cl]₂ (0.067 mmol) in 4 ml toluene at room temperature. The solution was stirred for 30 minutes at room temperature and the solvent was evaporated *in vacuo* afterwards. The residue was dissolved in 12 ml toluene and filtered. The solvent was again evaporated *in vacuo* to yield a dark red solid. Yield: 0.044 g (0.092 mmol, 69 %). Crystals of **15b**, suitable for X-Ray analysis, were obtained by layering a concentrated toluene solution with *n*-heptane.

¹H NMR (500 MHz, THF-*d*₈, 298 K): δ = 1.19 (q, *J*_{HH} = 6.8 Hz, 12H, CH₃), 1.38 (q, *J*_{HH} = 7.6 Hz, 12H, CH₃), 2.19 (hept, *J*_{HH} = 6.7 Hz, 4H, CH(CH₃)₂), 3.01 (dd, *J*_{PH} = 3.7 Hz, 4H, CH₂), 6.95 (d, *J*_{HH} = 7.6 Hz, 2H, 3-Py), 7.43 (t, *J*_{HH} = 7.7 Hz, 1H, 4-Py) ppm.

¹³C NMR (126 MHz, Tol-*d*₈, 298 K): δ = 17.62 (CH₃), 18.89 (vt, *J*_{CP} = 3.6 Hz, CH₃), 23.87 (vt, *J*_{CP} = 9.6 Hz, CH(CH₃)₂), 35.47 (vt, *J*_{CP} = 6.0 Hz, CH₂), 119.56 (vt, *J*_{CP} = 5.0 Hz, 3-Py), 128.80 (4-Py), 163.26 – 163.86 (vt, *J*_{CP} = 7.2 Hz, 4-Py) ppm.

³¹P NMR (202 MHz, THF-*d*₈, 298 K): δ = 46.36 (d, *J*_{RhP} = 152.5 Hz) ppm.

HRMS (ESI): Calculated for C₁₉H₃₅ClNOP₂Rh (MO)⁺ 493.0937, found 493.0934.

5 Appendix

Table 26: Crystallographic details of 15b.

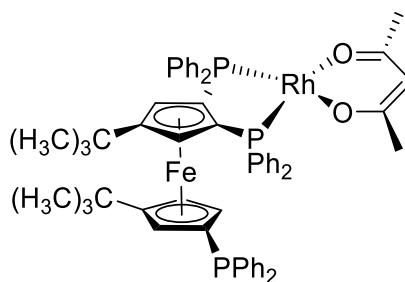
| | |
|--|------------------------|
| Chem. Formula | $C_{19}H_{35}ClNP_2Rh$ |
| Form. Wght. [$g\ mol^{-1}$] | 477.78 |
| Color | Red |
| Cryst. system | Trigonal |
| Space Group | $\bar{R}^3\ c:H$ |
| a [\AA] | 25.4887(11) |
| b [\AA] | 25.4887(11) |
| c [\AA] | 20.1260(9) |
| α [$^\circ$] | 90 |
| β [$^\circ$] | 90 |
| γ [$^\circ$] | 120 |
| V [\AA^3] | 11323.6(11) |
| Z | 18 |
| $\rho_{\text{calc.}}$ [$g\ cm^{-3}$] | 1.261 |
| μ [mm^{-1}] | 7.663 |
| $\lambda_{CuK\alpha}$ [\AA] | 1.54178 |
| T [K] | 150(2) |
| Reflections collected | 42641 |
| Independent reflections | 2234 |
| Reflections with $I > 2s(I)$ | 2148 |
| R_{int} | 0.039 |
| $F(000)$ | 4464 |
| R_1 (R [$F^2 > 2s(F^2)$]) | 0.0186 |
| wR_2 (F^2) | 0.0490 |
| Goodness-of-fit on F^2 | 1.061 |
| Parameters | 115 |

5.1.7 Hydroformylation experiments with PNP-complexes

The hydroformylation experiments with rhodium complexes with PNP-ligands were performed in a 16 ml autoclave (HEL group, Hertfordshire, Great Britain) equipped with a gas inlet stirrer, a thermocouple, a pressure controller as well as a gas flow meter. A high-grade pure syngas (99.997 %; CO/H₂ = 1:1) was used, which was purchased from Linde AG. Olefins were refluxed in an argon atmosphere over sodium metal and freshly distilled prior to use.

For the hydroformylation experiments the reaction solution was prepared under an atmosphere of argon. The complex was dissolved in 5 ml toluene. The mass of toluene was defined for GC analysis. Afterwards 0.80 g of 1-octene (7.040 mmol) was added. The prepared reaction solutions were filled into the autoclave and purged with argon and syngas (Linde; H₂ (99.999 %):CO (99.997 %) = 1:1) three times, respectively. Afterwards the stirred reaction solution was pressurized with 10 bar syngas and heated to the assigned temperature. After reaching the reaction temperature the pressure was elevated to the assigned pressure and the reaction was kept at constant pressure for 4 h. After the reaction time the autoclave was cooled down to room temperature, the pressure released and purged with argon. 0.1 ml of the reaction solution were diluted with 1 ml pentane and analyzed with gas chromatography (HP 5890 Series II plus, PONA, 50 m x 0,2 mm x 0,5 µm). The quantitative amount of remaining olefin and newly formed aldehyde were determined using toluene as internal standard.

5.1.8 Synthesis of HiersoPHOS-2 complexes

[Rh(HiersoPHOS-2)(acac)] (16):

To a stirred solution of 0.04 g rhodium(I) dicarbonyl acetylacetonate (0.162 mmol) in 8 ml toluene was added slowly dropwise to a solution of 0.14 g 1,1',2-tris(diphenylphosphino)-3',4-di-*tert*-butylferrocene (HiersoPHOS-2) (0.162 mmol) in 8 ml toluene at room temperature. The solution was stirred at room temperature for 18 h while the color changes from light green over yellow, orange and red to a dark red brown. The solvent was evaporated *in vacuo* to yield a dark brown solid. Yield: 0.170 g (0.162 mmol, >99 %).

^1H NMR (250 MHz, THF-*d*₈, 298 K): δ = 0.67 (s, 9H, C(CH₃)₃), 1.01 (s, 9H, C(CH₃)₃), 1.84 (s, 6H, CH₃), 3.55 (s, 1H, *H*-Cp), 4.23 (dt, $J_{\text{HH}} = 2.4$ Hz, $J_{\text{HH}} = 1.2$ Hz, 1H, *H*-Cp), 4.46 (d, $J_{\text{HH}} = 1.3$ Hz, 1H, *H*-Cp), 4.50 (d, $J_{\text{HH}} = 1.4$ Hz, 1H, *H*-Cp), 4.69 (td, $J_{\text{HH}} = 2.3$ Hz, $J_{\text{HH}} = 1.5$ Hz, 1H, *H*-Cp), 5.38 (s, 1H, CH), 6.76 – 6.87 (m, 2H), 6.90 – 7.01 (m, 6H), 7.12 – 7.31 (m, 12H), 7.33 – 7.43 (m, 6H), 8.09 – 8.23 (m, 4H) ppm.

^{31}P NMR (121 MHz, Tol-*d*₈, 298 K): δ = -19.5, 54.2 (dd, $J_{\text{RhP}} = 172.9$ Hz, $J_{\text{PP}} = 57.0$ Hz), 55.8 (dd, $J_{\text{RhP}} = 173.9$ Hz, $J_{\text{PP}} = 56.1$ Hz) ppm.

^{13}C NMR (63 MHz, THF-*d*₈, 298 K): δ = 28.1 (d, $J_{\text{CP}} = 2.7$ Hz), 30.7, 32.1, 32.4, 32.6, 69.4 (d, $J_{\text{CP}} = 3.7$ Hz), 70.3 (dd, $J_{\text{CP}} = 12.2$ Hz, $J_{\text{CP}} = 5.3$ Hz), 71.5 (d, $J_{\text{CP}} = 5.4$ Hz), 72.8, 73.3 (d, $J_{\text{CP}} = 2.3$ Hz), 75.8, 76.8 (dd, $J_{\text{CP}} = 25.2$ Hz, $J_{\text{CP}} = 1.2$ Hz), 79.1 (d, $J_{\text{CP}} = 14.1$ Hz), 99.8 (d, $J_{\text{CP}} = 1.8$ Hz), 108.2, 115.9, 127.7 – 128.0 (m), 128.0 (d, $J_{\text{CP}} = 2.1$ Hz), 128.1, 128.4 – 128.5 (m), 128.6, 128.6, 128.8 (d, $J_{\text{CP}} = 2.5$ Hz), 128.9 (d, $J_{\text{CP}} = 2.7$ Hz), 129.0, 129.1, 130.1, 130.9 (d, $J_{\text{CP}} = 2.0$ Hz), 131.0 (d, $J_{\text{CP}} = 3.8$ Hz), 131.9, 131.9, 132.0, 132.1, 132.5, 132.8, 134.3, 135.0, 135.1, 135.3, 135.8, 136.9, 137.1 (d, $J_{\text{CP}} = 2.1$ Hz), 137.1, 137.3, 137.3, 139.4, 139.7, 140.8, 141.4 (d, $J_{\text{CP}} = 3.0$ Hz), 142.1, 143.4, 143.7, 185.0 ppm.

HRMS (ESI): Calculated for C₅₉H₆₀O₂P₃⁵⁶FeRh (M⁺) 1052.2211, found 1052.2206.

Elemental analysis (calc. for C₅₉H₆₀O₂P₃FeRh = 1052.80 g/mol): C, 67.33 (67.31); H, 5.68 (5.74); P, 8.92 (8.83) %.

5.1.9 Hydroformylation with HiersoPHOS-2

The hydroformylation experiments of HiersoPHOS-2 were performed in a 150 ml autoclave (Premex Solutions GmbH, Switzerland) equipped with a gas inlet stirrer, a thermocouple, a storage vessel allowing the addition of substrate under pressure applied, a Bronkhorst hitec® pressure controller as well as a Bronkhorst hitec® gas flow meter. The autoclave periphery allowed us to fill in and to remove any media and reagents under exclusion of air. A high-grade pure syngas (99.997 %; CO/H₂ = 1:1) was used, which was purchased from Linde AG. Olefins were refluxed in an argon atmosphere over sodium metal and freshly distilled prior to use.

For the hydroformylation experiments the reaction solution was prepared under an atmosphere of argon. The mass of toluene was defined for GC analysis. The stirred reaction solution was pressurized with 6 bar (for 10 bar reactions), 12 bar (for reactions at 20 bar) or 32 bar (for reactions with 50 bar) syngas and heated to the assigned temperature. After reaching the reaction temperature the pressure was elevated to 8 bar, 18 bar or 46 bar and the 1-octene was added. The reaction was kept at constant pressure of 10 bar, 20 bar or 50 bar for 4 h. The current gas flow was determined in a time cycle of 3 seconds simultaneously to the reaction process. The gas consumption curve thus obtained was used to determine the observed 1st order velocity constant k_{obs} . The autoclave was cooled down to room temperature after the reaction time, the pressure released and purged with argon. 0.1 ml of the reaction solution were diluted with 1 ml pentane and analyzed with gas chromatography (HP 5890 Series II plus, PONA, 50 m x 0,2 mm x 0,5 µm). The quantitative amount of remaining olefin and newly formed aldehyde were determined using toluene as internal standard.

6 References

1. *Rhodium Catalyzed Hydroformylation*, van Leeuwen, P.W.N.M.; Claver, C.; Kluwer Academic Publishers: Dordrecht, Netherlands, 2000.
2. Franke, R.; Selent, D.; Börner, A., Applied hydroformylation. *Chem. Rev.* **2012**, *112*, 5675–5732, DOI: 10.1021/cr3001803.
3. *New syntheses with carbon monoxide: With 118 figures and 127 tables*, Falbe, J.; Reactivity and structure 11; Springer: Berlin Heidelberg, Germany, 1980.
4. Bohnen, H.-W.; Cornils, B., Hydroformylation of alkenes: An industrial view of the status and importance. *Adv. Catal.* **2002**, *47*, 1–64, DOI: 10.1016/S0360-0564(02)47005-8.
5. Cornils, B.; Herrmann, W. A.; Beller, M.; Paciello, R. *Applied Homogeneous Catalysis with Organometallic Compounds: A Comprehensive Handbook in Four Volumes*, 3rd edition; Wiley-VCH: Weinheim, Germany, 2017.
6. Wiese, K.-D.; Obst, D., Hydroformylation. In *Catalytic carbonylation reactions*; Beller, M., Ed.; Topics in Organometallic Chemistry 18; Springer: Berlin Heidelberg, Germany, op. 2006; pp 1–33.
7. Börner, A.; Franke, R. *Hydroformylation: Fundamentals, processes, and applications in organic synthesis*; Wiley-VCH: Weinheim, Germany, 2016.
8. Yan, Y.; Zhang, X.; Zhang, X., A tetraphosphorus ligand for highly regioselective isomerization-hydroformylation of internal olefins. *J. Am. Chem. Soc.* **2006**, *128*, 16058–16061, DOI: 10.1021/ja0622249.
9. Seiche, W.; Schuschkowski, A.; Breit, B., Bidentate Ligands by Self-Assembly through Hydrogen Bonding: A General Room Temperature/Ambient Pressure Regioselective Hydroformylation of Terminal Alkenes. *Adv. Synth. Catal.* **2005**, *347*, 1488–1494, DOI: 10.1002/adsc.200505174.
10. Selent, D.; Franke, R.; Kubis, C.; Spannenberg, A.; Baumann, W.; Kreidler, B.; Börner, A., A New Diphosphite Promoting Highly Regioselective Rhodium-Catalyzed Hydroformylation. *Organometallics* **2011**, *30*, 4509–4514, DOI: 10.1021/om2000508.
11. Petricci, E.; Cini, E., Domino reactions triggered by hydroformylation. *Top. Curr. Chem.* **2013**, *342*, 117–149, DOI: 10.1007/128_2013_463.
12. Settambolo, R., Rhodium-catalyzed hydroformylation in fused azapolycycles synthesis. *Top. Curr. Chem.* **2013**, *342*, 151–186, DOI: 10.1007/128_2013_432.

6 References

- Bates, R. W.; Kasinathan, S., Hydroformylation in natural product synthesis. *Top. Curr. Chem.* **2013**, *342*, 187–223, DOI: 10.1007/128_2013_428.
- Whiteker, G. T.; Cobley, C. J., Applications of Rhodium-Catalyzed Hydroformylation in the Pharmaceutical, Agrochemical, and Fragrance Industries. In *Organometallics as Catalysts in the Fine Chemical Industry*; Beller, M., Blaser, H.-U., Eds.; Topics in Organometallic Chemistry; Springer Berlin Heidelberg: Berlin, Heidelberg, Germany, 2012; pp 35–46.
- Gusevskaya, E. V.; Jiménez-Pinto, J.; Börner, A., Hydroformylation in the Realm of Scents. *ChemCatChem* **2014**, *6*, 382–411, DOI: 10.1002/cctc.201300474.
- Delolo, F. G.; Oliveira, K. C. B.; dos Santos, E. N.; Gusevskaya, E. V., Hydroformylation of biomass-based hydroxyolefins in eco-friendly solvents: New fragrances from myrtenol and nopol. *Mol. Catal.* **2019**, *462*, 1–9, DOI: 10.1016/j.mcat.2018.10.011.
- Vieira, C. G.; Freitas, M. C. de; Oliveira, K. C. B. de; Camargo Faria, A. de; dos Santos, E. N.; Gusevskaya, E. V., Synthesis of fragrance compounds from renewable resources: the aqueous biphasic hydroformylation of acyclic terpenes. *Catal. Sci. Technol.* **2015**, *5*, 960–966, DOI: 10.1039/C4CY01020E.
- Botteghi, C.; Paganelli, S.; Schionato, A.; Marchetti, M., The asymmetric hydroformylation in the synthesis of pharmaceuticals. *Chirality* **1991**, *3*, 355–369, DOI: 10.1002/chir.530030422.
- Lin, G.-Q.; Sun, X.-W., Chiral Drugs through Asymmetric Synthesis. In *Signposts to chiral drugs: Organic synthesis in action*; Sunjic, V., Parnham, M. J., Eds.; Springer: New York, USA, 2011; pp 29–76.
- Knifton, J. F.; Schwager, I. (Texaco Development Corp.), Verfahren zur Herstellung von Aldehyden durch Hydroformylierung von Olefinen, DE000002322751, 1973.
- Knifton, J. F.; Moss, P. H. (Texaco Development Corp.), Verfahren zur Herstellung linearer primaerer Alkylamine, DE000002811403, 1978.
- van Leeuwen, P. W.N.M.; Clément, N. D.; Tschan, M. J.-L., New processes for the selective production of 1-octene. *Coord. Chem. Rev.* **2011**, *255*, 1499–1517, DOI: 10.1016/j.ccr.2010.10.009.
- Rowe, D. J., Aroma Chemicals I: C, H, O Compounds. In *Chemistry and technology of flavors and fragrances*; Rowe, D. J., Ed.; Blackwell: Oxford, Great Britain, 2005; pp 56–84.
- Roelen, O. (Ruh Chemie AG), Verfahren zur Herstellung von sauerstoffhaltigen Verbindungen, DE000000849548, 1938.
- Roelen, O., Production of oxygenated carbon compounds, US000002327066, 1939.

6 References

26. Cornils, B.; Herrmann, W. A.; Rasch, M., Otto Roelen, Pioneer in Industrial Homogeneous Catalysis. *Angew. Chem. Int. Ed. Engl.* **1994**, *33*, 2144–2163, DOI: 10.1002/anie.199421441.
27. Slauch, L. H.; Mullineaux, R. D., Novel Hydroformylation catalysts. *J. Organomet. Chem.* **1968**, *13*, 469–477, DOI: 10.1016/S0022-328X(00)82775-8.
28. Canell, L. G.; Mullineaux, R. D.; Slauch, L. H. (Shell Int. Research), Verfahren zur Herstellung von Aldehyden und/oder Alkoholen durch die Oxo-Synthese, DE000001186455, 1961.
29. Sharma, S. K.; Jasra, R. V., Aqueous phase catalytic hydroformylation reactions of alkenes. *Catal. Today* **2015**, *247*, 70–81, DOI: 10.1016/j.cattod.2014.07.059.
30. Pospech, J.; Fleischer, I.; Franke, R.; Buchholz, S.; Beller, M., Alternative metals for homogeneous catalyzed hydroformylation reactions. *Angew. Chem. Int. Ed. Engl.* **2013**, *52*, 2852–2872, DOI: 10.1002/anie.201208330.
31. Pruchnik, F. P. *Organometallic Chemistry of the Transition Elements*; Modern Inorganic Chemistry; Springer: Boston, MA, USA, 1990.
32. Clarke, M. L.; Frew, J. J. R., Ligand electronic effects in homogeneous catalysis using transition metal complexes of phosphine ligands. In *Organometallic chemistry*; Fairlamb, I. J. S., Lynam, J. M., Eds.; Specialist Periodical Reports 35; Royal Society of Chemistry: Cambridge, Great Britain, 2009; pp 19–46.
33. Gillespie, J. A.; Dodds, D. L.; Kamer, P. C. J., Rational design of diphosphorus ligands - a route to superior catalysts. *Dalton Trans.* **2010**, *39*, 2751–2764, DOI: 10.1039/b913778e.
34. Gillespie, J. A.; Zuidema, E.; van Leeuwen, P. W. N. M.; Kamer, P. C. J., Phosphorus Ligand Effects in Homogeneous Catalysis and Rational Catalyst Design. In *Phosphorus (III) ligands in homogeneous catalysis: Design and synthesis*; Kamer, P., van Leeuwen, P. W. N. M., Eds.; Wiley-Blackwell: Oxford, Great Britain, 2012; pp 1–26.
35. Gual, A.; Godard, C.; La Fuente, V. de; Castellón, S., Design and Synthesis of Phosphite Ligands for Homogeneous Catalysis. In *Phosphorus (III) ligands in homogeneous catalysis: Design and synthesis*; Kamer, P., van Leeuwen, P. W. N. M., Eds.; Wiley-Blackwell: Oxford, Great Britain, 2012; pp 81–131.
36. Piras, I.; Jennerjahn, R.; Jackstell, R.; Baumann, W.; Spannenberg, A.; Franke, R.; Wiese, K.-D.; Beller, M., Synthesis of novel rhodium phosphite catalysts for efficient and selective isomerization–hydroformylation reactions. *J. Organomet. Chem.* **2010**, *695*, 479–486, DOI: 10.1016/j.jorganchem.2009.11.007.
37. Cogley, C. J.; Gardner, K.; Klosin, J.; Praquin, C.; Hill, C.; Whiteker, G. T.; Zanotti-Gerosa, A.; Petersen, J. L.; Abboud, K. A., Synthesis and application of a new bisphosphite ligand

6 References

- collection for asymmetric hydroformylation of allyl cyanide. *J. Org. Chem.* **2004**, *69*, 4031–4040, DOI: 10.1021/jo040128p.
38. van Leeuwen, P.W.N.M.; Roobeek, C. F., Hydroformylation of less reactive olefins with modified rhodium catalysts. *J. Organomet. Chem.* **1983**, *258*, 343–350, DOI: 10.1016/S0022-328X(00)99279-9.
39. van Rooy, A.; Orij, E. N.; Kamer, P. C. J.; van den Aardweg, F.; van Leeuwen, P. W. N. M., Hydroformylation of oct-1-ene with extremely high rates using rhodium catalysts containing bulky phosphites. *J. Chem. Soc., Chem. Commun.* **1991**, 1096–1097, DOI: 10.1039/c39910001096.
40. Jongsma, T.; Challa, G.; van Leeuwen, P.W.N.M., A mechanistic study of rhodium tri(*o*-*t*-butylphenyl)phosphite complexes as hydroformylation catalysts. *J. Organomet. Chem.* **1991**, *421*, 121–128, DOI: 10.1016/0022-328X(91)86436-T.
41. Roobeek, C. F.; van Leeuwen, P. W. N. M. (Shell Int. Research), A process for the hydroformylation of olefins., EP000000054986, 1981.
42. Abatjoglou, A. G.; Bryant, D. R.; Maher, J. M. (Union Carbide Chem Plastic), Stabilization of phosphite ligands in hydroformylation process, EP000000697391, 1995.
43. Abatjoglou, A. G.; Billig, E.; Bryant, D. R. (Union Carbide Corp.), Transition metal complex catalyzed processes, US000004668651, 1985.
44. Cuny, G. D.; Buchwald, S. L., Practical, high-yield, regioselective, rhodium-catalyzed hydroformylation of functionalized α -olefins. *J. Am. Chem. Soc.* **1993**, *115*, 2066–2068, DOI: 10.1021/ja00058a079.
45. Abatjoglou, A. G.; Billig, E.; Bryant, D. R. (Union Carbide Corp.), Bis-phosphite Compounds, EP000000213639, 1986.
46. Ayres, D. C.; Rydon, H. N., 219. The organic chemistry of phosphorous. Part V. The ester-interchange reaction between triphenyl phosphite and glycols. *J. Chem. Soc.* **1957**, 1109–1114, DOI: 10.1039/jr9570001109.
47. Cross, D. F. W.; Oakes, V. (Pure Chem Ltd.), Improvements relating to Alkyl Phosphites, GB000001173763, 1966.
48. Cobley, C. J.; Ellis, D. D.; Orpen, A. G.; Pringle, P. G., Calix[4]arene derived phosphites: their hydrolytic stability and complexes with gold(I), platinum(II), palladium(II) and iridium(I). *J. Chem. Soc., Dalton Trans.* **2000**, 1101–1107, DOI: 10.1039/a908960h.
49. Gavrilov, K. N.; Lyubimov, S. E.; Petrovskii, P. V.; Zheglov, S. V.; Safronov, A.; Skazov, R. S.; Davankov, V. A., Facile one-pot synthesis of BINOL- and H8-BINOL-based aryl phosphites

6 References

- and their use in palladium catalysed asymmetric allylation. *Tetrahedron* **2005**, *61*, 10514–10520, DOI: 10.1016/j.tet.2005.08.046.
50. Suárez, A.; Pizzano, A.; Fernández, I.; Khair, N., Monodentate phosphites with carbohydrate substituents and their application in rhodium catalysed asymmetric hydrosilylation reactions. *Tetrahedron: Asymmetry* **2001**, *12*, 633–642, DOI: 10.1016/S0957-4166(01)00082-9.
51. Börner, A.; Hess, D.; Kadyrov, R.; Röttger, D.; Selent, D. (Oxeno Olefinchemie GmbH), Neue Bisphosphitverbindungen und deren Metallkomplexe, DE000010031493, 2000.
52. Anschütz, L.; Marquardt, W., Phosphorigsäureester des 3.4-Dihydroxy-toluols und des 2.2'-Dihydroxy-biphenyls. *Chem. Ber.* **1956**, *89*, 1119–1123, DOI: 10.1002/cber.19560890507.
53. Selent, D.; Hess, D.; Wiese, K.-D.; Röttger, D.; Kunze, C.; Börner, A., New Phosphorus Ligands for the Rhodium-Catalyzed Isomerization/Hydroformylation of Internal Octenes. *Angew. Chem. Int. Ed.* **2001**, *40*, 1696–1698, DOI: 10.1002/1521-3773(20010504)40:9<1696:AID-ANIE16960>3.0.CO;2-2.
54. Börner, A.; Dyballa, K. M.; Franke, R.; Selent, D. (Evonik Degussa GmbH), One pot synthesis for the preparation of diphosphites and triphosphites, EP000003029046A1, 2014.
55. Kunze, C.; Selent, D.; Neda, I.; Schmutzler, R.; Spannenberg, A.; Börner, A., Synthesis of new calix[4]arene-based phosphorus ligands and their application in the Rh(I) catalyzed hydroformylation of 1-octene. *Heteroat. Chem.* **2001**, *12*, 577–585, DOI: 10.1002/hc.1088.
56. Börner, A.; Dyballa, K. M.; Franke, R.; Fridag, D.; Hess, D.; Selent, D. (Evonik Industries AG), New Quadridentate phosphorus ligands comprising Hostanox 03 conductive structure, WO002014177355, 2014.
57. Yan, Y.; Zhang, X.; Zhang, X., Retaining Catalyst Performance at High Temperature: The Use of a Tetrakisphosphine Ligand in the Highly Regioselective Hydroformylation of Terminal Olefins. *Adv. Synth. Catal.* **2007**, *349*, 1582–1586, DOI: 10.1002/adsc.200700017.
58. Evrard, D.; Lucas, D.; Mugnier, Y.; Meunier, P.; Hierso, J.-C., On the Mechanistic Behavior of Highly Efficient Palladium–Tetrakisphosphine Catalytic Systems for Cross-Coupling Reactions: First Spectroscopic and Electrochemical Studies of Oxidative Addition on Pd(0)/Multidentate Ferrocenylpolyphosphine Complexes. *Organometallics* **2008**, *27*, 2643–2653, DOI: 10.1021/om701279x.
59. Hierso, J.-C.; Amardeil, R.; Bentabet, E.; Broussier, R.; Gautheron, B.; Meunier, P.; Kalck, P., Structural diversity in coordination chemistry of tridentate and tetradentate

6 References

- polyphosphines of Group 6 to 10 transition metal complexes. *Coord. Chem. Rev.* **2003**, *236*, 143–206, DOI: 10.1016/S0010-8545(02)00221-7.
60. Hierso, J.-C.; Amardeil, R.; Bentabet, E.; Broussier, R.; Gautheron, B.; Meunier, P.; Kalck, P., Structural diversity in coordination chemistry of tridentate and tetradentate polyphosphines of Group 6 to 10 transition metal complexes. *Coord. Chem. Rev.* **2003**, *236*, 143–206, DOI: 10.1016/S0010-8545(02)00221-7.
61. Hierso, J.-C.; Beaupérin, M.; Meunier, P., Ultra-Low Catalyst Loading as a Concept in Economical and Sustainable Modern Chemistry: The Contribution of Ferrocenylpolyphosphane Ligands. *Eur. J. Inorg. Chem.* **2007**, *2007*, 3767–3780, DOI: 10.1002/ejic.200700405.
62. Hierso, J.-C.; Smaliy, R.; Amardeil, R.; Meunier, P., New concepts in multidentate ligand chemistry: effects of multidentarity on catalytic and spectroscopic properties of ferrocenyl polyphosphines. *Chem. Soc. Rev.* **2007**, *36*, 1754–1769, DOI: 10.1039/b701207c.
63. Yu, S.; Zhang, X.; Yan, Y.; Cai, C.; Dai, L.; Zhang, X., Synthesis and application of tetrphosphane ligands in rhodium-catalyzed hydroformylation of terminal olefins: high regioselectivity at high temperature. *Chem. Eur. J.* **2010**, *16*, 4938–4943, DOI: 10.1002/chem.200903109.
64. Börner, A.; Christiansen, A.; Franke, R.; Fridag, D.; Hess, D.; Kreidler, B.; Selent, D. (Evonik Oxeno GmbH), Novel organophosphorus compounds based on Anthracenetriol, WO002013068232A1, 2012.
65. Yu, S.; Chie, Y.-m.; Zhang, X., Highly Regioselective and Rapid Hydroformylation of Alkyl Acrylates Catalyzed by a Rhodium Complex with a Tetrphosphorus Ligand. *Adv. Synth. Catal.* **2009**, *351*, 537–540, DOI: 10.1002/adsc.200800676.
66. Shih, W.-C.; Ozerov, O. V., One-Pot Synthesis of 1,3-Bis(phosphinomethyl)arene PCP/PNP Pincer Ligands and Their Nickel Complexes. *Organometallics* **2015**, *34*, 4591–4597, DOI: 10.1021/acs.organomet.5b00671.
67. Peer, M.; Jong, J. C. de; Kiefer, M.; Langer, T.; Rieck, H.; Schell, H.; Sennhenn, P.; Sprinz, J.; Steinhagen, H.; Wiese, B.; Helmchen G., Preparation of chiral phosphorus, sulfur and selenium containing 2-aryloxazolines. *Tetrahedron* **1996**, *52*, 7547–7583, DOI: 10.1016/0040-4020(96)00267-0.
68. Casey, C. P.; Paulsen, E. L.; Beuttenmueller, E. W.; Proft, B. R.; Petrovich, L. M.; Matter, B. A.; Powell, D. R., Electron Withdrawing Substituents on Equatorial and Apical Phosphines Have Opposite Effects on the Regioselectivity of Rhodium Catalyzed Hydroformylation. *J. Am. Chem. Soc.* **1997**, *119*, 11817–11825, DOI: 10.1021/ja9719440.

6 References

69. Müller, G.; Klinga, M.; Leskelä, M.; Rieger, B. *Z. Anorg. Allg. Chem.* **2002**, *628*, 2839–2846, DOI: 10.1002/1521-3749(200213)628:13<2839:AID-ZAAC2839>3.0.CO;2-9.
70. Dahlhoff, W. V.; Nelson, S. M., Studies on the magnetic cross-over in five-co-ordinate complexes of iron(II), cobalt(II), and nickel(II). Part II. *J. Chem. Soc. A* **1971**, 2184–2190, DOI: 10.1039/j19710002184.
71. Kawatsura, M.; Hartwig, J. F., Transition Metal-Catalyzed Addition of Amines to Acrylic Acid Derivatives. A High-Throughput Method for Evaluating Hydroamination of Primary and Secondary Alkylamines. *Organometallics* **2001**, *20*, 1960–1964, DOI: 10.1021/om0009987.
72. Neumann, J.; Elangovan, S.; Spannenberg, A.; Junge, K.; Beller, M., Improved and General Manganese-Catalyzed *N*-Methylation of Aromatic Amines Using Methanol. *Chem. Eur. J.* **2017**, *23*, 5410–5413, DOI: 10.1002/chem.201605218.
73. Hermann, D.; Gandelman, M.; Rozenberg, H.; Shimon, L. J. W.; Milstein, D., Synthesis, Structure, and Reactivity of New Rhodium and Iridium Complexes, Bearing a Highly Electron-Donating PNP System. Iridium-Mediated Vinylic C–H Bond Activation. *Organometallics* **2002**, *21*, 812–818, DOI: 10.1021/om010719v.
74. Tripolszky, A.; Bálint, E.; Keglevich, G., Microwave-assisted synthesis of α -aminophosphine oxides. *Phosphorus Sulfur Silicon Relat. Elem.* **2019**, *194*, 345–348, DOI: 10.1080/10426507.2018.1541898.
75. Kosanovich, A. J.; Reibenspies, J. H.; Ozerov, O. V., Complexes of High-Valent Rhenium Supported by the PCP Pincer. *Organometallics* **2016**, *35*, 513–519, DOI: 10.1021/acs.organomet.5b00935.
76. Younus, H. A.; Ahmad, N.; Su, W.; Verpoort, F., Ruthenium pincer complexes: Ligand design and complex synthesis. *Coord. Chem. Rev.* **2014**, *276*, 112–152, DOI: 10.1016/j.ccr.2014.06.016.
77. Wu, Q.; Zhou, F.; Shu, X.; Jian, L.; Xu, B.; Zheng, X.; Yuan, M.; Fu, H.; Li, R.; Chen, H., Synthesis and application of PNP pincer ligands in rhodium-catalyzed hydroformylation of cycloolefins. *RSC Adv.* **2016**, *6*, 107305–107309, DOI: 10.1039/c6ra24144a.
78. Botteghi, C.; Paganelli, S.; Perosa, A.; Lazzaroni, R.; Uccello-Barretta, G., Hydroformylation of norbornene and 2,5-norbornadiene catalysed by platinum(0)-alkene complexes in the presence of methanesulfonic acid: determination of the stereochemistry of the reaction. *J. Organomet. Chem.* **1993**, *447*, 153–157, DOI: 10.1016/0022-328X(93)80285-J.

6 References

79. Yang, X.; Liang, H.; Fu, H.; Zheng, X.; Yuan, M.; Li, R.; Chen, H., Hydroformylation of 2,5-norbornadiene in organic/aqueous two-phase system and acceleration by cationic surfactants. *Appl. Organometal. Chem.* **2016**, *30*, 335–340, DOI: 10.1002/aoc.3436.
80. Tian, R.; Ng, Y.; Ganguly, R.; Mathey, F., A New Type of Phosphaferrocene–Pyrrole–Phosphaferrocene P-N-P Pincer Ligand. *Organometallics* **2012**, *31*, 2486–2488, DOI: 10.1021/om300061d.
81. Bianchini, C.; Meli, A.; Peruzzini, M.; Vizza, F.; Fujiwara, Y.; Jintoku, T.; Taniguchi, H., Rhodium complexes with the tripodal triphosphine MeC(CH₂PPh₂)₃ as highly reactive systems for hydrogenation and hydroformylation of alkenes. *J. Chem. Soc., Chem. Commun.* **1988**, 299–301, DOI: 10.1039/c39880000299.
82. Thaler, E. G.; Folting, K.; Caulton, K. G., η^3 -MeC(CH₂PPh₂)₃/rhodium complexes utilize phosphine arm dissociation mechanisms at 25 °C. *J. Am. Chem. Soc.* **1990**, *112*, 2664–2672, DOI: 10.1021/ja00163a029.
83. Rosales, M.; Soto, O.; González, B.; Pacheco, I.; Baricelli, P. J., Kinetics and mechanisms of homogeneous catalytic reactions: Part 15. Regio-specific hydroformylation of limonene catalysed by rhodium complexes of phosphine ligands. *Transition Met. Chem.* **2018**, *43*, 451–461, DOI: 10.1007/s11243-018-0232-6.
84. Phanopoulos, A.; Nozaki, K., Branched-Selective Hydroformylation of Nonactivated Olefins Using an N-Triphos/Rh Catalyst. *ACS Catal.* **2018**, *8*, 5799–5809, DOI: 10.1021/acscatal.8b00566.
85. Chen, C.; Li, P.; Hu, Z.; Wang, H.; Zhu, H.; Hu, X.; Wang, Y.; Lv, H.; Zhang, X., Synthesis and application of a new triphosphorus ligand for regioselective linear hydroformylation: a potential way for the stepwise replacement of PPh₃ for industrial use. *Org. Chem. Front.* **2014**, *1*, 947–951, DOI: 10.1039/C4QO00132J.
86. Chen, C.; Qiao, Y.; Geng, H.; Zhang, X., A novel triphosphoramidite ligand for highly regioselective linear hydroformylation of terminal and internal olefins. *Org. Lett.* **2013**, *15*, 1048–1051, DOI: 10.1021/ol400033k.
87. van Leeuwen, P. W. N. M.; Chadwick, J. C. *Homogeneous catalysts: Activity - stability - deactivation*; Wiley-VCH: Weinheim, Germany, 2011.
88. Christiansen, A.; Selent, D.; Spannenberg, A.; Köckerling, M.; Reinke, H.; Baumann, W.; Jiao, H.; Franke, R.; Börner, A., Heteroatom-substituted secondary phosphine oxides (HASPOs) as decomposition products and preligands in rhodium-catalysed hydroformylation. *Chem. Eur. J.* **2011**, *17*, 2120–2129, DOI: 10.1002/chem.201002823.

6 References

89. McIntyre, S. K.; Alam, T. M., ¹⁷O NMR investigation of phosphite hydrolysis mechanisms. *Magn. Reson. Chem.* **2007**, *45*, 1022–1026, DOI: 10.1002/mrc.2094.
90. van Leeuwen, P. W. N. M.; Roobeek, C. F.; Frijns, J. H. G.; Orpen, A. G., Characterization of the intermediates in the hydroformylation reaction catalyzed by platinum diphenylphosphinous acid complexes. *Organometallics* **1990**, *9*, 1211–1222, DOI: 10.1021/om00118a049.
91. Christiansen, A.; Selent, D.; Spannenberg, A.; Baumann, W.; Franke, R.; Börner, A., Reaction of Secondary Phosphine Oxides with Rhodium(I). *Organometallics* **2010**, *29*, 3139–3145, DOI: 10.1021/om100171p.
92. Christiansen, A.; Li, C.; Garland, M.; Selent, D.; Ludwig, R.; Franke, R.; Börner, A., Secondary Phosphane Oxides as Preligands in Rhodium-Catalyzed Hydroformylation. *ChemCatChem* **2010**, *2*, 1278–1285, DOI: 10.1002/cctc.201000114.
93. Johnson, B.; Keck-Antoine, K.; Dejolier, B.; Allen, N.; Ortuoste, N.; Edge, M., Impact of improved phosphite hydrolytic stability on the processing stabilization of polypropylene. *J. Vinyl Addit. Techn.* **2005**, *11*, 136–142, DOI: 10.1002/vnl.20052.
94. Oberhauser, W.; Manca, G., Catalytic Phosphite Hydrolysis under Neutral Reaction Conditions. *Inorg. Chem.* **2018**, *57*, 4824–4827, DOI: 10.1021/acs.inorgchem.8b00546.
95. Zhang, B.; Jiao, H.; Michalik, D.; Kloß, S.; Deter, L. M.; Selent, D.; Spannenberg, A.; Franke, R.; Börner, A., Hydrolysis Stability of Bidentate Phosphites Utilized as Modifying Ligands in the Rh-Catalyzed *n*-Regioselective Hydroformylation of Olefins. *ACS Catal.* **2016**, *6*, 7554–7565, DOI: 10.1021/acscatal.6b02185.
96. Börner, A.; Dyballa, K. M.; Franke, R.; Selent, D. (Evonik Degussa GmbH), Bis-phosphites with 2,3-biphenol unit as central component, EP000003029045, 2014.
97. Börner, A.; Dyballa, K. M.; Franke, R.; Selent, D. (Evonik Degussa GmbH), Phosphites with a dihydroxyterphenyl with a tetraphenyl dioxaphospholane, EP000003293192, 2016.
98. Börner, A.; Hess, D.; Kreidler, B.; Selent, D.; Wiese, K.-D. (Evonik Degussa GmbH), Bisphosphite ligands for hydroformylation catalyzed by transition metals, WO002008071508, 2007.
99. Selent, D. *Laboratory Journal: Nr. 28*. S. 95; Rostock, May 9, 2016.
100. Lu, W.; Li, P.; Shan, Y.; Su, P.; Wang, J.; Shi, Y.; Zhang, J., Discovery of biphenyl-based VEGFR-2 inhibitors. Part 3: design, synthesis and 3D-QSAR studies. *Bioorg. Med. Chem.* **2015**, *23*, 1044–1054, DOI: 10.1016/j.bmc.2015.01.006.

6 References

101. Hille, U. E.; Hu, Q.; Vock, C.; Negri, M.; Bartels, M.; Müller-Vieira, U.; Lauterbach, T.; Hartmann, R. W., Novel CYP17 inhibitors: Synthesis, biological evaluation, structure–activity relationships and modelling of methoxy- and hydroxy-substituted methyleneimidazolyl biphenyls. *Eur. J. Med. Chem.* **2009**, *44*, 2765–2775, DOI: 10.1016/j.ejmech.2009.01.002.
102. Fergusson, K. M.; Hird, M., The dramatic influence of the location of bend and of lateral fluoro substitution on the mesomorphic properties of angular chiral esters based on a 1,3-disubstituted benzene ring. *J. Mater. Chem.* **2010**, *20*, 3069, DOI: 10.1039/b923267b.
103. Boße, F.; Maier, M. E., Synthesis of a Tetrasubstituted Cyclohexene from a Bicyclo[2.2.2]octa-2,5-diene. *J. Prakt. Chem.* **2000**, *342*, 6–9, DOI: 10.1002/(SICI)1521-3897(200001)342:1<6:AID-PRAC6>3.0.CO;2-B.
104. Schmidt, B.; Riemer, M., Suzuki-Miyaura coupling of halophenols and phenol boronic acids: systematic investigation of positional isomer effects and conclusions for the synthesis of phytoalexins from pyrinae. *J. Org. Chem.* **2014**, *79*, 4104–4118, DOI: 10.1021/jo500675a.
105. Kloß, S., Stabilitätsuntersuchungen an Liganden für Hydroformylierungs-Katalysatoren. Master Thesis, Universität Rostock, Rostock, 2016.
106. Börner, A.; Dyballa, K. M.; Franke, R.; Selent, D. (Evonik Degussa GmbH), Phosphites with a Silyloxyphenol, EP000003293190, 2016.
107. Davies, J. S.; Higginbotham, C. L.; Tremeer, E. J.; Brown, C.; Treadgold, R. C., Protection of hydroxy groups by silylation: use in peptide synthesis and as lipophilicity modifiers for peptides. *J. Chem. Soc., Perkin Trans. 1* **1992**, 3043–3048, DOI: 10.1039/p19920003043.
108. Dyballa, K. M.; Franke, R. (Evonik Degussa GmbH), Novel monophosphite compound with an ester group, EP000003088407, 2016.
109. Börner, A.; Dyballa, K. M.; Franke, R.; Fridag, D.; Selent, D. (Evonik Degussa GmbH), Bis-phosphites with an asymmetric biaryl central component, EP000003029044, 2014.
110. Börner, A.; Dyballa, K. M.; Franke, R.; Fridag, D.; Geilen, F.; Hess, D.; Selent, D. (Evonik Degussa GmbH), Monophosphites with structural unit 4,4,5,5-tetraphenyl-1,3,2-dioxaphospholan as ligand for hydroformylation catalysts, EP000003029013, 2014.
111. Kloß, S.; Selent, D.; Spannenberg, A.; Franke, R.; Börner, A.; Sharif, M., Effects of Substitution Pattern in Phosphite Ligands Used in Rhodium-Catalyzed Hydroformylation on Reactivity and Hydrolysis Stability. *Catalysts* **2019**, *9*, 1036–1051, DOI: 10.3390/catal9121036.
112. Selent, D. *Zuarbeit für das Patent Monophosphit auf Basis von Benzopinakol*; Rostock, Sep 8, 2014.

6 References

113. Rybtchinski, B.; Oevers, S.; Montag, M.; Vigalok, A.; Rozenberg, H.; Martin, J. M.; Milstein, D., Comparison of steric and electronic requirements for C-C and C-H bond activation. Chelating vs nonchelating case. *J. Am. Chem. Soc.* **2001**, *123*, 9064–9077, DOI: 10.1021/ja016126t.
114. Rybtchinski, B.; Cohen, R.; Ben-David, Y.; Martin, J. M. L.; Milstein, D., Aromatic vs aliphatic C-H bond activation by rhodium(I) as a function of agostic interactions: catalytic H/D exchange between olefins and methanol or water. *J. Am. Chem. Soc.* **2003**, *125*, 11041–11050, DOI: 10.1021/ja029197g.
115. Windmüller, B.; Nürnberg, O.; Wolf, J.; Werner, H., A Novel Route to Cationic Four-Coordinate Rhodium(I) Complexes with Rh=C Bonds. *Eur. J. Inorg. Chem.* **1999**, *1999*, 613–619, DOI: 10.1002/(SICI)1099-0682(199904)1999:4<613:AID-EJIC613>3.0.CO;2-L.
116. Hahn, C.; Sieler, J.; Taube, R., Complex Catalysis, XLIX On the Coordination of Olefins and Secondary Amines at the Cationic [2,6-Bis(diphenylphosphanylmethyl)pyridine]rhodium(I) Fragment [Rh(PNP)]⁺ - Synthesis and Characterization of [Rh(PNP)(L)]X (L = Ethylene, Styrene, HNR₂; X = BF₄, PF₆, CF₃SO₃). *Chem. Ber.* **1997**, *130*, 939–945, DOI: 10.1002/cber.19971300720.
117. Feller, M.; Iron, M. A.; Shimon, L. J. W.; Diskin-Posner, Y.; Leitun, G.; Milstein, D., Competitive C-I versus C-CN reductive elimination from a Rh(III) complex. Selectivity is controlled by the solvent. *J. Am. Chem. Soc.* **2008**, *130*, 14374–14375, DOI: 10.1021/ja8046798.
118. Vasapollo, G.; Giannoccaro, P.; Nobile, C. F.; Sacco, A., Synthesis and reactivity toward gas molecules of chloro 2,6-di(diphenylphosphinomethyl)pyridine rhodium(I). *Inorg. Chim. Acta* **1981**, *48*, 125–128, DOI: 10.1016/S0020-1693(00)90077-X.
119. Feller, M.; Diskin-Posner, Y.; Leitun, G.; Shimon, L. J. W.; Milstein, D., Direct observation of reductive elimination of MeX (X = Cl, Br, I) from Rh(III) complexes: mechanistic insight and the importance of sterics. *J. Am. Chem. Soc.* **2013**, *135*, 11040–11047, DOI: 10.1021/ja401852c.
120. Smaliy, R. V.; Beaupérin, M.; Cattey, H.; Meunier, P.; Hierso, J.-C.; Roger, J.; Doucet, H.; Coppel, Y., Conformational Control of Metallocene Backbone by Cyclopentadienyl Ring Substitution: A New Concept in Polyphosphane Ligands Evidenced by “Through-Space” Nuclear Spin–Spin Coupling. Application in Heteroaromatics Arylation by Direct C–H Activation. *Organometallics* **2009**, *28*, 3152–3160, DOI: 10.1021/om8012162.
121. Beaupérin, M.; Job, A.; Cattey, H.; Royer, S.; Meunier, P.; Hierso, J.-C., Copper(I) Iodide Polyphosphine Adducts at Low Loading for Sonogashira Alkynylation of Demanding Halide Substrates: Ligand Exchange Study between Copper and Palladium. *Organometallics* **2010**, *29*, 2815–2822, DOI: 10.1021/om1003336.

6 References

122. Roy, D.; Mom, S.; Beaupérin, M.; Doucet, H.; Hierso, J.-C., A versatile palladium/triphosphane system for direct arylation of heteroarenes with chloroarenes at low catalyst loading. *Angew. Chem. Int. Ed.* **2010**, *49*, 6650–6654, DOI: 10.1002/anie.201002987.
123. Platon, M.; Cui, L.; Mom, S.; Richard, P.; Saeys, M.; Hierso, J.-C., Etherification of Functionalized Phenols with Chloroheteroarenes at Low Palladium Loading: Theoretical Assessment of the Role of Triphosphane Ligands in C-O Reductive Elimination. *Adv. Synth. Catal.* **2011**, *353*, 3403–3414, DOI: 10.1002/adsc.201100481.
124. Zinovyeva, V. A.; Mom, S.; Fournier, S.; Devillers, C. H.; Cattey, H.; Doucet, H.; Hierso, J.-C.; Lucas, D., Kinetic and electrochemical studies of the oxidative addition of demanding organic halides to Pd(0): the efficiency of polyphosphane ligands in low palladium loading cross-couplings decrypted. *Inorg. Chem.* **2013**, *52*, 11923–11933, DOI: 10.1021/ic401613w.
125. Brereton, R. G. *Chemometrics: Data analysis for the laboratory and chemical plant*, Repr; Wiley: Chichester, Great Britain, 2006.
126. Leardi, R., Experimental design in chemistry: A tutorial. *Anal. Chim. Acta* **2009**, *652*, 161–172, DOI: 10.1016/j.aca.2009.06.015.
127. Lewis, G. A.; Mathieu, D.; Phan, R. T. L. *Pharmaceutical experimental design; Drugs and the pharmaceutical sciences 92*; M. Dekker: New York, USA, 1999.
128. Shardt, Y. A.W. *Statistics for Chemical and Process Engineers: A Modern Approach*, 1st ed. 2015; Springer: Berlin Heidelberg, Germany, 2015.
129. Box, J. F., Guinness, Gosset, Fisher, and Small Samples. *Stat. Sci.* **1987**, *2*, 45–52, DOI: 10.1214/ss/1177013437.
130. Raine, J., Evaluation of drugs in humans. In *Clinical pharmacology*, 11th ed.; Bennett, P. N., Brown, M. J., Sharma, P., Eds.; Elsevier: Edinburgh, Great Britain, 2012; pp 37–54.